# Zebrafish *C9orf72* loss-of-function models of Amyotrophic Lateral Sclerosis and Frontotemporal Dementia

By

## Natalie Paige Rounding
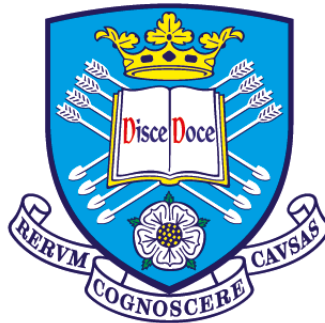
Sheffield Institute for Translational Neuroscience

University of Sheffield

## Submitted for the degree of Doctor of Philosophy (PhD)

November 2017

# Abstract

**Background:** A noncoding $(G_4C_2)_n$ hexanucleotide repeat expansion in chromosome 9 open reading frame 72 (*C9orf72*) is a major cause of both amyotrophic lateral sclerosis (ALS) and frontotemporal dementia (FTD), together referred to as C9-ALS/FTD. It is unknown how the repeat expansion causes C9-ALS/FTD, however there is evidence that C9orf72 mRNA levels are reduced in patients, suggesting *C9orf72* loss-of-function (LOF) via haploinsufficiency may contribute to C9-ALS/FTD. Understanding how haploinsufficiency may lead to the development of C9-ALS/FTD is dependent on a better understanding of C9orf72 protein function. Recent work from our laboratory and others in cell lines have shown that C9orf72 regulates autophagy, but the *in vivo* relevance of autophagy-deficits remains unclear.

**Objectives:** To investigate if *C9orf72* LOF via haploinsufficiency results in C9-ALS/FTD due to defective autophagy using a stable zebrafish *C9orf72* LOF model.

**Methods:** Genome editing techniques were used to target sequences within exon 1 and exon 7 of the zebrafish orthologue of *C9orf72* (*C13H9orf72; zgc10846*). To investigate the effects of *C13H9orf72* LOF, we characterised survival, motor function and anxiety-like behaviour. Immunohistochemical analysis of neuromuscular junctions (NMJs) was also performed. To investigate the role of C9orf72 in autophagy *in vivo*, autophagic flux was measured. Additionally, we looked for symptoms of splenomegaly, due to recent evidence that full ablation of *C9orf72* in mice resulted in immune system-related pathology.

**Results:** Three independent lines of zebrafish carrying different frameshift mutations in exon 1 (SH470) and exon 7 (SH448 and SH451) were characterised. Survival monitoring suggests that mutations in *C13H9orf72* do not lead to loss of viability. A subtle reduction in motor function is observed in adult *C13H9orf72* LOF zebrafish, but no corresponding NMJ pathology, and there is no evidence of anxiety-like behaviour in adults. Zebrafish C13H9orf72 was found to interact with a member of the autophagy initiation complex, but further work is needed to determine whether it plays a regulatory role in autophagy in zebrafish. Additionally, no signs of significant splenomegaly were observed in these zebrafish.

**Conclusions:** Results obtained do not support the hypothesis that *C9orf72* LOF is sufficient to cause C9-ALS/FTD alone, which complements published findings in *C9orf72* LOF mouse models.

**<u>Statement of contribution</u>**

I state that all work included in this thesis is my own. The only exception is the *in vitro* binding assay, discussed in chapter 5, which was performed in collaboration with Dr Christopher Webster, University of Sheffield.

## **Acknowledgments**

## Table of contents

## List of figures

# List of tables

## Abbreviations

| | |
|---|---|
| **AD** | Autosomal Dominant |
| **ALS** | Amyotrophic Lateral Sclerosis |
| **AMO** | Antisense Oligonucleotide Morpholino |
| **AR** | Autosomal Recessive |
| **ATG** | Autophagy-related Protein |
| **BB** | Bunina bodies |
| **BP** | Base pair |
| **BSA** | Bovine serum albumin |
| **bv-FTD** | Behavioural variant FTD |
| **C9-ALS/FTD** | ALS/FTD patients with a pathological $(G_4C_2)_n$ expansion in C9orf72 |
| **C9orf72** | Chromosome 9 open reading frame |
| **C13H9orf72** | Zebrafish C9orf72 (zgc 10846) |
| **CHAT** | Choline acetyltransferase |
| **CNS** | Central Nervous system |
| **CRISPR-Cas9** | Clustered Regularly Interspaced Short Palindromic Repeat (CRISPR) Associated 9 (Cas9) System |
| **DENN** | Differentially Expressed in Normal and Neoplastic Cells |
| **dH$_2$O** | Distilled water |
| **DM1** | Myotonic Dystrophy Type 1 |
| **DMSO** | Dimethyl Sulfoxide |
| **DNA** | Deoxyribonucleic acid |
| **DPF** | Days post fertilisation |
| **DPR** | Dipeptide Repeat Protein |
| **eIFα** | Eukaryotic Translation Initiation Factor 2 |
| **ER** | Endoplasmic Reticulum |
| **fALS** | Familial Amyotrophic Lateral Sclerosis |
| **FIP200** | Focal Adhesion Kinase Family Interacting Protein of 200 kD |
| **FTD** | Frontotemporal Dementia |
| **FUS** | Fused in Sarcoma |
| **GEF** | Guanine Nucleotide Exchange Factor |
| **GOF** | Gain-of-function |
| **GWAS** | Genome wide association study |
| **HCI** | Hyaline conglomerate inclusion |
| **HPF** | Hours post fertilisation |
| **HR** | Homologous recombination |
| **IHC** | Immunohistochemistry |
| **INDEL** | Insertion and deletion (mutation) |
| **iPSC** | Induced pluripotent stem cell |
| **kDa** | Kilo Daltons |
| **KD** | Knockdown |
| **KO** | Knockout |
| **LC3** | Microtubule-associated Protein 1 light chain 3 |
| **LMN** | Lower Motor Neuron |
| **LOF** | Loss-of-function |
| **MN** | Motor neuron |
| **MND** | Motor Neuron Disease |
| **mRNA** | Messenger-RNA |

| | |
|---|---|
| **mTOR** | Mammalian Target of Rapamycin |
| **NCIs** | Nuclear or Cytoplasmic Inclusions |
| **NGS** | Normal goat serum |
| **NHEJ** | Non homologous end joining |
| **NMJ** | Neuromuscular junction |
| **OPTN** | Optineurin |
| **p62/SQSTM1** | Sequestosome 1 |
| **PAM** | Protospacer adjacent motif |
| **PBP** | Progressive bulbar palsy |
| **PBS** | Phosphate buffered saline |
| **PCR** | Polymerase chain reaction |
| **PFA** | Paraformaldehyde |
| **PLS** | Primary lateral sclerosis |
| **PMA** | Progressive muscular atrophy |
| **PNFA** | Progressive nonfluent aphasia |
| **PNS** | Peripheral nervous system |
| **qPCR** | Quantitative polymerase chain reaction |
| **RAN** | Repeat-Associated, Non-ATG (translation) |
| **RBP** | RNA-Binding Protein |
| **RNA** | Ribonucleic acid |
| **RT** | Room Temperature |
| **sALS** | Sporadic Amyotrophic Lateral Sclerosis |
| **SD** | Semantic dementia |
| **SOD1** | Superoxide Dismutase 1 |
| **SV2** | Synaptic vesicle protein 2 |
| **TALENs** | Transcription Activator-like Effector Nucleases |
| **TARDBP** | TAR DNA Binding Protein |
| **TARDBPL** | TAR DNA Binding Protein-Like |
| **TDP-43** | TAR DNA Binding Protein (TARDBP) of 43 kDa |
| **UBI** | Ubiquitinated inclusions |
| **UBQLN-2** | Ubiquillin-2 |
| **U$_{crit}$** | Critical swimming speed |
| **ULK 1** | Unc-51 like Autophagy Activating Kinase 1 |
| **ULK2** | Unc-51 like Autophagy Activating Kinase 2 |
| **UMN** | Upper Motor Neuron |
| **UTR** | Untranslated region |
| **WT** | Wild-type |

# 1. Introduction

## 1.1. Amyotrophic Lateral Sclerosis

### 1.1.1. Background

Amyotrophic lateral sclerosis (ALS) is a rapidly progressive, fatal neurodegenerative disease. It is characterised by degeneration of motor neurons (MNs) within the cerebral cortex (known as upper motor neurons – UMNs), brainstem and the ventral horn of the spinal cord (lower motor neurons – LMNs) (Rowland and Shneider 2001) (see figure 1.1). The result of this degeneration is muscle weakness, wasting and eventual paralysis. The disease is fatal, usually within 2-5 years of diagnosis, due to respiratory failure. There are currently two treatments available, including Riluzole, which has a modest effect on life span, and more recently Edaravone, which has been reported to show efficacy in a small subset of people with ALS (Bensimon et al. 1994, Abe et al. 2017).
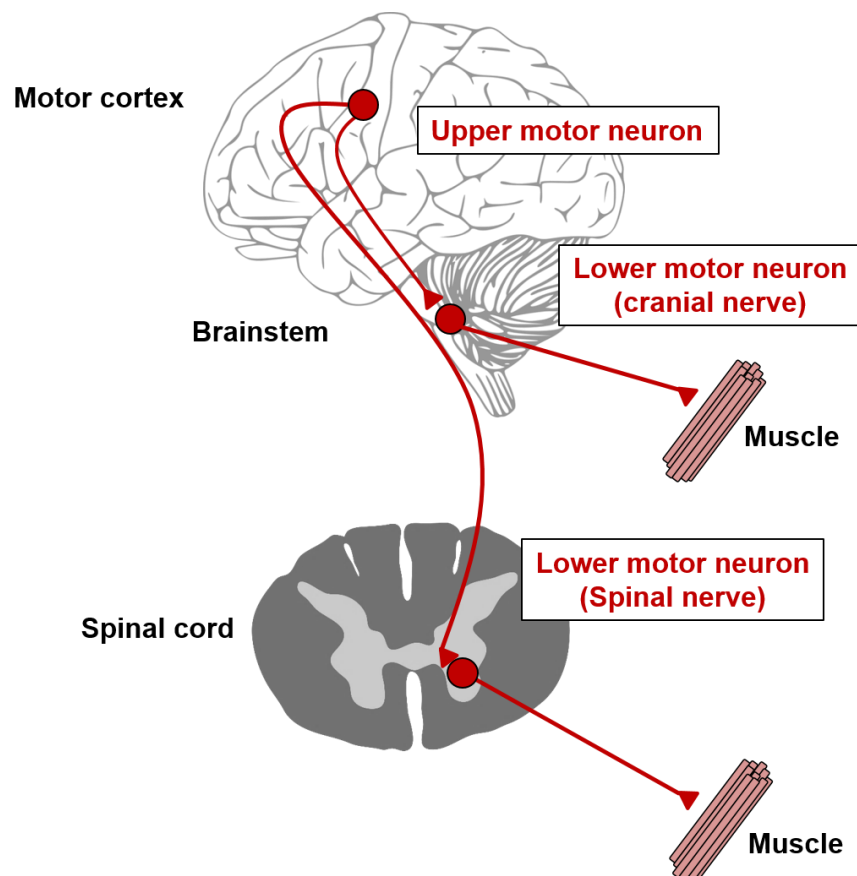


**Figure 1.1 Schematic diagram of upper and lower motor neurons.** Upper motor neurons (UMN) are motor neurons that originate in the motor region of the cerebral cortex. They carry motor information to lower motor neurons (LMN) located in the brainstem or the ventral horn of the spinal cord. The LMN innervate skeletal muscle fibres, acting as a link between UMN and muscles. (Rowland and Shneider 2001).

### 1.1.2. Clinical features of ALS

The term motor neuron disease (MND) describes a group of neurodegenerative disorders which selectively affect MNs. There are four main types of MND; ALS, Primary Lateral Sclerosis (PLS), Progressive Muscular Atrophy (PMA) and Progressive Bulbar Palsy (PBP). Although there is both clinical and neuropathological overlap between these different forms, each type has distinct features. ALS is the most common form of MND characterised by progressive degeneration of both UMNs and LMNs. Other less common forms of MND are characterised by the MNs initially affected. It is reported that less than 5% of cases are classified as PLS, which affects only the UMNs (Rowland and Shneider 2001). Additionally, PMA comprises around 10% of MND cases, characterised by initially affecting LMNs (Rowland and Shneider 2001). Finally, around 25% of cases are classified as PBP, although a recent study reported 87% of such patients eventually develop ALS, suggesting these are actually bulbar-onset ALS patients (Karam, Scelsa and MacGowan 2010).

The clinical hallmarks of ALS are due to a distinctive combination of signs of both LMN degeneration, including muscle weakness, atrophy and fasciculations, alongside features of UMN degeneration, such as muscular spasticity and hyperreflexia (Rowland and Shneider 2001). Interestingly, certain subgroups of LMNs appear to be resistant to degeneration throughout the disease course (Comley et al. 2016, Nijssen, Comley and Hedlund 2017). Oculomotor MNs, including the oculomotor (CNIII), trochlear (IV) and abducens (VI) nuclei appear to be spared during disease (Gizzi et al. 1992). These are involved in regulating eye movement; thus eye-tracking devices can be used which enable ALS patients to communicate when they can no longer speak (Caligari et al. 2013). Additionally, MNs in the Onuf's nucleus of the sacral spinal cord, which innervate the pelvic floor muscles, remain relatively unaffected (Carvalho, Schwartz and Swash 1995). This means that ALS patients do not suffer from incontinence. However, the reasons for this differential vulnerability in MNs is not fully understood.

Approximately 70% of ALS patients present with limb-onset disease, with around 25% suffering from bulbar-onset disease (Kiernan et al. 2011). In contrast, symptom onset involving the trunk or respiratory muscles is rare (Swinnen and Robberecht 2014). Typically, symptoms rapidly progress throughout the course of the disorder before culminating in a debilitating failure of the neuromuscular system. Incidence rates of ALS are estimated to be 2.16 per 100,000 persons-years in western populations (Logroscino et

al. 2010). Additionally, it has been reported that incidence rates are higher amongst males (3.0 per 100,000 person-years) compared to females (2.4 per 100,000 persons-years) in Europe (Logroscino et al. 2010). It is reported that the lifetime risk of developing ALS is 1 in 400 (Johnston et al. 2006). The peak age of onset is 58-63 for sporadic disease and 47-52 for familial disease (Kiernan et al. 2011); however there are also rare juvenile variants of ALS, such as ALS2, where onset of symptoms occurs in either the first or second decade of life (Yang et al. 2001).

The disease is usually fatal within 2 to 5 years post initial diagnosis, due to respiratory failure (Kiernan et al. 2011). However, around 5-10% of patients can survive up to 10 years post initial diagnosis (Chio et al. 2009). It has been observed that older age at symptom onset, bulbar-onset disease and onset of disease within the trunk or respiratory muscles are all linked to reduced survival (Swinnen and Robberecht 2014, Talbot 2009). Alternatively, a younger age of symptom onset and limb-onset disease are linked to prolonged survival (Swinnen and Robberecht 2014, Talbot 2009). There are currently two treatments available. Firstly, Riluzole, which has a modest effect on life span (Bensimon et al. 1994). Secondly, there is Edaravone, which has recently been reported to show efficacy in a small subset of people with ALS (Abe et al. 2017). Aside from this, standard treatment for ALS is palliative and involves multidisciplinary care, including nutritional and respiratory support.

It has been observed that ALS patients have clinical, pathological and genetic overlap with other neurodegenerative diseases. Loss of cortical neurons in the frontal and/or temporal lobes is commonly seen, resulting in a condition called frontal temporal dementia (FTD). The link between ALS and FTD will be covered in greater detail in section 1.1.6.

### 1.1.3. Neuropathological features of ALS

Regarding neuropathology, it was discovered in 1988 that ubiquitinated inclusions (UBIs) are hallmarks of ALS (Leigh et al. 1988, Lowe et al. 1988). Microscopically, UBIs are observed as skein-like aggregates or dense, round structures. They are most commonly observed in neurons, but have also been reported in glial cells (Arai et al. 2003). For many years, the protein constituents of UBIs were unknown. It is now known that TAR DNA-binding protein 43 (TDP-43) is the major constituent of UBIs in both ALS and FTD patients (Neumann et al. 2006). Although inclusions positive for TDP-43 are noted in the majority of ALS cases, they are not seen in fused in sarcoma (FUS)- or Cu/Zn superoxide

dismutase 1 (SOD1)-linked ALS. The characteristic pathology in FUS-ALS are UBIs positive for FUS, but negative for TDP-43, tau and α-synuclein (Kwiatkowski et al. 2009, Vance et al. 2009). Additionally, in SOD1-ALS, UBIs positive for SOD1, but negative for TDP-43 are observed (Mackenzie et al. 2007).

In addition to UBIs, there are several other pathognomonic features of ALS. Bunina bodies (BBs) are small, eosinophilic inclusions observed in the remaining LMNs in approximately 80-100% of patients (Piao et al. 2003). BBs stain positive for cystatin C and transferrin (Okamoto et al. 1993, Mizuno et al. 2006b), but negative for a variety of proteins associated with neurodegeneration such as tau, p62, α-synuclein and amyloid precursor protein (Okamoto et al. 1993, Mizuno et al. 2006b, Sasaki and Iwata 2006, Mizuno et al. 2006a). However, the biological significance of BBs is still not fully understood. Additionally, large multifocal accumulations of phosphorylated and non-phosphorylated neurofilament subunits, called hyaline conglomerate inclusions (HCIs), have been observed (Ince, Lowe and Shaw 1998). However, these are also noted in other diseases and in normal patients, questioning their specificity to ALS (Leigh et al. 1989, Sobue et al. 1990).

As well as the pathognomonic neuropathology reported, it has been observed that genetic variants of ALS show distinct pathology in patients. For example, C9-ALS/FTD patients have been reported to have p62/SQSTM1 positive, TDP-43 negative UBIs in the cerebellum, hippocampus and neocortex (Al-Sarraj et al. 2011, Cooper-Knock et al. 2012), aggregates of dipeptide repeat (DPRs) proteins in the cerebellum, hippocampus and frontotemporal neocortex (Ash et al. 2013, Mori et al. 2013c, Mori et al. 2013a, Zu et al. 2013), and RNA foci in the frontal cortex, motor cortex, hippocampus, cerebellum and spinal cord (Cooper-Knock et al. 2014b, Mizielinska et al. 2013). These will be discussed in further detail in section 1.2.4.

### 1.1.4. Genetics of ALS

Sporadic ALS cases (sALS), where a patient has no evident family history of ALS, are estimated to account for 90-95% of all ALS cases, with familial ALS cases (fALS), where a patient has a family history of ALS in a first- or second-degree relative, account for 5-10% of ALS cases. Typically, fALS is inherited in an autosomal dominant (AD) manner; however, there are rare cases of both autosomal recessive (AR) and X-linked disease. Since the discovery that mutations in SOD1 cause around 20% of fALS cases more than two decades ago (Rosen et al. 1993), more than 20 ALS-causing genes have subsequently been identified, revealing the genetic heterogeneity of this disorder. It is reported that the genetic etiology for around two-thirds of fALS and 11% of sALS is now known (Renton, Chio and Traynor 2014). The genes identified to be associated with fALS and fALS/FTD are summarised in table 1.1, with the original references.

**Table 1.1 Causal genetic mutations in fALS and fALS/FTD.** Chromosomal loci, function and inheritance of genes found to be involved in fALS.

| Gene | Chromosome | Pathology/Function | Inheritance | Phenotype | Reference(s) |
|------|------------|--------------------|-------------|-----------|--------------|
| *SOD1* | 21q22 | Oxidative stress, UPS and autophagy | AD | ALS | (Rosen et al. 1993) |
| *ALSIN* | 2q33 | Endosomal trafficking and cell signalling | AR | ALS | (Yang et al. 2001) |
| *DCTN1* | 2p13 | Axonal transport | AD | ALS | (Puls et al. 2003) |
| *Unknown* | 18q21 | -- | AD | ALS | (Hand et al. 2002) |
| *SETX* | 9q34 | RNA processing | AD | ALS | (Chen et al. 2004) |
| *SPG11* | 15q21.1 | DNA damage repair and axonal growth | AR | ALS | (Orlacchio et al. 2010) |
| *FUS* | 16p11.2 | RNA processing | AD | ALS, FTD | (Kwiatkowski et al. 2009, Vance et al. 2009) |
| *Unknown* | 20p13 | -- | AD | ALS | (Sapp et al. 2003) |
| *VAPB* | 20q13.32 | Vesicle trafficking, UPR and ER stress | AD | ALS | (Nishimura et al. 2004) |
| *ANG* | 14q11.2 | RNA metabolism and angiogenesis | AD | ALS, FTD | (Greenway et al. 2006) |
| *TARDBP* | 1p36.22 | RNA metabolism | AD | ALS, FTD | (Sreedharan et al. 2008) |
| *FIG4* | 6q21 | Endosomal trafficking | AD | ALS | (Chow et al. 2009) |
| *OPTN* | 10p13 | Autophagy | AD and AR | ALS | (Maruyama et al. 2010) |
| *VCP* | 9p13.3 | Autophagy | AD | ALS, FTD | (Johnson et al. 2010) |
| *UBQLN2* | Xp11.21 | UPS and autophagy | XD | ALS/FTD | (Deng et al. 2011) |
| *SIGMAR1* | 9p13.3 | UPR, ER stress and proteasome | AD | ALS/FTD | (Luty et al. 2010, Al-Saif, Al-Mohanna and Bohlega 2011) |
| *CHMP2B* | 3p11.2 | Endosomal trafficking and autophagy | AD | ALS, FTD | (Parkinson et al. 2006) |
| *PFN1* | 17p13.2 | Cytoskeleton and axonal growth | AD | ALS, FTD | (Wu et al. 2012) |
| *ERBB4* | 2q34 | Neuronal development | AD | ALS | (Takahashi et al. 2013) |
| *HNRNPA1* | 12q13.13 | RNA metabolism | AD | ALS | (Kim et al. 2013) |
| *MATR3* | 5q31.2 | RNA metabolism | AD | ALS | (Johnson et al. 2014) |
| *C9orf72* | 9p21.2 | RNA metabolism, endosomal trafficking and autophagy | AD | ALS/FTD | (Renton et al. 2011, DeJesus-Hernandez et al. 2011) |
| *CHCHD10* | 22q11.23 | Mitochondrial maintenance | AD | ALS/FTD | (Bannwarth et al. 2014) |
| *SQSTM1* | 5q35.2 | Autophagy and protein degradation | AD | ALS/FTD | (Fecto et al. 2011) |
| *TBK1* | 12q14.2 | Autophagy and neuroinflammation | AD | ALS/FTD | (Cirulli et al. 2015, Freischmidt et al. 2015) |
| *TUBA4A* | 2q35 | Cytoskeleton | AD | ALS | (Smith et al. 2014) |
| *ANXA11* | 10q22.3 | Vesicular trafficking protein | AD | ALS | (Smith et al. 2017) |

### 1.1.4.1. Genetic risk factors in ALS

In addition to known ALS causal genes, several genetic risk factors have been identified that increase the risk of developing ALS and/or to modify the disease phenotype in patients, via methods such as genome-wide association studies (GWAS) or whole-exome sequencing. Such genetic risk factors include *ATXN2* (Elden et al. 2010). Large expansions of repeats within the trinucleotide CAG in *ATXN2* have previously been reported to cause spinocerebellar ataxia type 2 (Imbert et al. 1996). However, in 2010 it was identified that intermediate-length expansions increased the risk for ALS (Elden et al. 2010). These intermediate-length expansions in *ATXN2* have now been reported as the most important risk factor for ALS-FTD, as they have been observed to coincide with C9orf72 repeat expansions in C9-ALS/FTD patients (Ciura et al. 2016). In addition to *ATXN2,* other genetic risk factors have been identified including *UNC13A* (van Es et al. 2009), *SMN1* (Corcia et al. 2006) and *EPHA4* (Van Hoecke et al. 2012). Identification of genetic risk factors could help to explain why members of the same family, who inherit the same causal mutation, present with ALS at different ages and sites of onset for example. Further understanding these variants in the future may help in developing more effective therapies to treat ALS.

### 1.1.4.2. The oligogenic nature of ALS

An emerging theme in ALS is oligogenic inheritance. This refers to a situation in which mutations in two or more ALS-linked genes may be required to develop disease (Lattante et al. 2015a). Several large scale studies have revealed the oligogenic nature of ALS. For example, in 5/97 fALS probands, mutations in more than one ALS-associated gene were identified, including: FUS and TARDBP mutations in combination with ANG mutations; and C9orf72 repeat expansions with TARDBP, SOD1 and FUS mutations (van Blitterswijk et al. 2012b). Additionally an Irish population-based study examining over 400 ALS cases reported that 1.6% of the cohort had mutations in more than one ALS gene (Kenna et al. 2013). Interestingly, oligogenic inheritance of *C9orf72* with other ALS-linked genes is the most commonly reported combination, with over 10 ALS-causing genetic variants described (Lattante et al. 2015a).

As expansions in C9orf72 are so common, it is important to re-evaluate ALS cases where the causal mutation was identified before the discovery of *C9orf72,* as this may increase the number of cases with mutations in two or more ALS-linked genes. It could be that one of the mutations is weakly penetrant, thus both are needed to develop disease in a

synergistic or additive way. Alternatively, it could be one of the mutations, or the whole gene itself, has been falsely related to ALS. In the future, large-scale global studies will be needed to investigate the relevance of oligogenic inheritance to ALS. Additionally, cellular and animal models will be required to model oligogenic disease to functionally characterise how identified genes interact to cause disease.

### 1.1.5. General pathogenic mechanisms

The identification of multiple ALS-causing genes has enabled researchers to elucidate potential molecular mechanisms underlying the disorder. In common with other neurodegenerative diseases, pathogenic mechanisms are multifactorial and not yet fully understood. The general consensus is that a complex interplay between several mechanisms leads to the selective degeneration of UMNs and LMNs observed in ALS. Some of the cellular events believed to cause such destruction include; oxidative stress, excitotoxicity, mitochondrial dysfunction, protein aggregation, impaired axonal transport, defective RNA/DNA processing and activation of non-neuronal cells (Ferraiuolo et al. 2011) – all of which share commonality with other neurodegenerative disorders. See table 1.2 for an overview of these mechanisms.

Understanding the potential molecular mechanisms in ALS is not only important in further understanding clinical features of ALS, but it is also essential in unmasking potential targets for neuroprotective therapies. For example, ameliorating excitotoxicity via the use of Riluzole has been a successful pharmacological strategy to slow down the progression of ALS (Lacomblez et al. 1996, Bensimon et al. 1994). Additionally, the newly approved Edaravone, a neuroprotective drug with properties of a free radical scavenger, has been shown to reduce oxidative stress and slow down the progression of ALS (Abe et al. 2017). There is a growing need to further understand the genetics and pathogenic mechanisms underlying ALS, in order to develop more effective disease modifying therapies.

**Table 1.2 Summary of general pathogenic mechanisms involved in ALS.**

| Pathogenic mechanism | Key evidence with reference(s) |
|---|---|
| *Oxidative stress;* Imbalance in generation and/or removal of reactive oxygen species (ROS), coinciding with inability of the system to remove and/or repair ROS-induced damage | - Oxidative stress results in structural damage, including DNA, RNA and proteins, and disrupts redox-sensitive signalling pathways<br>- Mutations in the gene *SOD1*, which encodes major antioxidant protein, account for approx. 20% of fALS cases (Rosen et al. 1993)<br>- Biosamples from ALS patients show elevated levels of free radical damage (Simpson et al. 2004)<br>- Increased levels of oxidative damage to proteins, lipids and DNA found in sALS and SOD1-related fALS post-mortem tissue (Shaw et al. 1995)<br>- Oxidative damage occurs in cellular and murine models of SOD1 related ALS (Ferraiuolo et al. 2011) |
| *Excitoxicity;* Excitoxicity results in excessive stimulation of glutamate receptors resulting in increased calcium influx into post-synaptic neurons, which results in toxicity | - Raised levels of glutamate found in CSF of ALS (Rothstein et al. 1990)<br>- KO of EAAT2 *in vitro* and *in vivo* (astrocytic glutamate transporter) results in neuronal death (Rothstein et al. 1996)<br>- Overexpression of EAAT2 in mutant SOD1 transgenic mouse delayed onset of motor deficits (Guo et al. 2003)<br>- Reduction in spinal cord EAAT2 protein in end-stage SOD1 rodent models of ALS (Bruijn et al. 1997, Howland et al. 2002)<br>- Only disease-modifying drug to date, Riluzole, has anti-glutamatergic activity (Doble 1996) |
| *Mitochondrial dysfunction;* Mitochondria are critical to cell survival, acting as an energy source, buffering intracellular calcium and regulating apoptosis | - Defective respiratory chain function found in tissue from ALS patients and mSOD1 rodent models, associated with oxidative damage to mitochondrial proteins and lipids (Wiedemann et al. 2002, Mattiazzi et al. 2002)<br>- Thus dysregulated energy metabolism likely to contribute to MN dysfunction in ALS<br>- Calcium buffering impaired in mitochondria purified from CNS of mSOD1 mice (Damiano et al. 2006)<br>- Altered mitochondrial morphology observed in spinal MNs from ALS patients (Sasaki and Iwata 2007)<br>- This is also observed in primary motor neurons and NSC-34 cells expressing mutant SOD1 (Menzies et al. 2002) |
| *Protein aggregation;* Insoluble protein aggregates are a hallmark of ALS, suggesting a collapse in protein homeostasis (see section 1.2) | - Inclusions found in both degenerating neurons and surrounding glia (Piao et al. 2003, Zhang et al. 2008, Nishihira et al. 2008) |

| | |
|---|---|
| | - Most common inclusions contain ubiquitinated proteins, indicating a problem with the ubiquitin-proteasome system (UPS) and autophagy degradation pathways (Neumann et al. 2006, Blokhuis et al. 2013)
- Several ALS-linked genes play role in protein trafficking or degradation pathways, including *UBQLN2, p62/SQSTM1, VCP, C9orf72, OPTN, TBK-1* (see table 1.1)
- Evidence of ER stress in ALS patient CNS tissue, plus cellular and animal models (Matus et al. 2013) |
| *Impaired axonal transport;* Efficient axonal transport is critical for axonal function | - Many ALS-linked genes are involved with axonal transport and/or the cytoskeleton (see table 1.1), suggesting impaired axonal transport contributes to ALS pathogenesis
- Defective axonal transport occurs early in disease in mSOD1 mice and impairs anterograde transport of mitochondria (De Vos et al. 2007, Kieran et al. 2005, Williamson and Cleveland 1999, Bilsland et al. 2010)
- Mutations in *DCTN1*, essential for retrograde transport, led to degeneration of MNs and premature death in rodents (Puls et al. 2003, Laird et al. 2008) |
| *Dysregulated RNA metabolism;* Numerous RNA/DNA binding proteins associated with fALS, including TDP-43, FUS, ANG, ATXN-2 and hnRNPA1 (see table 1.1) | - TDP-43 forms the characteristic neuronal inclusions in most ALS cases (Neumann et al. 2006), minus fALS cases linked to FUS and SOD1 mutations (Mackenzie et al. 2007, Vance et al. 2009, Kwiatkowski et al. 2009)
- Sense and antisense RNA transcripts are present in intranuclear foci in C9-ALS cases (Gendron et al. 2013), which are reported to sequester a number of RNA binding proteins and perturb their function, including: hnRNP A3, hnRNP A1, hnRNP-H1/F, SRSF2, ALYREF and ADARB2 (Mori et al. 2013b, Xu et al. 2013, Lee et al. 2013, Donnelly et al. 2013, Cooper-Knock et al. 2014b) |
| *Activation of non-neuronal cells;* Widely accepted concept that ALS is a non-cell autonomous process (Ferraiuolo et al. 2011) | - Survival of mice expressing SOD1$^{G93A}$ in MNs improved when surrounded by WT non-neuronal cells (Clement et al. 2003)
- Survival of SOD1$^{G93A}$ transgenic mice is prolonged by eliminating mutant SOD1 gene from several non-neuronal cell types (Yamanaka et al. 2008, Boillee et al. 2006, Kang et al. 2013)
- ALS-derived astrocytes have been shown to be toxic to MNs *in vitro (Nagai et al. 2007)*
- Astrocytes and microglia are activated in ALS, resulting in an increase in pro-inflammatory cytokine activity, which is seen in CNS tissues from ALS patients (Philips and Robberecht 2011) |

### 1.1.6. The ALS-FTD spectrum

ALS patients often show a loss of cortical neurons in the frontal and/or temporal lobes. Such neurodegeneration is characteristic of a condition called FTD, which is the leading cause of dementia after Alzheimer's disease. It presents in individuals under 65, with an incidence rate of 3.5-4.1 per 100 000 person-years in the 45-64 age group (Van Langenhove, van der Zee and Van Broeckhoven 2012). Disease duration is approximately 6-8 years post diagnosis and there is currently no cure (Hodges et al. 2003, Vossel and Miller 2008). It is a heterogeneous condition and there are three clinically recognised subgroups of the disease, with variable symptoms and distinct locations of neurodegeneration (Van Langenhove et al. 2012) (see table 1.3). There is a strong genetic contribution to FTD and around 50% of cases are thought to be familial. Mutations in the microtubule associated protein tau (*MAPT*) (Hutton et al. 1998) and progranulin (*PGRN*) (Baker et al. 2006, Cruts et al. 2006) are believed to explain around 10-20% of these cases. Accumulating evidence has revealed that ALS and FTD are linked clinically, pathologically and genetically, with both disorders recognised as two extremes of a clinico-pathological continuum.

**Table 1.3 Subgroups of frontotemporal dementia (FTD).**

| FTD subtype | Characteristic neuropathology | Main clinical characteristics |
|---|---|---|
| Behavioural variant FTD (bvFTD) | Prefrontal neurodegeneration | Disinhibition, apathy, lack of emotional concern, stereotypic behaviour, executive dysfunction and hyperorality |
| Progressive non-fluent aphasia (PNFA) | Left perisylvian atrophy | Labored speech and aggramatism |
| Semantic dementia (SD) | Atrophy of anterior temporal lobes | Comprehension deficits, naming error with fluent speech |

Clinically, in addition to the characteristic motor dysfunction observed in ALS, it has been estimated that up to 50% of patients show evidence of cognitive or behavioural impairment (Ringholz et al. 2005). Two studies on large ALS patient cohorts revealed around 15-18% of such patients met the clinical criteria for FTD (see table 1.3) (Ringholz et al. 2005, Lomen-Hoerth et al. 2003). Additionally, it is estimated around 15% of FTD patients have motor dysfunction, meeting the clinical criteria of ALS (Lomen-Hoerth et al. 2002, Burrell et al. 2011). The cognitive changes in patients with both ALS and FTD usually resembles bvFTD (Lillo et al. 2010), however there are reports describing PNFA

or SD in association with ALS (Ostberg and Bogdanovic 2011, Catani et al. 2004). Interestingly, FTD-ALS patients sometimes develop hallucinations or delusions, which is not often seen in pure FTD (Mendez et al. 2008, Lillo et al. 2010). In the majority of cases, FTD symptoms precede those of ALS (Van Langenhove et al. 2012).

A major breakthrough in elucidating shared pathogenic mechanisms between ALS and FTD occurred in 2006, when evidence revealed that TDP-43 was the major ubiquitinated protein found within UBIs in both disorders (Neumann et al. 2006). Subsequently, it was identified that mutations in the gene encoding TDP-43, were causative in ALS (Sreedharan et al. 2008) and FTD (Borroni et al. 2009) cases. Additionally, mutations in the gene encoding FUS, were discovered to account for rare ALS and FTD cases (Van Deerlin et al. 2008, Kwiatkowski et al. 2009, Vance et al. 2009). Interestingly, both of these are RNA binding proteins and play a role in RNA metabolism. Therefore, this suggests that aberrant RNA processing may be a central pathogenic mechanism in the causation of ALS, ALS/FTD and/or FTD.

Additionally, several other genes which encode proteins involved in protein degradation pathways or maintaining protein homeostasis, have been identified to cause ALS, ALS/FTD and/or FTD. This non-exhaustive list includes: ubiquillin-2 (*UBQLN-2*) (Deng et al. 2011); valosin containing protein (*VCP*) (Johnson et al. 2010); optineurin (*OPTN*) (Maruyama et al. 2010); vesicle-associated membrane protein-associated protein B (*VAPB*) (Nishimura et al. 2004); charged multivesicular body protein 2B or chromatin modifying protein 2B (*CHMP2B*) (Parkinson et al. 2006); and p62/sequestosome (*SQSTM1*) (Fecto et al. 2011). Alongside the characteristic protein aggregates identified in both ALS and FTD, these discoveries indicate a disruption in proteostasis may also be a central pathogenic mechanism in both diseases, as well as aberrant RNA processing.

In 2011 a non-coding hexanucleotide repeat expansion in chromosome 9 open reading frame 72 (*C9orf72*) was identified as the most common mutation found in ALS (40% of fALS and 6-20% sALS) and FTD (25% of fFTD and 6% sFTD) (DeJesus-Hernandez et al. 2011, Renton et al. 2011). This genetic variant will be discussed in detail in section 1.2.

### 1.2. Chromosome 9 open reading frame 72 (C9orf72)
#### 1.2.1. Identification of *C9orf72* as an ALS- and FTD-disease gene

In 2006, genetic linkage analysis performed by two individual groups (Vance et al. 2006, Morita et al. 2006) on families affected by both ALS and FTD revealed linkage of ALS-FTD to chromosome 9p. Subsequent genetic linkage reports indicated this shared chromosomal region was located at 9p21.2-9p21.1 (Van Langenhove et al. 2012). Additionally, several genome wide association studies (GWAS) on large cohorts of unrelated ALS patients and controls (van Es et al. 2009, Shatunov et al. 2010, Laaksovirta et al. 2010) also reported linkage to chromosome 9p region, located at 9p21. This trend was also demonstrated in a GWAS on a large group of FTD-TDP patients (Van Deerlin et al. 2010). Amalgamation of these reports indicated that genetic variation within the identified chromosomal region affected both familial and sporadic ALS and FTD cases. In 2010, the identified locus which linked these families on chromosome 9p was narrowed to a 232 kb interval, which was shown to contain three protein encoding genes: *C9orf72, MOBKL2B, IFNK* (Laaksovirta et al. 2010). Finally, in 2011, two individual research teams reported that the causative mutation within this region was a $(G_4C_2)_n$ hexanucleotide repeat expansion in intron 1 of *C9orf72* (DeJesus-Hernandez et al. 2011, Renton et al. 2011). This was later confirmed in a separate study (Gijselinck et al. 2012).

#### 1.2.2. $(G_4C_2)_n$ hexanucleotide repeat expansions in C9orf72

As discussed, a non-coding hexanucleotide repeat expansion in *C9orf72* is the most common mutation found in ALS (40% of fALS and 6-20% sALS) and FTD (25% of fFTD and 6% sFTD) (DeJesus-Hernandez et al. 2011, Renton et al. 2011). The human *C9orf72* gene (ENST00000619707.4) has 11 exons in total, 10 of which are coding exons, and is reported to be alternatively spliced into three protein-coding transcript variants, V1-V3 (DeJesus-Hernandez et al. 2011, Renton et al. 2011) (Figure 1.2). It is predicted that these three transcripts lead to the expression of two alternative isoforms of the C9orf72 protein. Firstly, a long protein isoform (C9orf72L) of 481 amino acids (aa), encoded by V1 and V3. Secondly, a short protein isoform (C9orf72S) of 222aa, encoded for by V2. It is reported that these isoforms are widely expressed in a number of brain regions and peripheral tissues (DeJesus-Hernandez et al. 2011, Waite et al. 2014). However, such data has been hampered by the fact that reliable anti-C9orf72 antibodies were not commercially available. Recently, a group designed antibodies which specifically recognise the two C9orf72 protein isoforms (Xiao et al. 2015). It was reported that the two isoforms are localised to distinct parts of the cell. For example, C9orf72L is

localised diffusely throughout the cytoplasm in cerebellar Purkinje cells, and C9orf72S expression is localised to the nuclear membrane of Purkinje cells (Xiao et al. 2015)
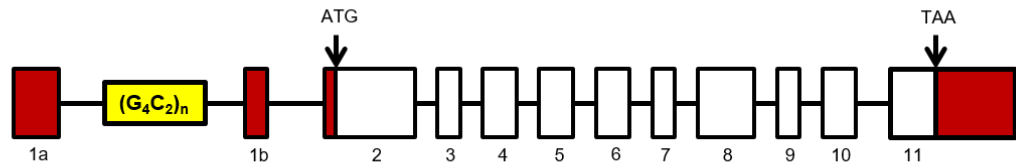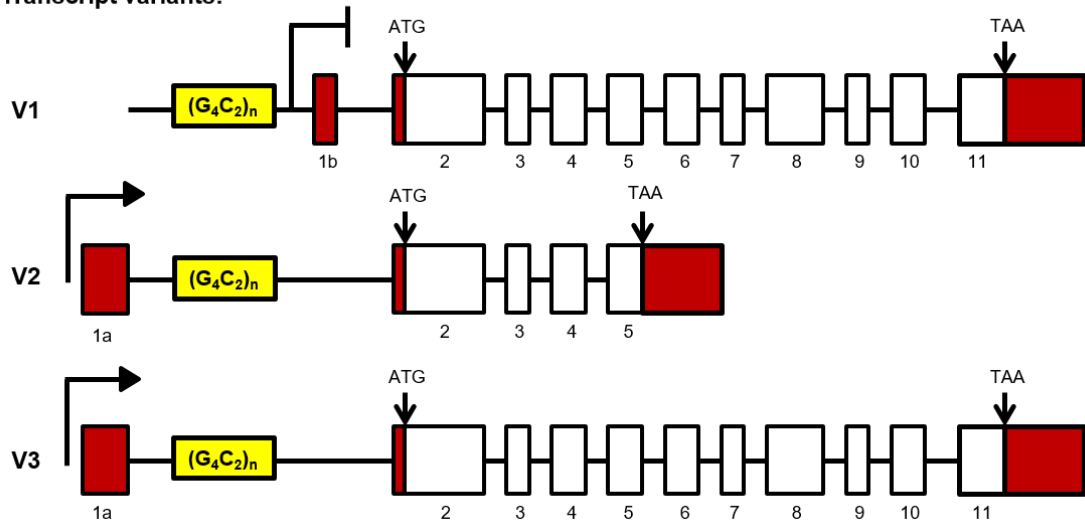


**Figure 1.2 Schematic diagram of C9orf72.** Introns are represented by lines and exons by boxes; white boxes are coding exons whereas red boxes are non-coding exons/UTRs. The $(G_4C_2)_n$ repeat expansion is located between the non-coding exons 1a and 1b of *C9orf72*, as indicated by the yellow box. *C9orf72* is alternatively spliced into three protein-coding transcripts; V1-V3. Transcript variants V1 and V3 encode the long isoform (C9orf72-L). Transcript variant V2 encodes the short isoform (C9orf72-S). The transcription start site is upstream of exon 1A and the $(G_4C_2)_n$ repeat in V2 and V3. However, in V1 the $(G_4C_2)_n$ repeat is upstream of the transcription start site. Adapted from (DeJesus-Hernandez et al. 2011)

Repeat-primed PCR (rpPCR) assays were often used to determine whether a sample carries a large pathogenic expansion. However, this technique could only reliably predict size up to a maximum of 30 repeats (Renton et al. 2011), thus amplification of the entire pathogenic *C9orf72* repeat expansion was not possible by this method. Southern blotting is a much more reliable method to predict true repeat size. Using this technique, 'normal' repeat size in healthy individuals is estimated to be <30 units, although approximately 90% have fewer than 10 units (Picher-Martel et al. 2016). Conversely, the number of repeats in ALS patients can range from several hundred to several thousand units (Beck et al. 2013, Buchman et al. 2013, van Blitterswijk et al. 2013).

In many repeat expansion disorders, the size of the pathological repeat expansion influences the observed clinical phenotype. For example, myotonic dystrophy type I (DM1) is caused by a $(CTG)_n$ repeat expansion in a noncoding region of *DMPK* (Brook et al. 1992, Mahadevan et al. 1992). The number of repeats in *DMPK* is reported to show a high degree of instability, which appear to predispose the repeat toward further expansion (van Blitterswijk, DeJesus-Hernandez and Rademakers 2012a). Additionally, longer expansions have been reported to correlate with more severe symptoms and an earlier age of onset in successive generations (genetic anticipation) (van Blitterswijk et al. 2012a). Regarding *C9orf72,* sizing of the $(G_4C_2)_n$ repeat expansion via southern blotting has revealed somatic heterogeneity within individuals, with different expansion lengths observed in different tissues (Beck et al. 2013, van Blitterswijk et al. 2013, Harms et al. 2013, Huebers et al. 2014). Somatic heterogeneity suggests instability within the $(G_4C_2)_n$ repeat expansion and evidence of genetic anticipation in C9-ALS/FTD has been reported, with decreasing onset age of 7-11 years in subsequent generations (Benussi et al. 2014, Chio et al. 2012, Gijselinck et al. 2012, Hsiung et al. 2012, Stewart et al. 2012). However, genetic anticipation is not seen in all cohorts (DeJesus-Hernandez et al. 2011, Renton et al. 2011). It is still not clear whether the observed genetic anticipation in C9-ALS/FTD patients is related to expansion size. Although, a recent study reported an increase in expansion size from parent to offspring (Gijselinck et al. 2016).

### 1.2.3.   Clinical features of C9-ALS/FTD

In general, the ALS and/or FTD phenotypes associated with the $(G_4C_2)_n$ repeat expansion are representative of the whole clinical spectrum. However, some distinct phenotypes have been reported. There is a higher incidence of bulbar-onset disease (Cooper-Knock et al. 2012, Millecamps et al. 2012, Stewart et al. 2012). An earlier age of onset is often

observed in *C9orf72*-linked ALS (C9-linked) (Byrne et al. 2012, Cooper-Knock, Shaw and Kirby 2014a). Some cohorts report that male C9-linked ALS patients present at a younger age of onset than non-C9 ALS cases (Williams et al. 2013). There is also evidence for a shorter disease duration in patients carrying the $(G_4C_2)_n$ repeat expansion (Cooper-Knock et al. 2014a). There is a higher prevalence of cognitive and/or behavioural changes in C9-linked ALS patients, with co-morbid dementia observed in approximately 50% of C9-linked ALS patients compared to only 12% in non-C9 ALS cases (Byrne et al. 2012). The cognitive changes in C9-linked ALS and/or FTD resembles bvFTD (Lillo et al. 2010). Additionally, a higher frequency of psychotic symptoms, including hallucinations and delusions, is often observed in C9-linked FTD compared to classical FTD (Mendez et al. 2008, Lillo et al. 2010). There is also a higher than expected incidence of parkinsonism in patients carrying the $(G_4C_2)_n$ repeat expansion, displaying symptoms such as hypokinesia/bradykinesia (Wilke et al. 2016). However, the $(G_4C_2)_n$ repeat expansion does not seem to be associated directly with Parkinson's Disease (Cooper-Knock et al. 2013).

The basis for the clinical heterogeneity noted in patients carrying the $(G_4C_2)_n$ repeat expansion is not fully understood. A potential explanation is that there is a correlation between expansion size and clinical phenotype. There is evidence for this in C9-linked FTD, where repeat size in the cerebellum has been identified to correlate with disease (van Blitterswijk et al. 2013). However, there is no conclusive data to support this in ALS (Cooper-Knock et al. 2014a). Additionally, patients carrying the repeat expansion in *C9orf72* are often observed to have mutations in other ALS-linked genes. Interestingly, it has been identified that *C9orf72* repeat expansions coinciding with TDP-43, FUS or SOD1 mutations are linked to causing pure ALS (Lattante et al. 2015a). Alternatively, *C9orf72* repeat expansions coinciding with tau or p62/SQSTM1 mutations are linked to causing pure FTD (Lattante et al. 2015a). This suggests that *C9orf72* repeat expansions may be a risk factor for developing ALS, ALS/FTD and/or FTD in patients, with the second mutation potentially contributing to where along the spectrum the patient lies. However, the molecular mechanisms underlying the oligogenic hypothesis would need to be further investigated, using cellular and animal models.

### 1.2.4. Neuropathological features of C9-ALS/FTD

In relation to pathology, patients with the repeat expansions exhibit typical characteristics noted in classical ALS. However, there are a number of neuropathological changes which appear to be specific to *C9orf72* patients.

Firstly, several studies have reported the presence of dotlike or star shaped p62/SQSTM1 and/or ubiquillin-2 positive nuclear or cytoplasmic inclusions (NCIs) which are negative for TDP-43 (Al-Sarraj et al. 2011, Cooper-Knock et al. 2012, Stewart et al. 2012). It is believed that these inclusions are a specific feature of ALS caused by pathological repeat expansions in *C9orf72* (Al-Sarraj et al. 2011, Cooper-Knock et al. 2012). These inclusions have been found to be located in regions such as the cerebellum, hippocampus and frontotemporal neocortex (Cooper-Knock et al. 2012). The presence of these inclusions suggest that there is a coinciding pathomechanism to TDP-43 aggregates in C9-linked ALS.

Secondly, it is known that the *C9orf72* repeat expansion is transcribed in both a sense and antisense direction. This results in the presence of both sense $(G_4C_2)_n$ and antisense $(C_2G_4)_n$ RNA foci in several locations in the CNS of patients, including; the frontal cortex, motor cortex, hippocampus, cerebellum and spinal cord (Gendron et al. 2013, Mizielinska et al. 2013, Lagier-Tourenne et al. 2013). Whilst the majority of RNA foci are neuronal, it has been reported that they are present in astrocytes, microglia and oligodendrocytes at a much lower frequency (Mizielinska et al. 2013). Several studies have observed that these RNA foci co-localise with various RNA binding proteins, which could perturb their function (Mori et al. 2013b, Xu et al. 2013, Lee et al. 2013, Donnelly et al. 2013, Cooper-Knock et al. 2014b).

Lastly, it is reported that the $(G_4C_2)_n$ sense and $(C_4G_2)_n$ antisense transcripts undergo repeat-associated non-ATG (RAN) translation in all reading frames, resulting in the synthesis of five aggregation-prone dipeptide repeat (DPR) proteins (Ash et al. 2013, Mori et al. 2013a, Mori et al. 2013c). All five of these DPR proteins co-aggregate in the characteristic p62 positive, TDP-43 negative inclusions seen in C9FTD/ALS patients (Mori et al. 2013b, Mori et al. 2013c, Mori et al. 2013a, Ash et al. 2013), in locations such as the cerebellum, hippocampus and frontotemporal neocortex. Additionally, it is suggested that DPR protein aggregation may precede TDP-43 pathology, with evidence of some DPRs within TDP-43 positive inclusions (Mori et al. 2013c).

### 1.2.5. C9orf72 protein function

Currently, the function(s) of the C9orf72 protein are beginning to be elucidated, but are not fully understood. It is imperative to gain a better knowledge on the normal function of this protein in order to both understand C9-linked disease mechanisms and to identify novel neuroprotective targets for future therapies. Evidence for some of the potential roles of C9orf72 is detailed in this section.

### 1.2.5.1. C9orf72: a novel DENN protein?

There is emerging evidence that C9orf72 may play a role in protein trafficking, as a member of the DENN-like superfamily (Levine et al. 2013, Zhang et al. 2012). The tripartite DENN (meaning 'differentially expressed in normal and neoplastic cells') module, consists of; an N-terminal longin domain, a central DENN domain and a C-terminal d-DENN domain. The DENN domain is an evolutionary conserved protein module, and its best characterised function is as a specific guanine nucleotide exchange factor (GEF) for Rab GTPases (Levivier et al. 2001). The role of these GEFs is to catalyse the exchange of GDP for GTP, which results in the activation of Rab GTPases. The human genome is thought to encode up to 66 Rab GTPases (Kloepper et al. 2012), many of which are master regulators of intracellular membrane trafficking (Zerial and McBride 2001). Once activated, GTP-bound Rab interacts with various effector proteins to mediate numerous functions, including directing vesicles to the correct site of fusion (Hutagalung and Novick 2011).

C9orf72L is a full-length homologue containing all three DENN domains, whereas the short isoform appears to show homology only to the N-terminal longin domain (Levine et al. 2013). However, the implications of these differences are not known, as the distinct roles of each of the DENN domains are not fully understood. Consistent with the prediction that C9orf72 may be a DENN-like protein, an initial report showed that C9orf72 co-localised and co-immunoprecipitated with Rab proteins implicated in both autophagy and endocytic trafficking, including Rab-1, -7 and -11 (Farg et al. 2014). However, clear mechanistic details were lacking. Recently, data from our lab has shown that C9orf72 interacts with Rab1a (Webster et al. 2016a). Interestingly, it was found that it preferentially binds to GTP-bound Rab1a, suggestive that C9orf72 functions as an effector of Rab1a rather than a GEF, as would be expected of a DENN-like protein (Webster et al. 2016a). Additionally, it was shown that as a Rab1a effector, C9orf72 was essential in mediating the Rab1a-mediated translocation of the ULK-1 complex to the

phagophore, essential in initiating autophagosome formation (Webster et al. 2016a, Hara et al. 2008). Conversely, it has also been reported recently that C9orf72 acts as a GEF for Rab8a and Rab39b, in complex with SMCR8, another DENN-like protein, and WDR41 (Sellier et al. 2016). However, the interaction of C9orf72/SMCR8/WDR41 complex with these particular Rabs appears to be mediated by SMCR8, as GEF activity is only observed when SMCR8 is present in the complex (Sellier et al. 2016). It is known that Rab GTPases can act in Rab GEF/GAP cascades. In such cascades, the upstream Rab, and its effectors, recruit the GEF for the downstream Rab, whilst the downstream Rab simultaneously recruits the GAP for the upstream Rab (Hutagalung and Novick 2011). Thus, our lab suggests that C9orf72 acts in a Rab cascade (Webster et al. 2016b). Therefore, it is likely that C9orf72 links autophagy initiation to downstream events via a Rab GEF/GAP cascade, with Rab1a upstream, and Rab8a and Rab39b downstream (Webster et al. 2016b).

### 1.2.5.2.    C9orf72 and autophagy

DENN domain-containing proteins function as GDP/GTP exchange factors (GEFs) for Rab GTPases, which are involved in regulating a number of cellular trafficking events, including autophagy (Zerial and McBride 2001, Kloepper et al. 2012). Recent research has revealed a direct mechanistic role for C9orf72 in macroautophagy (hereafter referred to as autophagy). Autophagy is a conserved lysosomal degradation pathway which involves the degradation of cytoplasmic components, such as misfolded proteins and damaged organelles, within an autophagolysosome, for bulk degradation or recycling (Klionsky et al. 2012). This important cellular process can be divided into four sequential steps: translocation and initiation; elongation and recruitment; completion; lysosome fusion and degradation (figure 1.3) (Bento et al. 2016). Autophagy is known to be essential for neuronal health; for example, neuronal-specific knockout (KO) of essential autophagy genes - such as *ATG7, ATG5* and *FIP200* - results in the inhibition of autophagy in neurons and subsequently neurodegeneration in mouse models (Hara et al. 2006, Komatsu et al. 2006, Liang et al. 2010). Furthermore, there are increasing reports that defective autophagy plays a role in the pathogenesis of ALS (Menzies et al. 2017). As mentioned, UBIs are a neuropathological hallmark of C9-linked ALS, as well as non-
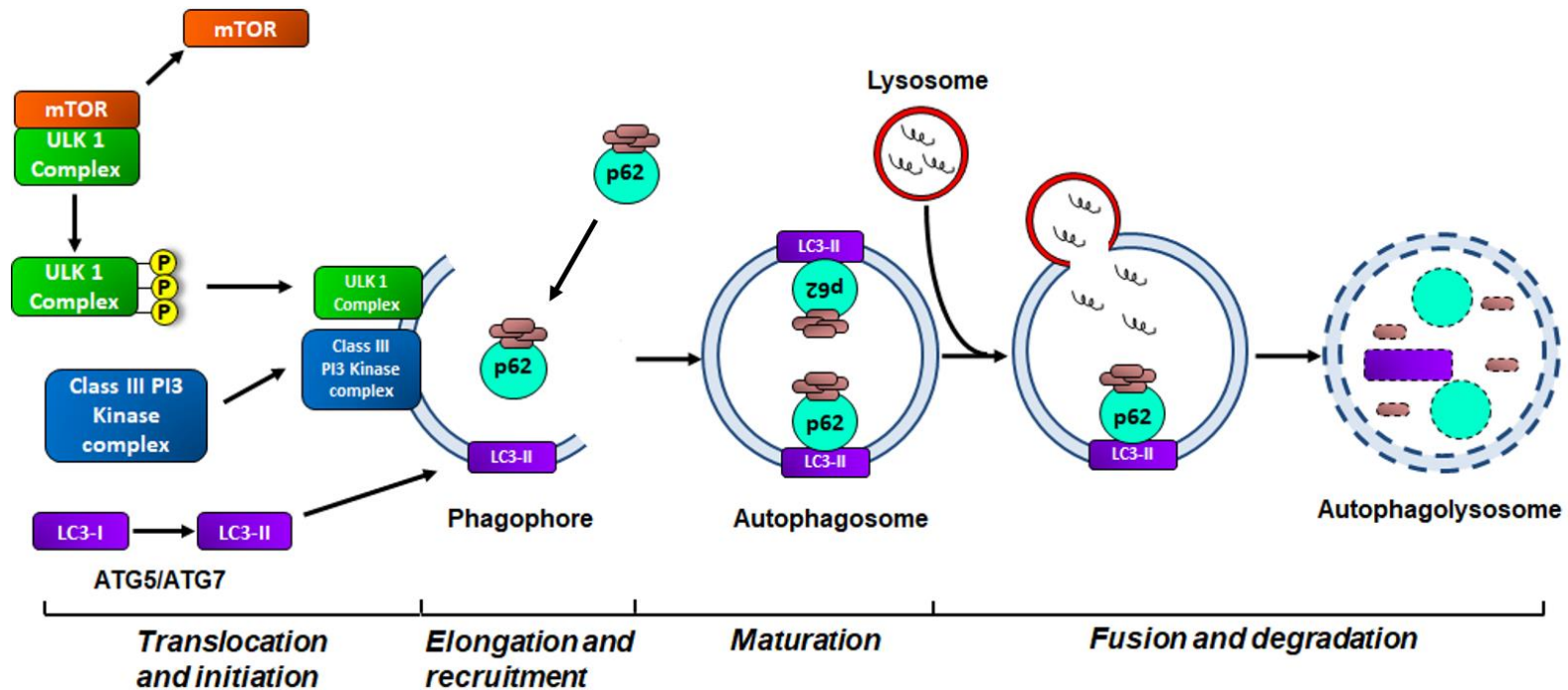
**Figure 1.3 The autophagy pathway.** Schematic diagram of the autophagy pathway. Inhibition of mTOR (in nutrient poor conditions) releases the ULK1 complex. ULK 1 then phosphorylates ATG13 and FIP200, activating the complex, which then translocates to the phagophore. This is the first step of autophagy initiation. The Class III PI3 Kinase Complex then translocates to the phagophore, which is essential for elongation of the membrane. Cargo is transported to the growing phagophore by autophagy receptors, such as p62/SQSTM1, which bind to both the poly-ubiquitin chains on the cargo (via the ubiquitin binding (UBI) domain) and LC3-II on the phagophore membrane (via the LC3 interacting region (LIR) domain). Mature autophagosomes then fuse with the lysosome. Autophagosome-lysosome fusion results in an autophagolysosome, where cargo is degraded via lysosomal hydrolases. Conversely in nutrient rich conditions, mTOR suppresses the ULK1 complex via phosphorylating ULK 1/2 and ATG13. This suppresses autophagy initiation.

C9 linked ALS (Menzies et al. 2017). Additionally, several ALS-linked genes are known to encode proteins which function within the pathway, including: *p62/SQSTM1, UBQLN2, OPTN, TBK-1* and *VCP* (see table 1.1). Therefore, the implication that C9orf72 also plays a role in autophagy is consistent with the fact that autophagy is an important pathway in ALS.

A characteristic neuropathology observed in C9-ALS/FTD patients is p62/SQSTM1 positive, TDP-43 negative inclusions (Cooper-Knock et al. 2012, Al-Sarraj et al. 2011). The protein p62/SQSTM1 targets ubiquitinated proteins to the autophagy pathway for degradation (Bento et al. 2016) and accumulation of this protein has been associated with inhibition of autophagy (Hara et al. 2006). Thus this pathology, alongside early evidence for C9orf72 haploinsufficiency, suggested the possibility of defective autophagy via loss of C9orf72 function in C9-ALS/FTD. There is now increasing evidence in our lab and others, that the C9orf72 protein is a key regulator of autophagy (Amick, Roczniak-Ferguson and Ferguson 2016, Sellier et al. 2016, Sullivan et al. 2016a, Webster et al. 2016b, Webster et al. 2016a, Yang et al. 2016). In particular, there are a wealth of reports that show C9orf72 plays a role upstream, regulating initiation of the pathway. As shown in figure 1.3, autophagy can be activated by the ULK-1 complex, which consists of ULK-1, FIP200, ATG13 and ATG101. This complex is kept inactive via the phosphorylation of ULK-1 by mTOR. Inactivation of mTOR, for example in nutrient poor conditions, results in the release of the ULK-1 initiation complex. ULK-1 is then able to phosphorylate FIP200 and ATG13, activating the complex and initiating autophagy (Jung et al. 2009, Ganley et al. 2009). Overexpression of C9orf72 has been shown to activate autophagy (Webster et al. 2016a). Furthermore, following disruption of the ULK-1 initiation complex, via depletion of FIP200, overexpression of C9orf72 no longer activated the pathway, indicating that C9orf72 may also function at the level of the ULK-1 complex (Webster et al. 2016a). Strengthening this association, it is reported that C9orf72 directly interacts with several members of this complex, including; ULK-1, FIP200 and ATG13 (Behrends et al. 2010, Webster et al. 2016a). Also, recent studies have published that depletion of C9orf72, in both cell lines and primary neurons, results in defective autophagy initiation and accumulation of p62/SQSTM1, similar to the pathology seen in C9-ALS/FTD patients (Farg et al. 2014, Yang et al. 2016, Sellier et al. 2016, Sullivan et al. 2016a, Webster et al. 2016a). Adding to the story, our lab has also identified that the C9orf72 protein is an effector of Rab1a, facilitating trafficking of the

ULK-1 initiation complex to the phagophore, which is essential for autophagosome formation (Webster et al. 2016a). Conversely, others have demonstrated that a complex consisting of C9orf72/SMCR8/WDR41 acts as a GEF for Rab8a and Rab39b, which act further downstream the autophagy pathway, during autophagosome maturation (Sellier et al. 2016). However, the GEF activity of the C9orf72/SMCR8/WDR41 appears to be dependent on SMCR8 (Sellier et al. 2016). Adding further complexity to its function, C9orf72 co-localises with lysosomes in cells when starved of amino acids (Amick et al. 2016), consistent with the lysosome being an important site of function for C9orf72. Overall, although different roles have been suggested, recent evidence supports the involvement of C9orf72 in autophagy regulation.

### 1.2.6. C9orf72 specific pathogenic mechanisms

Due to the discovery of the $(G_4C_2)n$ hexanucleotide repeat expansion in *C9orf72*, ALS and FTD are now part of a growing class of 'non-coding repeat expansion disorders', including myotonic dystrophies, fragile-X associated tremor/ataxia and several spinocerebellar ataxias (La Spada and Taylor 2010). Research into these has elucidated various mechanisms by which non coding repeat expansions may cause disease. Regarding the *C9orf72* repeat expansion, three principal mechanisms have gained particular attention; haploinsufficiency, RNA toxicity and repeat-associated, non-ATG (RAN) translation (figure 1.4). The pathogenic mechanism underlying *C9orf72*-linked ALS may be attributable to just one of these mechanisms or involve a combination of all three.
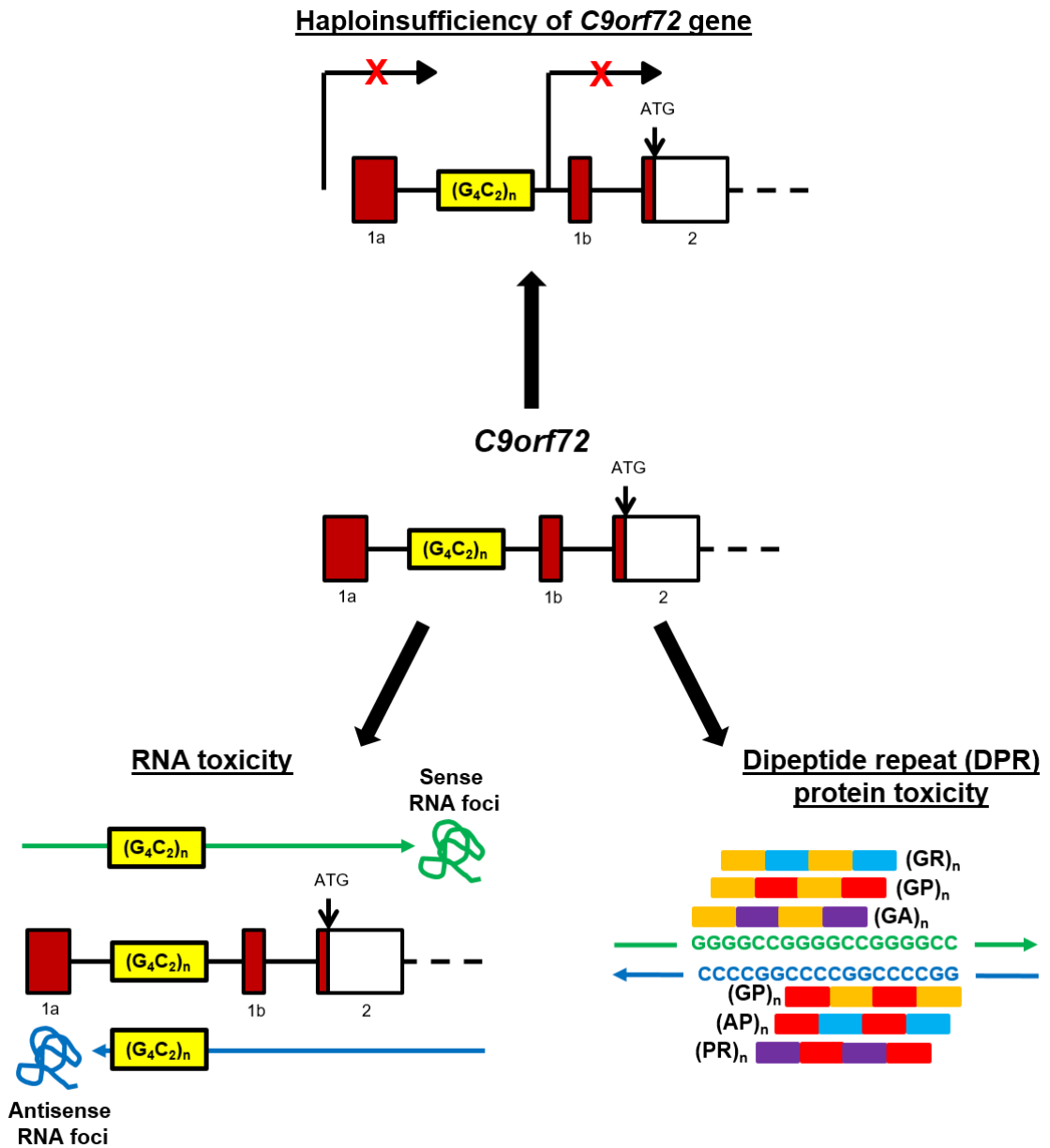
**Figure 1.4 Potential disease mechanisms associated with C9orf72 (G4C2)n repeat expansion.** There are currently three potential mechanisms by which the *C9orf72* associated hexanucleotide expansion could cause neurotoxicity. Firstly, transcriptional silencing of *C9orf72* via hypermethylation or transcription abortion may lead to reduced C9orf72 expression and haploinsufficiency. Secondly, the hexanucleotide repeat is transcribed in a sense and antisense direction. This $(G_4C_n)_2$ and/or $(C_4G_2)_n$ repeat containing RNA form foci, which may sequester RNA binding proteins, perturbing their function and causing toxicity. Finally, the $(G_4C_n)_2$ and/or $(C_4G_2)_n$ repeat containing RNA undergoes repeat-associated non-ATG (RAN) translation producing dipeptide repeat (DPR) proteins, which aggregate and cause toxicity.

### 1.2.6.1. Haploinsufficiency

The haploinsufficiency model suggests partial or complete loss of function of the repeat containing allele. This pathogenic mechanism has been reported to underlie other repeat expansion disorders such a Fragile X Syndrome (FXS) (Wen et al. 2017). A reduction in variant-specific or total *C9orf72* messenger RNA (mRNA) in various CNS tissues, lymphoblast cells and iPSC-derived neurons from *C9orf72* repeat expansion carriers has been observed by several groups (DeJesus-Hernandez et al. 2011, Gijselinck et al. 2012, Belzil et al. 2013, Fratta et al. 2013, Almeida et al. 2013). Additionally, it has been reported that C9orf72 protein levels are reduced in various regions of the CNS in *C9orf72* repeat expansion carriers (Waite et al. 2014, Xiao et al. 2015). There are several reports suggesting that the decrease in *C9orf72* mRNA expression may be due to epigenetic alterations, such as varying levels of DNA and histone methylation, which are events known to repress gene expression. It has been reported that trimethylated histones (H3K9, H3K27, H3K79, H4K20) bind the pathogenic repeat expansion of C9orf72 in brain regions that correspond to decreased C9orf72 mRNA levels in patients (Belzil et al. 2013). In addition, it has been shown that aberrant CpG island methylation 5' of the $(G_4C_2)_n$ hexanucleotide repeat is significantly associated with C9-ALS/FTD and that levels of methylation are inversely correlated with disease onset (Xi et al. 2013). However, others have reported that this aberrant methylation may actually be protective (Liu et al. 2014). Additionally, another recent report suggests that this decrease in *C9orf72* mRNA may be a result of stalled transcription. The formation of distinct polymorphic structures within the *C9orf72* hexanucleotide repeat expansion, including G-quadruplexes and RNA•DNA hybrids (R-loops), may cause the RNA polymerase processivity to be impaired in the repeat region (Haeusler et al. 2014).

In order to establish whether decreased C9orf72 expression contributes to disease pathogenesis, a number of *C9orf72* knock down (KD) or knock out (KO) models have been generated, with varying results. Deletion of *ALFA-1*, the *C.elegans* orthologue of *C9orf72*, resulted in age-dependent progressive motor defects with an increased sensitivity to stress induced paralysis (Therrien et al. 2013). Additionally, transient KD of *C9orf72* during embryonic development has been shown to result in locomotor and axonal deficits in zebrafish (Ciura et al. 2013). In mice, *C9orf72* has been conditionally removed in neuronal and glial cells using the Nestin-Cre system or constitutively removed in all cell types using targeted genome editing techniques (Wen et al. 2017). Although it

is reported that the *C9orf72* KO mouse models do not show signs of neurodegeneration (Koppers et al. 2015, Sudria-Lopez et al. 2016, O'Rourke et al. 2016, Atanasio et al. 2016), two KO mouse models did show mild motor defects (Atanasio et al. 2016) and decreased survival (Sudria-Lopez et al. 2016). However, these phenotypes may be attributed to other underlying conditions rather than ALS/FTD, as these models have consistently reported symptoms such as enlarged spleens and lymph nodes, microglia activation with abnormal lysosomal activity and altered cytokine production (Atanasio et al. 2016, O'Rourke et al. 2016, Sudria-Lopez et al. 2016). In addition to animal models, two studies of human C9-ALS/FTD have provided contradictory evidence for a LOF disease mechanism. Firstly, a case report on a patient homozygous for the *C9orf72* repeat expansion argued against haploinsufficiency, as if it was the major disease mechanism it would be expected that this patient would have a more severe phenotype, but analysis revealed that the phenotype was no more severe than a patient heterozygous for the *C9orf72* repeat expansion (Fratta et al. 2013). Conversely, a recent study reported the presence of a novel LOF *C9orf72* splice site mutation in a patient with ALS, supporting haploinsufficiency as a disease mechanism in C9-ALS/FTD (Liu et al. 2016).

Taken together, these findings suggest that haploinsufficiency may not be the sole pathogenic mechanism in C9-ALS/FTD. However, normal function of C9orf72 still remains poorly understood, particularly *in vivo*. Experiments to define the biological role of C9orf72 are necessary to guide research into how alterations in its function may contribute to disease. C9orf72 is thought to function in autophagy, thus partial or complete loss of its function may disrupt the pathway, exacerbating RNA toxicity or dipeptide repeat (DPR) protein toxicity (see section 1.2.6.2 and 1.2.6.3).

### 1.2.6.2. RNA toxicity

The RNA toxicity hypothesis proposes that transcripts containing the $(G_4C_2)_n$ repeat expansion aggregate to form RNA foci and subsequently sequester RNA-binding proteins (RBPs). This is hypothesised to result in the perturbed physiological function of such RBPs. This is an attractive pathogenic mechanism as it is seen in other non-coding repeat expansion disorders such as myotonic dystrophy type 1 (DM1) (La Spada and Taylor 2010). Evidence of RNA foci in ALS was first reported in 2011, when they were observed in the frontal cortex and spinal cord of two patients carrying the repeat expansion (DeJesus-Hernandez et al. 2011). Several groups have reported that the *C9orf72* repeat expansion is transcribed in both a sense and antisense direction, resulting in the presence

of both sense $(G_4C_2)_n$ and antisense $(C_2G_4)_n$ RNA foci in several locations in the CNS of patients, including; the frontal cortex, motor cortex, hippocampus, cerebellum and spinal cord (Gendron et al. 2013, Mizielinska et al. 2013, Lagier-Tourenne et al. 2013, Zu et al. 2013). Whilst the majority of RNA foci are neuronal, it has been reported that they are present in astrocytes, microglia and oligodendrocytes at a much lower frequency (Mizielinska et al. 2013). A number of RBPs have been reported to be sequestered by the $(G_4C_2)_n$ repeat *in vitro*, including; hnRNP A3, hnRNP A1, hnRNP-H1/F, hnRNP-H, SRSF2, ALYREF, ADARB2, nucleolin, Pur-α, ASF/SF2, RanGAP1 (Mori et al. 2013b, Xu et al. 2013, Lee et al. 2013, Donnelly et al. 2013, Cooper-Knock et al. 2014b, Haeusler et al. 2014, Sareen et al. 2013, Reddy et al. 2013, Zhang et al. 2015). It is hypothesised that this will lead to lost or reduced function of these RBPs. Interestingly, transcriptomic analysis of C9-ALS/FTD patient tissue has shown dysregulation of RNA splicing, which may be due to sequestration of particular RBPs (Cooper-Knock et al. 2015).

To investigate whether the RNA foci seen in patients are sufficient to cause neurodegeneration, a number of models have been made. Expression of 30 $G_4C_2$ repeats in Drosophila was found to be sufficient to cause neurodegeneration, resulting in decreased locomotor activity and disrupted eye morphology (Xu et al. 2013). Pur-α was found to interact with the repeat in this study and overexpression of this RBP rescued the phenotype (Xu et al. 2013). Additionally, in a zebrafish model expressing 38 or longer $G_4C_2$ repeats, RNA foci formed and initiated apoptotic cell death via sequestration of hnRNP-H (Lee et al. 2013) Although this provides evidence that RNA foci are toxic and possibly mediate their effect through sequestration of RBPs, mouse models have provided contradictory results. Two mouse models expressing a patient derived *C9orf72* gene containing either 500 or 800 $G_4C_2$ repeats had abundant sense and antisense RNA foci, as well as RAN translated DPR proteins throughout the CNS, but had no neurodegeneration or change in survival, motor or cognitive function (O'Rourke et al. 2015, Peters et al. 2015a). Additionally, a mouse model expressing 66 $G_4C_2$ repeats in the CNS via AAV delivery had abundant sense RNA foci, sense derived DPR proteins and phosphorylated TDP-43 inclusions (Chew et al. 2015). Conversely to the aforementioned mouse models, this model also had neuronal loss and behavioural abnormalities reminiscent of C9-ALS/FTD patients, including anxiety, antisocial behaviour and motor defects (Chew et al. 2015). Contradictory evidence in several *in vivo* models suggests that RNA foci alone may not be sufficient to cause neurodegeneration. However, future work

should focus on elucidating the effect of sequestration of identified RBPs *in vivo*, to understand which one, if any, is critical for disease pathogenesis.

### 1.2.6.3. Dipeptide repeat (DPR) protein toxicity

The repeat-associated non-ATG (RAN) translation hypothesis proposes that tracts of expanded repeats are translated despite the absence of an initiating AUG codon, resulting in the production of polypeptides composed of repeating units of two amino acids, called dipeptide repeat (DPR) proteins (Zu et al. 2011). RAN translation was first reported in the repeat expansion disorders myotonic dystrophy type 1 and spinocerebellar ataxia type 8 (Zu et al. 2011). It has been reported that the repeat expansion in *C9orf72* is able to undergo bidirectional RAN translation of both the $(G_4C_2)_n$ sense and $(C_4G_2)_n$ antisense transcripts (Ash et al. 2013, Mori et al. 2013a, Mori et al. 2013c), resulting in the synthesis of five DPR proteins: poly-(glycine-alanine, GA), poly-(glycine-proline, GP), poly-(glycine-arginine, GR), poly-(proline-arginine, PR) and poly-(proline-alanine, PA) (Mori et al. 2013a, Zu et al. 2013, Ash et al. 2013, Mori et al. 2013c). All five of these DPR proteins co-aggregate in the characteristic p62 positive, TDP-43 negative inclusions seen in C9FTD/ALS patients (Mori et al. 2013b, Mori et al. 2013c, Mori et al. 2013a, Ash et al. 2013), in locations such as the cerebellum, hippocampus and frontotemporal neocortex. Poly-(GA) has been found to be the most prevalent in these inclusions (Mori et al. 2013c), with poly-(GP) and poly-(GR) present to a lesser extent. It is suggested that DPR protein aggregation may precede TDP-43 pathology, with evidence of poly-(GA) aggregate cores inside TDP-43 positive inclusions (Mori et al. 2013c).

Several groups have now demonstrated in various *in vitro* and *in vivo* models that DPRs are toxic. Many studies have focussed on poly-GA, as this is the most abundant DPR species in patients carrying the repeat expansion (Mori et al. 2013c). For example, expression of poly-GA in primary neurons, in the absence of RNA foci, resulted in neurotoxicity due to impaired proteasome activity and induction of endoplasmic reticulum (ER) stress (Zhang et al. 2014). Expression of poly-GA in zebrafish was found to be highly toxic (Ohki et al. 2017). Additionally, transgenic mice with abundant poly-GA pathology have neurodegeneration and ALS/FTD-like symptoms (Zhang et al. 2016). As well as poly-GA, arginine rich DPR proteins (poly-GR and -PR) have been extensively studied. Expression of GR or PR caused toxicity and early lethality in a Drosophila model (Wen et al. 2014). Interestingly, a sophisticated study generated two Drosophila models, one with a pure $(G_4C_2)_n$ repeat and one with a $(G_4C_2)_n$ repeat engineered to contain regular

interruptions with stop codons to prevent translation. Both pure and interrupted repeats formed RNA foci. However, unlike the pure repeat, the interrupted repeats could not be RAN translated to form DPRs. Expression of the pure repeats caused toxicity and early lethality, whereas the interrupted repeats had no effect. This supports the idea that RNA foci are not toxic, but the DPRs are (Mizielinska et al. 2014).

The aforementioned models indicate that DPRs are toxic, but do not confirm that this drives pathogenesis in humans. If DPRs are the major pathogenic mechanism underlying C9-ALS/FTD, if would be expected that DPRs accumulate in regions commonly affected during disease, for example motor neurons. However, in general it is reported that there is a low abundance of DPR proteins in these areas in patient post mortem tissue (Mackenzie, Frick and Neumann 2014, Mackenzie et al. 2015). This may be explained, as if accumulation of DPRs is toxic and results in neuronal death, the surviving neurons found in post mortem tissue may never have had abundant DPR pathology to begin with, which would explain why they survived. Interestingly, pathological findings from three *C9orf72*-FTD patients who died prematurely after disease onset (two from bronchopneumonia and one from myocardial infarction) suggested that DPR pathology preceded TDP-43 pathology, and DPRs were abundant throughout cerebral cortical regions, hippocampus and cerebellum (Baborie et al. 2015). This highlights that developing minimally invasive techniques to detect DPRs in patients during the disease course would be useful to understand the role of DPR proteins in early-stage disease pathogenesis.

### 1.3. Modelling neurodegenerative disorders in zebrafish
#### 1.3.1. Advantages of Zebrafish

The zebrafish (*Danio rerio*) was established as a vertebrate model to study developmental processes in the 1980s. Since then, the experimental value of the zebrafish has been demonstrated and it is increasingly being recognised as a model organism of human disease, including neurodegeneration. Zebrafish possess several characteristics that make them beneficial to scientists. They are vertebrates which develop *ex utero* in transparent eggs, known as chorions, enabling scientists to monitor developing embryos (Kimmel et al. 1995). Embryonic development is rapid, with all major organs formed within 1-day post fertilisation (dpf) (Kalueff, Stewart and Gerlai 2014), which is an advantage in comparison to higher vertebrate models such as rodents, which have longer gestation periods. Zebrafish reach sexual maturity at 3-4 months and are excellent breeders, with a single female able to produce hundreds of fertile eggs each week (Kalueff et al. 2014). Due to their small size they are able to be kept in a relatively small space, which means they are ideal for high-throughput genetic and drug screens.

The zebrafish genome is fully sequenced and is known to have 25 pairs of chromosomes, containing >26,000 protein coding genes (Howe et al. 2013). The genetic homology is relatively high between zebrafish and mammals, including humans, supporting the translational value of the zebrafish. The nucleotide sequences of zebrafish genes show approximately 70% homology with human genes and around 84% of human disease genes have zebrafish counterparts, including those linked to neurodegenerative disorders (Howe et al. 2013). In genetic studies it is important to consider the genome duplication which occurred during teleost evolution, resulting in duplicate copies of many genes in zebrafish (Kalueff et al. 2014, Howe et al. 2013, Phillips and Westerfield 2014). However, despite this, zebrafish have a similar number of chromosomes to humans and the duplicated CNS genes seem to mostly encode proteins with similar or substantially overlapping function and properties (Kalueff et al. 2014, Howe et al. 2013, Phillips and Westerfield 2014). As the zebrafish genome is fully sequenced they are susceptible to genetic manipulation (section 1.3.2). Interestingly, the study of embryonic lethal mutations is possible in zebrafish, as they do not require a functional circulatory system to survive in the first week, relying on their yolk and passive diffusion of oxygen, and undeveloped embryos are not resorbed, as mouse embryos are (Kabashi et al. 2010a). Thus, analysis of the whole-organism phenotype can be conducted due to their *ex utero* development.

The zebrafish has a conserved, yet simplified, nervous system with other higher vertebrates (Babin, Goizet and Raldua 2014). In general, although much smaller, the CNS and PNS have a similar overall organisation, including cell types and neuron structure (Babin et al. 2014). Key similarities include: fore-, mid- and hind-brain (including diencephalon, telencephalon and cerebellum); peripheral nervous system with motor and sensory components; a functional blood-brain barrier; main neurotransmitter systems such as the cholinergic and dopaminergic pathways are present; higher vertebrate behaviours and integrated neural function such as memory and social behaviour (Wullimann and Mueller 2004, Panula et al. 2006, Jeong et al. 2008, Lieschke and Currie 2007, Babin et al. 2014). Conversely, there are some structural differences, including: no direct telencephalic projections into the spinal cord, such as the corticospinal tract; smaller cerebral hemispheres; zebrafish muscle is polyneuronally innervated throughout its lifetime; fish behaviour and cognitive function are simplified in comparison to 'higher' vertebrates; presence of teleost specific sensory organs such as the lateral line (Wullimann and Mueller 2004, Lieschke and Currie 2007, Babin et al. 2014, Westerfield, McMurray and Eisen 1986).

It is important to acknowledge that despite similarities, no model organism can reproduce and accurately model all aspects of human neurodegenerative diseases. There are still significant differences between zebrafish and humans in terms of genetics, lifespan and architecture of the nervous system, for example. It is important to understand both the advantages and limitations when interpreting results in all model organisms, including zebrafish.

### 1.3.2. Genetic tools

The zebrafish has proven to be an essential model organism for validating pathogenicity of novel genes or alleles in human patients. Due to its fully sequenced genome, there are multiple known targets for reverse genetic techniques. Genes can be easily manipulated by loss- or gain-of-function approaches in simple, transient assays of gene function and by creation of stable disease models using targeted genome editing techniques. The zebrafish offers an inexpensive and rapid alternative to generating models of neurodegenerative disease in comparison to murine models, which are labour-intensive and costly.

In this project, the main focus is generation of LOF mutations. The easiest approach to study LOF mutations in zebrafish is the injection of antisense morpholino

oligonucleotides (AMOs), and this method has been particularly exploited over the past few decades for this reason (Nasevicius and Ekker 2000). AMOs are a synthetic derivative from DNA, with two major changes resulting in a neutral charge: i) a six-membered morpholine ring replaces the standard deoxyribose ring; ii) a non-ionic phosphorodiamidate linkage replaces anionic phosphodiester bond (Summerton and Weller 1997). Knockdown (KD) can be easily achieved by the microinjection of AMOs at the 1- to 4-cell embryonic stage. The neutral charge and small size (around 25 bases in length) allows the AMO to diffuse throughout the embryo following microinjection (Nasevicius and Ekker 2000). AMOs bind complementary sequences of RNA or single-stranded DNA, and can be designed to temporarily downregulate gene expression by either blocking translation or splicing (Eisen and Smith 2008).

The use of AMOs has significantly helped to solidify the relevance of investigating zebrafish orthologues of human disease genes. However, the technique is often confounded by off-target effects, which are often caused by the induction of p53 that leads to apoptosis, but can also be p53-independent (Kok et al. 2015). These inconsistencies have resulted in questions about its relevance in the advent of novel genome editing techniques in recent years. The potential for off-target effects has been demonstrated in zebrafish models of neurodegeneration, such as MND. KD of a *Tardbp* orthologue in zebrafish using translation blocking AMOs has been reported to cause shorter, disorganised motor neuron axons (Kabashi et al. 2010b). Subsequently, two independent studies demonstrated that stable loss of *Tardbp* was fully compensated by alternative splicing of a second *Tardbp* orthologue in the zebrafish, *Tardbpl* (Schmid et al. 2013, Hewamadduma et al. 2013). Thus, the *Tardbp* KD-induced phenotype was not observed in these stable *Tardbp* mutants (Schmid et al. 2013, Hewamadduma et al. 2013). Interestingly, one of the groups microinjected the same AMO used in the Kabashi study into both wild-type and stable *Tardbp* knock-out (KO) mutants (Hewamadduma et al. 2013). They found that this resulted in severe defects in both genotypes, suggesting that the AMO used in the Kabashi paper may have had off-target effects which contributed to the observed phenotype (Hewamadduma et al. 2013). In addition, AMO-mediated KD of *C13H9orf72* in zebrafish has been reported to result in locomotor deficits and axonopathy of the motor neurons (Ciura et al. 2013). However, we have evidence which suggests that stable loss of *C13H9orf72* does not recapitulate these same phenotypes, again suggesting the phenotypes observed in the KD study were due in part to off-target effects (chapter

4). As well as this, a recent study by the same group reported that AMO-mediated KD of p62/SQSMT1 in zebrafish again caused locomotor deficits and axonopathy of the motor neurons (Lattante et al. 2015b). Currently, this is the only zebrafish model of p62/SQSTM1, therefore it will be essential to investigate the effects of p62/SQSTM1 LOF in a stable KO model to validate the AMO phenotype, given the aforementioned discrepancies for *Tardbp* and *C13H9orf72*.

It is important not to disregard off-target effects, as they may result in others unintentionally classifying these as genuine effects of the gene under investigation. This is a particularly sensitive issue with regards to peer reviewers from disparate fields, who may not have the necessary experience to distinguish AMO-induced toxicity from gene-specific AMO-induced phenotypes. The use of appropriate controls is essential so that investigators can ensure that the phenotype they observe is specific to the gene of interest. For example, control AMOs should always be used, which could include mismatch or scrambled AMOs. However, even if the 'control' AMO causes no phenotype, this doesn't rule out that the phenotype observed with the 'specific' AMO wasn't caused by an off-target effect. Therefore, additional controls to test for specificity should be used. This includes using at least two AMOs for any gene targeted, with each AMO tested individually to ensure they result in similar phenotypes. Additionally, at least one of these should be a splice-inhibiting AMO, therefore even if relevant antibodies are unavailable, quantification of the effect of the AMO could be performed using qRT-PCR. Specificity could also be determined by mRNA rescue. However, this technique is only effective if the genes are ubiquitously expressed or have no overexpression phenotype. If the target gene is expressed in a restricted manner or has a strong overexpression phenotype, this method would not be suitable. Alternatively, one could compare phenotypes observed to existing mutants. However, clearly this method is limited to whether another mutant has been generated. This topic has recently been addressed by publication of a set of guidelines for the use of morpholinos in zebrafish (Stainier et al. 2017).

In addition to off-target effects, the transient nature of the technique means it is not appropriate for studying the late-onset disease related phenotypes of many neurodegenerative diseases, such as adult-onset MND. To circumvent this issue, the recent development of genome-editing techniques such as transcription activator-like effector nucleases (TALENs) (Joung and Sander 2013) and clustered regularly interspaced short palindromic repeats (CRISPR) (Hruscha et al. 2013, Chang et al. 2013,

Hwang et al. 2013), have enabled researchers to induce targeted, heritable mutations in the zebrafish genome. Both of these techniques consist of a sequence-specific DNA targeting subunit and a double stranded DNA cleaving nuclease. TALENs consist of a pair of DNA binding proteins fused to a fok1 nuclease. The pair bind opposite sides of the target site, separated by a spacer region of 14-20 nucleotides, within which fok1 cuts the DNA (Joung and Sander 2013). Additionally, CRISPR consists of a complex between a cas9 nuclease and a target specific single guide RNA (gRNA). The gRNA directs the cas9 nuclease to a 20 nucleotide target site, immediately followed by a protospacer adjacent motif (PAM) site, where it cuts the DNA (Hruscha et al. 2013, Chang et al. 2013, Hwang et al. 2013). The induction of double stranded breaks in the genome initiates two DNA repair pathways: i) non-homologous end joining (NHEJ), which ligates the DNA strands without a template, frequently producing small insertion or deletion (indel) mutations; ii) homologous recombination (HR), which repairs the break with a homologous DNA template (Schmid and Haass 2013). Despite both techniques being able to induce heritable mutations, they both have specific advantages and disadvantages, as detailed in table 1.4.

Overall, the ease at which potentially pathogenic genes can be transiently depleted in zebrafish, has been exploited over the past few decades. This technique, alongside rescue of LOF mutations with the human wild-type mRNA but not human disease mRNA, enables researchers to demonstrate the specificity and pathogenicity of certain human disease genes. However, the generation of stable LOF models in recent years has shed light on the potential pitfalls of transient techniques such as AMOs. This calls in to question past research and highlights the importance of making stable models of these genetic variants in the future, to further confirm pathogenicity. As techniques such as CRISPR/Cas9 are inexpensive and rapid to perform, the next few years should see a wealth of new zebrafish disease models.

**Table 1.4 Advantages and Disadvantages of TALENs and CRISPR/Cas9.**

| Genome editing technique | Advantages | Disadvantages |
|---|---|---|
| Transcription activator-like effector nucleases **(TALENs)** | - High target specificity<br>- In theory, can be targeted to any position within the genome as they are not constrained by a PAM site<br>- Off-target effects less of an issue, as the DNA binding site is very long (approx. 36 base pairs) therefore rarely, if ever, found elsewhere in the genome (Mussolino et al. 2011, Miller et al. 2011)<br>- Another reason for less off target effect is that double stranded breaks (DSB) only occur after correct positioning and dimerization of Fok1 (Christian et al. 2010) | - More expensive<br>- More time consuming to generate<br>- TALEN specificity/binding is dependent on protein-DNA interactions which can be affected by epigenetic status, such as sensitivity to methylation (Bultmann et al. 2012) – this is thought to explain the little or no mutagenesis activity in some cases |
| Clustered regularly interspersed short palindromic sequences **(CRISPR)/Cas9** | - Easy and simple to design<br>- Less cost-intensive than TALENs<br>- High target specificity<br>- Have been reported to have higher mutation efficiency - indel formation of up to 70% reported (Wang et al. 2014)<br>- Not sensitive to methylation like TALENS<br>- Multiplexed mutations – mutations can be introduced in multiple genes at the same time via injection of multiple gRNAs (Wang et al. 2013)<br>- Cas9 nickase mutants used to increase specificity and reduce off-target effects (Ran et al. 2013). | - Target site selection can be limited, due to dependency on PAM site (Sternberg et al. 2014)<br>- Off-target effects reported to occur more frequently than TALENs (Boettcher and McManus 2015) – one reason is that gRNA can tolerate up to 5 mismatches (non-Watson-Crick base pairing) (Fu et al. 2013) |

### 1.3.3. Examining motor function in adult zebrafish models of neurodegeneration

Several neurodegenerative diseases are characterised by motor dysfunction, including Parkinson's disease, Huntington's disease and motor neuron diseases, such as ALS. The zebrafish is increasingly being acknowledged as a model organism to study normal and/or pathological motor function throughout its lifetime for several reasons. For example, as a vertebrate model, it has conserved organisation of organs and tissues, including the brain and spinal cord. Additionally, neurogenesis begins around 10 hours post fertilisation (hpf), synaptogenesis around 18 hpf and hatching around 52 hpf in the zebrafish (Kimmel et al. 1995). The aforementioned qualities mean that both larval and adult zebrafish are ideal to study motor dysfunction associated with many human neurodegenerative disorders.

As gene overexpression or KD can be easily achieved using injections of RNA (or cDNA) or AMOs at the embryonic stage, there are a number of transient embryonic models which have been used to model the toxic effects of genetic mutations associated with neurodegenerative disease, including changes in motor function. Behavioural responses to touch and swimming can be monitored shortly after hatching in such models, as they already have a repertoire of stereotyped motor behaviours at this stage (Drapeau et al. 2002, Wolman and Granato 2012). For example, by 24 hpf wild-type zebrafish spontaneously contract their tail muscles and by 48 hpf, zebrafish exhibit controlled swimming behaviours (Sztal et al. 2016). Reduction or other alterations in these movements may indicate a motor dysfunction. There are two main approaches to measure swimming behaviour in early development, including; the touch-evoked escape response (TEER) and high-throughput locomotion assays. The TEER, involves measuring acceleration during a burst of swimming, following an external stimulus to the head or tail. Additionally, locomotion assays can be performed using commercially available automated tracking systems, such as Zebralab by ViewPoint (France), providing reliable and high-throughput measurements of motor function. This test is also suitable for high-throughput *in vivo* drug or mutagenesis screens. However, although advantageous to have a disease model with phenotypes at these early stages, it is not representative of human neurodegeneration. Therefore, in order to fully understand the progressive nature of motor dysfunction in these disorders, stable genetic models of neurodegeneration must be developed for long-term phenotypic studies in adult zebrafish.

There are several ways in which motor function can be investigated in both health and disease in adult zebrafish. A study generated a fish that expressed mutant zebrafish *sod1* (Ramesh et al. 2010) and a swim tunnel test was utilised to test the motor abilities in this transgenic line, at several different ages. This test measures swimming endurance against an increasing flow of water. Critical swimming speed ($U_{crit}$) is calculated for each individual, as the maximum swimming velocity a fish can sustain for a set duration (Plaut 2000, Brett 1964). The transgenic zebrafish generated in this study showed a marked decline in $U_{crit}$ with increasing age compared to controls, which eventually resulted in paralysis at end stage disease (Ramesh et al. 2010). This transgenic model recapitulates the progressive trait of ALS. Other models of neuromuscular degeneration, such as the *Mfn2*-linked Charcot Marie Tooth (CMT) disease Type 2 zebrafish model, utilised the same technique (Chapman et al. 2013). They also showed progressive swimming defects, with adult *Mfn2* mutants displaying a decreasing $U_{crit}$ with age, in comparison to controls (Chapman et al. 2013). In the future, other models of neuromuscular degeneration would benefit from using this method of testing motor performance. Another method which has been used to observe motor function in adult zebrafish models of neurodegeneration involves using various video tracking systems to monitor swimming activity of individuals in a tank over a set period (Sakowski et al. 2012, Wang et al. 2017, Da Costa et al. 2014). For example, it was reported that swimming velocity of a stable transgenic zebrafish, expressing human G93A-*SOD1,* decreased over time in comparison to controls (Sakowski et al. 2012), showing that this method is also sensitive in detecting changes in motor function. However, the disadvantage to these studies is that they are time consuming to perform on large cohorts. A novel test, called the spinning task, has the ability to rapidly measure swimming endurance in adult zebrafish (Blazina, Vianna and Lara 2013). However, it is yet to be tested and published on adult zebrafish models of neurodegeneration.

In addition to identifying motor dysfunction, defects at the neuromuscular junction (NMJ) and a decrease in the number of motor neurons (MNs) were also observed in the fish expressing mutant zebrafish *sod1* (Ramesh et al. 2010). The NMJs were analysed in this model, as effects at the NMJ are one of the earliest defects in mouse models of ALS (Frey et al. 2000, Schaefer, Sanes and Lichtman 2005, Fischer et al. 2004). To do this, whole-mount staining for synaptic vesicle 2 (SV2 – a presynaptic marker) and α-bungarotoxin (α-BTX – a postsynaptic marker) was performed on larvae (11dpf) and adult (12 months)

muscle tissue (Ramesh et al. 2010). They found a significant reduction in SV2 and α-BTX co-localisation in transgenic fish at 12 months in comparison to controls, indicating dysfunctional NMJs (Ramesh et al. 2010). In addition, the MNs were analysed as NMJ degeneration is followed by MN loss in ALS patients and transgenic ALS rodents (Frey et al. 2000, Fischer et al. 2004). To analyse this, spinal cords were taken at end stage disease from transgenic *sod1* fish and processed for choline acetyl transferase (ChAT) immunostaining to examine MNs (Ramesh et al. 2010). End stage, transgenic zebrafish had a 38% reduction of MNs in comparison to controls (Ramesh et al. 2010). These results suggest the degeneration of NMJs and subsequent loss of MNs in the transgenic zebrafish underlie the progressive motor dysfunction observed. Several groups have used the same method of examining NMJs for different adult *sod1* mutants (Da Costa et al. 2014, McGown et al. 2013, Sakowski et al. 2012) and adult *Mfn2* mutant zebrafish (Chapman et al. 2013). The main difference is the method in which co-localisation was measured. For example, one study used the Pearson's Correlation Coefficients test (Ramesh et al. 2010), whereas another study used the Intensity Correlation Quotient (ICQ) (Chapman et al. 2013, Li et al. 2004). It may be useful in the future to standardise which method is used. Additionally, other groups have reported using Cresyl violet Nissl Stain, instead of ChAT immunostaining, in order to count MNs in spinal cord cross sections from control and transgenic fish expressing human G93A-*SOD1* (Sakowski et al. 2012). However, both methods of MN counting are sensitive to detecting changes in MN number.

Despite advantages of using adult zebrafish to study motor function, there are some limitations which must be acknowledged when interpreting results. For example, it has been shown that zebrafish muscle is polyneuronally innervated throughout its lifetime (Westerfield et al. 1986) and that adult zebrafish have the capability to regenerate motor neurons (Reimer et al. 2008), unlike mice and humans. It is possible that this capability could affect the severity of motor phenotypes observed in zebrafish models of neurodegenerative disease. However, it has been reported that zebrafish do develop severe motor defects in several models of neurodegenerative disease, highlighting its relevance to study such disorders (Ramesh et al. 2010, McGown et al. 2013, Chapman et al. 2013, Sakowski et al. 2012). Overall, there are multiple effective methods to study both motor function and the underlying pathology in adult zebrafish, showing that they are an excellent model to study motor function in long-term phenotypic studies.

### 1.3.4. Examining behaviour in adult zebrafish models of neurodegeneration

In addition to motor dysfunction (section 1.3.3), disruptions in emotional, cognitive and social behaviour are common phenotypes observed in several neurodegenerative diseases, including Alzheimer's Disease, FTD, Parkinson's Disease and ALS. Therefore, it is essential when modelling these diseases that changes in behaviour and/or cognition can be detected. The zebrafish is rapidly gaining popularity in behavioural research as a useful organism to study normal and/or pathological behaviours. Their behavioural responses are robust and appear to be conserved, resembling those seen in mammalian species, such as humans (Kalueff et al. 2014, Stewart et al. 2014, Norton and Bally-Cuif 2010). As discussed previously, the zebrafish has a conserved, yet simplified, nervous system compared with other higher vertebrates (Babin et al. 2014). They possess the major neuromediator systems, including similar neurotransmitter receptors, transporters, plus enzymes of synthesis and metabolism (Kalueff et al. 2014). Zebrafish also have well-developed, conserved neuroendocrine systems. For example, stress responses are mediated by cortisol activated by a cascade of hypothalamo-pituitary hormones and acting via glucocorticoid receptors in zebrafish, similar to humans (Ziv et al. 2013). In addition, they are sensitive to major neurotropic drugs (such as antipsychotics, anxiolytic, antidepressants, ethanol, sedatives and antiepileptics) and respond to these in a similar manner to humans (Kalueff et al. 2014, Stewart et al. 2014). These similarities all support the translational value of studying behaviour in zebrafish and the potential value of testing new drugs for major brain disorders.

Larvae can be used to measure a number of simple behaviours. For example, with the application of automated video tracking tools, robust anxiety-like or anxiolytic-like responses can be detected at this early stage in high throughput screens. However, for larval stages the most common endpoints for these assays are locomotory, such as distance travelled and immobility, which may subsequently increase or decrease with anxiety (Kalueff et al. 2013, Ahmad et al. 2012). Although these endpoints may be useful when studying the effects of anxiogenic or anxiolytic drugs for example, they may not be suitable when studying larval zebrafish models of neurodegenerative diseases, as motor function may be affected by alternate factors, such as degeneration of motor neurons. Additionally, it is reported that certain complex behaviours are not prominent in larval zebrafish, such as social behaviours. A recent study suggests that social behaviours, such as social preference, begin to emerge when zebrafish are around 2 weeks old (Dreosti et

al. 2015). Analysis of social behaviours are relevant for several neurodegenerative disorders, where patients may experience aberrant social behaviours, such as depression, disinhibition or apathy, for example. Although the number of stable genetic models of neurodegeneration are limited, the increasing use of genome editing techniques, such as TALENs and CRISPR/Cas9, will hopefully accelerate their development, allowing for a better understanding into the progressive nature of behavioural phenotypes in neurodegenerative disease.

Although more difficult to manipulate than larvae, adult zebrafish display a whole host of mature behaviours which make it an enticing model organism to study changes in behaviour and/or cognition, complementary to existing rodent models. Adult zebrafish are a powerful tool to model behaviours including aggression, anxiety, learning, memory and social behaviour, which are relevant to many neurodegenerative diseases (Norton and Bally-Cuif 2010). Additionally, the availability of reliable, commercially available video tracking systems, such as the Zebralab by ViewPoint (France), markedly strengthens neurobehavioral analysis in adult zebrafish. Several groups have developed a wealth of behavioural assays which enable the study of aggression, anxiety, learning, memory and social behaviours in adult zebrafish, taking advantage of these video tracking systems (Stewart et al. 2014, Norton and Bally-Cuif 2010).

The focus of this study is ALS and as discussed, it has been reported that 50% of ALS patients carrying the repeat expansion in *C9orf72* have behavioural and/or cognitive impairments (Ringholz et al. 2005). Additionally, it has been reported that around 15% of these patients meet the clinical criteria for FTD, particularly the behavioural variant of FTD (bvFTD) (Ringholz et al. 2005). Patients exhibit symptoms such as anxiety, disinhibition, apathy and memory loss (Mahoney et al. 2012). There are several established protocols available to investigate these behaviours in adult zebrafish. For example, methods available to monitor spatial learning and memory in the zebrafish include the T-maze, which is similar to a test used on rodents (Darland and Dowling 2001, Norton and Bally-Cuif 2010). There are also several aquatic 'novelty' tests, such as the novel tank diving test, open field test and light-dark box which have been extensively validated to monitor anxiety-like behaviour and are conceptually similar to rodent anxiety tests, such as the open field test (Lopez-Patino et al. 2008, Egan et al. 2009, Norton and Bally-Cuif 2010, Serra, Medalha and Mattioli 1999). These tests have been used on adult zebrafish models of neurodegeneration. For example, a group reported that rotenone

treatment of adult zebrafish induced Parkinson's disease-like motor and non-motor symptoms, including anxiety-like behaviour as shown by using the light-dark test (Wang et al. 2017). As well as this, zebrafish are naturally social animals and prefer to swim in shoals. This behaviour can be disrupted by environmental, pharmacological or genetic factors and can be easily assessed in adult zebrafish (Norton and Bally-Cuif 2010).

### 1.3.5. C9orf72-ALS/FTD zebrafish models

As discussed, a noncoding $(G_4C_2)_n$ hexanucleotide repeat expansion in *C9orf72* is a major cause of both ALS and FTD. In addition, it is not fully understood how the repeat expansion causes disease, but three principal mechanisms have gained particular attention, including; haploinsufficiency, RNA toxicity and repeat-associated, non-ATG (RAN) translation. The pathogenic mechanism underlying *C9orf72*-linked ALS may be attributable to just one of these mechanisms or involve a combination of all three. Zebrafish are an excellent organism to utilise as a model of C9-ALS/FTD. As discussed, not only do they possess several characteristics which make it an ideal organism to model motor neuron diseases in general, but they have a highly conserved *C9orf72* orthologue (*C13H9orf72*), sharing 68.55% nucleotide identity with the human gene. Zebrafish have only one copy of the *C9orf72* orthologue and they are predicted to possess 3 protein-coding transcripts, encoding two protein isoforms of different lengths, as observed in humans (Ciura et al. 2013). It has been reported that *C13H9orf72* mRNA is expressed in regions of the CNS including forebrain, hindbrain and spinal cord in 24hpf zebrafish embryos (Ciura et al. 2013). In adult zebrafish, *C13H9orf72* mRNA is present more extensively in a number of organs and tissues, with notable expression in regions of the CNS such as the forebrain, midbrain, hindbrain and spinal cord (Ciura et al. 2013). Both loss-of-function (LOF) and gain-of-function (GOF) models of C9-ALS/FTD have been generated in zebrafish, which are discussed in sections 1.3.5.1 and 1.3.5.2.

### 1.3.5.1. Loss-of-function models

To address the LOF hypothesis, a group generated a genetic model of *C9orf72* haploinsufficiency via transient KD of *C13H9orf72* transcripts in zebrafish (Ciura et al. 2013). KD was achieved by designing specific AMOs to target two ATG translation start sites for all three predicted transcripts (Ciura et al. 2013). AMO-mediated knockdown of *C13H9orf72* resulted in disrupted aborization and shortening of the motor neuron axons (Ciura et al. 2013), a phenotype which has previously been reported in other KD models of ALS in zebrafish, including TDP-43 (Kabashi et al. 2010b). In addition, impaired

touch-evoked escape response (TEER) and spontaneous swimming behaviour was also observed in this model (Ciura et al. 2013). Despite the fact the level of KD was not quantified, due to lack of available anti-C9orf72 antibodies at the time of publication, co-injection of human *C9orf72* mRNA rescued both the axonopathy and locomotor defects, supporting the specificity of the observed phenotypes (Ciura et al. 2013). Despite promising results, data from AMO KD should be treated with caution, as the technology has various limitations, ranging from its transient efficacy to its potential for off-target effects, as previously discussed. In addition to this, ALS is principally an adult onset disorder in humans, therefore it is desirable to use a complementary approach to the AMOs in order to study the adult phenotype in zebrafish. The aforementioned reasons highlight the necessity to develop a stable zebrafish *C13H9orf72* LOF model. Recently, a group utilised the CRISPR/Cas9 system to generate zebrafish *C13H9orf72* LOF alleles (Hruscha et al. 2013). They reported that the identified LOF mutations successfully transmitted through the germline, however, to date there are no publications phenotypically characterising this potential model.

### 1.3.5.2. Gain-of-function models

The relative contribution of RNA and DPR toxicity in the context of C9-ALS/FTD is still under debate, since many conflicting results have been obtained from a variety of model systems. Regarding zebrafish, RNA injections of 8x, 38x and 72x $G_4C_2$ repeats has previously been reported to result in RNA foci and cell death by apoptosis at 24 hpf, in a repeat length-dependent manner, although no C9-ALS/FTD-like motor or behavioural phenotypes were reported (Lee et al. 2013). Additionally, this study did not report evidence of RAN translation products from the repeat RNA injections in these zebrafish. Another recent study generated two independent transgenic zebrafish lines carrying x80 $G_4C_2$ repeats (Ohki et al. 2017). It was observed that this model had key pathological features of C9-ALS/FTD at 28 hpf, such as RNA foci present in the spinal cord, however RAN translation products were not detected (Ohki et al. 2017). This is possibly because no RAN translation occurs in early development or it was below the detection limit of the antibodies used. This model showed mild toxicity, with mild pericardial oedema commonly observed (Ohki et al. 2017). However, as DPRs were not detected, it cannot be determined that this mild toxicity was due to RNA foci or low level DPR protein expression. Interestingly, this group also generated two additional transgenic zebrafish lines carrying a translation initiation codon (ATG) in front of the x80 $G_4C_2$ repeats,

driving expression of poly-GA DPR proteins (Ohki et al. 2017). This study focussed on poly-GA, as this is most abundant DPR species in patients carrying the repeat expansion (Mori et al. 2013c). In addition to the presence of RNA foci in the spinal cord at 28 hpf, this model also had abundant poly-GA inclusions and increased toxicity, including severe pericardial oedema, circulatory defects and decreased survival (Ohki et al. 2017). Blocking production of poly-GA using an antisense approach partially rescued the observed phenotype, demonstrating that poly-GA is toxic *in vivo* and targeting DPR proteins might be a useful therapeutic method in the future (Ohki et al. 2017). Unfortunately, due to larval lethality of this model, analysis of possible neurodegenerative phenotypes in adulthood was not possible. Further development of inducible GOF zebrafish models will be necessary to further dissect the relative contribution and/or synergistic effect of repeat RNA and DPRs to toxicity in C9-ALS/FTD zebrafish models.

### 1.4. Aims and Objectives

There are two major gaps in our knowledge regarding this *C9orf72*. Firstly, it is not fully understood how the repeat expansion causes C9-ALS/FTD, however there is evidence that C9orf72 mRNA and protein levels are reduced in patients (DeJesus-Hernandez et al. 2011, Gijselinck et al. 2012, Belzil et al. 2013, Fratta et al. 2013, Almeida et al. 2013, Waite et al. 2014, Xiao et al. 2015), suggesting that *C9orf72* LOF via haploinsufficiency may be causative in C9-ALS/FTD. Secondly, the function of the C9orf72 protein is not fully understood, however there is increasing evidence that C9orf72 plays a regulatory role in autophagy (Farg et al. 2014, Yang et al. 2016, Sellier et al. 2016, Sullivan et al. 2016a, Webster et al. 2016a). It is essential that gaps in our knowledge are filled in order to identify novel therapeutics for preclinical development, which have the potential to help the majority of ALS and FTD patients. Thus, the objective of this project is to test the hypothesis that loss of C9orf72 expression causes ALS/FTD by disruption of C9orf72 function in autophagy. To investigate this, the overall aims of this project are:

1. To generate a stable zebrafish *C13H9orf72* LOF model using targeted genome editing techniques
2. To characterise the model generated to determine whether loss of C13H9orf72 expression results in any ALS- or FTD-like phenotypes
3. To investigate the function of C13H9orf72 *in vivo*

As discussed the initial aim of this project is to generate a stable zebrafish *C13H9orf72* LOF model. Developing *in vivo* models recapitulating C9-ALS/FTD is essential in order to further elucidate the pathomechanisms which underlie this disorder and to aid in evaluating the potential efficacy of novel therapies. This can be achieved by the development of zebrafish models, as they hold several characteristics which make it an advantageous model to use in the study of neurodegenerative disorders such as ALS and we know there is high homology between human ALS-linked genes and the corresponding zebrafish orthologue. Importantly, there is 68.55% nucleotide identity and 76.14% amino acid identity between human *C9orf72* and the zebrafish orthologue, *C13H9orf72* (zgc: 100846). Therefore, it is expected that functional role of C9orf72 is likely to be similar in zebrafish and humans, thus disease mechanisms are expected to be conserved. As discussed, AMOs have been utilised to transiently KD both isoforms of the zebrafish *C13H9orf72*, resulting in both locomotor and axonal deficits (Ciura et al. 2013), which is consistent with the aetiology of ALS. However, as ALS is an adult onset disorder it is critical to generate a stable LOF model in order to study the potential adult phenotype in the zebrafish. In addition, a recent identification of a novel LOF *C9orf72* splice site mutation in a patient with ALS, supports haploinsufficiency as a disease mechanism in C9-ALS/FTD and further highlights the importance of generating this model (Liu et al. 2016). In order to produce zebrafish *C13H9orf72* LOF alleles, we will utilise targeted genome editing techniques to target coding exons 1 and 7 of *C13H9orf72*, to generate LOF mutations in either both isoforms or the long isoform, respectively (chapter 3).

Validated zebrafish *C13H9orf72* LOF mutants will be used for characterisation studies to address our second aim in determining whether loss of *C13H9orf72* results in any ALS/FTD-like phenotypes, such as changes in survival, motor dysfunction or changes in behaviour (chapter 4). As there are currently no publications characterising a stable zebrafish *C13H9orf72* LOF model of ALS/FTD, the phenotypic characterisation of the generated lines will be highly important during this project. To determine the possibility of lethal effects of the *C13H9orf72* mutations, survival will be monitored as has been done previously in our group (Chapman et al. 2013). During larval stages, they will be monitored twice per day, with dead larvae collected for genotyping. Additionally, the mutants will also be monitored throughout their lifetime, as it may be expected that survival decreases during adulthood, as ALS/FTD is mainly an adult onset disorder in

humans. To determine whether the zebrafish *C13H9orf72* LOF mutants have a motor deficit, two approaches will be used. Firstly, the spinning task will be utilised to monitor swimming endurance (Blazina et al. 2013). Secondly, the swim tunnel will be utilised to measure critical swimming velocity ($U_{crit}$) in the zebrafish, which has been used to characterise other zebrafish models of ALS previously (Ramesh et al. 2010). Furthermore, we will confirm the basis for any altered motor function by quantitative assessment of neuromuscular junctions (NMJs). In addition, C9-ALS/FTD patients are known to exhibit a number of behavioural changes such as: anxiety, disinhibition, apathy, memory loss (Mahoney et al. 2012). There are now several protocols established to measure behaviours such as anxiety, aggression, social preference, memory and learning in adult zebrafish (Norton and Bally-Cuif 2010). Thus, we aim to examine anxiety-like behaviour in our mutants via utilising two tests which robustly measure this behaviour in zebrafish; the novel tank diving test and the open field analysis test.

The final aim of this project is to investigate the *C9orf72*-linked disease mechanisms by investigating and identifying the function of the C9orf72 protein *in vivo*. A characteristic phenotype of C9-ALS/FTD is the presence of p62/SQSTM1 positive, TDP-43 negative inclusions found in the cerebellum, hippocampus and the neocortex (Cooper-Knock et al. 2012, Al-Sarraj et al. 2011). p62/SQSTM1 targets ubiquitinated proteins to the autophagy pathway for degradation and accumulation of this protein has been associated to inhibition of autophagy, suggesting C9orf72 may function within this protein clearance pathway (Hara et al. 2006). The presence of these pathognomonic inclusions, alongside the identification of C9orf72 haploinsufficiency in patients, suggests that defective autophagy via loss of C9orf72 function may be causative in C9-ALS/FTD. Further supporting this hypothesis, recent studies published that disruption of C9orf72 function, in both cell lines and primary neurons, results in an inhibition of autophagy initiation and accumulation of p62/SQSTM1, similar to the pathology seen in C9-ALS/FTD patients (Farg et al. 2014, Yang et al. 2016, Sellier et al. 2016, Sullivan et al. 2016a, Webster et al. 2016a). Therefore, the investigation of the role of C9orf72 *in vivo,* using the stable zebrafish *C13H9orf72* LOF models, is an important aspect of this project (chapter 5). This not only has the potential to allow for further investigation into the possible role of autophagy deficits in disease progression, but will provide a useful tool for studying C9orf72 function *in vivo.*

## 2. Materials and Methods

### 2.1. Materials

#### 2.1.1. General reagents

All general chemicals and reagents, unless otherwise stated, were purchased from VWR, Lutterworth, UK. For polymerase chain reaction all primers were purchased from Sigma-Aldrich, Poole, UK and all restriction enzymes from New England Biolabs (NEB), Ipswich, USA.

**Table 2.1 General reagents.**

| | |
|---|---|
| **E3 Embryo Medium** | 5mM NaCl; 0.17mM KCl; 0.33mM $CaCl_2$; 0.33mM $Mg_2SO_4$; 0.1mg/l Methylene Blue in $dH_2O$ |
| **Tricaine** | 400mg Tricaine powder (Sigma, #A-5040), 97.9ml $dH_2O$, ~2.1ml 1M Tris (pH 9). Adjust if required to ~ pH 7 |
| **50x TAE stock solution** | 242g Tris Base, 57.1ml acetic acid, 0.5M EDTA pH 8.8, up to volume with $dH_2O$ |
| **Embryo Deyolking Buffer** | 55mM NaCl, 1.8mM $NaHCO_3$, made up to volume with $dH_2O$ |
| **Embryo Washing Buffer** | 110mM NaCl, 3.5mM KCl, 2.7mM $CaCl_2$, 10mM Tris.HCl pH 8.5 |
| **BRB80 Lysis Buffer** | 80mM PIPES pH6.8, 1mM EDTA, 1mM $MgCl$, 150mM NaCl, 1% v/v NP40 |
| **RIPA Lysis Buffer** | 50 mM Tris HCl pH 6.8, 150 mM NaCl, 1 mM EDTA, 1 mM EGTA, 0.1% SDS, 0.5% Deoxycholic acid, 1% Triton X-100 |
| **IP150 Lysis Buffer** | 150mM NaCl, 1mM EDTA, 1mM DTT, 0.5% (v/v) Triton-X-100, 50mM HEPES, 10% (v/v) Glycerol, pH 7.5 |
| **5x Laemmlli Sample Buffer** | 300mM Tris pH 6.8, 25% v/v glycerol, 10% w/v SDS, 0.01% w/v bromophenol blue, 25% v/v β-mercaptoethanol, made up to volume with $dH_2O$ |
| **Resolving Gel Buffer** | 1.5M Tris.HCl pH 8.8, made up to volume with $dH_2O$ |
| **Stacking Gel Buffer** | 0.5M Tris.HCl pH 6.8, made up to volume with $dH_2O$ |
| **For a 1mm thick 15% polyacrylamide resolving gel (25ml for 4 gels)** | 12.50ml of Ultra-Pure ProtoGel® 30% (w/v) Acrylamide, 6.25ml resolving gel buffer, 250µl 10% w/v SDS, 5.7ml $dH_2O$, 250µl 10% w/v ammonium persulfate (APS), 25µl |

| | N, N, N, N'-tetra methylethylethylnediamine (TEMED) |
|---|---|
| **For a 1mm thick 10% polyacrylamide resolving gel (25ml for 4 gels)** | 8.33ml of Ultra-Pure ProtoGel® 30% (w/v) Acrylamide, 6.25ml resolving gel buffer, 250$\mu$l 10% w/v SDS, 10ml dH$_2$O, 250$\mu$l 10% w/v ammonium persulfate (APS), 25$\mu$l TEMED |
| **For a 1mm thick 6% stacking gel** | 1ml 30% acrylamide, 1.25ml stacking gel buffer, 50$\mu$l 10% w/v SDS, 3ml dH$_2$O, 30$\mu$l 10% w/v APS, 15$\mu$l TEMED |
| **10x Running Buffer Stock (10L)** | 300g Tris, 1440g Glycine, made to volume with dH$_2$O |
| **Running Buffer (1L)** | 100ml 10x Running Buffer Stock, 10ml 10% w/v SDS, made up to volume with dH$_2$O |
| **Transfer Buffer (2L)** | 200ml 10x Running Buffer Stock, 400ml Methanol, made to volume with dH$_2$O |
| **Tris-buffered saline (TBS) (1L)** | For 20X stock: 48.46g Tris, 160.16g NaCl, 30ml HCl, up to volume with dH$_2$O |
| **TBS-T** | 1X TBS, 0.1% v/v TWEEN-20, made up to volume with dH$_2$O |
| **Blocking Buffer** | 5% w/v non-fat dry milk (Marvel) in TBS-T |
| **PBS (1L)** | For 25X stock: 200g NaCl, 5g KCl, 5g KH$_2$PO$_4$, 28.6g Na$_2$HPO$_4$ up to volume with dH$_2$O |
| **PBD-T** | 50ml 1X PBS, 0.5g BSA, 500$\mu$l DMSO, 250$\mu$l Triton-X-100 |
| **Fish gelatin** | 27.5ml fish gelatin (Sigma, #G7765), 7.5g Sucrose, up to 50ml with dH$_2$O |
| **Coomassie Stain** | 50% Methanol, 10% Glacial acetic acid, 40% H$_2$O, 3g/L Coomassie Brilliant Blue R250 |

### 2.2. General zebrafish methods

All zebrafish maintenance and experiments were performed at the Bateson Centre or Sheffield Institute for Translational Neuroscience (SITraN), University of Sheffield. All procedures were conducted in accordance with the Animal Scientific Procedures Act (ASPA) 1986, under the authority of both project and personal licences granted by the Home Office, UK.

#### 2.2.1. Wild-type strains

All zebrafish stocks were kept in tanks at 28°C on a 14-hour light, 10-hour dark cycle at the Bateson Centre, University of Sheffield. The wild-type line AB was used for all zebrafish procedures unless otherwise stated in the protocols.

#### 2.2.2. Zebrafish breeding and embryo collection

Zebrafish were marbled or paired the previous afternoon in order to stimulate the production of embryos at the start of the light-dark cycle. Embryos were collected the morning after marbling or pairwise mating. Following this, embryos were reared in E3 embryo medium and kept at 28°C up to 5 days post fertilisation (dpf), maximum.

#### 2.2.3. Fin biopsies

Fin biopsies were taken at >3 months for genotyping. A 96-well plate was prepared with approximately 200µl of aquaria system water in each well. Fish were put in 200ml of Tricaine solution (4.2ml tricaine per 100ml aquaria system water) to anaesthetise them. Once anaesthetised, individual fish are removed from the solution and a small section of the tail is cut with scissors. Fish are put into a tank to recover from the anaesthetic. The fin clip is placed in one well of the PCR plate and the tank is labelled with the corresponding number of the well to allow for identification.

#### 2.2.4. Dechorionating zebrafish embryos

The removal of the chorion was performed at 24hpf. Using a light microscope for guidance, forceps were used to manually pull the chorion apart and release the embryo. Dechorionated embryos were then kept in E3 embryos medium at 28°C until required.

### 2.3. General molecular biology techniques

#### 2.3.1. Making LB broth and LB agar plates

Sterile LB broth (10g/L Tryptone, 5g/L Yeat extract, 10g/L NaCl) (Fisher Scientific) was made by resuspending 25g of LB broth powder in 1L of distilled water (dH₂O). Additionally, sterile LB agar (10g/L Tryptone, 5g/L Yeat extract, 10g/L NaCl, 15g/LAgar) (Fisher Scientific) was made by resuspending 40g of LB agar powder in 1L of dH₂O. The mix was then autoclaved and allowed to cool for around 30 minutes. 50μg/ml of the appropriate antibiotic was added to the LB agar in sterile conditions. The LB agar solution was poured into 10cm petri dishes and allowed to set at RT, before being stored at 4°C.

#### 2.3.2. Preparation of glycerol stocks

Single colonies from LB agar plates were picked and grown in 5ml of LB broth with 50μg/ml of the appropriate antibiotic. These were left overnight on a shaker at 37°C. To make the glycerol stock, 500μl of the bacterial culture and 500μl of sterile 50% glycerol was mixed in a microcentrifuge tube. All glycerol stocks were stored at -80°C.

#### 2.3.3. Preparation and purification of plasmid DNA

To obtain plasmid DNA, E.coli colonies containing the plasmid of interest were picked and grown in 5ml LB broth containing 50μg/ml of the appropriate antibiotic. These were then left overnight at 37°C on a shaker. The next day, these were centrifuged at 4000 x g for 10 minutes in order to pellet the bacterial cells. Plasmid DNA was then extracted using the NucleoSpin® Plasmid DNA, RNA and protein purification kit (Macehery Nagel), following manufacturer's instructions.

#### 2.3.4. Quantification of plasmid DNA

Plasmid DNA was quantified using the NanoDrop Spectrophotometer ND-1000 (NanoDrop Technologies, Wilmington, USA). The NanoDrop was initiated with 1μl of nuclease free water. Subsequently, it was then blanked with 1μl of the elution buffer used in the NucleoSpin® Plasmid DNA, RNA and protein purification kit. To assess concentration, 1μl of sample plasmid DNA was then tested.

### 2.4. Cloning of zebrafish C9orf72 (C13H9orf72)
#### 2.4.1. Zebrafish C13H9orf72 plasmids

**Table 2.2 Zebrafish C13H9orf72 plasmids.**

| Plasmid name | Construct | Insert Size | Vector Backbone | Cloning strategy |
|---|---|---|---|---|
| *myc-C13H9orf72* | C13H9orf72 | 1389bp | pci-neo | Subcloned as NotI/XhoI PCR fragment from pDNR-LIB |
| *GST-C13H9orf72* | C13H9orf72 | 1389bp | pGEX-6p-1 | Subcloned as NotI/XhoI PCR fragment from pCI-neo |

#### 2.4.2. Site-Directed Mutagenesis of C13H9orf72 construct
##### 2.4.2.1. QuickChange lightning site-directed mutagenesis kit

The QuickChange lightning site-directed mutagenesis kit (Agient Technologies, #210518-5) was used in order to modify the C13H9orf72 construct. Primers used are shown in table 2.3. For this, the following reaction was prepared: 5μl of 10x reaction buffer; 1.9μl (25ng) of dsDNA template; 1.25μl (125ng) of oligonucleotide primer #1 and #2 (100ng/μl stock); 1μl of dNTP mix; 1.5μl of QuickSolution reagent; made up to 50μl final volume with dH$_2$O. In addition, 1μl of QuickChange Lightning enzyme was added. The following cycling parameters were used:

| | |
|---|---|
| **Temperature** | 95°C for 2 minutes |
| **x18 cycles** | 95°C 20 seconds |
| | 60°C 10 seconds |
| | 68°C 30 seconds/kb of plasmid length |
| **Temperature** | 68°C 5 minutes |
| **Infinite hold** | 10°C |

**Table 2.3 Primers for site-directed mutagenesis of C13H9orf72 construct.**

| Name | Forward (5'-3') | Reverse (5'-3') |
|------|-----------------|-----------------|
| *C109T* | GGAACAGCCGCAAGTCTGAAG ATGAGAGCTGAT | ATCAGCTCTCATCTTCAGA CTTGCGGCTGTTCC |
| *C9plus2* | GCTGATGATACGTGTGCTCGTG GCAGGGTG | CACCCTGCCACGAGCACCG TATCATCAGC |

Following this, 2μl of DpnI restriction enzyme was added to each amplification reaction. The reaction was thoroughly mixed via pipetting up and down several times and a brief spin down. The reaction was then immediately incubated at 37°C for 5 minutes in order to digest the parental supercoiled dsDNA.

### 2.4.2.2. Molecular cloning of C13H9orf72

The QuickChange lightning site-directed mutagenesis kit suggests to transform XL-10 Gold® Ultracompetent cells (Agilent Technologies) with the mutagenesis reaction. However, the mutagenized plasmid contained a chloramphenicol resistance marker, and these *E.coli* are resistant to both chloramphenicol and tetracycline, therefore an alternative strain of competent cells had to be used. OneShot® TOP10 competent *E.coli* (ThermoFisher Scientific) were instead transformed. OneShot® TOP10 competent *E.coli* were stored long-term at -80°C and for transformations, aliquots were thawed on ice for approx. 10 minutes. To 25μl of these competent cells, 2μl of the mutagenesis reaction was added and the mixture left on ice for 30 minutes. After this time, the competent cells were heat shocked for 45s at 42°C and subsequently placed on ice for a further 2 minutes. Following this, 250μl of LB broth was added and the mixture incubated at 37°C for 1 hour on a shaker. After 1 hour, the sample was centrifuged at 2500 x g for 2 minutes to pellet the bacterial cells. In sterile conditions, approx. 200μl of the LB broth was pipetted off and the pellet was then resuspended in the remaining LB broth. All of the resuspended pellet was spread on a LB agar plate containing 50μg/ml of the appropriate antibiotic in sterile conditions. Once dry, the plates were then incubated upside down at 37°C overnight to allow bacterial cultures to grow. Single colonies were picked from the bacterial plates and plasmid DNA prepared, purified and quantified as stated in sections 2.3.3 and 2.3.4. To sequence, 10μl of 100ng/μl of purified plasmid DNA made up in dH$_2$O was sent to the Core Genetics Service at the University of Sheffield, to ensure that

the mutagenesis had worked successfully. Once completed, the sequence data was analysed using Sequencher Demo Version 5.0.1 (Genecodes, USA).

### 2.4.3. Subcloning C13H9orf72 into pCI-neo-myc mammalian expression vector

#### 2.4.3.1. Producing a blunt ended PCR product using the Phusion® High Fidelity PCR kit

In order to subclone the construct into pCI-neo mammalian expression vector, flanking XhoI and NotI restriction enzyme sites were required. To do this, the Phusion® high fidelity PCR kit (NEB #E0553) was used, according to manufacturer's instructions, using primers containing the XhoI or NotI restriction sites (see table 2.4 below). Following this, 1µl of the reaction was run on a gel to ensure the product was the predicted size.

**Table 2.4 XhoI and NotI primer sequences.**

| Restriction cut site inserted | Primer sequence (5'-3') |
| --- | --- |
| XhoI | CTCGAGATGTCTTCAGCCTGTCCTCC |
| NotI | GCGGCCGCTCAGAAGTTGATGAGGAGG TCG |

#### 2.4.3.2. Zero blunt® TOPO® PCR cloning kit

Following high fidelity PCR, the blunt ended PCR product was subcloned into the pCR™-Blunt II-TOPO® Vector, using the Zero blunt® TOPO® PCR cloning kit, according to manufacturer's instructions. The reaction was then transformed in to XL-10 Gold® Ultracompetent cells as described below.

#### 2.4.3.3. Molecular cloning of C13H9orf72

XL-10 Gold® Ultracompetent cells were stored at -80°C and for transformations, aliquots were thawed on ice for approx. 10 minutes. To 25µl of these competent cells, 1µl of β-mercaptoethanol was added to improve transformation efficiency. To this, 3µl of the TOPO reaction was added and the mixture was left on ice for 30 minutes. After this time, the competent cells were heat shocked for 45s at 42°C and subsequently placed on ice for a further 2 minutes. Following this, 250µl of LB broth was added and the mixture incubated at 37°C for 1 hour on a shaker. After 1 hour, the sample was centrifuged at 3893 x g for 2 minutes to pellet the bacterial cells. In sterile conditions, approx. 200µl of the LB broth was pipetted off and the pellet was then resuspended in the remaining LB broth. All of the resuspended pellet was spread on a LB agar plate containing 50µg/ml of

the appropriate antibiotic in sterile conditions. Once dry, the plates were then incubated upside down at 37°C overnight to allow bacterial cultures to grow. Single colonies were picked from the bacterial plates and plasmid DNA prepared, purified and quantified as stated in sections 2.3.3 and 2.3.4. To sequence, 10μl of 100ng/μl of purified plasmid DNA made up in dH$_2$O was sent to the Core Genetics Service at the University of Sheffield. Once completed, the sequence data was analysed using Sequencher Demo Version 5.0.1 (Genecodes, USA).

### 2.4.4. Restriction digests using XhoI and NotI

The C13H9orf72 construct was digested using XhoI and NotI. For this, the following reaction was set up: 2ug C13H9orf72 construct; 0.5ul XhoI; 0.5ul NotI; 1x fast digest buffer (made from 10x stock solution) in dH$_2$O and digested for 10 minutes at 37°C. Pre-cut pCI-neo vector was used (courtesy of Emma Smith), cut using XhoI and NotI fast digest enzymes (Thermo Fisher Scientific, Delaware, USA).

### 2.4.5. DNA extraction from agarose gel

To separate linear DNA fragments following restriction digest, agarose gel electrophoresis was used. All of the sample was loaded on to a 1% agarose (Melford, UK) gel, containing 2μl Ethidium Bromide (EtBr) per 100ml agarose gel. Samples were loaded adjacent to 3μl of Hyperladder I (Bioline). Gels were run in DNA electrophoresis tanks (Geneflow, UK) in 1x TAE buffer. Samples were visualised using a UV transilluminator and DNA bands of the desired size were cut manually using a scalpel. The DNA was then extracted and purified using the GenElute™ Gel Extraction Kit (Sigma), according to manufacturer's instructions. The amount of purified DNA was quantified using a NanoDrop spectrophotometer ND-1000 (Thermo Fisher Scientific, Delaware, USA).

### 2.4.6. Ligation of DNA fragments

To ligate the purified DNA fragment and linearized pCI-neo vector (as described in section 2.4.4 and 2.4.5), the Quick Ligation™ kit was used (#M2200, NEB). For this, 50ng of vector was combined with a 3-fold molar excess of insert. To this 10μl of 2X Quick Ligation buffer was added to the mix, followed by 1μl of Quick T4 DNA ligase. Volume was adjusted to a total of 20μl with dH$_2$O. The mixture was centrifuged briefly and left at RT for 10 minutes. Following this, 1μl of ligation mix was transformed into XL-10 Gold® Ultracompetent cells (as described in section 2.4.3.3).

### 2.4.7. Colony screening

Following transformation, a colony PCR was used to screen for successful ligations in the transformed *E.coli* colonies. Single colonies were picked using a sterile p200 tip, re-streaked on an LB agar plate containing 50μg/ml of the appropriate antibiotic (see section 2.4.7.1) and then incubated in 10μl of PCR reaction mix; 6μl of nuclease-free (NF)-water, 2μl of 5x FIREPol® master mix with 7.5mM $MgCl_2$ (Solis BioDyne), 1μl of 10μM T7 EEV forward primer (Sigma), 1μl of 10μM T3 reverse primer (Sigma). The following cycling parameters were used:

| | |
|---|---|
| **Lid temperature** | 110°C |
| **Temperature** | 95°C for 5 minutes |
| **30x conventional cycles** | 95°C for 40 seconds |
| | 57°C for 45 seconds |
| | 72°C for 2 minute 30 seconds |
| **Temperature** | 72°C for 10 minutes |
| **Infinite hold** | 10°C |

5μl of each sample was loaded on to a 1.5% agarose (Melford, UK) gel, containing 2μl Ethidium Bromide (EtBr) per 100ml agarose gel. Samples were loaded adjacent to 3μl of Hyperladder I (Bioline, UK). Gels were run in DNA electrophoresis tanks (Geneflow, UK) in 1x TAE buffer. Samples were visualised using the gel imager GENi (Syngene, UK). Selected colonies with the correct construct size were picked from the re-streaked bacterial plates (see section 2.4.7.1) and plasmid DNA prepared, purified and quantified as stated in sections 2.3.3 and 2.3.4. To sequence, 10μl of 100ng/μl of purified plasmid DNA made up in $dH_2O$ was sent to the Core Genetics Service at the University of Sheffield. Once completed, the sequence data was analysed using Sequencher Demo Version 5.0.1.

### 2.4.7.1. Re-streaking bacterial plates

Alongside running the colony PCR as described in section 2.4.7, the single *E.coli* colonies picked for screening were also re-streaked on a new LB agar plate, containing 50μg/ml of the appropriate antibiotic, for further use. A grid with numbers was taped to the bottom of the plate. When a colony was picked, it was streaked across a number and then placed into a well containing the PCR mix, with the same number. This meant that colonies which produced positive results during screening could be identified in the future.

### 2.4.8. Subcloning C13H9orf72 into a pGEX-6p-1-GST expression vector

For the TnT® Quick Coupled Transcription Translation Binding assay (see section 2.10), the C13H9orf72 construct had to be subcloned into the pGEX-6p-1 GST expression vector (GE Healthcare Life Sciences). To do this the C13H9orf72 construct was cut using XhoI and NotI as described previously in section 2.4.4. Following this the digested product was run on an agarose gel and purified as described previously in section 2.4.5. The C13H9orf72 construct was ligated with the pre-cut pGEX-6p-1 GST expression vector and transformed into XL-10 Gold® Ultracompetent cells, as described in section 2.4.6. Following this, single colonies were screened using colony PCR as described in section 2.4.7, using the programme below and primers detailed in table 2.5:

| | |
|---|---|
| **Temperature** | 94°C for 3 minutes |
| **Conventional cycle (30 cycles)** | 95°C for 40 seconds |
| | 57°C for 45 seconds |
| | 72°C for 1 minute 30 seconds |
| **Temperature** | 72°C for 10 minutes |
| **Infinite hold** | 10°C |

**Table 2.5 GST forward and reverse primers.**

| Name | Forward (5'-3') | Reverse (5'-3') |
|---|---|---|
| *GST* | GCTGGCAAGCCACGTTTGGTG | ATGTGTCAGAGGTTTTCACCG |

Selected colonies with the correct insert size (1389bp) were picked from the re-streaked bacterial plates (see section 2.4.7.1) and plasmid DNA prepared, purified and quantified as stated in sections 2.3.3 and 2.3.4. To sequence, 10μl of 100ng/μl of purified plasmid DNA made up in $dH_2O$ was sent to the Core Genetics Service at the University of Sheffield. Once completed, the sequence data was analysed using Sequencher Demo Version 5.0.1 (Genecodes, USA).

### 2.5. Methods for targeted genome-editing in zebrafish

In order to generate *C13H9orf72* LOF zebrafish, two modes of targeted genome editing were used: transcription activator-like effector nucleases (TALENs), to target coding exon 7, and Clustered Regularly Interspaced Short Palindromic Repeats (CRISPR) and CRISPR-associated (Cas) gene 9 (CRISPR/Cas9), to target coding exon 1. Target sites were designed in both exon 1 and exon 7, to produce LOF mutations in both isoforms or just the long isoform respectively of zebrafish C9orf72. It would not be possible however to generate a zebrafish with LOF mutations affecting only the short isoform, as the entire sequence for the short isoform is included in the long isoform.

#### 2.5.1. TALENs

TALENs were previously generated and microinjected by Dr Andrew Grierson prior to the start of the current project. The TALEN site used was as follows (spacer region underlined):

TATATTTCAGGACGTGAT<u>gcacaaagacacgcttgtg</u>AAGTCTTTCATAGATGA

#### 2.5.2. CRISPR/Cas9 target site design

The CRISPR/Cas9 genome editing system was used in order to produce targeted insertion and/or deletion (INDEL) mutations in exon 1 of zebrafish *C9orf72 (C13H9orf72; zgc: 100846)*. The guide RNA (gRNA) antisense oligonucleotide sequence (5'-3') was as follows (Integrated DNA technologies):

*AAAGCACCGACTCGGTGCCACTTTTTCAAGTTGATAACGGACTAGCCTTATTTTAA CTTGCTATTTCTAGCTCTAAAA*<u>CTCACTGAGCAGCAGCAACCC</u>**CTATAGTGAG TCGTATTA**CGC

with the gRNA scaffold shown in italics, the target sequence shown underlined and the T7 site shown in bold. The target sequence was adopted from (Hruscha et al.,2013).

#### 2.5.3. In vitro RNA transcription of the gRNA and nCas9 for microinjection

##### 2.5.3.1. gRNA in vitro RNA transcription

In order for direct *in vitro* transcription to occur, the $10\mu M$ of the custom gRNA antisense oligonucleotide was annealed to the $10\mu M$ T7 primer (TAATACGACTCACTATAG). Conditions were as follows: 95°C for 5 minutes, then cooled at room temperature overnight. The gRNA was then *in vitro* transcribed using the MEGAshortscript-T7 kit (Ambion), following the manufacturer's protocol. The transcribed RNA was then

purified using the MEGAclear™ kit (Ambion), again following manufacturer's instructions. The concentration of gRNA produced was 108 ng/μl.

### 2.5.3.2. nCas9 in vitro RNA transcription

The nuclear Cas 9 (nCas9) plasmid (pCS2-nCas9n; Addgene #47929) was obtained from Addgene (Jao et al., 2013). For this protocol, purified nCas9 plasmid DNA was originally obtained from Mr Rich Lucas (SITraN), at a concentration of 3μg/μl. Firstly, the plasmid DNA was linearised using the NotI restriction enzyme (NEB) (30 units per 10μg of plasmid DNA) and left at 37° overnight. Following this, 1μl of linearised plasmid was loaded on a 1% agarose gel in comparison to the same volume of an undigested control to ensure the digestion had been successful. After linearization, the nCas9 mRNA was *in vitro* transcribed using the mMESSAGE mMACHINE kit (Ambion) following the manufacturer's instructions, using 1μg of linearised plasmid DNA as template. The transcribed RNA was then purified using the MEGAclear™ kit (Ambion) according the manufacturer's instructions.

### 2.5.4. Microinjection of CRISPR/Cas9 into zebrafish embryos

The injection mix was made with 1μl of RNA-grade phenol red dye, added to 5μl gRNA (540 ng/ul), 2μl nCas9 (6μg/ul) and up to 10μl final volume with NFW. Glass capillaries (World Precision Instruments) were pulled on a Model P-97 Flaming/Brown micropipette pulling machine (Sutter Instruments Co., USA) to produce capillary needles suitable for microinjection. The needle was placed in an Eppendorf containing the injection mix and the needle loaded by capillary action. The loaded capillary needle was placed in a micromanipulator (Leica Microsysems, Wetzlar, Germany). The needle was calibrated using a graticule so that two pulses injected a volume of 1nl. Zebrafish were paired the night before injection as described in section 2.2.2. The following morning fertilised, one-cell staged embryos were collected, as described in section 2.2.2. The embryos were placed on a 1% agarose gel mould and excess E3 buffer removed using a Pasteur pipette so the mould was dry to prevent the embryos moving during injection. They were then injected into the yolk sac with 2nl of the gRNA/Cas9 injection mixture using an air pressure injector, with final concentration of gRNA 108pg and Cas9 1.2ng (Narashige IM-300 gas line injector). Injected embryos were collected, placed in fresh E3 and incubated at 28°C. For each batch of injected embryos, a plate of un-injected embryos from the same pair was kept as a control. After 48 hours, a selection of injected embryos was collected for genotyping.

### 2.5.4.1. PCR analysis

DNA was extracted from injected embryos at 48 hpf as described in section 2.6.1. The resulting DNA was genotyped as described in section 2.6.4 using Exon 1 primers (see table 2.6).

## 2.6. Genotyping mutant lines
### 2.6.1. DNA extraction

To extract DNA for genotyping, single embryos or fin clips were placed in 30µl of QuickExtract™ DNA Extraction solution (Epicentre UK, #QE09050). Samples were then incubated at 65°C for 2 hours, 99°C for 2 minutes to terminate the reaction and held at 10°C.   DNA extract from fin clips was diluted 1:5 with nuclease-free water before use.

### 2.6.2. Genotyping primers

**Table 2.6 Genotyping primers.**

| Name | Forward (5'-3') | Reverse (5'-3') | Product size (bp) |
|---|---|---|---|
| *Exon 7 primer 1* | GCGCAGACGTACAA AATCAACGTCA | GCTTCCTCCGCTTT GGCCTTGA | 220 |
| *Exon 7 primer 2* | TGTAAAACGACGGC CAGTCGTCTCCAGTA ATGTCACGGT | ACACTACGCAGAG ACAGACCT | 492 |
| *-6 primer* | TACAGAGAACATGA GAGTCACTAACTAA | TGTAAAACGACGG CCAGTTCAAGGCC AAAGCGGAGGAA GC | 175 |
| *+6 primer* | TACAGAGAACATGA GAGTCACTAACTATT AC | TGTAAAACGACGG CCAGTTCAAGGCC AAAGCGGAGGAA GC | 181 |
| *Exon 1 primer* | TGCTTTGTGAGCCTG ACGGTCT | CGGCGTGCAGAGG CAGGTAG | 436 |

### 2.6.3. Detecting TALEN-induced mutations via restriction fragment length polymorphism (RFLP)

TALEN-induced insertion or deletion (INDEL) mutations were detected by RFLP analysis of an MslI site overlapping the TALEN target site. Loss of the MslI site indicates the presence of an INDEL mutation produced by the TALEN. Each PCR was prepared as a 10 µl reaction, including; 7.525µl of nuclease-free (NF)-water, 1µl of 10x Standard *Taq* Reaction Buffer (NEB #B90145), 0.2µl of deoxynucleotide (dNTP) solution mix (NEB #N64475), 0.1µl of 100mM Exon 7 primer 2 (forward), 0.1µl of 100µM Exon 7 primer 2 (reverse), 1µl of template DNA (diluted 1:5) and 0.075µl of *Taq* DNA polymerase (NEB #M0273S). The samples were then run using the following protocol:

| | |
|---|---|
| **Initial denature** | **94°C for 3 minutes** |
| **Touchdown (x15 cycles)** | 94°C for 30 seconds |
| | 65°C - 50°C for 45 seconds* |
| | 72°C for 1 minute 30 seconds |
| | ***decreases by 1°C per cycle** |
| **Conventional cycle ('n' cycles)** | 94°C for 30 seconds |
| | 58°C for 45 seconds |
| | 72°C for 1 minute 30 seconds |
| **Temperature** | 72°C for 10 minutes |
| **Infinite hold** | 10°C |

When using DNA extracted from fin clips 20 conventional cycles were used and when from embryos 40 conventional cycles were used. Once completed, 1µl of the restriction enzyme MslI (NEB #R0571L) was added to PCR product in each well. Samples were then incubated at 37°C for 12 hours and held at 10°C. After digestion, 5x DNA loading buffer (Bioline, UK, #37045) was added to each sample in order to monitor migration rate of the samples during electrophoresis. 5µl of each sample was loaded on to a 2.5% agarose (Melford, UK) gel, containing 2µl Ethidium Bromide (EtBr) per 100ml agarose gel. Samples were loaded adjacent to 3µl of Hyperladder IV (Bioline, UK) to enable estimation of fragment sizes every 100bp. Gels were run in DNA electrophoresis tanks (Geneflow, UK) in 1x TAE buffer. Samples were visualised using the gel imager GENi (Syngene, UK).

### 2.6.4. Detecting CRISPR/Cas9-induced mutations via restriction fragment length polymorphism (RFLP)

CRISPR/Cas9-induced insertion or deletion (INDEL) mutations were detected by RFLP analysis of an DdeI site overlapping the CRISPR/Cas9 target site. Loss of the DdeI site indicates the presence of an INDEL mutation produced by the CRISPR/Cas9. Each PCR was prepared as a 10 µl reaction, including; 6.8µl of nuclease-free (NF)-water, 2µl of 5x FIREPol® master mix with 7.5mM $MgCl_2$ (Solis BioDyne), 0.1µl of 100µM Exon 1 primer (forward), 0.1µl of 100µM Exon 1 primer (reverse) and 1µl of template DNA. The samples were then run using the following protocol:

| | |
|---|---|
| **Initial denature** | **94°C for 3 minutes** |
| **Touchdown (x15 cycles)** | 94°C for 30 seconds |
| | 65°C - 50°C for 45 seconds* |
| | 72°C for 1 minute 30 seconds |
| | **\*decreases 1°C per cycle** |
| **Conventional cycle ('n' cycles)** | 94°C for 30 seconds |
| | 58°C for 45 seconds |
| | 72°C for 1 minute 30 seconds |
| **Temperature** | 72°C for 10 minutes |
| **Infinite hold** | 10°C |

When using DNA extracted from fin clips 20 conventional cycles were used and when from embryos 40 conventional cycles were used. Once completed, the following mix was added to PCR product in each well:  7.75 µl of nuclease-free (NF)- water, 2 µl of CutSmart Buffer (Biolabs, #B7204S) and 0.25 µl DdeI (NEB, #RO175L). Samples were then incubated at 37°C for 12 hours and held at 10°C. After digestion, 10µl of each sample was loaded on to a 2.5% agarose (Melford, UK) gel, containing 2µl Ethidium Bromide (EtBr) per 100ml agarose gel. Samples were loaded adjacent to 3µl of Hyperladder IV (Bioline) to enable estimation of fragment sizes every 100bp. Gels were run in DNA electrophoresis tanks (Geneflow, UK) in 1x TAE buffer. Samples were visualised using the gel imager GENi (Syngene).

### 2.6.5. Sequencing

Sequence analysis was used to confirm that loss of the restriction site was due to TALEN- or CRISPR/Cas9-induced mutations at the target site. To amplify DNA for sequencing, the -6 primer (forward and reverse) and +6 primer (forward and reverse) were used for the TALEN lines (see table 2.6). The exon 1 primers (forward and reverse) were used for the CRISPR/Cas9 lines (see table 2.6). Each PCR was prepared as a 10μl reaction, including; 6.8μl of nuclease-free (NF)-water, 2μl of 5x FIREPol® master mix with 7.5mM $MgCl_2$ (Solis BioDyne), 0.1μl of the appropriate forward primer (100μM), 0.1μl of the appropriate reverse primer (100μM) and 1μl of template DNA. The PCRs were run using the PCR cycle detailed in sections 2.6.3 and 2.6.4. Once completed, 4μl of each PCR product was loaded on to a 2.5% agarose (Melford, UK) gel, containing 2μl EtBr per 100ml buffer. PCR products were loaded adjacent to 3μl of Hyperladder IV (Bioline UK) to enable estimation of fragment sizes every 100bp. Gels were run in DNA electrophoresis tanks (Geneflow, UK), in 1x TAE buffer. Products were visualised using the gel imager GENi (Syngene). DNA from the amplified PCR products are prepared for sequencing by ExoSAP, including: 0.05μl Exonuclease 1 (NEB, #M0293S), 1μl SAP (Affymetrix, #78390) and 3.95μl deionised water. The product was then incubated at 37°C for 45 min, 80°C for 15 min to terminate reaction and held at 10°C. PCR products were sequenced by the Core Genetics Service at the University of Sheffield. Once completed, the sequence data was analysed using Sequencher Demo Version 5.0.1 (Genecodes, USA). Subsequent analysis of the sequences was performed using ExPASy translate tool (http://web.expasy.org/translate/) and ClustalW2 (http://www.ebi.ac.uk/).

### 2.6.6. Real Time Quantitative Polymerase Chain Reaction (RT-qPCR)
#### 2.6.6.1. RT-qPCR primers

**Table 2.7 RT-qPCR primers.**

| Name | Forward (5'-3') | Reverse (5'-3') | Optimised concentration |
|------|-----------------|-----------------|-------------------------|
| *C13H9orf72 exon 9-10* | CCCTGACGCTGCTCA GATAC | TCCACCGTCAGGTCCA AATC | *2.5μM* |
| *EF1a* | GGATTGCCACACGGC TCACATT | GGTGGATAGTCTGAGA AGCTCTC | *5μM* |

#### 2.6.6.2. DNA extraction

From the lines raised, heterozygous carriers for the identified mutations were incrossed and offspring raised to 5 dpf. At 5 days, 24 larvae were collected and placed into individual 0.5ml tubes. Larvae were suspended in 15μl of Trizol reagent (Invitrogen) and incubated for 10 minutes at RT. The larvae were then homogenised using a handheld homogeniser, ensuring the homogeniser tips were cleaned between each larvae. Homogenised larvae were incubated at RT for 5 minutes. 3μl of chloroform was added to each sample and incubated at RT for 2 minutes. Samples were then centrifuged for 15 minutes at 12000 x g at 4°C. This leads to the formation of a lower organic phase (containing DNA and denatured proteins) and an upper aqueous phase (containing RNA). The upper aqueous layer was removed, placed into a sterile 0.5ml tube and snap frozen in liquid nitrogen. The upper aqueous layer was stored at -80°C until genotyping had been completed. To the lower organic phase 1μl of glycoblue (Ambion #AM9515) and 5μl of 100% ethanol was added. Samples were vortexed and centrifuged for 10 minutes at 15500 x g at 4°C. The resulting supernatant was discarded and the following mix was added to each pellet: 1μl of glycoblue (Ambion #AM9515), 1μl of 7.5M ammonium acetate, 14μl dH$_2$O and 15μl of 100% ethanol. The ammonium acetate and ethanol stabilise the nucleic acids via neutralising the backbone of the nucleic acids and by decreasing the dielectric constant. This makes the backbone stronger and less hydrophilic respectively. The samples were then incubated for 30 minutes at RT and subsequently centrifuged for 10 minutes at 16000 x g at RT. The supernatant was discarded, the pellet was washed in 15μl of 75% ethanol and then centrifuged for 10 minutes at 15871 x g at RT. The resulting

supernatant was removed and the pellet allowed to dry to complete the removal of ethanol. The pellet was then re suspended in 30μl dH$_2$O and stored at 4°C for genotyping.

### 2.6.6.3. Genotyping

The extracted DNA was genotyped as described in sections 2.6.3 or 2.6.4 depending on the lines being analysed. For the PCR cycle, 40 conventional cycles were used. Individual homozygous mutants and wild type siblings were identified for RNA extraction (see section 2.6.6.4).

### 2.6.6.4. RNA extraction

The upper aqueous layer collected from all identified homozygous mutants and identified wild type siblings were pooled together into two separate 0.5ml tubes. 0.5ml of isopropanol per 1ml of trizol was added to precipitate the RNA and incubated at RT for 10 minutes. The samples were then centrifuged for 10 minutes at 12000 x g at 4°C. The RNA precipitate formed a pellet at the side of the tube and the resulting supernatant was carefully removed. The pellet was washed with 1ml of 75% ethanol (made to volume with NFW) per 1ml of trizol, vortexed and centrifuged for 5 minutes at 12000 x g at 4°C. The supernatant was removed and the pellet allowed to air dry. The pellet was then re suspended in 10μl of NFW before it was quantified using a NanoDrop spectrophotometer ND-1000 (Thermo Fisher Scientific, Delaware, USA).

### 2.6.6.5. Reverse transcription and complementary DNA (cDNA) synthesis

1-2μg of RNA was added to a 0.2ml tube with 1μl of DNAse buffer (Invitrogen), 1μl of DNAse (NEB #M03035) and made up to 10μl with NFW. Samples were then incubated at 37°C for 10 minutes. The reaction was terminated by adding 1μl of 25mM EDTA pH 8.0 and incubating at 75°C for 10 minutes. Following this, 2μl of 25mM dNTP mix (NEB #N64475) and 1μl of oligo(dT)$_{18}$ (Thermo Scientific #S0132), which primes the polyA tail and ensure amplification of spliced mRNA only, was added and incubated at 65°C for 5 minutes. The sample was then chilled on ice for 5 minutes and collected by brief centrifugation. To each sample, 4μl of 5x first strand buffer (Invitrogen) and 2μl of 0.1M dithiothreitol (DTT) (Invitrogen) was added. Samples were incubated at 25°C for 5 minutes before adding 0.5μl of Superscript II (Invitrogen). Samples were then maintained at 25°C for a further 5 minutes, 50°C for 50 minutes and 70°C for 15 minutes to terminate the reaction. cDNA samples were stored at -20°C.

### 2.6.6.6. RT-qPCR

Prior to performing RT-qPCR, primer concentrations were optimised and reaction efficiency determined via using a standard curve. All RT-qPCR primers and their optimised concentrations are detailed in table 2.7. RT-qPCR was performed using the Stratagene Mx3000P™ Real Time Thermal Cycler (Agilent Technologies Ltd) and MxPro v4.10 software. The cDNA samples were amplified in triplicate 20µl reactions using 10µl 2x Brilliant-II ultrafast SYBR® green qPCR master mix (Agilent technologies #600882), 2µl of forward primer and 2µl of reverse primer (at their optimised concentration – see table 2.7), 1µl cDNA and made up to a final volume of 20µl with dH$_2$O. Cycling conditions were as follows: 95°C for 10 min to denature followed by 35 cycles of 95°C for 30 s, 60°C for 1 min. Levels of mRNA were quantified relative to EF1α mRNA levels according to the ΔΔC$t$ method.

### 2.7. Characterisation of mutant lines
#### 2.7.1. Survival monitoring

To monitor survival of the numerous lines, heterozygous mutant carriers were incrossed (as described in section 2.2.2), producing offspring with a mixture of genotypes (approx. 25% wild-type, 25% homozygous and 50% heterozygous for the inherited mutation). The larvae were raised in tanks containing up to 60 fish. The tanks were checked twice a day up to 21dpf. Dead fish were collected and genotyped (as described in sections 2.6.3 and 2.6.4). A Kaplan–Meier survival plot was generated using Prism v6 software (Graphpad Software, USA).

### 2.7.2. Methods to examine motor function
#### 2.7.2.1. Swimming endurance test

Critical swimming speed ($U_{crit}$), which is the maximum velocity a zebrafish can maintain for a set time, was measured using a custom-built swim tunnel apparatus as described in Plaut., 2000 and Ramesh et al., 2010. Adult zebrafish were individually introduced into the water flow chamber. The water current flow rate started at 6.58 cm/min. The adult zebrafish were then subjected to this flow rate for 5 minutes. The flow rate was then increased in 6.58 cm/min increments every 5 minutes. This was done until either 30 minutes had been reached, at a maximum flow rate of 39.47 cm/sec, or until the zebrafish could no longer swim and fell into a mesh net at the end of the water flow chamber. If fatigued, the zebrafish were given another opportunity to re-enter the highest achieved flow rate by pausing the time, reducing flow and slowly increasing the flow rate back to the fatigue velocity. If the zebrafish could still no longer swim in this current, the time was recorded when the zebrafish stopped swimming. $U_{crit}$ was calculated based on the following formula as previously described in Ramesh et al., 2010, Brett., 1964, Plaut., 2000: $U_{crit}=U_i + (U_{ii}T_i/T_{ii})$, where $U_i =$ the highest velocity maintained for a whole interval (cm/sec), $U_{ii} =$ the velocity increment (6.58 cm/sec), $T_i =$ the time elapsed at fatigue velocity (minutes) and $T_{ii} =$ the time interval (5 minutes).

#### 2.7.2.2. Spinning task

An alternative method to observe swimming endurance in our pilot cohort was the Spinning Task (Blazina et al. 2013). This test was conducted in a 1L beaker, which contained 800 mL of system water and a magnetic stir bar. The beaker was placed on a magnetic stirrer and placed within an opaque box to avoid external interference. Adult zebrafish were individually placed in the beaker and allowed to habituate for 2 minutes. Following this, the stirrer speed was gradually increased until the desired speed was

obtained. The individual zebrafish were subjected to speeds of 400 rotations per minute (rpm) and 500 rpm. The water current generated by the magnetic stirrer produces a visible whirlpool. A stopwatch was used to measure the swimming time, defined as the time taken for the zebrafish to be swept into the whirlpool at each speed.

### 2.7.3. Methods to examine behaviour

All behavioural analysis was performed between 13.00h-17.00h, using the equipment and related software included in the ViewPoint analysis suite (ViewPoint Life Science, Lyon, France). All analysis was done within a soundproof box, in the light and when possible the experimenter was located outside the area to avoid any interference with the behavioural responses.

#### 2.7.3.1. Novel tank diving test

In order to measure anxiety levels in adult zebrafish, the novel tank diving test was employed as described in (Parker et al. 2014). The test was carried out in trapezoid tanks (17cm height $\times$ 27.3cm top $\times$ 24cm bottom $\times$ 10.2cm width) which were filled with system water from the main aquarium supply. For consistency, system water was taken from the aquarium the zebrafish were originally housed in. Prior to the test, the zebrafish were transported into the behavioural test room and allowed to habituate for 1 hour to acclimatise to test room conditions. Each adult zebrafish was individually placed into the novel tank and immediately filmed over a 5-minute time period. During this time, the duration of time spent in the bottom half of the tank and total distance travelled was recorded. The filming and analysis was carried out using the ViewPoint system. After the test, the zebrafish were placed back into the holding tank. The water in the testing tank was changed after each individual fish, to control for possible odour cues left by the previous individual. Statistical analysis performed on R3.3.2 for windows, using a one-way ANOVA with repeated measures. Graphs show mean ± standard deviation, unless otherwise stated, and this was performed using GraphPad Prism 7.

#### 2.7.3.2. Open field analysis

The open field analysis was designed to be conceptually similar to the rodent open field test, in order to measure thigmotaxis. Thigmotaxis was initially measured in a rectangular tank (26.3cm length $\times$ 16.6cm width $\times$ 15.3cm height) filled with system water to a height of 10cm. The outer zone was defined as the region 6 cm from the edge of the tank, and the time spent in this zone was determined. From 13-months onwards, thigmotaxis was measured in a white opaque polypropylene circular tank (27.5cm height $\times$ 20.5cm

diameter) filled with system water to a height of 10cm. The outer zone was defined as the region 5 cm from the edge of the tank, and the time spent in this zone was determined. Prior to the test, the zebrafish were transported into the behavioural test room and allowed to habituate for 1 hour (as mentioned in section 2.5.3.1). Zebrafish were individually placed into the centre of the arena and filmed for a total of 6 minutes using the ViewPoint system, with the first 1 minute discounted for acclimatisation. Each behavioural session was filmed by a camera placed above the open field apparatus. During recording time, the duration of time spent in the periphery of the arena, duration of time spent in the centre and total distance travelled was recorded. Following the test, the zebrafish were gently netted back to a holding tank. The water in the testing arena was changed after each individual fish, for reasons described in section 2.5.3.1. Temporal analysis (per minute) of the percentage of time spent in the periphery of the open field apparatus (i.e. thigmotaxis) was calculated in the following way: *Thigmotaxis (% time spent in the periphery) = (Time spent in the periphery (s) / Time spent in the periphery + centre (s)) * 100*. Graphs show mean ± standard deviation, unless otherwise stated, and this was performed using GraphPad Prism 7.

### 2.7.4. Staining adult zebrafish muscle
#### 2.7.4.1. Collection, fixing and sectioning of adult muscle

11-month adult zebrafish were terminally anaesthetized in tricaine. Muscle was dissected using micro dissection tools under the microscope and subsequently fixed overnight in 4% PFA at 4°C. The tissue was then washed 3-5 times in 1ml of $dH_2O$ to wash away any remaining PFA. Muscle tissue was embedded in fish gelatine and snap frozen on dry ice, before being stored at -80°C. Before snap freezing, the position of the embedded tissue was confirmed under the microscope and a line drawn on the mould to aid orientation during sectioning. In each block, 1 piece of muscle was embedded. Serial 16μm cryostat sections of the tissue were performed on the Leica CM3050S cryostat, with both objective temperature (where the block is mounted) and chamber temperature set to -30°C. Sections were collected on silane-coated microscope slides (CellPath) and stored at -80°C until needed. Muscle sections were taken as lateral sections in order to give the best neuro-muscular junction (NMJ) structures for staining and imaging.

#### 2.7.4.2. Immunostaining of muscle samples

Immunostaining of NMJs in adult muscle tissue was performed using synaptic vesicle 2 (SV2 – a presynaptic marker) and α-bungarotoxin (BTX – a post synaptic NMJ marker).

The samples were allowed to air dry at RT for 2 hours, after being removed from -80°C. Sections were rehydrated 3x 5mins in PBD-T. The sections were then blocked using PBD-T with 5% normal goat serum (NGS) for 30 minutes. Following this, sections were incubated for 30 minutes in PBD-T containing 5% NGS along with alexa 488 conjugated α-bungarotoxin (molecular probes, 1:100, #B14322). After incubation, the sections were washed 3x 15mins in PBD-T. Sections were then incubated with the anti-SV2 antibody (Developmental Studies Hybridoma Bank, 1:50 of supernatant) in PBD-T with 5% NGS overnight at 4°C. The following day, the samples were washed 6x 15mins in PBD-T and incubated in AlexaFluor-568 donkey anti-mouse secondary antibody (Invitrogen, 1:200) in PBD-T with 2% NGS at 4°C overnight. The sections were then washed 6x 15mins in PBD-T and the slides then mounted with VectaShield Hardest with DAPI (Vector labs). Sections were imaged at 5μm intervals using confocal microscopy (TCS Sp5 2, Leica). Following this, z-stacks were generated using Image J Software (National Institute of Health). Intensity correlation quotient (ICQ) (Li et al. 2004) and pre- and post-synaptic area were determined using the intensity correlation analysis and particle analysis plugins for ImageJ.

### 2.7.5. Collection, fixing and measuring of adult zebrafish spleens

24-month adult zebrafish were terminally anaesthetized in tricaine. Spleens were dissected using micro dissection tools under the microscope and subsequently fixed overnight in 4% PFA at 4°C. The tissue was then washed 3-5 times in 1ml of dH$_2$O to wash away any remaining PFA. Images of the spleens were taken using a light microscope and the area of each spleen was subsequently calculated using Image J Software (National Institute of Health).

### 2.8. Autophagic flux assay
#### 2.8.1. Drug treatments for autophagic flux assay

Embryos were collected as stated in section 2.2.2. At 2 dpf, 10-30 dechorionated embryos were incubated in 5ml of each of the treatments detailed in table 2.8 below for 24 hours at 28°C. Treatments were made in a volume of 10ml and made up to volume using E3 embryo medium, with a 2% final DMSO concentration. Following drug treatment, dechorionated embryos were transferred into chilled 1.5ml tubes in order to prepare lysates (see section 2.9.1)

**Table 2.8 Drug treatments for autophagic flux assay.** Information adapted from (Klionsky et al. 2012).

| Treatment | Stock concentration | Working concentration | Effect |
|---|---|---|---|
| DMSO (Sigma) | n/a | 2% | Control (no effect on the autophagy pathway) |
| Torin-1 (Tocris) | 1mM | 1$\mu$M | Potent and selective MTOR inhibitor resulting in the induction of autophagy |
| Trehalose (Sigma) | n/a | 2% | Induces autophagy in a MTOR-independent manger via activation of AMPK |
| Rapamycin (Fisher Bioreagents) | 1mM | 100nM | Inhibits MTOR via binding RAPTOR, resulting in the induction of autophagy |
| INK128 (Cayman Chemicals) | 2mM | 250nM-1$\mu$M | This compound is a rapalog (synthetic drugs that are analogues of rapamycin), thus induces autophagy in the same way as rapamycin |
| Ridafiromilus (APExBIO) | 2mM | 250nM-1$\mu$M | This compound is a rapalog (synthetic drugs that are analogues of rapamycin), thus induces autophagy in the same way as rapamycin |
| AZD8055 (LKT Lab) | 2mM | 250nM-1$\mu$M | This compound is a rapalog (synthetic drugs that are analogues of rapamycin), thus induces autophagy in the same way as rapamycin |
| Temsirolimus (Cayman Chemicals) | 2mM | 250nM-1$\mu$M | This compound is a rapalog (synthetic drugs that are analogues of rapamycin), thus induces autophagy in the same way as rapamycin |
| Bafilomycin (LKT Lab) | 100$\mu$M | 100nM | A V-ATPase inhibitor, which neutralises lysosomal pH and ultimately prevents autophagosome-lyosome fusion, resulting in autophagy inhibition |
| Ammonium Chloride (Acros Organics) | 1M | 100mM | Neutralises lysosomal pH, which results in autophagy inhibition |
| Chloroquine (Sigma) | 500mM | 50$\mu$M | Neutralises lysosomal pH, which results in autophagy inhibition |

### 2.9. Preparation of lysates for western blotting
#### 2.9.1. Collecting tissue from zebrafish embryos < 5dpf

Prior to protein extraction, zebrafish embryos < 5dpf must be deyolked. It is essential to remove the yolk sac before immunoblotting, as it is enriched with the protein Vitellogenin, which can cause overloading effects whilst blotting (Mathai, Meijer and Simonsen 2017, Link, Shevchenko and Heisenberg 2006). Firstly, dechorionated embryos were placed in a 1.5ml tube, to which 1ml of embryo deyolking buffer was added. A p1000 was used to pipette the zebrafish embryos up and down in order to disrupt the yolk sac. Once all yolk sacs had been disrupted, the deyolking buffer was removed and replaced with 1ml of embryo washing buffer. Following this each tube was centrifuged at 13000 x g for 2 minutes in embryo washing buffer. Embryo washing buffer was removed from the resulting pellet, ready for homogenisation (see section 2.9.3)

#### 2.9.2. Collecting tissue from zebrafish > 5dpf

Prior to protein extraction, zebrafish > 5dpf were prepared for lysis. As there is no yolk sac at this age, protein was extracted from the heads of fish > 5dpf, which were removed using a sterile scalpel before being placed into a 1.5ml tube ready for protein extraction. Tissue was kept on ice at all times to prevent degradation.

#### 2.9.3. Protein extraction method

For protein extraction, collected tissue (via either method described in 2.9.1 and 2.9.2) was homogenised in a lysis buffer. For embryos, the final volume of BRB80 lysis buffer added was equal to 2µl of lysis buffer per embryo. For the tissue collected from zebrafish > 5dpf, a total of 40µl of RIPA lysis buffer was added to each head.  Firstly, the lysis buffer minus detergent was added and the tissue was homogenised for 30 seconds using a handheld homogeniser (Anachem Ltd, UK). Once homogenised, an equal volume of lysis buffer containing 2x concentration of detergent (either NP40 or Triton-X-100) was added and samples were lysed on ice for 30 minutes. 1x of a 100x stock of protease inhibitor cocktail (PIC) (Thermo Scientific) was added to the lysis buffer. Following lysing, samples were then centrifuged at 18 000 x g for 20 minutes at 4°C.

#### 2.9.4. Protein concentration assay

The total protein concentration of each sample was quantified using the Bio-Rad protein assay, following the manufacturer's protocol. The pheraSTAR FS plate reader (BMG Labtech) was used to measure the absorbance of each sample at a wavelength of 595nm, and the total protein concentration was calculated by comparing values with the known concentrations of bovine serum albumin (BSA) standards. Once the concentrations of the

samples were established, appropriate dilution volumes of 5x laemmlli buffer and deionised water were added to the samples.

### 2.10. Western blotting
### 2.10.1. SDS-polyacrylamide gel electrophoresis (PAGE)

SDS-page was carried out using the Bio-Rad mini-PROTEAN® tetra system. Approximately 25μg of each sample was loaded onto either a 10% or 15% (*w/v*) polyacrylamide resolving gels with a 6% (*w/v*) stacking gel. 3μl of Precision Plus Protein™ all blue standard (Bio-Rad) was run adjacent to the samples as a marker. The samples were electrophoresed at 100V in running buffer, until the dye front reached the bottom of the gel.

### 2.10.2. Immunoblotting

Once SDS-PAGE was complete, proteins were transferred electrophoretically for 1 hour at 100V. For autophagic flux assays, proteins were transferred onto an immun-blot® PVDF membrane (Bio-Rad), which needed to be activated by methanol beforehand. Everything else was transferred onto nitrocellulose unless otherwise stated. Transfer of protein to the membrane was verified via reversible staining with Ponceau S stain (0.1% ponceaux, 5% acetic acid, made to volume with deionised water). Membranes were washed with deionised water and blocked in blocking buffer for 1 hour at RT. The membranes were then incubated with the appropriate primary antibody, diluted in blocking buffer for 1 hour at RT (or at 4°C overnight). Membranes were washed three times with TBS-T for a total of 30 minutes. The membranes were then incubated in secondary antibody, conjugated to horseradish peroxidase (HRP) and diluted in TBS-T for 1 hour at RT. This was again followed by washes, as described.

Antibody binding was detected by using enhanced chemiluminescence (ECL; Thermo Scientific, #34080), following the manufacturers protocol. Images were obtained either by using the G:box (Syngene) or by exposing films in a dark room. In the dark room, the membrane was placed in an autoradiography cassette and exposed on Amersham hyperfilm ECL (GE Healthcare) for an appropriate length of time. The film was then immersed in 1x Ilford multigrade developer (Harman technology Ltd) for 1 min, rinsed in water and then placed in 1x Ilford hypam fixer (Harman technology Ltd) for a further 2 min. The film was then again rinsed in water and allowed to dry at RT. Films were scanned using the CanoScan LiDE 60 scanner (Canon) and semi-quantitative densitometry was performed using ImageJ.

### 2.10.3. Antibodies for western blotting

**Table 2.9 Primary and Secondary Antibodies for Western Blotting.**

| Antibody | Host species | Specificity | Dilution | Company |
|---|---|---|---|---|
| *Primary Antibody* | | | | |
| Anti-LC3 (NB100-2331) | Rabbit | Between residues 25-121 of human LC3 protein | 1:500 | Novus biologicals |
| Anti-LC3 (NB100-2220) | Rabbit | Between residues 1-100 of human LC3 protein | 1:1000 | Novus biologicals |
| DM1a (T9026) | Mouse | α-tubulin | 1:1000 | Sigma |
| Anti-actin (#MAB1501) | Mouse | Highly specific to vertebrate actin | 1:5000 | Millipore |
| p62/SQSTM1 (PM045) | Rabbit | Recombinant human p62 (120-440aa) | 1:500 | MBL |
| Anti-C9orf72 (SC-138763) | Rabbit | Internal region of C9orf72 of human origin | 1:250 | Santa Cruz |
| Anti-C9orf72 (HPA023873) | Rabbit | Recombinant Protein Epitope Signature Tag (PrEST) antigen Sequence, corresponding to residues 110-281(human) | 1:250 | Sigma ATLAS |
| Anti-C9orf72 (22637-1-AP) | Rabbit | C9orf72 fusion protein ag18326, corresponding to residues 1-310 (human) | 1:250 | ProteinTech |
| *Secondary antibody* | | | | |
| Anti-Rabbit immunoglobulin/HRP (P0448) | Goat | Rabbit immunoglobulins | 1:5000 | Dako |
| Anti-mouse immunoglobulin/HRP (ab97040) | Goat | Mouse immunoglobulins | 1:5000 | Abcam |

## 2.11. TnT® Quick Coupled Transcription Translation Kit
### 2.11.1. Transforming Rosetta™ Competent Cells

Rosetta™ pLysS Competent Cells were transformed with the pGEX6p1 vector containing either zebrafish C13H9orf72 (see section 2.4.8) or human C9orf72L. The human C9orf72 construct was obtained from glycerol stocks produced by Dr Chris Webster, SITraN. Rosetta pLysS cells were removed from -80°C and thawed on ice for 10 minutes prior to transformation. 500 ng of pGEX6p1 control, pGEX6p1-C13H9orf72 or pGEX6p1-hC9orf72L plasmid DNA was transformed in to 80μl of Rosetta™ pLysS Competent Cells. The transformation and heat shock protocol was performed as described previously (see section 2.4.3.3). After 1 h at 37°C, bacteria were plated onto LB-ampicillin/chloramphenicol agar plates. Ampicillin resistance is conferred by the pGEX6p1 vector, while chloramphenicol resistance is conferred by the T7 lysozyme plasmid carried by the Rosetta pLysS cells.

### 2.11.2. Inoculation of start-up culture for TnT® Quick Coupled Transcription Translation Binding assay

50ml of terrific broth (TB), supplemented with ampicillin and chloramphenicol, was inoculated with multiple colonies from the agar plates. These were incubated overnight on a shaker at 37°C.

### 2.11.3. Inducing expression of GST protein

To 750ml of TB, 50μg/ml of ampicillin was added. Chloramphenicol was not added as this can inhibit protein translation. In a cuvette, 1ml of broth was taken as a blank for the $OD_{600}$ reading, which measures cell density, on the S1200 Diode Array Spectrophotometer (WPA). Following this, bacteria from the start-up culture were added to the broth, until the $OD_{600}$ reached an optimal 0.05. At this point, a glycerol stock was made (as detailed in section 2.6.2) and stored at -80°C. The inoculated cultures were then left on a shaker at 37°C and $OD_{600}$ measured every 30 minutes. When culture reached $OD_{600}$ 0.7 and the bacteria were in the exponential growth phase, 300mM of IPTG was added directly to the culture at 37°C to induce expression of the protein of interest from the pGEX6p1 vector. This was left on a shaker at 37°C for 3 hours. The post-induction broth was poured into 500ml Beckman Tubes and centrifuged at 4000rpm for 15 mins at 4°C to form bacterial pellets (Avanti J-26 XP centrifuge, Beckman Coulter, JA-10 rotor).

### 2.11.4. TnT® Quick Coupled Transcription Translation Binding assay

The following reaction mix was made in a 1.5ml Eppendorf using the T7 quick system (TnT® Quick Coupled Transcription/Translation System, Promega, L1170): 8μl of

reticulocyte lysate mix, 500ng in 1.5ml of the DNA template (ATG13), 0.5µl $^{35}$S-Methionine and nuclease-free water up to a final volume of 10µl. This reaction was set up for each interaction to be investigated. The mix was then incubated at 30°C for 1.5 hours. During incubation, 0.1g of the GST bacterial cell pellet or 0.25g of the GST-C9 bacterial pellets weighed out in an individual Eppendorf. 1ml of RB100 lysis buffer (25 mM Hepes (pH 7.5), 100 mM KOAc, 10 mM $MgCl_2$, 1 mM DTT, 0.05% Triton X-100, 10% (vol/vol) glycerol) was added to each bacterial pellet and sonicated at 99% amplitude for 5s, followed by 20s on ice. This was repeated 3 times overall and the bacteria were incubated at 4°C for 1 hour. During this time, 30µl of Glutathione Sepharose High performance (GSH) beads (GE healthcare, UK) per reaction tube were washed in RB100 lysis buffer. Following lysis, the bacteria were centrifuged at 17 000 x g for 5 minutes at 4°C. 1ml of the cleared bacterial lysate was added to the pre-washed GSH beads and incubated at 4°C for 1 hour on a roller. Following this, the beads were washed 3x using RB100 buffer to remove any unbound GST proteins and finally re suspended in 400µl of RB100. Approx. 8-9µl of the *in vitro* translated radiolabelled ATG13 protein was added to each reaction and incubated at 4°C for 1 hour on a roller. The beads were then washed 3x in 1ml RB100 and GST proteins were eluted from the beads in 40µl Elution Buffer (50 mM Tris-HCl (pH 7.5), 100 mM NaCl, 40 mM reduced glutathione) for 10 minutes at RT.

### 2.11.5. Preparing samples for SDS-PAGE and detection

For input controls, 0.5µl of pure reticulocyte was added to 15.5µl of elution buffer and 4µl 5x laemmli. For the GST control, 1µl of the eluted GST was added to 15µl of elution buffer and 4µl of 5x laemmli. For samples of interest, 16µl of the eluted protein was added to 4µl of 5x laemmli. The expression of the GST control is higher than the GST-tagged proteins of interest, and also binds to the GSH beads with a higher affinity. For this reason, less GST control sample was loaded compared to the proteins of interest. Samples were given a pulse spin and boiled at 100°C for 5 minutes before loading. All samples were run on an appropriate percentage stacking/resolving gel and run at 100V until the dye front had run off the gel. The gel was then stained with coomassie and subsequently de-stained. The de-stained gel was then dried using a BioRad Gel Dryer (Model 583). To detect radioactivity, the dry gel was placed in a cassette with a phosphoscreen for 4-7 days, depending on the signal (which was checked using a Geiger

Counter). The signal was then detected using a GE healthcare Typhoon FLA7000 phosphoimager.

# 3. Generation of C13H9orf72 loss-of-function zebrafish models of ALS/FTD

## 3.1. Introduction

Amyotrophic lateral sclerosis (ALS) is a progressive neurodegenerative disease characterised by the degeneration of upper- and lower- motor neurons, resulting in weakness and eventual paralysis of nearly all of the muscles. It is known that approximately 90% of all cases are sporadic and 10% are familial. By studying familial ALS cases, over 30 genes have been implicated in the pathogenesis of this disease (Peters, Ghasemi and Brown 2015b), highlighting the genetic heterogeneity of this disorder. Of particular importance was the identification that a non-coding $(G_4C_2)_n$ hexanucleotide repeat expansion, within intron 1 of *C9orf72,* was the most common cause of ALS responsible for approximately 40-50% of all fALS cases and 8-10% of sALS (DeJesus-Hernandez et al. 2011, Renton et al. 2011, Gijselinck et al. 2012). It is unknown how the repeat expansion causes C9-ALS, however there is evidence for three possible, non-exclusive pathogenic mechanisms. Reduced levels of C9orf72 mRNA in patients has been reported, suggesting C9orf72 loss-of-function (LOF) via haploinsuffiency may be causative in C9-ALS. Alternatively, pathogenic mechanisms may involve a toxic gain-of-function (GOF) of the repeat containing transcripts via RNA toxicity and/or repeat-associated non-ATG (RAN) translation into aggregation-prone, dipeptide repeat (DPR) proteins (C9RAN proteins).

Developing *in vivo* models recapitulating C9-ALS is essential in order to further elucidate the pathomechanisms which underlie this disorder and to aid in evaluating the potential efficacy of novel therapies. One way in which this can be achieved is with the development of zebrafish models. Zebrafish hold several characteristics which make it an advantageous model to use in the study of neurodegenerative disorders such as ALS. It is a low-cost vertebrate system, which produces a large number of offspring, with a short generation time and a conserved, yet simplified, vertebrate nervous system (Babin et al. 2014). Importantly, its genome is fully sequenced and we know there is high homology between many human ALS-linked genes and the corresponding zebrafish orthologue. Importantly, there is 68.55% nucleotide identity and 76.14% amino acid identity between human *C9orf72* and the zebrafish orthologue (zgc: 100846). Therefore, it is expected that the functional role of C9orf72 is likely to be similar in zebrafish and humans, thus disease mechanisms are expected to be conserved. In addition, the potential to genetically

manipulate genes with a variety of techniques in zebrafish makes it a powerful genetic tool for studying disease.

This study focuses on whether haploinsuffiency of *C9orf72* results in the development of ALS and in order to investigate this, methods leading to both transient and stable loss of C9orf72 can be utilised. Previously, antisense morpholinos oligonucleotides (AMOs) have been utilised to transiently knock down (KD) both isoforms of the zebrafish *C9orf72*, resulting in both locomotor and axonal deficits (Ciura et al. 2013), which is consistent with the aetiology of ALS. Despite promising results, data from AMO knockdown should be treated with caution. The technology has various limitations, ranging from its transient efficacy to its potential for off-target effects. Regarding the latter point in particular, the same group that published the C9orf72 morpholino phenotype previously reported that morpholino-mediated knockdown of *tardbp,* the gene encoding TDP-43, resulted in motor neuron axonopathy in zebrafish embryos (Kabashi et al. 2010b). However, subsequent groups have not managed to recapitulate this effect (Schmid et al. 2013, Hewamadduma et al. 2013) indicating that in some situations the phenotypic changes observed in morpholino studies may be due to off-target effects, as previously discussed.

ALS is principally an adult onset disorder in humans, therefore it is essential to use a complementary approach to the AMOs in order to study the adult phenotype in zebrafish. As such, this present study aimed to generate stable lines of zebrafish carrying LOF mutations in *C9orf72,* using targeted genome editing techniques. Additionally, as a LOF mutation has been reported in one ALS case (Liu et al. 2016), it is especially important to use *in vivo* models to further investigate this. The highly conserved zebrafish orthologue is predicted to encode two different protein isoforms, which in humans includes; a long protein isoform encoding a 481 amino acid protein, and a short protein isoform encoding a 222 amino acid protein which lacks a number of exons encoding the c-terminus of the protein. It is unclear whether these isoforms have different functions, therefore target sites were designed in both exon 1 and exon 7, to produce LOF mutations in both isoforms or just the long isoform respectively of zebrafish C9orf72. It would not be possible however to generate a zebrafish with LOF mutations affecting only the short isoform, as the entire sequence for the short isoform is included in the long isoform, represented in figure 1.2.

Originally, transcription activator-like effector nucleases (TALENs) were used to target both exon 1 and 7 of zebrafish *C9orf72,* in order to produce LOF mutants by either nonsense or frameshift mutations. It was also desirable that these mutations would either disrupt a restriction enzyme cut site and therefore be detected by restriction fragment length polymorphism (RFLP) analysis, or alternatively, be large enough to genotype easily throughout the process. However, TALENs initially failed to produce such mutations in exon 1. Therefore, exon 1 was targeted again utilising the CRISPR/Cas9 system, which has been shown to transmit mutations in *C9orf72* successfully through the germline, with low off-target effects in zebrafish (Hruscha et al. 2013). The effect of the identified mutations were characterised at the ribonucleic acid (RNA) level and successful LOF mutants taken forward for further characterisation of the ALS phenotype (chapter 4).

### 3.2. Generating *C13H9orf72* loss of function models using transcription activator-like effector nucleases (TALENs)
#### 3.2.1. Comparisons between human *C9orf72* and the zebrafish orthologue

The zebrafish *C9orf72* orthologue (*C13H9orf72*) is highly conserved and shares 68.55% nucleotide identity with the human gene. Zebrafish only have one copy of *C13H9orf72*, there is no gene duplication. The zebrafish orthologue (ENSDART00000015127.6) has 10 exons in total, 9 of which are coding exons, with a total length of 17.24 kb (figure 3.1a). Transcript length is 2.427 kb and translation length 462 amino acids (aa). The human gene (ENST00000619707.4) has 11 exons in total,10 of which are coding exons, with a total length of 27.32 kb (figure 3.1b). Transcript length is 3.339 kb and translation length 481 aa.



**A) *Danio rerio*** (ENSDART00000015127.6)

17.24 kb
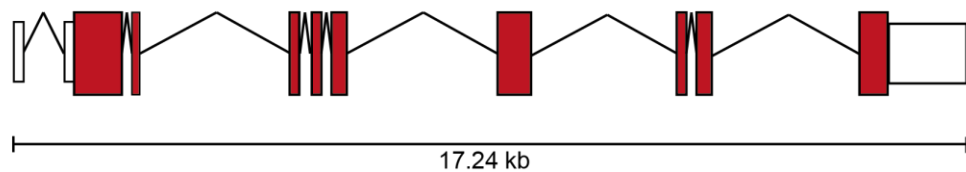
**B) *Homo sapiens*** (ENST00000619707.4)

27.32 kb

■ Coding exon
□ Non-coding exon/UTR
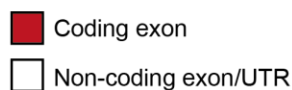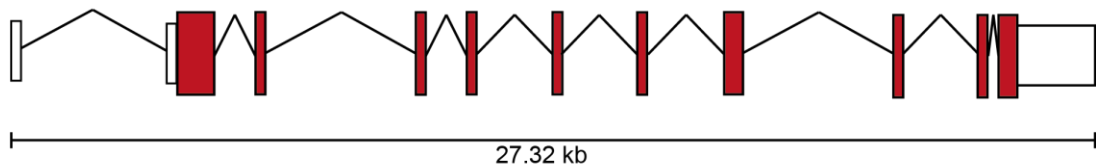
**Figure 3.1 Diagram of human *C9orf72* and the zebrafish orthologue.** Schematic diagram representing A) zebrafish (*Danio rerio*) *C13H9orf72* and B) human (*Homo sapiens*) *C9orf72*.

Protein sequences, obtained from ensembl, for both human *C9orf72* and the zebrafish orthologue indicate that the missing coding exon in zebrafish corresponds to human exon 3, as indicated by the protein alignment (figure 3.2). This could be because ensembl did not predict the existence of exon 3 in zebrafish based on homology for the zebrafish orthologue of *C9orf72,* therefore this region was excluded. However, it may also be that fish species do not harbour this exon in *C9orf72*.

```
Danio rerio 1-462      MSSACPPQSPAVAKTEVLVDDCCPVLAATFAYWDNILGPRVRHIWAPKSQGLLLLSDGEV
Homo sapiens 1-481     MSTLCPPPSPAVAKTEIALSGKSPLLAATFAYWDNILGPRVRHIWAPKTEQVL-LSDGEI
                       **:.*** ********: :.. .*:*********************:: :* *****:

Danio rerio 1-462      TFLANHTLNGEILRSAESGAVDVKFFVLAEKGVIIVSLIFDGELKGDKNTCALSIILPQS
Homo sapiens 1-481     TFLANHTLNGEILRNAESGAIDVKFFVLSEKGVIIVSLIFDGNWNGDRSTYGLSIILPQT
                       **************.*****:*******:**************: :**:.* .*******:

Danio rerio 1-462      ELSFYLPLHAVCVERLKHVIRKGRICMQK--------------------GYNIISMLSSE
Homo sapiens 1-481     ELSFYLPLHRVCVDRLTHIIRKGRIWMHKERQENVQKIILEGTERMEDQGQSIIPMLTGE
                       ********* ***:** *:****** *:*                    * .**.**:.*

Danio rerio 1-462      IVPIMELLTSMKKHSVPEEVDLKDTVLNDDDIGDSCHEDFLHKAISSHLQTCGCSMVVGS
Homo sapiens 1-481     VIPVMELLSSMKSHSVPEEIDIADTVLNDDDIGDSCHEGFLLNAISSHLQTCGCSVVVGS
                       ::*:****:***.******:*: **************.** :***********:****

Danio rerio 1-462      NPEKVNKIVLTLCLFLTPAERKCSRLCHPDGSFKYDTGLFVQGLLKDSTGSFVFPYRQVL
Homo sapiens 1-481     SAEKVNKIVRTLCLFLTPAERKCSRLCEAESSFKYESGLFVQGLLKDSTGSFVLPFRQVM
                       ..******* ****************..:.****::*****************:*:***:

Danio rerio 1-462      YSPYPTTHIDVDINTVKQMPPCHEHTYHQRRYMRAELSALWKAASEDDFSSDNLINAQDS
Homo sapiens 1-481     YAPYPTTHIDVDVNTVKQMPPCHEHIYNQRRYMRSELTAFWRATSEEDMAQDTIIYTDES
                       *:**********:*********** *:******:**:*:*:*:**:*::.*.:* :::*

Danio rerio 1-462      YTPDLNIFQDVMHKDTLVKSFIDEVFLLKPGLSLRSVYLSHFLLLLHRKALTLLRYIEDE
Homo sapiens 1-481     FTPDLNIFQDVLHRDTLVKAFLDQVFQLKPGLSLRSTFLAQFLLVLHRKALTLIKYIEDD
                       :**********:*:*****:*:*:** ********.:*::***:********::****:

Danio rerio 1-462      TQKGKKPFRSLRNLKTDLDLTVEGDLNIIMAMAEKLRAGLHSFVFGKSFLTSVQERDLLI
Homo sapiens 1-481     TQKGKKPFKSLRNLKIDLDLTAEGDLNIIMALAEKIKPGLHSFIFGRPFYTSVQERDVLM
                       ********:****** *****.*********:***::.*****:**:.* *******:*:

Danio rerio 1-462      NF
Homo sapiens 1-481     TF
                        .*
```

**Figure 3.2 Protein sequence alignment of human C9orf72 and the zebrafish orthologue C13H9orf72.** Protein sequences of the wild type human (Homo sapiens) *C9orf72* and the zebrafish (Danio rerio) orthologue *C13H9orf72* are shown. The online tool Clustal Omega was used to perform alignments of these protein sequences. The position of human exon 3 is shown in red, with the corresponding gap in zebrafish *C13H9orf72* also highlighted.

Firstly, to ensure that the sequencing data obtained from ensembl was correct and that this exon was in fact missing, RNA was extracted from wild-type AB zebrafish embryos. cDNA was synthesised via reverse transcription and the area surrounding this region was amplified via PCR and subsequently sequenced. It was identified that the ensembl sequence was correct and this exon was missing.

Following this, we investigated whether this region was missing in all fish orthologues of human *C9orf72*. A multiple sequence alignment was generated (figure 3.3). This alignment included protein sequences of all fish orthologues of *C9orf72*, as well as lamprey, human, rodent and bird. The region under investigation was highly conserved for the human, rodent and bird protein sequences. However, there was virtually no conservation between the mammals and other non-mammalian species investigated. There do appear to be a number of strongly hydrophobic amino acids encoded by this exon in all species, however in the context of the whole protein this region is not particularly hydrophobic. In six out of the ten fish orthologues this exon was missing. Since the lamprey, which is evolutionary ancestral to all the species investigated, has a non-conserved protein sequence in this region we suggest that during evolution the common ancestor of all fish species lost this exon, and then subsequently several fish species re-gained the exon, while others, including zebrafish, did not.

We are unclear what the role of exon 3 is in C9orf72 protein. The *C9orf72* gene in humans encodes two protein isoforms that share structural homology with the Differentially Expressed in Normal and Neoplasia (DENN) proteins and the long isoform of C9orf72 (C9-L, 462aa in length), is predicted to harbour all three domains: u-DENN residues 23-151; central DENN residues 212-322; d-DENN on c-terminus, exact location unpublished (Levine et al. 2013, Zhang et al. 2012). Exon 3 is located between the predicted u-DENN and central DENN domains, suggesting that this region may have a spacer role, regulating the distance between these two domains.

```
Zebrafish      ILPQSELSFYLPLHAVCVERLKHVIRKGRICMQK----------------------GYN
Lamprey        VLRLAPRPLCVRAHTLAAARLAHATRVLRVLMYKSRLCIVARPVILNATLM--FVQDSDN
Human          ILPQTELSFYLPLHRVCVDRLTHIIRKGRIWMHKERQENVQKIILEGTE---RMEDQGQS
Mouse          ILPQTELSFYLPLHRVCVDRLTHIIRKGRIWMHKERQENVQKIVLEGTE---RMEDQGQS
Rat            ILPQTELSFYLPLHRVCVDRLTHIIRKGRIWMHKERQENVQKIVLEGTE---RMEDQGQS
Chicken        ILPQSELAFYLPLHRVCVDRLTHIIRKGRIWMHKERQEHFQKIVLEGTE---RMEDQGQS
Amazon Molly   ILPQTELAFYLPLHAACVERLTHGIRKGRIWMQK---------------------GYN
Cave           ILPQSELNFYLPLHSVCVERLKHIVRKGRICMQK--------------------GYS
Cod            ILPQTELAFYLPLHAICVERFQHVIRKGRIWMQK--------------------GYN
Spotted Gar    ILPQTELSFYLPLHTVCVERLKHIIRKGRIWMQK--------------------GYN
Stickleback    ILPQTELPFYLPLHTVCVERLKHVIRKGRISMQK--------------------GYN
Fugu           ILPQTELAFYLPLHNICVERLKHVIRKGRIWMQKPRDECVGLCCIR-------KWLQGYN
Medaka         ILPQTELSFYLPLHAVCVDRLKHAVRKGRICMQKDLVLSVYVPELMTIGEYWNEDQPGFN
Tetraodon      ILPQTELAFYLPLHNICVDRLKHVIRKGRIWMQKKRLQNICLVTIRSLKS--IDYVQGYN
Tilapia        ILPQTELAFYLPLHTICVERLKHVIRKGRIWMQKVASTYRHLAL-----A--CTEEQGYN
               :*   :    : :   *   ..  *:  *    *    *:  *                  ..
```

**Figure 3.3 Multiple sequence alignment between wild-type zebrafish C13H9orf72 and orthologues from various species.** The online tool Clustal Omega was used to perform multiple sequence alignments of these protein sequences. The position of human exon 3 is shown in red, with the corresponding position in the various orthologues also highlighted.

### 3.2.2. Investigation of polymorphisms surrounding the target locus in exon 7

As discussed in section (2.6.3), to detect TALEN-induced genome modifications within exon 7 of *C13H9orf72,* restriction fragment length polymorphism (RFLP) analysis was utilised. Evidence of mutation was confirmed by the loss of MslI restriction enzyme cleavage, described in figure 3.4.
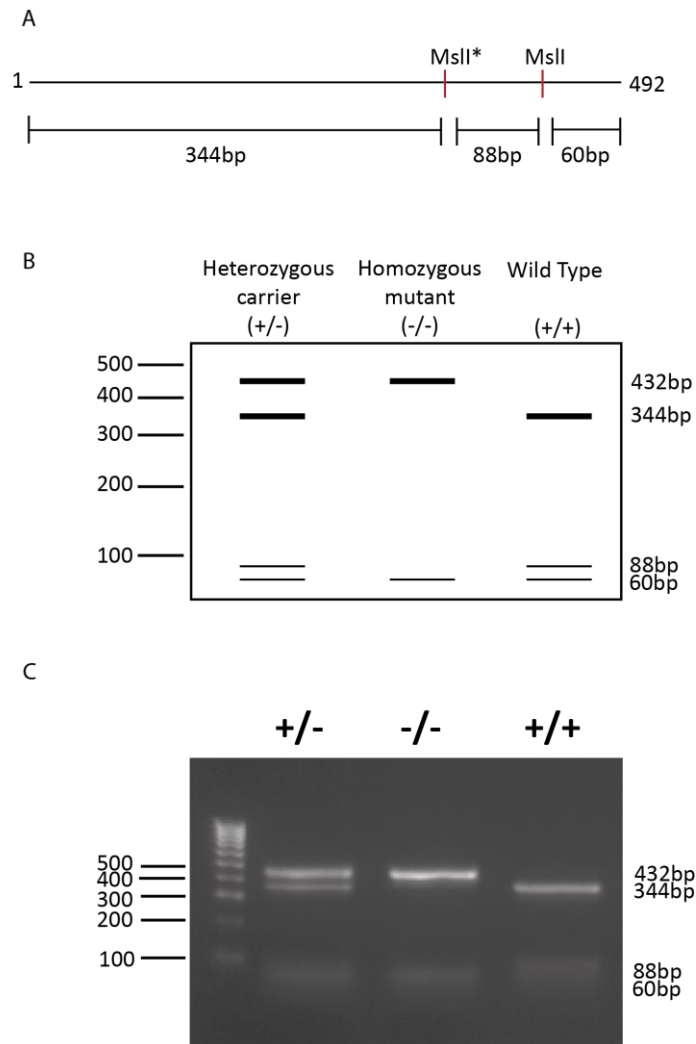


**Figure 3.4 Detection of mutation at exon 7 TALEN target site using restriction fragment length polymorphism (RFLP) analysis.** A) Schematic diagram representing the size of the amplified PCR product using the exon 7 primers (top) and the size of the fragments following restriction enzyme digest with MslI (bottom). B) Schematic representation of expected bands for homozygous mutants (432 and 60bp), wild-types (344, 88 and 60bp) and heterozygous carriers (432, 344, 88 and 60bp) product are run on an agarose gel. C) Image of an actual agarose gel showing product from all three genotypes. Bands at approximately 88 and 60bp are usually faint and hard to distinguish. However, the larger bands allow for accurate genotyping. Asterisk marks the MslI site within the TALEN spacer region.

Once loss of MslI cleavage was determined, sequence analysis was performed on undigested PCR product to confirm that this loss was due to a TALEN-induced insertion and/or deletion (INDEL) mutation at the target site, resulting in a frameshift.

Initially, PCR amplification in preparation for sequence analysis was performed using 'exon 7 primer 1' (table 2.6). However, it was found that this resulted in unreadable sequencing data, predominantely consisting of uncalled bases. As a result, 'exon 7 primer 2' (table 2.6) were designed. These were situated further from the TALEN spacer region, as it was possible the distance between the original primers and spacer region was too short, thus reading straight into the heterozygous region. However, the resulting sequencing data was still unreadable.

Further analysis of the sequencing data revealed the presence of two novel polymorphisms either side of the target site (figure 3.5). This included a six base pair INDEL (*TTACTA*) upstream of the TALEN spacer region, between coding exons 6 and 7. It also included a microsatellite situated downstream, a seven dinucleotide (14bp) stretch of GT, between coding exons 7 and 8. Both polymorphisms lay between the TALEN spacer region and the forward or reverse 'exon 7 primer 2', resulting in double sequence reads which were impossible to interpret.
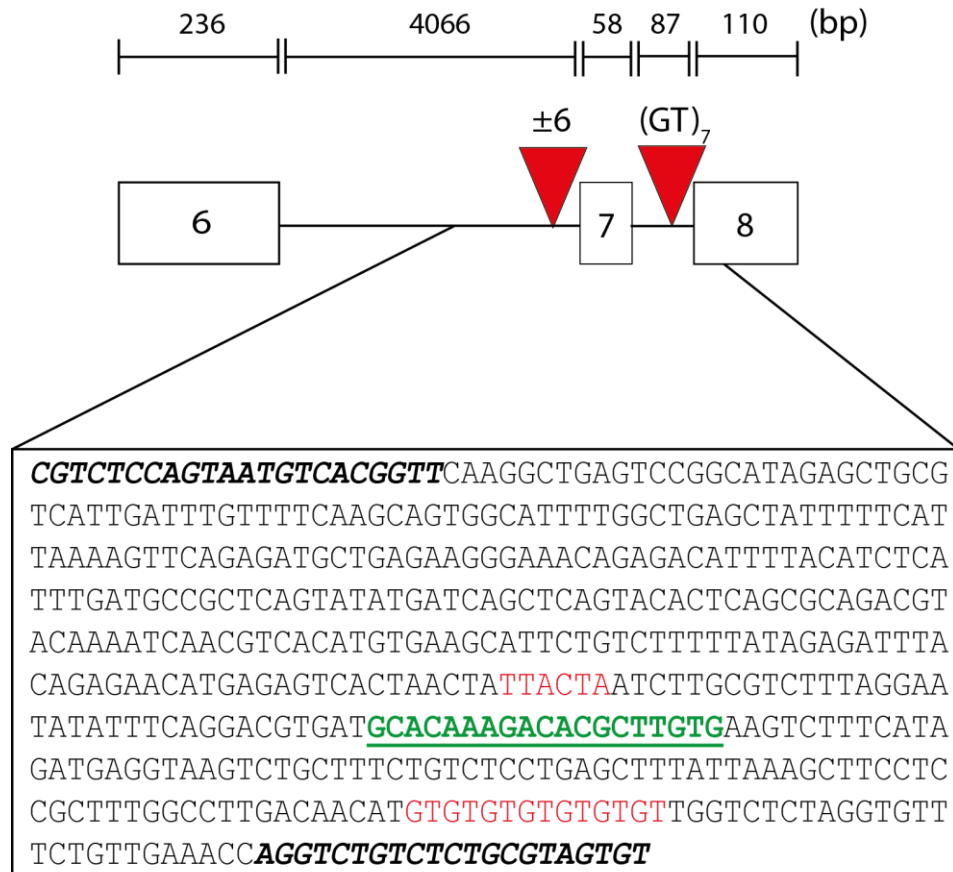
**Figure 3.5 Diagram detailing the position of the novel polymorphisms discovered surrounding the TALEN target site in exon 7.** The red arrows indicate the position of the polymorphisms. The six base pair INDEL lies between coding exons 6 and 7. Conversely the microsatellite lies between coding exons 7 and 8. The length of each intron and exon is represented (top). The text represents the diagram as the corresponding nucleotide sequence. Bold text indicates the 'exon 7 primer 2' sequences. Red text indicates the polymorphisms. Green text indicates the TALEN spacer region within coding exon 7 of *C13H9orf72*.

To allow the generation of readable sequence data, allele specific forward primers were designed so that the alleles with 6 bp deleted (termed the minus 6 allele; -6 – table 2.6) and those including the 6 bp (termed the plus 6 allele; +6 – table 2.6) could be amplified in separate PCR reactions. In addition, the reverse primer was designed to lie upstream of the microsatellite. Optimal conditions for these primers were determined using genomic DNA extracted from fin biopsies, which were confirmed to have the following genotypes; homozygous for minus 6 allele (-6/-6), homozygous for plus 6 allele (+6/+6) and heterozygous for both alleles (-6/+6). Using the PCR programme noted in section 2.6.3, optimal cycle numbers were identified as described in figure 3.6.
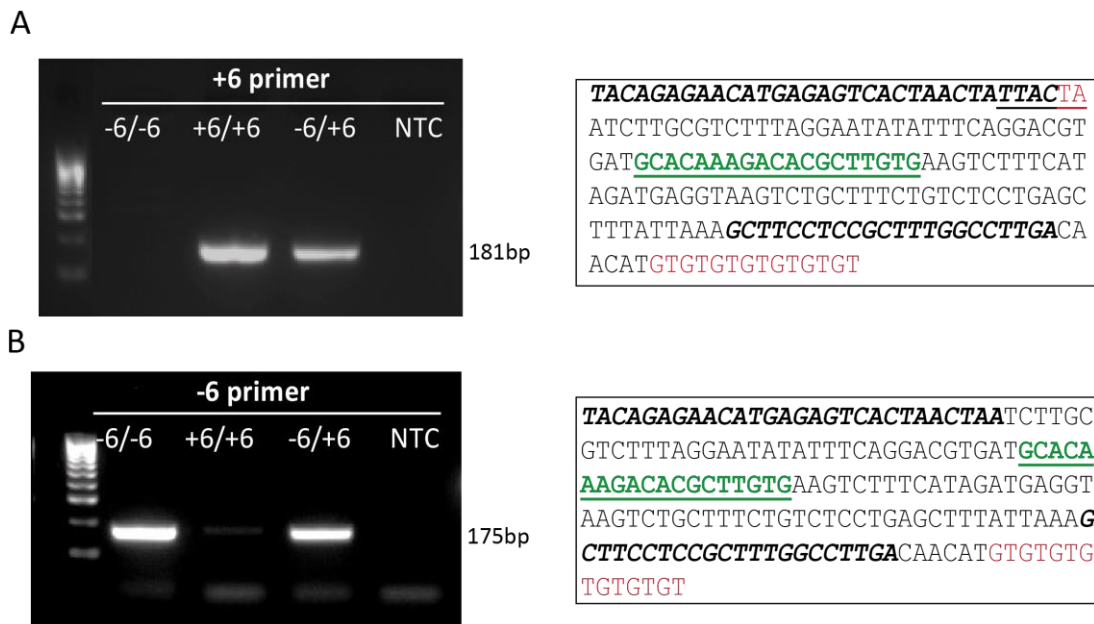


**Figure 3.6 Testing the allele specific primers.** PCR amplification of the genomic DNA extracted from fin biopsies with the following genotypes; -6/-6 (homozygous for minus 6 allele), +6/+6 (homozygous for plus 6 allele) and -6/+6 (heterozygous for both alleles) was performed. A) Shows the result using the 'exon 7 +6' primers. A product of 181bp is only present in samples with a +6 allele. The corresponding sequence is shown on the RHS. Primers are in black, polymorphisms are underlined or red, TALEN spacer region is green. B) Shows the result using the 'exon 7 -6' primers. A product of 175bp is only seen in samples with a -6 allele. The corresponding sequence is shown on the RHS. Colours are the same as previous. The cycle numbers optimised for use with the touchdown PCR were A) 25 cycles B) 20 cycles.

Subsequently, all PCR amplification in preparation for sequence analysis was performed using the allele specific primers throughout the genotyping process. As well as improving the quality of the sequencing data obtained, it revealed that all identified frameshift mutations were in linkage disequilibrium with the minus 6 allele.

### 3.2.3. Identification and raising mutant lines generated using TALENs

Initially, before the start of this project, fertilised, one-cell staged zebrafish embryos were successfully microinjected with the TALEN targeted against exon 7 of *C13H9orf72* and raised to adulthood (F0 founders). TALENs consist of a pair of DNA binding proteins fused to a fok1 nuclease. The pair bind opposite sides of the target site, separated by a spacer region of 14-20 nucleotides, within which fok1 cuts the DNA, resulting in a double stranded break (DSB) (Joung and Sander 2013). The cell responds to this with endogenous repair mechanisms such as homologous recombination (HR) and non-homologous end joining (NHEJ) (discussed in chapter 1, section 1.3.2). HR-directed DSB repair is mainly error-free, utilising the genetic information contained in the undamaged sister chromatid in a template (Li and Heyer 2008). Conversely, NHEJ is error-prone, involving direct ligation of the broken ends and can result in insertion and deletion (INDEL) mutations (Lieber 2010). In this study, we wanted to detect INDELs within the target site which produce frameshift mutations, as these will alter the position of the stop codon and most likely result in a non-functional protein.

For phenotypic characterisation of any TALEN-induced mutations to occur, zebrafish with mutations in germline cells needed to be generated. To achieve this, F0 founders transmitting frameshift mutations through the germline were identified. Fin biopsies were taken from F0 founders for screening, using methods described previously (section 2.6), identifying all those with evidence of somatic mutations within the target site. The selected zebrafish were subsequently outcrossed with wild-type AB zebrafish. The resulting offspring (F1) were screened and sequenced for evidence of TALEN-induced mutations within exon 7 of *C13H9orf72,* in order to determine germline transmission rate from the F0 founders. For this locus, out of the 9 F1 clutches screened, four were identified to carry mutations (44%).

F1 offspring produced from transmitting F0 founders were then raised to adulthood. Fin biopsies from all F1 offspring raised were screened and sequenced, in order to identify those heterozygous for frameshift mutations. Figure 3.7 summarises all the frameshift mutations identified.
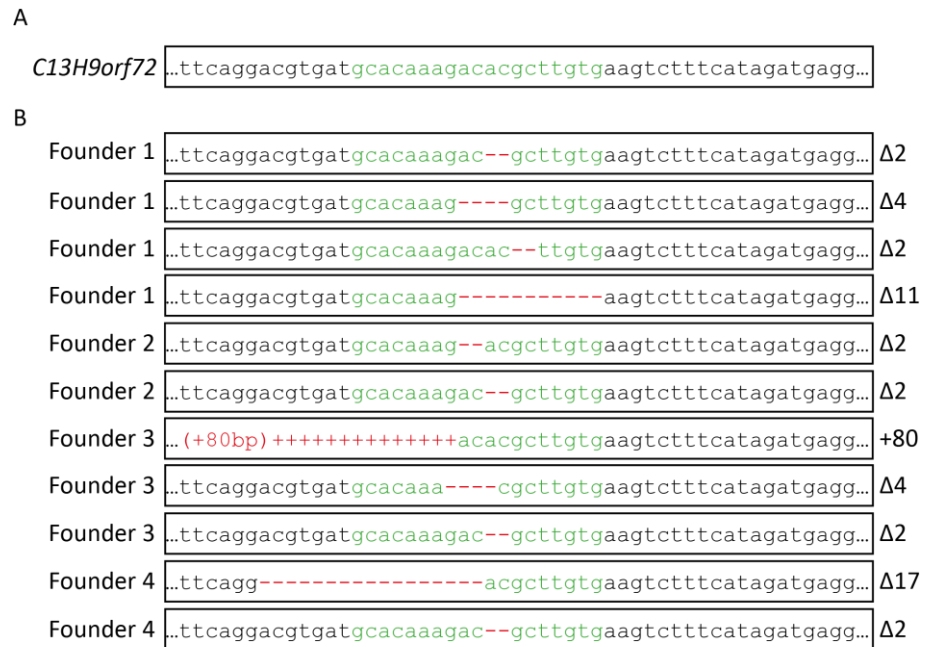
**Figure 3.7 Diagram detailing all frameshift mutations identified in F1 offspring.**
A) The wild-type *C13H9orf72* sequence (coding exon 7) (Ensembl: ENSDARG00000011837). Sequence highlighted in green is the TALEN spacer region. B) The sequences derived from the mutant F1 alleles of F0 founders 1, 2, 3 and 4, injected with the TALEN targeted against coding exon 7 of *C13H9orf72*. Sequence highlighted in green is the TALEN spacer region. Mutations are shown in red.

In order to produce a large batch with identical mutations, four F1 zebrafish identified as heterozygous carriers for frameshift mutations were selected, ensuring that the zebrafish chosen were each produced from a different F0 founder. The selected zebrafish were outcrossed with wild-type AB zebrafish. Figure 3.8 summarises the four F1 mutants outcrossed. The resulting offspring (F2) were raised to adulthood.
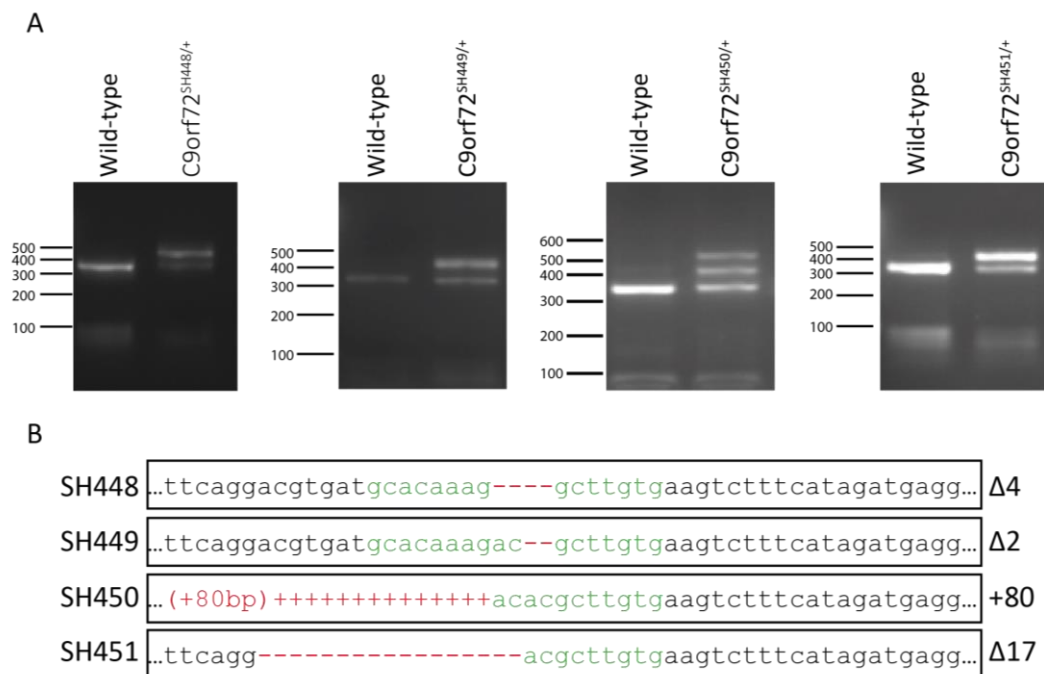


**Figure 3.8 Summary of F1 offspring heterozygous for frameshift mutations in exon 7 which were selected to outcross.** A) PCR amplification of the genomic DNA extracted from fin biopsies taken from F1 offspring SH448, SH449, SH50 and SH451 using exon 7 primers. Following digestion with MslI, the digested PCR product was run on a 2.5% agarose gel. Digested bands for each heterozygous carrier are compared to a wild-type sibling control.  B) Shows the corresponding mutations identified after sequencing. Sequence highlighted in green is the TALEN spacer region. Mutations are shown in red.

F1 offspring with these particular frameshift mutations were selected to be outcrossed, as they were predicted to result in truncated forms of the C13H9orf72 protein and it is expected that these are most likely to result in LOF mutations. An online translation tool, ExPASy, was used to translate the complementary DNA (cDNA) sequences of wild-type *C13H9orf72* and of the mutated *C13H9orf72* alleles as previously described (figure 3.8) in to the corresponding protein sequences. The online tool ClustalW2 was then used to perform multiple sequence alignments of these protein sequences (figure 3.9).

```
C13H9orf72    MSSACPPQSPAVAKTEVLVDDCCPVLAATFAYWDNILGPRVRHIWAPKSQGLLLLSDGEV
SH448         MSSACPPQSPAVAKTEVLVDDCCPVLAATFAYWDNILGPRVRHIWAPKSQGLLLLSDGEV
SH449         MSSACPPQSPAVAKTEVLVDDCCPVLAATFAYWDNILGPRVRHIWAPKSQGLLLLSDGEV
SH450         MSSACPPQSPAVAKTEVLVDDCCPVLAATFAYWDNILGPRVRHIWAPKSQGLLLLSDGEV
SH451         MSSACPPQSPAVAKTEVLVDDCCPVLAATFAYWDNILGPRVRHIWAPKSQGLLLLSDGEV
              ************************************************************


C13H9orf72    TFLANHTLNGEILRSAESGAVDVKFFVLAEKGVIIVSLIFDGELKGDKNTCALSIILPQS
SH448         TFLANHTLNGEILRSAESGAVDVKFFVLAEKGVIIVSLIFDGELKGDKNTCALSIILPQS
SH449         TFLANHTLNGEILRSAESGAVDVKFFVLAEKGVIIVSLIFDGELKGDKNTCALSIILPQS
SH450         TFLANHTLNGEILRSAESGAVDVKFFVLAEKGVIIVSLIFDGELKGDKNTCALSIILPQS
SH451         TFLANHTLNGEILRSAESGAVDVKFFVLAEKGVIIVSLIFDGELKGDKNTCALSIILPQS
              ************************************************************


C13H9orf72    ELSFYLPLHAVCVERLKHVIRKGRICMQKGYNIISMLSSEIVPIMELLTSMKKHSVPEEV
SH448         ELSFYLPLHAVCVERLKHVIRKGRICMQKGYNIISMLSSEIVPIMELLTSMKKHSVPEEV
SH449         ELSFYLPLHAVCVERLKHVIRKGRICMQKGYNIISMLSSEIVPIMELLTSMKKHSVPEEV
SH450         ELSFYLPLHAVCVERLKHVIRKGRICMQKGYNIISMLSSEIVPIMELLTSMKKHSVPEEV
SH451         ELSFYLPLHAVCVERLKHVIRKGRICMQKGYNIISMLSSEIVPIMELLTSMKKHSVPEEV
              ************************************************************


C13H9orf72    DLKDTVLNDDDIGDSCHEDFLHKAISSHLQTCGCSMVVGSNPEKVNKIVLTLCLFLTPAE
SH448         DLKDTVLNDDDIGDSCHEDFLHKAISSHLQTCGCSMVVGSNPEKVNKIVLTLCLFLTPAE
SH449         DLKDTVLNDDDIGDSCHEDFLHKAISSHLQTCGCSMVVGSNPEKVNKIVLTLCLFLTPAE
SH450         DLKDTVLNDDDIGDSCHEDFLHKAISSHLQTCGCSMVVGSNPEKVNKIVLTLCLFLTPAE
SH451         DLKDTVLNDDDIGDSCHEDFLHKAISSHLQTCGCSMVVGSNPEKVNKIVLTLCLFLTPAE
              ************************************************************


C13H9orf72    RKCSRLCHPDGSFKYDTGLFVQGLLKDSTGSFVFPYRQVLYSPYPTTHIDVDINTVKQMP
SH448         RKCSRLCHPDGSFKYDTGLFVQGLLKDSTGSFVFPYRQVLYSPYPTTHIDVDINTVKQMP
SH449         RKCSRLCHPDGSFKYDTGLFVQGLLKDSTGSFVFPYRQVLYSPYPTTHIDVDINTVKQMP
SH450         RKCSRLCHPDGSFKYDTGLFVQGLLKDSTGSFVFPYRQVLYSPYPTTHIDVDINTVKQMP
SH451         RKCSRLCHPDGSFKYDTGLFVQGLLKDSTGSFVFPYRQVLYSPYPTTHIDVDINTVKQMP
              ************************************************************


C13H9orf72    PCHEHTYHQRRYMRAELSALWKAASEDDFSSDNLINAQDSYTPDLNIFQDVMHKDTLVKS
SH448         PCHEHTYHQRRYMRAELSALWKAASEDDFSSDNLINAQDSYTPDLNIFQDVMHKGLStop
SH449         PCHEHTYHQRRYMRAELSALWKAASEDDFSSDNLINAQDSYTPDLNIFQDVMHKDACEVF
SH450         PCHEHTYHQRRYMRAELSALWKAASEDDFSSDNLINAQDSYTPDLNIFQDVMHKDSVRGG
SH451         PCHEHTYHQRRYMRAELSALWKAASEDDFSSDNLINAQDSYTPDLNIFQDACEVFHRStop
              **************************************************


C13H9orf72    FIDEVFLLKPGLSLRSVYLSHFLLLLHRKALTLLRYIEDETQKGKKPFRSLRNLKTDLDL
SH450         VSRGCGRVGRAATPPAPPSPSTRLStop
SH449         HRStop


C13H9orf72    TVEGDLNIIMAMAEKLRAGLHSFVFGKSFLTSVQERDLLINFStop
```

**Figure 3.9 Multiple sequence alignment of wild-type and mutated C13H9orf72 protein sequence from TALEN generated lines.** Complementary DNA (cDNA) sequences of the wild type *C13H9orf72* and of the mutated *C13H9orf72* alleles, as previously described in figure 5, were translated in to the corresponding protein sequences using ExPASy. The online tool Clustal Omega was then used to perform multiple sequence alignments of these protein sequences. The effects of each insertion or deletion allele on protein truncation are shown.

Fin biopsies taken from F2 offspring raised to adulthood (SH448, SH449, SH450 and SH451) were screened in order to identify those heterozygous carriers for the selected frameshift mutations. The expected Mendelian inheritance pattern of 50% wild-type and 50% heterozygous carriers was observed in all lines. Once identified, heterozygous carriers from all of the lines (SH448, SH449, SH450 and SH451) were incrossed to produce offspring (F3), in order to study any effects on early survival (chapter 4). It is expected from such an incross to see the following Mendelian inheritance pattern; 25% wild-type, 25% homozygous mutant and 50% heterozygous carriers for the previously identified mutations

Following this, F3 offspring were raised to adulthood from lines SH448 and SH451, in order to have two TALEN lines for adult phenotypic characterisation. Fin biopsies taken from F3 offspring raised to adulthood were screened and subsequently wild-types and homozygous mutants were selected for characterisation, following appropriate power calculations (chapter 4).

### 3.2.4. Identification of null alleles in TALEN-generated lines

As previously discussed, the identified mutations in lines SH448, SH449, SH450 and SH451 were predicted to result in a truncated form of C13H9orf72 (see figure 3.9). Initially, in order to try and detect endogenous C13H9orf72 protein levels in the wild-type and homozygous mutant zebrafish, western blotting using three commercially available anti-C9orf72 antibodies was performed (figure 3.10).
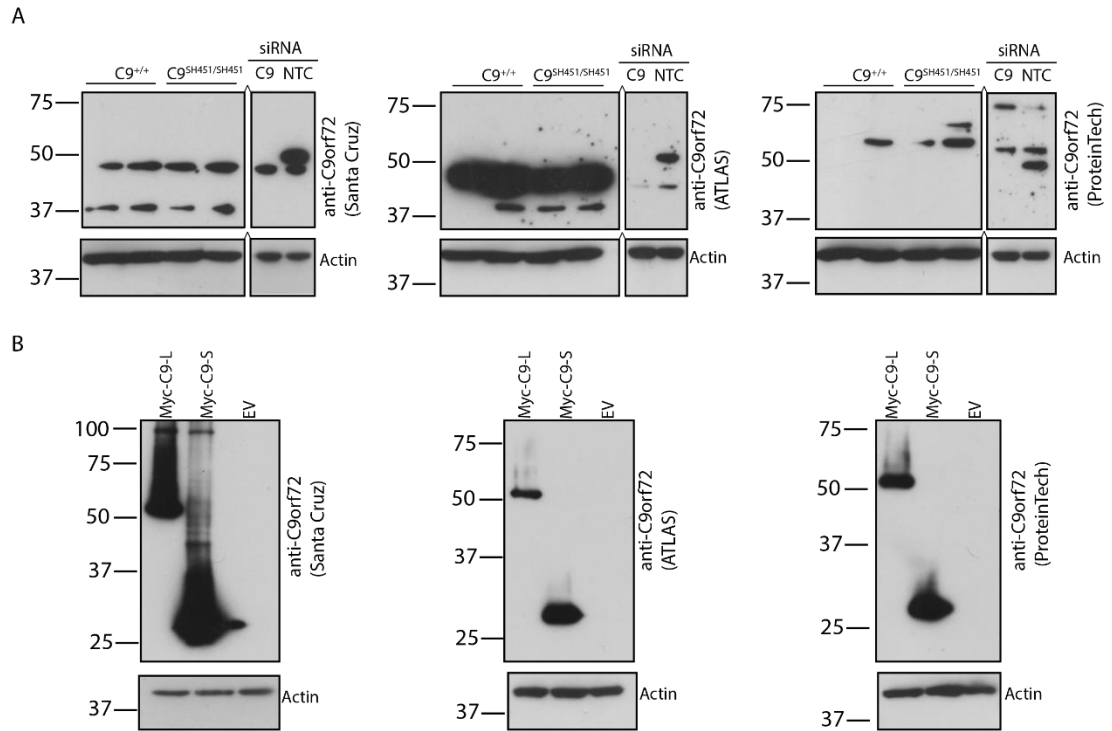
**Figure 3.10 Observing C13H9orf72 protein levels in zebrafish.** A) Untreated wild type or C13H9orf72$^{SH451/SH451}$ lysates were run alongside HEK293 cells treated with C9orf72 siRNA or non-targeting (NTC). Levels of endogenous C9orf72 were determined on immunoblots using three commercially available anti-C9orf72 antibodies (all 1:250). B) HEK293 were transfected with Myc-C9L, Myc-C9S or empty vector control. Levels of C9orf72 were determined on immunoblots using the same anti-C9orf72 antibodies.

It was expected that the full-length zebrafish C13H9orf72 protein would run at 52 kDa, whereas the C13H9orf72$^{SH451/SH451}$ protein will either not be visible, if the protein is not expressed, or if the truncated protein is expressed, produce a band around 40kDa. However, no band was visible at these predicted kDa values with any of the commercial anti-C9orf72 antibodies used (figure 3.10A), only non-specific bands also seen in the siRNA treated cell lysates. The human C9orf72-L was expected to run at 54 kDa and human C9orf72-S at 25kDa. Endogenous C9orf72-S was not observed in any of the cell lysates. However, endogenous C9orf72-L was observed when HEK-293 were treated with non-targeting siRNA with two of the commercial anti-C9orf72 antibodies used (Santa Cruz and ATLAS, figure 3.10A). As expected, overexpressed Myc-C9orf72L and Myc-C9orf72S was observed with all antibodies tested (figure 3.10B), indicating that these antibodies are able to detect both C9orf72 isoforms.

Due to the lack of reliable antibodies to detect C13H9orf72 protein levels, RT-qPCR was performed to investigate *C13H9orf72* mRNA levels. This was carried out to determine

whether the predicted truncated *C13H9orf72* transcripts are degraded by nonsense-mediated decay. RT-qPCR analysis revealed a significant decrease in total *C13H9orf72* transcript levels in homozygous mutants in comparison to wild-type siblings in all lines (figure 3.11); SH448 (*C13H9orf72*$^{+/+}$ mean 1.01±0.01 vs *C13H9orf72*$^{SH448/SH448}$ 0.33±0.09, unpaired t-test, p = <0.0001); SH449 (*C13H9orf72*$^{+/+}$ 1.01±0.01 vs *C13H9orf72*$^{SH449/SH449}$ 0.34±0.11, unpaired t-test, p = <0.0001); SH450 (*C13H9orf72*$^{+/+}$ 1.05±0.04 vs *C13H9orf72*$^{SH450/SH450}$ 0.23±0.16, unpaired t-test, p=0.0006); SH451 (*C13H9orf72*$^{+/+}$ 1.00±0.00 vs *C13H9orf72*$^{SH451/SH451}$ 0.17±0.04, unpaired t-test, p = <0.0001).
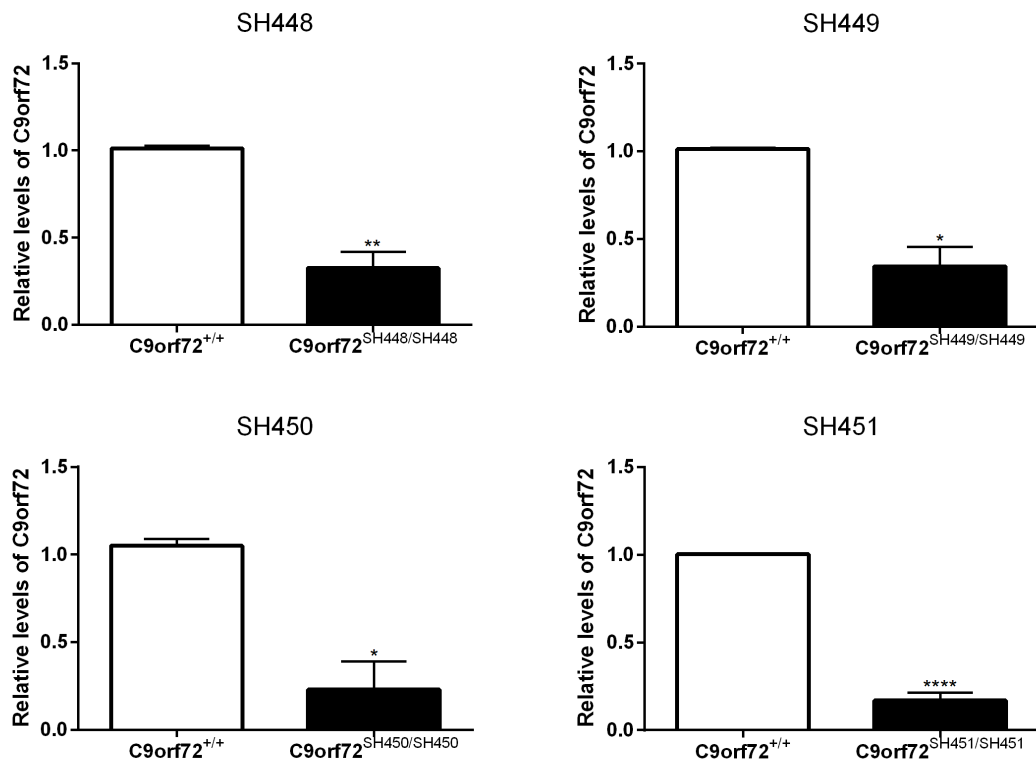


**Figure 3.11 Identified frameshift mutations in coding exon 7 of C13H9orf72 gene lead to reduced levels of C13H9orf72 transcripts in zebrafish.** Result from RT-qPCR to investigate whether truncated C13H9orf72 transcripts are degraded by nonsense-mediated decay. In comparison to wild type siblings, homozygous mutants show a reduction in *C13H9orf72* transcript levels of approximately 60-80% (n=3) in lines A) SH448 (unpaired t-test, p = <0.0001, n=2); B) SH449 (unpaired t-test, p = <0.0001, n=2); C) SH450 (unpaired t-test, p=0.0006, n=2); D) SH451 (unpaired t-test, p = <0.0001, n=3). Levels of mRNA were quantified relative to loading control EF1α mRNA levels according to the ΔΔC*t* method. Error bars represent standard deviation of the mean of n=2-3 biological repeats. Each biological repeat contains 3-10 zebrafish pooled together per genotype.

## 3.3. Generating *C13H9orf72* loss of function models using the CRISPR/Cas9 system

### 3.3.1. Investigation of polymorphisms surrounding the target locus in exon 1

In addition to the TALEN designed to target exon 7 of *C13H9orf72* prior to the start of this project, a TALEN was also designed to target exon 1 of *C13H9orf72*. Embryos injected with this TALEN were not taken forward to be raised at this point, as it was unsuccessful in producing TALEN-induced genome modifications within this target locus. As a result, this region was targeted again utilising an alternative targeted genome editing technique, the CRISPR/Cas9 system. We used a previously published CRISPR/Cas9 target site within exon 1 of *C13H9orf72* (Hruscha et al. 2013) (section 2.5.2 and figure 3.12-A)

In preparation for this, genomic DNA from AB zebrafish was amplified using 'exon 1 primer' (table 2.6) and the undigested PCR product, including the potential CRISPR site in exon 1, was sequenced. This was done in order to identify possible polymorphisms in this region, due to the previous identification of polymorphisms surrounding the target locus in exon 7 of *C13H9orf72*.

Analysis of the sequencing data revealed a polymorphism located between the forward primer and potential CRISPR target site within exon 1 (figure 3.12). This involved a single base pair change from thymine to guanine (ZGC_100846:c.66 T>G), resulting in a codon change from TGT to TGG. The codon change corresponds to an amino acid change from cysteine to tryptophan. These amino acids have different properties; cysteine is a polar amino acid with a neutral side chain, whereas tryptophan is an aromatic amino acid with a hydrophobic side chain. However, this is a known missense variant (rs40965738). The polymorphism occurs in a poorly conserved region of C9orf72 and this cysteine is non-conserved in other fish species as well as in higher mammals.

A



553 (bp)

T or G

1

tgctttgtgagcctgacggtctataggtttgtataagcccctatc
ATGTCTTCAGCCTGTCCTCCACAATCTCCAGCCGTGGCCAAGACT
GAAGTTCTGGTTGACGACTGTTGTCCTGTTCTGGCTGCGACCTTC
GCTTACTGGGACAACATCCTCGGACCTCGTGTCCGGCACATCTGG
GCACCGAAAAGCCAAGGGTTGCTGCTGCTCAGTGACGGAGAGGTC
ACATTTCTGGCCAATCACACGCTGAACGGTGAGATTTTGCGCAGC
GCAGAGAGCGGCGCGGTGGATGTCAAGTTCTTCGTCTTGGCTGAA
AAGGGAGTCATCATCGTCTCTCTGATATTTGACGGAGAACTCAAG
GGTGATAAGAACACTTGCGCGCTGTCAATCATCTTGCCGCAGTCA
GAGCTTAGCTTCTACCTGCCTCTGCACGCCG

B



**Figure 3.12 Schematic diagram to show position of polymorphism surrounding target locus in exon 1.** A) The nucleotide sequence represents a portion of *C13H9orf72* including the 5' UTR and coding exon 1. C9E1 primer sequences are shown in black and italicised. The identified polymorphism is shown in red. The CRISPR target sequence is shown in green. The PAM site shown in blue. B) Shows part of the chromatogram obtained after sequencing this region. The uncalled base 'n' represents the site of the polymorphism.

### 3.3.2. Identification and raising mutant lines generated using CRISPR/Cas9

As described in section 3.3.1, the CRISPR/Cas9 system was utilised to target exon 1 of zebrafish *C13H9orf72* and we used a previously published CRISPR/Cas9 target site within exon 1 of *C13H9orf72* (Hruscha et al. 2013) (section 2.5.2 and figure 3.12-A). CRISPR/Cas9 is a complex between a target-specific single guide RNA (gRNA) and a Cas9 nuclease. The gRNA directs the Cas9 to the target site, which is directly followed by a PAM site, resulting in DSBs. As discussed in section 3.2.3, the cell responds to this with endogenous repair mechanisms such as HR and NHEJ. In this study, we wanted to detect INDELs within the target site which produce frameshift mutations, as these will alter the position of the stop codon and most likely result in a non-functional protein (figure 3.13). Within the target site there is a restriction enzyme site for DdeI. This restriction enzyme has a 5bp recognition sequence, which is optimal for rapidly detecting CRISPR/Cas9-induced INDEL mutations for genotyping.

The published gRNA (Hruscha et al. 2013) was co-injected with *Cas9* mRNA into fertilised, one-cell stage zebrafish embryos (0-0.75hpf). The embryos used originated from the wild-type line AB, consistent with the TALEN lines produced previously. A portion of the injected embryos were screened at 48hpf for CRISPR/Cas9-induced genome modifications at the target site. PCR products were amplified using 'exon 1 primers' (table 2.6) and analysed via RFLP for evidence of INDEL mutations. Evidence of mutation was confirmed by the loss of DdeI restriction enzyme cleavage, described in figure 3.14. At this stage, digested and un-digested bands were seen in samples where the CRISPR/Cas9 injection was successful, resembling a heterozygous carrier, as the injected embryos are genetically mosaic at this point. Following confirmation of genome modifications at the target site, the remaining injected zebrafish embryos (F0 founders) were raised to adulthood.
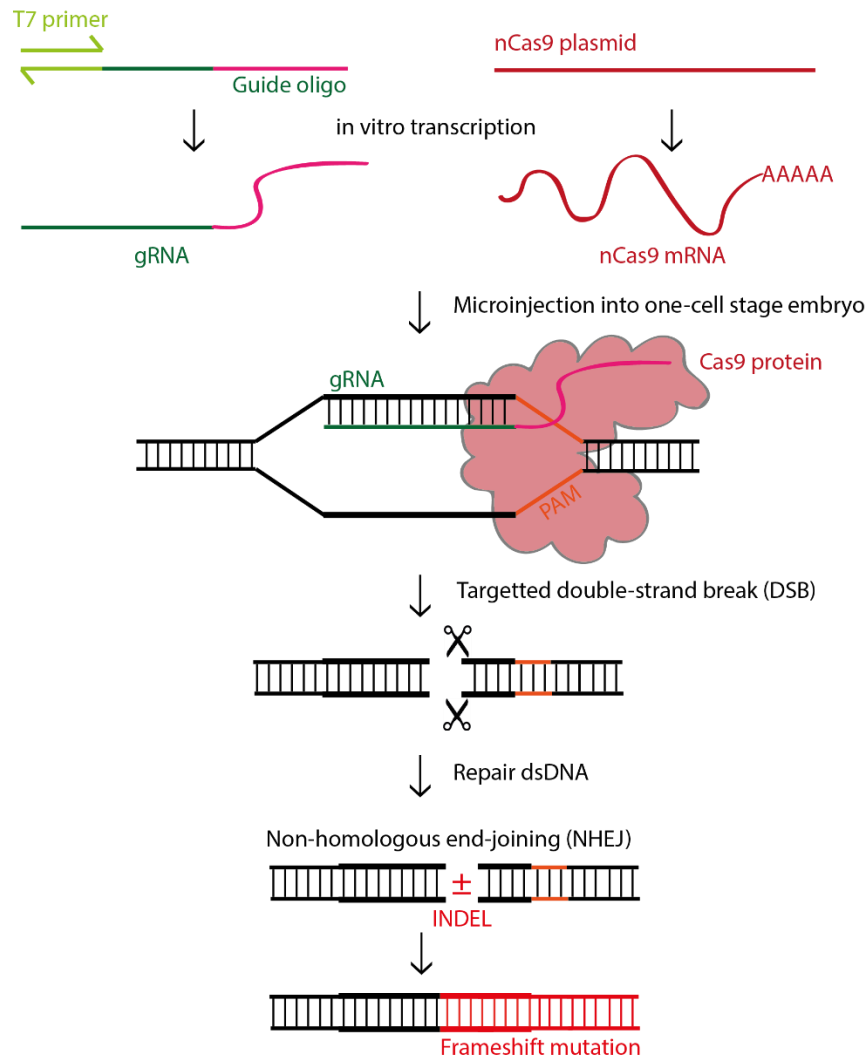
**Figure 3.13 Diagram to show how CRISPR/Cas9 system result in non-homologous end-joining (NHEJ).** Guide oligonucleotides containing a T7 RNA polymerase binding domain were annealed with a T7 primer (green). gRNA containing a target binding site (dark green) and the nCas9 plasmid were *in vitro* transcribed. gRNA and nCas9 mRNA were co-injected into one-cell stage zebrafish embryos. The gRNA recruits the Cas9 protein to the target site to induce double-strand breaks (DSB) close to the protospacer adjacent motif or PAM sequence (orange). In the absence of donor DNA template, the DSB are repaired by non-homologous end joining (NHEJ). NHEJ results in small insertions or deletions (INDEL) which may result in frameshift mutations.
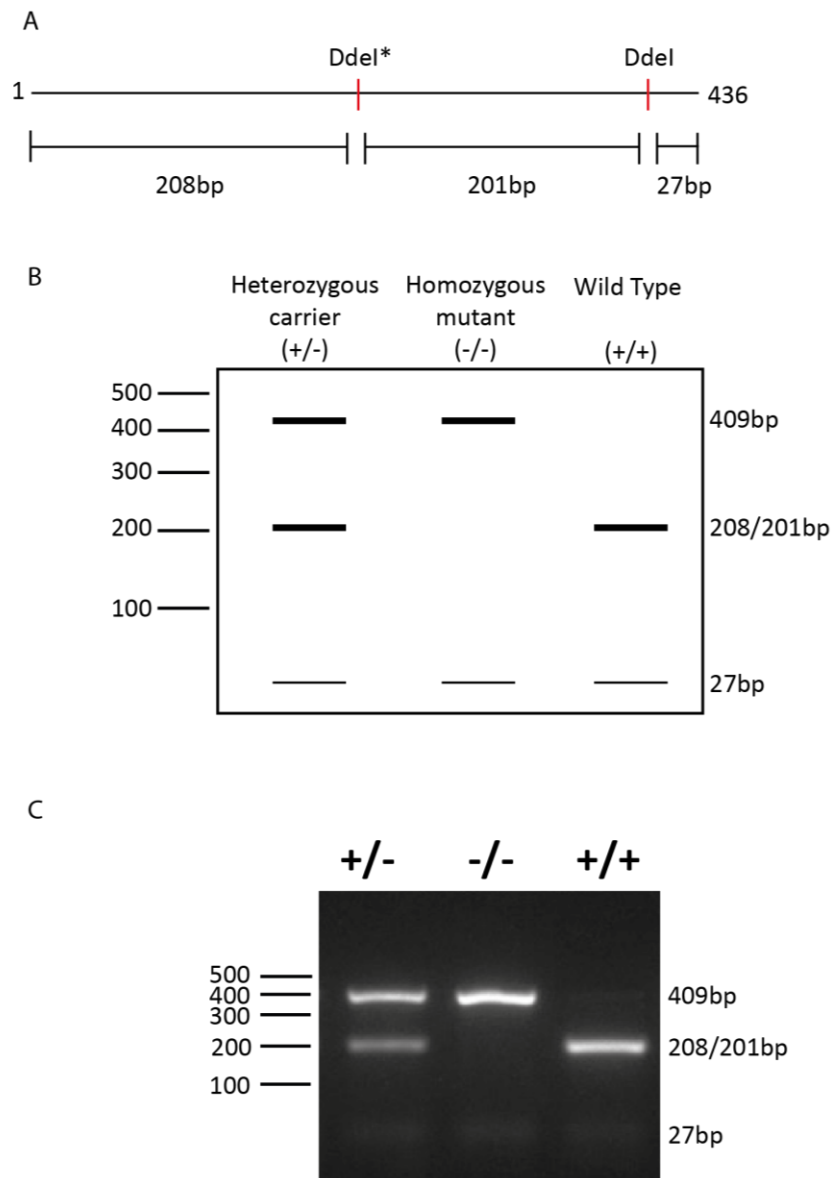
**Figure 3.14 Detection of mutation at exon 1 CRISPR/Cas9 target site using restriction fragment length polymorphism (RFLP) analysis.** A) Schematic diagram representing the size of the amplified PCR product using the exon 1 primers (top) and the size of the fragments following restriction enzyme digest with DdeI (bottom). B) Schematic representation of expected bands for homozygous mutants (409 and 27bp), wild-types (208, 201 and 27bp) and heterozygous carriers (409, 208, 201 and 27bp) product are run on an agarose gel. C) Image of an actual agarose gel showing product from all three genotypes. Bands at approximately 27bp are usually faint and hard to distinguish. However, the larger bands allow for accurate genotyping. Asterisk marks the DdeI site within the CRISPR/Cas9 target site.

Once F0 founders had reached adulthood, those transmitting frameshift mutations through the germline were identified, as previously discussed in section 3.2.3. Fin biopsies were taken from F0 founders for screening, using methods described previously (section 2.6), identifying all those with evidence of somatic mutations within the exon 1 target site. The selected zebrafish were subsequently outcrossed with wild-type AB zebrafish. The resulting F1 offspring were screened and sequenced for evidence CRISPR/Cas9-induced mutations within exon 1 of *C13H9orf72,* in order to determine germline transmission rate from the F0 founders. For this locus, out of the 4 F1 clutches screened, three were identified to carry mutations (75%).

F1 offspring produced from transmitting F0 founders were then raised to adulthood. Again, fin biopsies from all F1 offspring raised were screened and sequenced, in order to identify those heterozygous for frameshift mutations, as done previously. Figure 3.15 summarises all the frameshift mutations identified.
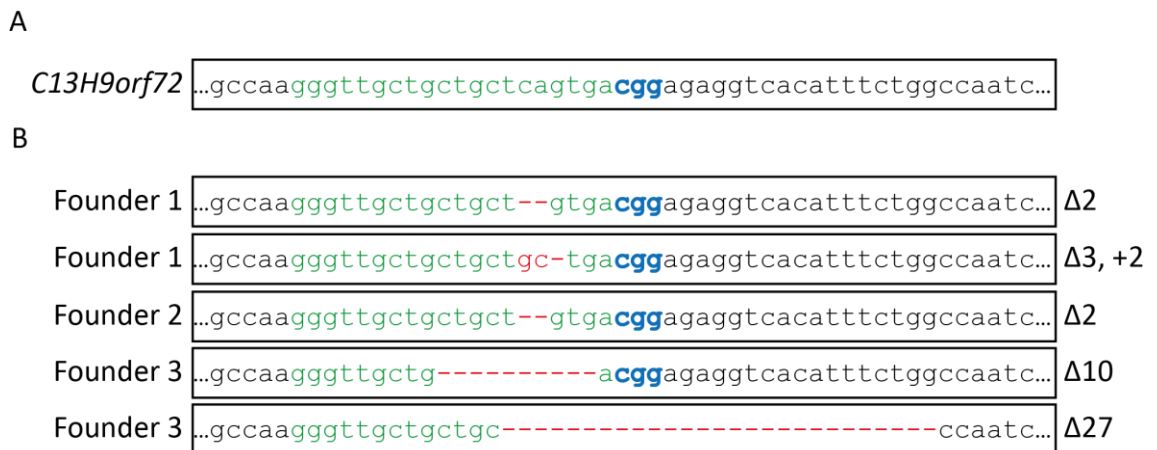


**Figure 3.15 Diagram detailing all frameshift mutations identified in CRISPR/Cas9 generated F1 offspring.** A) The wild-type *C13H9orf72* sequence (coding exon 1) (Ensembl: ENSDARG00000011837). Sequence highlighted in green is the CRISPR target site. B) The sequences derived from the mutant F1 alleles of F0 founders 1, 2 and 3, injected with the CRISPR/Cas9 targeted against coding exon 1 of *C13H9orf72*. Sequence highlighted in green is the CRISPR target site. Mutations are shown in red. PAM site shown in blue.

In order to produce a large batch with identical mutations, three F1 zebrafish identified as heterozygous carriers for frameshift mutations were selected, again ensuring that the zebrafish chosen were each produced from a different F0 founder. The selected zebrafish were outcrossed with wild-type AB zebrafish. Figure 3.16 summarises the three F1 mutants outcrossed. The resulting F2 offspring were raised to adulthood.
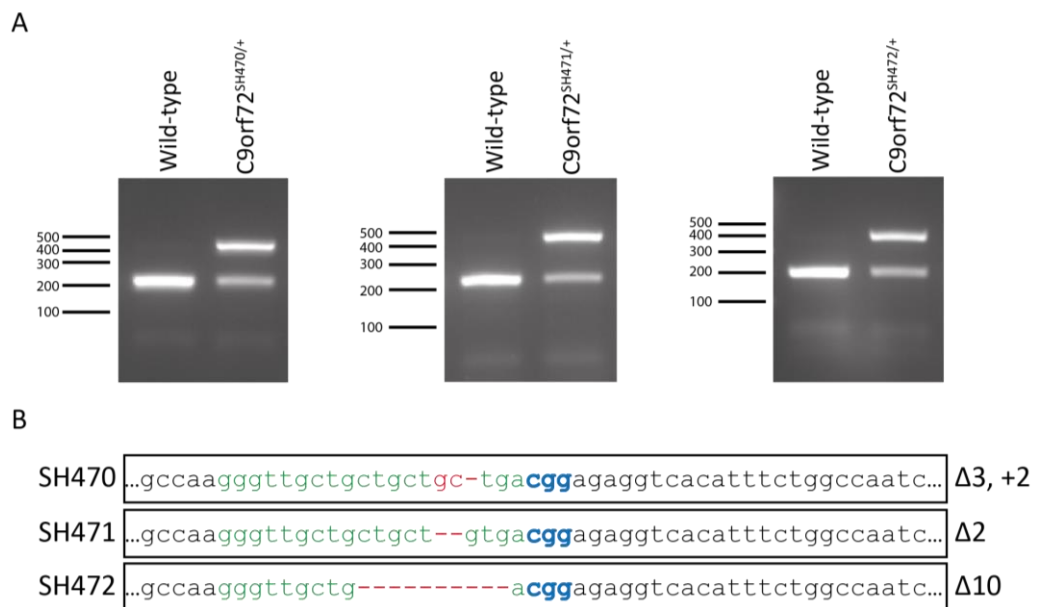


**Figure 3.16 Summary of the F1 offspring heterozygous for frameshift mutations in exon 1 which were selected to outcross.** A) PCR amplification of the genomic DNA extracted from fin biopsies taken from F1 offspring SH470, SH471 and SH472 using C9E1 primers. Following digestion with DdeI, the digested PCR product was run on a 2.5% agarose gel. Digested bands for each heterozygous carrier are compared to a wild-type sibling control. B) Shows the corresponding mutations identified after sequencing. Sequence highlighted in blue is the CRISPR target site. Mutations are shown in red. PAM site shown in blue

As before, F1 offspring with these particular frameshift mutations were selected to be outcrossed, as they were predicted to result in truncated forms of the C13H9orf72 protein and it is expected that these are most likely to result in LOF mutations. Figure 3.17 shows the multiple sequence alignments of the mutated C13H9orf72 protein sequences compared to the wild-type protein sequence. This was carried out in the same way as described in section 3.2.3.

```
C13H9orf72    MSSACPPQSPAVAKTEVLVDDCCPVLAATFAYWDNILGPRVRHIWAPKSQGLLLLLSDGEV
SH470         MSSACPPQSPAVAKTEVLVDDCCPVLAATFAYWDNILGPRVRHIWAPKSQGLLLLLTERS
SH471         MSSACPPQSPAVAKTEVLVDDCCPVLAATFAYWDNILGPRVRHIWAPKSQGLLLLStop
SH472         MSSACPPQSPAVAKTEVLVDDCCPVLAATFAYWDNILGPRVRHIWAPKSQGLL---TERS
              ****************************************************

C13H9orf72    TFLANHTLNGEILRSAESGAVDVKFFVLAEKGVIIVSLIFDGELKGDKNTCALSIILPQS
SH470         HFWPITRStop
SH472         HFWPITRStop

C13H9orf72    ELSFYLPLHAVCVERLKHVIRKGRICMQKGYNIISMLSSEIVPIMELLTSMKKHSVPEEV

C13H9orf72    DLKDTVLNDDDIGDSCHEDFLHKAISSHLQTCGCSMVVGSNPEKVNKIVLTLCLFLTPAE

C13H9orf72    RKCSRLCHPDGSFKYDTGLFVQGLLKDSTGSFVFPYRQVLYSPYPTTHIDVDINTVKQMP

C13H9orf72    PCHEHTYHQRRYMRAELSALWKAASEDDFSSDNLINAQDSYTPDLNIFQDVMHKDTLVKS

C13H9orf72    FIDEVFLLKPGLSLRSVYLSHFLLLLHRKALTLLRYIEDETQKGKKPFRSLRNLKTDLDL

C13H9orf72    TVEGDLNIIMAMAEKLRAGLHSFVFGKSFLTSVQERDLLINFStop
```

**Figure 3.17 Multiple sequence alignment of wild-type and mutated C13H9orf72 protein sequence from CRISPR/Cas9 generated lines.** Complementary DNA (cDNA) sequences of the wild type *C13H9orf72* and of the mutated *C13H9orf72* alleles, as previously described in figure 3.16, were translated in to the corresponding protein sequences using ExPASy. The online tool Clustal Omega was then used to perform multiple sequence alignments of these protein sequences. The effects of each insertion or deletion allele on protein truncation are shown.

Fin biopsies taken from F2 offspring raised to adulthood (SH470, SH471 and SH472) were screened in order to identify those heterozygous carriers for the selected frameshift mutations. As before, the expected Mendelian inheritance pattern of 50% wild-type and 50% heterozygous carriers was observed in all lines. Once identified, heterozygous carriers from all of the lines (SH470, SH471 and SH471) were incrossed to produce F3 offspring, in order to study any effects on early survival (chapter 4). It is expected from this incross to see the following Mendelian inheritance pattern; 25% wild-type, 25% homozygous mutant and 50% heterozygous carriers for the previously identified mutations

Following this, F3 offspring were raised to adulthood from line SH470, in order to have a CRISPR/Cas9 line for adult phenotypic characterisation. Fin biopsies taken from F3 offspring raised to adulthood were screened and subsequently wild-types and homozygous mutants were selected for characterisation, following appropriate power calculations (chapter 4).

### 3.3.3. Identification of null alleles in CRISPR/Cas9-generated lines

As previously discussed in section 3.2.4, the identified mutations in lines SH470, SH471 and SH472 were predicted to result in a truncated form of C13H9orf72 (figure 3.16). Due to the lack of reliable antibodies to detect C13H9orf72 protein levels (see figure 3.10), RT-qPCR was performed to investigate *C13H9orf72* mRNA levels, to determine whether the predicted truncated *C13H9orf72* transcripts are degraded by nonsense-mediated decay. RT-qPCR analysis revealed a significant decrease in total *C13H9orf72* transcript levels in homozygous mutants compared to wild-type siblings (figure 3.18), in lines SH470 and SH471; SH470 (*C13H9orf72*$^{+/+}$ $1.01\pm0.02$ vs *C13H9orf72*$^{SH470/SH470}$ $0.46\pm0.07$, unpaired t-test, p = $<0.0001$); SH471 (*C13H9orf72*$^{+/+}$ $1.03\pm0.04$ vs *C13H9orf72*$^{SH471/SH471}$ $0.38\pm0.00$, unpaired t-test, p = $<0.0001$). However, there was not a biologically relevant difference in total C9orf72 transcript levels observed between homozygous mutants and wild-type siblings in line SH472; SH472 (*C13H9orf72*$^{+/+}$ $1.02\pm0.03$ vs *C13H9orf72*$^{SH472/SH472}$ $0.88\pm0.02$, unpaired t-test, p = $<0.05$).
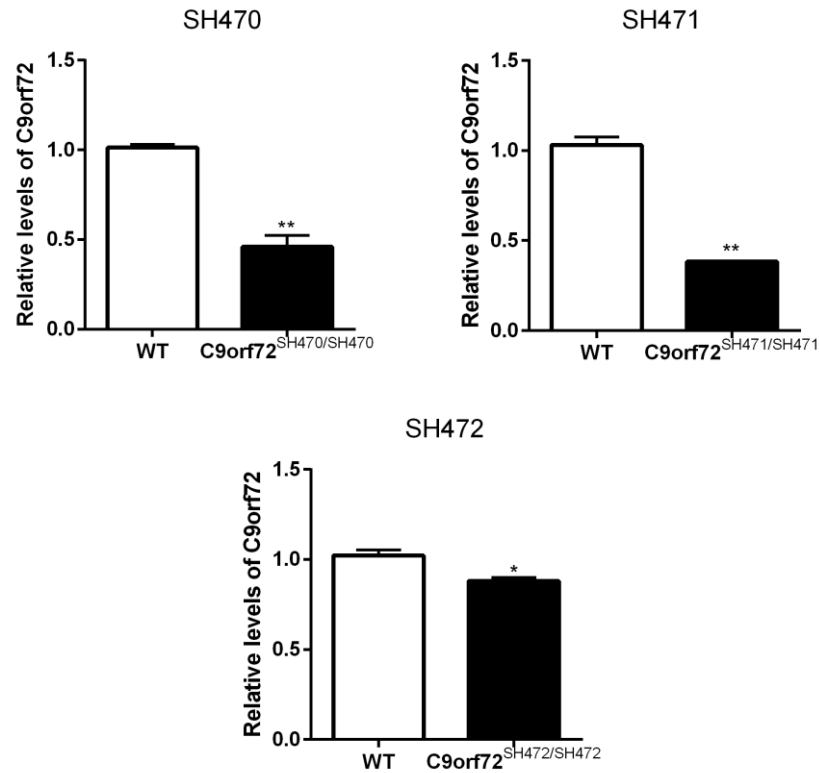
**Figure 3.18 Identified frameshift mutations in coding exon 1 of C13H9orf72 gene lead to reduced levels of C13H9orf72 transcripts in zebrafish.** Result from RT-qPCR to investigate whether truncated C13H9orf72 transcripts are degraded by nonsense-mediated decay. In comparison to wild type siblings, homozygous mutants show a significant reduction in *C13H9orf72* transcript levels in lines A) SH470 (unpaired t-test, p = <0.0001, n=2); B) SH471 (unpaired t-test, p = <0.0001, n=2); C) but not SH472 (unpaired t-test, p = <0.05, n=2). Levels of mRNA were quantified relative to loading control EF1α mRNA levels according to the ΔΔC*t* method. Error bars represent standard deviation of the mean of n=2 biological repeats. Each biological repeat contains 3-10 zebrafish pooled together per genotype.

### 3.4. Discussion

The initial aim of this project was to produce a stable zebrafish *C9orf72* LOF model of C9-ALS/FTD, using targeted genome editing techniques. As discussed, it is not fully understood how the repeat expansion in *C9orf72* results in ALS/FTD, however there is evidence for three possible, non-exclusive pathogenic mechanisms. It is essential to model all three potential mechanisms in order to understand their contribution to disease and this project focuses particularly on how *C9orf72* LOF via haploinsufficiency may contribute to C9-ALS/FTD. This project utilised zebrafish for the generation of the model, which harbour a highly conserved orthologue of the human *C9orf72,* called *C13H9orf72*. Currently, only one group has published data investigating *C9orf72* LOF in zebrafish. As discussed, this group used AMOs to transiently KD *C13H9orf72* in their zebrafish model, and observed ALS-like phenotypes (Ciura et al. 2013). The stable zebrafish *C9orf72* LOF models which have been produced in this project are highly important, as currently no other stable zebrafish model has been characterised. As ALS is mainly an adult-onset disorder in humans, it is essential to study the phenotypes of a stable LOF model throughout its lifetime. This will enable further understanding as to how this gene contributes to C9-ALS/FTD and to investigate protein function *in vivo*.

### 3.4.1. Comparisons between targeted genome editing techniques: TALENs vs CRISPR/Cas9

Two targeted genome editing techniques were utilised in order to generate the stable zebrafish *C13H9orf72* LOF model. As discussed, before the start of this project, TALENs were used to target exon 1 and exon 7 of *C13H9orf72*. TALENs are comprised of a pair of DNA-binding proteins, which bind to opposite sides of the target site and are separated by a spacer region consisting of around 14-20 nucleotides. Within this spacer region, the nonspecific fok-1 nuclease fused to the DNA binding proteins makes double-stranded breaks. Although successful in targeting exon 7, the TALEN targeting exon 1 initially failed. As a result, the CRISPR/Cas9 system was used to target exon 1, utilising a gRNA which has been previously published (Hruscha et al. 2013). CRISPRs are a complex between a target specific guide RNA (gRNA) and a cas9 nuclease. The gRNA guides the cas9 to a 20 nucleotide target site, immediately followed by a PAM site, causing double-stranded breaks. This technique was chosen as during the project the CRISPR/Cas9 system was becoming more widely used, due to the ease of design and high mutation efficiency of the technique. However, it is important to note that both techniques

successfully exploited DNA repair mechanisms such as NHEJ, resulting in INDEL mutations within the chosen target regions of *C13H9orf72*.

As previously mentioned, in order for phenotypic characterisation of the CRISPR/Cas9- and/or TALEN-induced mutations to occur, zebrafish with mutations in germline cells need to be generated. The F0 founders injected with either CRISPR/Cas9 or TALENs were raised to adulthood and their offspring (F1) screened for germline transmission (section 3.2.3 and 3.3.2). Interestingly, when F1 clutches were screened, it was observed that several mutations were passed through the germline from the same founder (figures 3.7 and 3.15). This variety of inherited mutations is to be expected, as the injected F0 founder fish are genetically mosaic. Due to the mosaic nature of the founders, it is important to select specific F1 offspring heterozygous carriers for frameshift mutations to outcross. As a result, all heterozygous carriers identified in F2 offspring will have identical mutations.

Additionally, it was noted in this project that the F0 founders injected with the CRISPR/Cas9 system had a high germline transmission rate of 75% compared to those injected with TALENS, at only 44%. Interestingly, the germline transmission rate produced by the CRISPR/Cas9 injection was higher than that observed with the same gRNA in (Hruscha et al. 2013), who observed only 20%. It is possible that whilst screening for loss of the DdeI restriction site, that the authors may have missed some frame-shift mutations that did not disrupt this site and were therefore not detected. In the future, due to ease of design and high germline transmission rate, the CRISPR/Cas9 system would be the method of choice over TALENs for rapidly generating INDEL mutation in desired target sites.

### 3.4.2. Genotyping mutations in C13H9orf72

Identification of CRISPR/Cas9- and TALEN-induced mutations was done via RFLP, using the restriction enzymes DdeI and MslI, respectively. A limitation of this method is that it only allows identification of mutations which have disrupted the restriction enzyme cut site. Therefore, it will not detect mutations which are present in the region but have not disrupted the restriction cut site. This suggests that there could be more mutations present in the founder population which were not discovered. However, the restriction enzyme MslI was particularly advantageous to use to avoid this limitation, as it has a long cut site of 10bp (CAYNNNNRTG), which means it should detect the majority of

insertions and deletions within the target region. A further limitation of RFLP is that it only provides information on whether a mutation is present, not if it is an in-frame or frameshift mutation. Therefore, it was essential to sequence undigested PCR product in order to determine what the mutation was, which elongates the genotyping process. However, it is essential to do this step, as frameshift mutations are more likely to result in truncated and/or non-functional protein products. In the future, techniques such as High Resolution Melt (HRM) analysis and SURVEYOR mutation detection kits could be utilised to speed up the genotyping process. These methods are advantageous when mutating regions without good restriction sites.

Novel polymorphisms were identified to surround the target region in exon 7 of *C13H9orf72*, therefore it was impossible to obtain readable sequencing data with the original primers (section 3.2.2). As a result, before injection of the CRISPR/Cas9, the region surrounding the target site in exon 1 of *C13H9orf72* was fully sequenced to ensure there were no polymorphisms surrounding it. This led to the identification of a nonsynonymous amino acid substitution in a non-conserved region.  Luckily, in both cases, the identified polymorphisms were avoidable with the design of new primers. However, in the future it should be essential to sequence the region surrounding a potential target site before generating a new model. This is important, particularly in zebrafish, as their genomes are highly polymorphic (Nasiadka and Clark 2012). This is also critical to consider as whole genome sequencing was performed on the Tuebingen strain of zebrafish (Howe et al. 2013). Therefore, when using other strains to generate models, such as the AB strain in this project, there may be variations in the sequence of a particular region due to the polymorphic nature of their genomes.

Originally, it was hoped that the targeted genome editing techniques used would produce large INDEL mutations. This would have been advantageous, as these could be simply genotyped by resolving the bands on an agarose gel. This would negate the use of RFLP, speeding up the genotyping process.  An allele produced via injection with TALENs, SH450, harboured an +80bp insertion in exon 7 of *C13H9orf72,* which could be easily observed on an agarose gel without digestion. However, upon further analysis, when cDNA produced from zebrafish carrying this mutation was sequenced, an alternatively spliced transcript was identified. The transcript carried an in-frame Δ168bp, corresponding to the deletion of exons 7 and 8. As the mutation was in-frame, these transcripts could potentially produce functioning protein, therefore this line was not taken

forward. In the future, it will be important to sequence cDNA from zebrafish carrying large INDELs to ensure that the expected truncated transcript is present before continuing with characterisation.

### 3.4.3. Identified frameshift mutations in exon 1 and 7 of *C13H9orf72* result in truncated transcripts

The identified frameshift mutations chosen to be taken forward were selected as they are predicted to result in a truncated form of C13H9orf72 (figures 3.9 and 3.17). The full length C13H9orf72 consists of 462 residues. The TALEN-induced frameshift mutations located in exon 7 of *C13H9orf72* were predicted to result in truncations from the following amino acid residues: SH448 residue 356; SH449 residue 362; SH450 residue 384; SH451 residue 357. Additionally, the CRISPR/cas9-induced frameshift mutations located in exon 1 of *C13H9orf72* were predicted to result in truncations from the following amino acid residues: SH470 residue 67; SH471 residue 55; SH472 residue 64.

Our RT-qPCR data demonstrates that the predicted truncated transcripts are degraded by nonsense mediated decay before they are able to be translated into protein (discussed further below). However, it is possible that a small amount of mutant mRNA may be translated into truncated, aberrant proteins. The result this has would be dependent on the role of C13H9orf72. As mentioned previously, the *C9orf72* gene in humans encodes two protein isoforms that share structural homology with the Differentially Expressed in Normal and Neoplasia (DENN) proteins (Levine et al. 2013, Zhang et al. 2012). DENN proteins are implicated in membrane trafficking events as GDP/GTP exchange factors (GEF) of Rab GTPases. The tripartite DENN module consist of the following domains in eukaryotes: u-DENN domain on the N-terminus; a central DENN domain; a d-DENN domain on the C-terminus (Levivier et al. 2001). The long isoform of C9orf72 (C9-L, 462aa in length), is predicted to harbour all three domains: u-DENN residues 23-151; central DENN residues 212-322; d-DENN on c-terminus, exact location unpublished (Levine et al. 2013, Zhang et al. 2012). The short isoform of C9orf72 (C9-S, 212aa in length) is predicted to contain only the u-DENN and part of the central DENN domain, due to it lacking a portion of the C-terminus of the protein. Due to high conservation between human and zebrafish C9orf72 (76.14% amino acid identity), it is expected that the functional role of C9orf72 is likely to be similar in both species. Therefore, it could be predicted that if a small amount of mutant mRNA is translated, the CRISPR/Cas9-induced frameshift mutations resulting in truncations at residues 55-67 would result in a

more severe phenotype in the zebrafish, as the truncated protein would only contain part of the u-DENN. This would be dependent on whether the location of the three DENN domains are similar in zebrafish. It is important to note the distinct roles of each of the DENN domains are not fully understood, but it will certainly be interesting to investigate whether mutations located in exon 1 are more severe than those in exon 7 during characterisation of the models.

Ideally, western blot analysis would be utilised to examine protein levels of C13H9orf72 in zebrafish carrying mutant alleles vs wild-type siblings. However, as shown in section 3.2.4, the commercially available antibodies used were not able to detect endogenous protein levels in the zebrafish. A reason for this may be due to the immunogen sequence these antibodies were raised against. For example, the polyclonal ATLAS and ProteinTech anti-C9orf72 antibodies were raised against immunogen sequences which include human exon 3, which as discussed in section 3.2.1, is not present in zebrafish. Additionally, an important limitation to consider when using these commercially available anti-C9orf72 antibodies is that they do not discriminate between the two protein isoforms of C9orf72. However, pioneering work by (Xiao et al. 2015) has led to the development of antibodies which are able to detect C9orf72-L and C9orf72-S individually. In the future, it would be interesting to test these antibodies on protein extracted from the zebrafish lines generated, as the epitopes are well conserved between human and the zebrafish orthologue.

As a result of the lack of reliable, commercially available anti-C9orf72 antibodies during this project, RT-qPCR was performed on cDNA produced from identified homozygous mutants and their wild-type siblings from all lines (section 3.2.4 and 3.3.3). A reduction in C13H9orf72 mRNA levels in homozygous mutants would provide evidence for degradation by nonsense mediated decay (NMD). NMD is an important surveillance mechanism which exists in eukaryotes. It ensures that mRNA transcripts containing premature translation termination codons (PTCs), are degraded and thus cannot be translated into potentially aberrant proteins (Kurosaki and Maquat 2016). It is known that the zebrafish genome encodes orthologues for most of the genes essential for NMD to occur (Wittkopp et al. 2009). If NMD is occurring, a lower steady state of mutant mRNA would be expected. This is what was reported in sections 3.2.4 and 3.3.3, for most lines tested. However, it is important to acknowledge the limitations in studying NMD by examination of mRNA levels via RT-qPCR. For example, it cannot be assumed that the

level of mRNA is directly proportional to the level of protein expression. Factors to consider which effect this correlation include post-transcriptional processes which are essential in determining the final synthesis of the protein (Greenbaum et al. 2003). Therefore, in the future it is hoped that there will be anti-C9orf72 antibodies available to study the endogenous C13H9orf72 protein levels in these zebrafish in order to compare to the RT-qPCR result.

### 3.4.4. Determining loss-of-function alleles to take forward for phenotypic characterisation

Following generation of frameshift mutations in both exon 1 and exon 7, using CRISPR/Cas9 and TALENs respectively, it had to be decided which LOF alleles would be taken forward for phenotypic characterisation.

Following initial injection of the TALEN targeted against exon 7 of *C13H9orf72*, the following four lines were generated: SH448 (Δ4bp exon 7); SH449 (Δ2bp exon 7); SH450 (+80bp ins exon 7); SH451 (Δ17bp exon 7). As previously discussed in section 3.4.2, the allele SH450 was not taken forward for characterisation due to the presence of an alternative transcript harbouring an in-frame Δ168bp, corresponding to the deletion of exon 7 and 8 of *C13H9orf72*. It was shown from the RT-qPCR results that zebrafish homozygous mutant for the other three mutant alleles had a significant reduction in *C13H9orf72* mRNA level in comparison to wild-type siblings (section 3.2.4). As a result, it was decided to take two alleles forward, SH448 and SH451, for phenotypic characterisation. Two lines were chosen to allow confirmation of any phenotypic changes observed. This would strengthen confidence that any effects were due to a mutation truncating the c-terminus of the protein, and not any side effect in the genetic background of that particular line.

Additionally, following injection of the CRISPR targeted against exon 1 of *C13H9orf72,* the following lines were generated: SH470 (+2bp ins, Δ1bp exon 1); SH471 (Δ2bp exon 1); SH472 (Δ10bp exon 1). It was noted from the RT-qPCR result in section 3.3.3, that zebrafish homozygous mutant for the SH472 allele only had a minimal decrease in *C13H9orf72* mRNA level (10-14%) in comparison to wild-type siblings. As RT-qPCR primers were designed against the 3'-end of the transcript, it was predicted that this mutation would not lead to a LOF and that full-length protein would be expressed.

Therefore, it was decided not to take forward the SH472 allele for phenotypic characterisation.

RT-qPCR results from zebrafish homozygous mutant for the other two mutant alleles had a significant reduction in *C13H9orf72* mRNA level in comparison to wild-type siblings (section 3.3.3). Initially, it was decided to take forward both alleles for phenotypic characterisation, for the same reason noted for the TALEN-generated lines. However, allele SH471 was unable to be taken forward due to issues regarding breeding. There was a sex skew bias towards males in the F2 generation, with only one female a heterozygous carrier for the SH471 mutant allele. As a result, the F2 generation were outcrossed again with wild-type AB to produce a better ratio of males:females heterozygous carriers for the SH471 allele. However, by the time this generation was raised, it was too late in the project to incross these and produce an F3 generation to obtain any meaningful characterisation data on. As a result, only one allele, SH470, was taken forward to observe the effect of mutations in exon 1 of *C13H9orf72*.

### 3.4.5. Conclusion

In conclusion, the initial aim of this project was achieved and stable zebrafish *C13H9orf72* LOF models have been generated to take forward and characterise in the future. To summarise, a total of four TALEN-generated lines (SH448, SH449, SH450 and SH451) and two CRISPR/Cas9-generated lines (SH470 and SH471) showed a significant reduction in *C13H9orf72* transcript levels (section 3.2.4. and 3.3.3). As a result, two TALEN-generated lines (SH448 and SH451) and one CRISPR/Cas9-generated line (SH470) were taken forward for phenotypic characterisation into adulthood, as covered in chapter 4.

## 4. Characterisation of C13H9orf72 loss-of-function zebrafish models of ALS/FTD
### 4.1. Introduction

As previously discussed, there is a link between ALS and FTD in patients who carry the repeat expansion in *C9orf72,* therefore observed phenotypes may include both motor dysfunction and behavioural and/or cognitive changes in humans. Following the generation of stable *C13H9orf72* loss-of-function (LOF) zebrafish, as discussed in chapter 3, this study focussed on investigating whether loss of *C13H9orf72* results in any ALS- or FTD-like phenotypes similar to those seen in patients. There is currently no characterised stable *in vivo* model of C9-ALS/FTD in the zebrafish; therefore, an important component of this project is the phenotypic characterisation of these zebrafish. If loss of *C13H9orf72* results in the development of ALS/FTD in the zebrafish, we will expect to see changes in phenotypes such as survival, motor function and pathology, as has been shown in other models of ALS in zebrafish.

Regarding survival, previous AMO experiments suggest that knockdown (KD) of *C13H9orf72* produces viable embryos (Ciura et al. 2013). It is possible that complete loss of *C13H9orf72* will result in embryonic or larval lethality. However, if this was the case, these zebrafish could still be utilised. Due to their external development and availability in large numbers, they can be studied easily to the end of life, unlike embryonic lethal murine models. Additionally, zebrafish that are heterozygous carriers of the frameshift mutations could also be utilised, as C9-ALS/FTD patient mRNA levels are similar to what we would expect to see in these fish. To determine whether the frameshift mutations in *C13H9orf72* result in early loss of viability in these fish, survival monitoring will be performed during larval stages by monitoring tanks twice per day and removing dead larvae for genotyping as previously described (Chapman et al. 2013).

In order to observe any changes in motor function of adult *C13H9orf72* LOF zebrafish, two main approaches will be utilised, including the spinning task (Blazina et al. 2013) and the swim tunnel (Ramesh et al. 2010, Plaut 2000). As loss of muscle strength is a hallmark phenotype seen in C9-ALS/FTD, these two techniques will aim to examine the swimming endurance of the zebrafish. It is expected that if the zebrafish carrying frameshift mutations in *C13H9orf72* develop ALS/FTD-like phenotypes, a reduction in swimming endurance will be observed as noted in previous models of ALS (Ramesh et al. 2010). In order to confirm the basis for any alteration in motor function observed,

quantitative assessment of neuromuscular junctions (NMJs) will be performed, as carried out previously in (Chapman et al. 2013, Ramesh et al. 2010).

Additionally, due to the link between ALS and FTD in patients harbouring the repeat expansion in *C9orf72*, behavioural changes will be investigated in these zebrafish. As previously mentioned, there are a number of established protocols which are able to investigate behavioural changes in zebrafish, and for this study a battery of such tests were performed on the adult *C9orf72* LOF zebrafish.

## 4.2. Characterisation of survival in stable *C13H9orf72* loss of function zebrafish

C9-ALS/FTD patients typically survive 30.5 months after diagnosis (Cooper-Knock et al. 2012). To address whether *C13H9orf72* LOF zebrafish had a shorter lifespan, we analysed survival over time, as reported in section 4.2.1 and 4.2.2.

### 4.2.1. Investigating whether frameshift mutations in exon 1 of *C13H9orf72* lead to loss of viability

#### 4.2.1.1. Viability up to 21dpf

To address whether frameshift mutations in exon 1 of *C13H9orf72* resulted in early loss of viability in the zebrafish, survival monitoring was performed during larval stages for all lines generated. Heterozygous carriers from each line were in-crossed and the resulting offspring were monitored twice a day, with dead larvae removed for genotyping as previously described in section 2.7.1.

There was no significant difference in survival at larval stages for lines SH471 and SH472, with all three genotypes showing 96-100% survival up to 21dpf (figure 4.1, B and C). However, there was a significant decline in survival at larval stages in line SH470 ($p = 0.0006$, Mantel-Cox log-rank test; figure 4.1 A), with knockout of *C13H9orf72* in the *C13H9orf72$^{SH470/SH470}$* embryos resulting in only 41% survival by 21dpf in the observed offspring, compared to 68% for *C13H9orf72$^{+/+}$* and 74% for *C13H9orf72$^{SH470/+}$*.
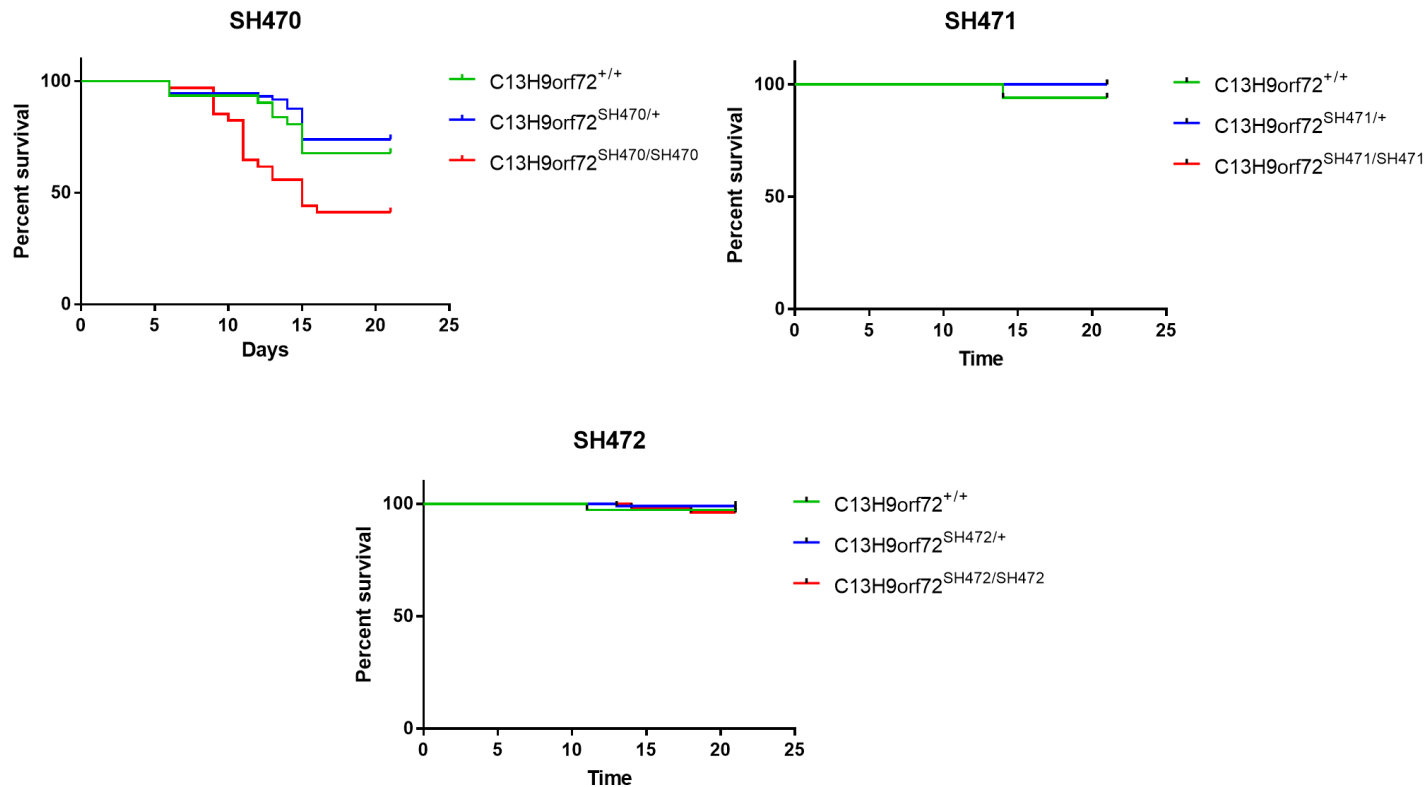
**Figure 4.1 Survival characterisation in zebrafish carrying frameshift mutations in exon 1 of C13H9orf72.** Figure shows Kaplan-Meier plots for lines A) SH470 (n = 3 clutches, p=0.0006, Mantel-Cox log-rank test) B) SH471 (n=1 clutch, ns, Mantel-Cox log-rank test) and C) SH472 (n=4 clutches, ns, Mantel-Cox log-rank test), up to 21 dpf. Survival of wild-types are shown in green, heterozygous carriers in blue and homozygous mutants in red. Plots generated using GraphPad Prism 6.

### 4.2.1.2. Viability up to 90dpf

Heterozygous carriers from line SH470 were in-crossed and raised to adulthood for phenotypic characterisation. Fin biopsies were taken for genotyping at 90dpf. A chi-squared ($\chi^2$) test was calculated, comparing the observed and expected Mendelian inheritance patterns for line SH470 at 90dpf (table 4.1). A non-significant interaction was found ($\chi^2$ (2) = 4.380, p = 0.1119), which indicates that the observed pattern was not significantly different from the expected Mendelian ratio.

**Table 4.1 Expected and observed Mendelian inheritance patterns at 90dpf for line SH470**

| Line | Genotype | Expected Mendelian inheritance at 90dpf (%) | Observed Mendelian inheritance at 90dpf (%) |
|---|---|---|---|
| SH470 | C13H9orf72$^{+/+}$ | 25 | 27 |
| | C13H9orf72$^{SH470/+}$ | 50 | 57 |
| | C13H9orf72$^{SH470/SH470}$ | 25 | 16 |

In addition, the survival for this batch was better than observed previously (section 4.2.1.1), as knockout of *C13H9orf72* in the *C13H9orf72$^{SH470/SH470}$* embryos resulted in an average survival of 68% by 90dpf, with an average of 96% survival for *C13H9orf72$^{+/+}$* and 100% for *C13H9orf72$^{SH470/+}$*. This indicates that the result seen previously (figure 4.1) may have been due to variability in husbandry.

### 4.2.1.3. Survival at end stage

Following the genotyping at 90dpf, groups of 11 wild-type and 11 homozygous mutants from line SH470 were selected, based on power calculations from swim tunnel data obtained from a transgenic *SOD-1* zebrafish model of ALS (Ramesh et al. 2010). Table 4.2 below summarises the original and end-stage group sizes in this cohort, indicating there was no further decrease in survival by 12 months. A chi-squared ($\chi^2$) test was calculated, comparing the original and end-stage group sizes for each clutch. A non-significant interaction was found for line SH470 ($\chi^2$ (1) = 0, p = 1).

**Table 4.2 Group sizes at end stage for line SH470**

| Line | Genotype | DOB | Age at end stage | Original group size | End stage group size |
|---|---|---|---|---|---|
| SH470 | C13H9orf72$^{+/+}$ | 30.3.16 | 12 months | 11 | 11 |
| | C13H9orf72$^{SH470/SH470}$ | 30.3.16 | 12 months | 11 | 11 |

### 4.2.1. Investigating whether frameshift mutations in exon 7 of *C13H9orf72* lead to loss of viability

#### 4.2.1.1. Viability up to 21dpf

To address whether frameshift mutations in exon 7 of *C13H9orf72* resulted in early loss of viability in the zebrafish, survival monitoring was performed during larval stages for all lines generated, as described in section 2.7.1.

There was no significant difference in the survival of lines SH449, SH450 and SH451 up to 21dpf, with all three genotypes surviving at a similar rate (figure 4.2, B-D). However, there was a significant decline in survival at larval stages in line SH448 (p = 0.03, Mantel-Cox log-rank test; see figure 4.2 A), with average survival up to 21dpf for *C13H9orf72$^{SH448/SH448}$* and *C13H9orf72$^{SH448/+}$* embryos were 37% and 48%, respectively, compared to 55% for *C13H9orf72$^{+/+}$*. It is important to note that survival overall, especially for lines SH448, SH449 and SH450 (figure 4.2, A-C) appears lower for all genotypes in comparison to the other lines tested in section 4.2.1 and 4.2.2.
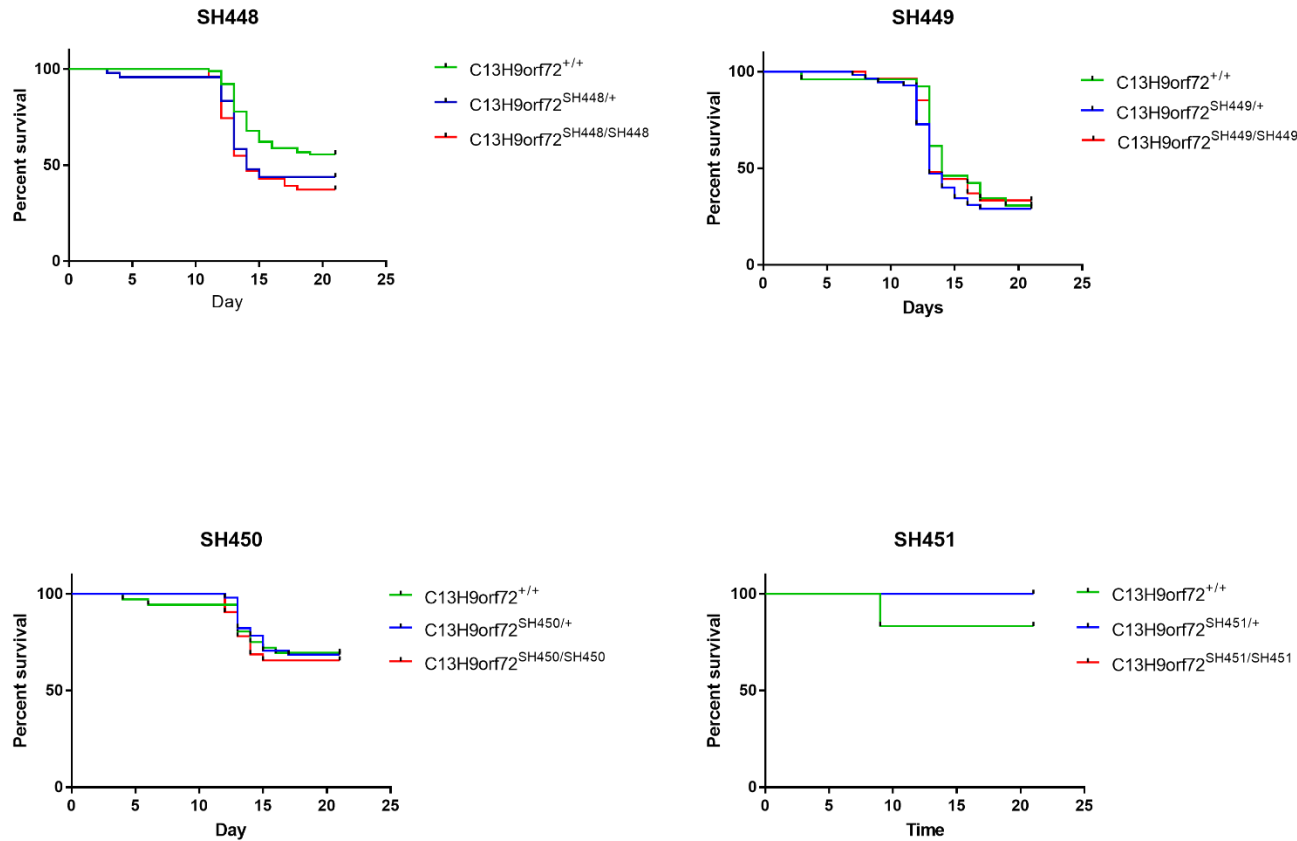
**Figure 4.2 Survival characterisation in zebrafish carrying frameshift mutations in exon 7 of C13H9orf72.** Figure shows Kaplan-Meier plots for lines A) SH448 (n = 3 clutches, p = 0.03, Mantel-Cox log-rank test) B) SH449 (n = 3 clutches, ns, Mantel-Cox log-rank test) C) SH450 (n = 2 clutches, ns, Mantel-Cox log-rank test) and D) SH451 (n = 1 clutch, ns, Mantel-Cox log-rank test), up to 21 dpf. Survival was performed during larval stages. Survival of wild-types are shown in green, heterozygous carriers in blue and homozygous mutants in red. Plots generated using GraphPad Prism 6.

#### 4.2.1.2. Viability up to 90dpf

Heterozygous carriers from lines SH448 and SH451 were in-crossed and raised to adulthood for phenotypic characterisation. Fin biopsies were taken for genotyping at 90dpf. A chi-squared ($\chi^2$) test was calculated, comparing the observed and expected Mendelian inheritance patterns for both lines at 90dpf (table 4.3). For each line, 2 clutches were raised for phenotypic characterisation. A non-significant interaction was found for line SH448 clutch 1 ($\chi^2$ (2) = 0.09, p = 0.9560) and clutch 2 ($\chi^2$ (2) = 5.94, p = 0.0513). Additionally, a non-significant interaction was found for line SH451 clutch 1 ($\chi^2$ (2) = 0.04, p = 0.9802) and clutch 2 ($\chi^2$ (2) = 2.46, p = 0.2923). Therefore, this shows that the observed patterns were not significantly different from the expected Mendelian ratios resulting from a heterozygous in-cross, in any of the lines raised.

**Table 4.3 Expected and observed Mendelian inheritance patterns at 90dpf for lines SH448 and SH451**

| Line | Genotype | Expected Mendelian inheritance at 90dpf (%) | Observed Mendelian inheritance at 90dpf (%) |
|---|---|---|---|
| SH448 clutch 1 | C13H9orf72$^{+/+}$ | 25 | 24.25 |
| | C13H9orf72$^{SH448/+}$ | 50 | 51.5 |
| | C13H9orf72$^{SH448/SH448}$ | 25 | 24.25 |
| SH448 clutch 2 | C13H9orf72$^{+/+}$ | 25 | 22.5 |
| | C13H9orf72$^{SH448/+}$ | 50 | 42 |
| | C13H9orf72$^{SH448/SH448}$ | 25 | 35.5 |
| SH451 clutch 1 | C13H9orf72$^{+/+}$ | 25 | 24.5 |
| | C13H9orf72$^{SH451/+}$ | 50 | 51 |
| | C13H9orf72$^{SH451/SH451}$ | 25 | 24.5 |
| SH451 clutch 2 | C13H9orf72$^{+/+}$ | 25 | 19 |
| | C13H9orf72$^{SH451/+}$ | 50 | 51 |
| | C13H9orf72$^{SH451/SH451}$ | 25 | 30 |

In addition, the survival for line SH448 was better than observed previously (section 4.2.2.1), as knockout of *C13H9orf72* in the *C13H9orf72$^{SH448/SH448}$* embryos resulted in an average survival of 75% by 90dpf, with an average of 84% survival for *C13H9orf72$^{+/+}$* and 81% for *C13H9orf72$^{SH448/+}$*. This indicates that the result seen previously (figure 4.2) may have been due to variability in husbandry.

### 4.2.1.3. Survival at end stage

Following the genotyping at 90dpf, groups of 11 wild-type and 11 homozygous mutants from lines SH448 and SH451 were selected, based on power calculations from swim tunnel data obtained from a transgenic *SOD-1* zebrafish model of ALS (Ramesh et al. 2010). However, group sizes of 10 wild-type and 10 homozygous mutants were selected for SH451 clutch 2, as we were limited by the number of available wild-types. A chi-squared ($\chi^2$) test was calculated, comparing the original and end-stage group sizes for each clutch. The use of a chi-square test is usually inappropriate if the expected frequency is below 5 in more than 20% of your cells. However, in the 2x2 case of the chi-square test of independence, expected frequencies less than 5 are usually considered acceptable if Yates' correction is employed, which was done here (table 4.4). In addition, a continuity correction of 0.5 was added to each cell. A non-significant interaction was found for line SH448 clutch 1 ($\chi^2$ (1) = 0.178, p = 0.6731) and clutch 2 ($\chi^2$ (1) = 0, p = 1). Additionally, a non-significant interaction was found for line SH451 clutch 1 ($\chi^2$ (1) = 0, p = 1) and clutch 2 ($\chi^2$ (1) = 0, p = 1). Therefore, this shows that end-stage group sizes were not significantly different from the original group sizes, in any of the lines.

**Table 4.4 Group sizes at end stage for line SH448 and SH451**

| Line | Genotype | DOB | Age at end stage | Original group size | End stage group size |
|---|---|---|---|---|---|
| SH448 clutch 1 | C13H9orf72$^{+/+}$ | 28.1.15 | 24 | 11 | 8 |
| | C13H9orf72$^{SH448/SH448}$ | 28.1.15 | 24 | 11 | 6 |
| SH448 clutch 2 | C13H9orf72$^{+/+}$ | 13.1.16 | 12 | 11 | 8 |
| | C13H9orf72$^{SH448/SH448}$ | 13.1.16 | 12 | 11 | 9 |
| SH451 clutch 1 | C13H9orf72$^{+/+}$ | 18.3.15 | 24 | 11 | 11 |
| | C13H9orf72$^{SH451/SH451}$ | 18.3.15 | 24 | 11 | 10 |
| SH451 clutch 2 | C13H9orf72$^{+/+}$ | 25.2.16 | 12 | 10 | 9 |
| | C13H9orf72$^{SH451/SH451}$ | 25.2.16 | 12 | 10 | 10 |

## 4.3. Characterisation of motor function in a stable *C13H9orf72* loss of function zebrafish

As discussed previously, loss of muscle strength is a hallmark phenotype seen in C9-ALS/FTD. Thus, the next aim of this project was to examine swimming endurance of the adult zebrafish carrying frameshift mutations in *C13H9orf72*. It was expected that if the zebrafish develop ALS/FTD-like phenotypes, a reduction in swimming endurance would be observed. In order to investigate this, two methods were used. Firstly, the swim tunnel was used to measure critical swimming speed ($U_{crit}$) of individual zebrafish (Plaut 2000). This method had previously been used to examine motor function in zebrafish models of motor neuron dysfunction, including in our lab (Chapman et al. 2013, Ramesh et al. 2010). Secondly, a novel method called the Spinning Task was used to examine swimming endurance (Blazina et al. 2013). This method had an advantage over the swim tunnel in that it was quicker to test motor function of large clutches of zebrafish, taking only a few minutes per individual, compared to up to 30 minutes using the swim tunnel (section 4.3.2).

### 4.3.1. Pilot study examining swimming endurance using the Spinning Task in adult zebrafish

The Spinning Task is represented in figure 4.3, consists of individually placing a zebrafish in to a beaker of system water containing a magnetic stirrer. The latency of the individual to be swept into the whirlpool was recorded, at both 400rpm (figure 4.4) and 500rpm (figure 4.5). The line SH448 (DOB 24.09.14) were the first line carrying LOF mutations raised to adulthood. Therefore, this line was used as the pilot cohort for this experiment. Group sizes consisted of n=6 wild-type (5 males and 1 female) and n=6 homozygous mutants (4 males and 2 females). At first, each individual was recorded for 60 seconds. However, this was increased up to 300s at 7 months onwards. This was done to ensure the latency of being swept into the whirlpool was recorded accurately.
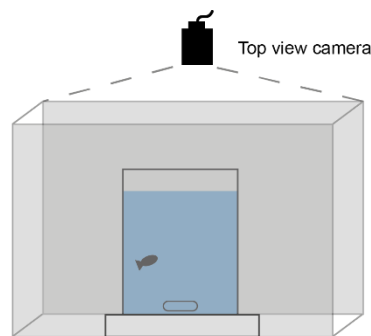


**Figure 4.3 Schematic of Spinning Task apparatus.** Design of the apparatus used for the spinning task. A 1-L beaker is placed on top of a stirrer with 800mL of aquarium system water, inside opaque walls made of cardboard.
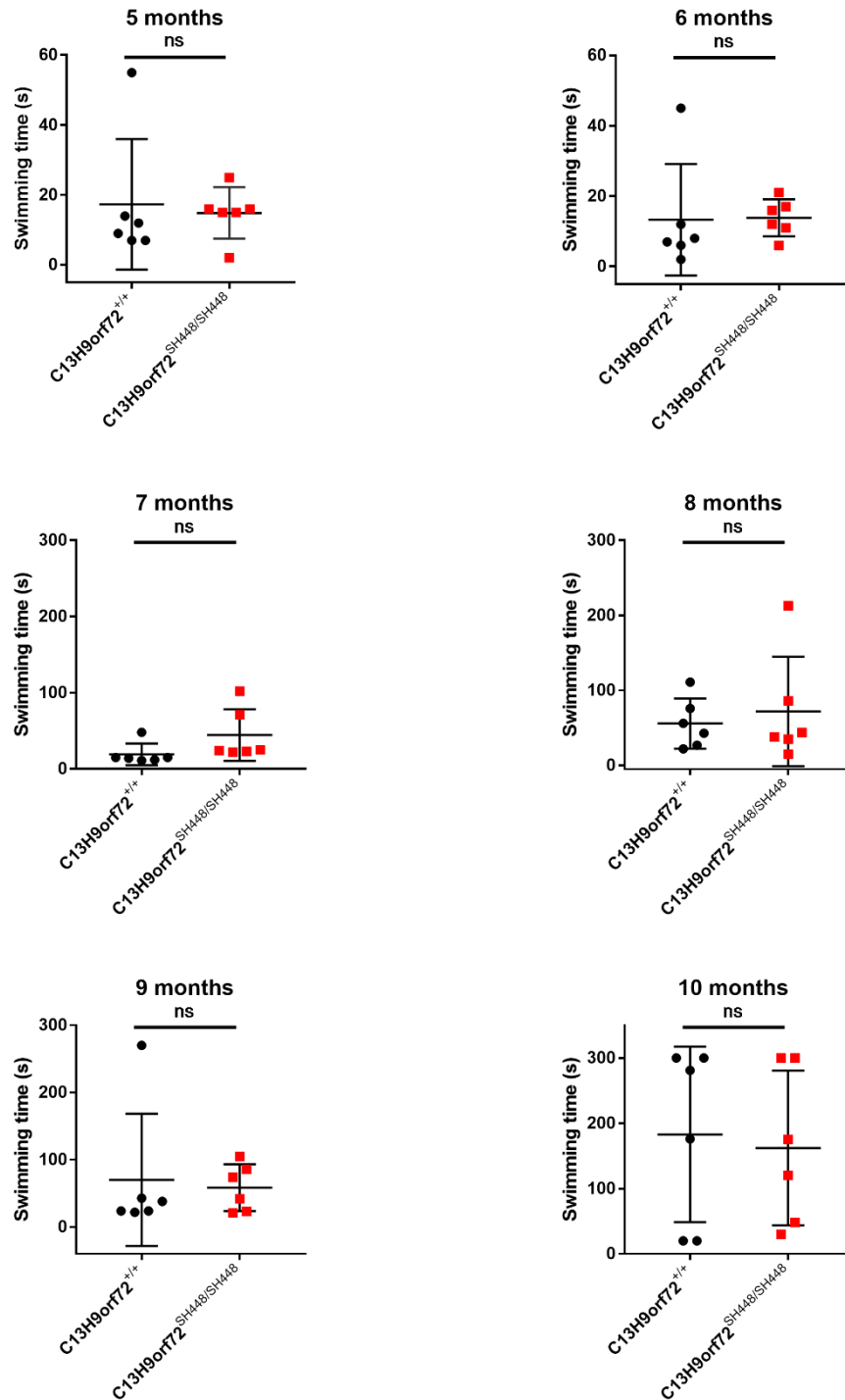
**Figure 4.4 Spinning task at 400rpm.** Time taken to be swept into the whirlpool at 400rpm is represented for both genotypes (C13Horf72$^{+/+}$ n=6 and C13H9orf72$^{SH448/SH448}$ n=6) at months 5-10. Mean average time for the group and standard deviation is shown. An unpaired t-test revealed that there is no significant difference at any time point tested.
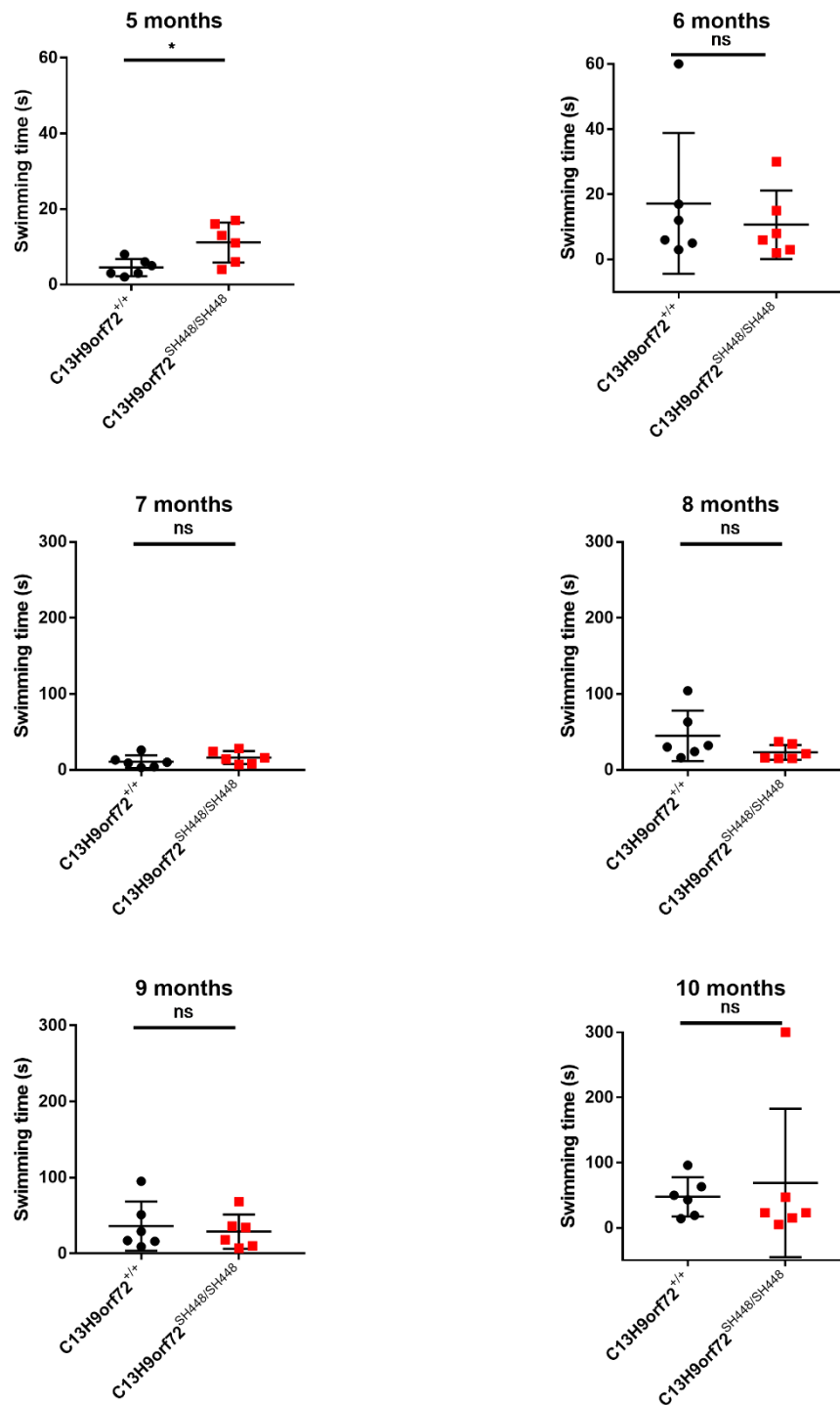
**Figure 4.5 Spinning task at 500rpm.** Time taken to be swept into the whirlpool at 500rpm is represented for both genotypes (C13H9orf72^{+/+} n=6 and C13H9orf72[SH448/SH448] n=6) at months 5-10. Mean average time for the group and standard deviation is shown. An unpaired t-test revealed that there is no significant difference at time points 6-10 months. At 5 months, there is a significant difference, *; p=0.0173.

There was no significant difference observed between $C13H9orf72^{SH448/SH448}$ mutants and their wild-type siblings at any time point tested (5-10 months) at 400rpm (figure 4.4). Additionally, there was no significant difference observed between $C13H9orf72^{SH448/SH448}$ mutants and their wild-type siblings at time points 6-10 months at 500rpm (figure 4.5). However, a significant difference was seen at 5 months (unpaired t-test, p=0.0173), with homozygous mutants swimming longer against the current than their wild-type siblings.

Additionally, the coefficient of variation was high at both speeds tested (table 4.5). The coefficient of variation is the standard deviation as a percentage of the mean. The higher this percentage is, the greater the level of dispersion around the mean. For example, the average coefficient of variation of wild-types in the spinning task was 95.68% at 400rpm and 80.34% at 500rpm. In comparison, the average coefficient of variation of wild-types in the swim tunnel was 11.67% (table 4.7, SH448 clutch 1), indicating the swim tunnel method is less variable than the spinning task. As a result, the spinning task was no longer used and the primary method chosen for examining motor output was the swim tunnel.

**Table 4.5 Summary of mean ± SD plus coefficient of variation at 400 and 500rpm**

| Genotype | Time point (month) | Speed (rpm) | 'N' number | Mean (s) ± SD | Coefficient of variation |
|---|---|---|---|---|---|
| C13H9orf72$^{+/+}$ | 5 | 400 | 6 | 17.33±18.66 | 107.66% |
| C13H9orf72$^{SH448/SH448}$ | 5 | 400 | 6 | 14.83±7.36 | 49.62% |
| **C13H9orf72$^{+/+}$** | **5** | **500** | **6** | **4.50±2.26** | **50.18%** |
| **C13H9orf72$^{SH448/SH448}$** | **5** | **500** | **6** | **11.17±5.27** | **47.19%** |
| C13H9orf72$^{+/+}$ | 6 | 400 | 6 | 13.33±15.85 | 118.84% |
| C13H9orf72$^{SH448/SH448}$ | 6 | 400 | 6 | 13.83±5.27 | 38.09% |
| **C13H9orf72$^{+/+}$** | **6** | **500** | **6** | **17.50±22.40** | **128.02%** |
| **C13H9orf72$^{SH448/SH448}$** | **6** | **500** | **6** | **10.67±10.54** | **98.80%** |
| C13H9orf72$^{+/+}$ | 7 | 400 | 6 | 19.17±14.22 | 74.18% |
| C13H9orf72$^{SH448/SH448}$ | 7 | 400 | 6 | 44.50±33.99 | 76.39% |
| **C13H9orf72$^{+/+}$** | **7** | **500** | **6** | **10.83±8.33** | **76.88%** |
| **C13H9orf72$^{SH448/SH448}$** | **7** | **500** | **6** | **16.17±8.45** | **52.25%** |
| C13H9orf72$^{+/+}$ | 8 | 400 | 6 | 55.83±33.44 | 59.89% |
| C13H9orf72$^{SH448/SH448}$ | 8 | 400 | 6 | 71.83±72.99 | 101.60% |
| **C13H9orf72$^{+/+}$** | **8** | **500** | **6** | **44.83±33.11** | **73.85%** |
| **C13H9orf72$^{SH448/SH448}$** | **8** | **500** | **6** | **23.00±9.98** | **43.39%** |
| C13H9orf72$^{+/+}$ | 9 | 400 | 6 | 70.17±98.27 | 140.06% |
| C13H9orf72$^{SH448/SH448}$ | 9 | 400 | 6 | 58.50±34.92 | 59.69% |
| **C13H9orf72$^{+/+}$** | **9** | **500** | **6** | **36.17±32.39** | **89.55%** |
| **C13H9orf72$^{SH448/SH448}$** | **9** | **500** | **6** | **28.83±22.63** | **78.49%** |
| C13H9orf72$^{+/+}$ | 10 | 400 | 6 | 182.83±134.29 | 73.45% |
| C13H9orf72$^{SH448/SH448}$ | 10 | 400 | 6 | 162.17±118.69 | 73.19% |
| **C13H9orf72$^{+/+}$** | **10** | **500** | **6** | **47.50±30.18** | **63.53%** |
| **C13H9orf72$^{SH448/SH448}$** | **10** | **500** | **6** | **68.83±114.10** | **165.76%** |

### 4.3.2. Examination of critical swimming speed ($U_{crit}$) using the Swim Tunnel in adult zebrafish

As discussed in section 4.3.1, the primary method chosen for examining motor output was the swim tunnel. As noted in tables 4.7 – 4.11, coefficient of variation is relatively low for both genotypes tested at all the time points, providing confidence that this protocol has low variability and is sensitive to detect significant changes in motor function. This method involved placing the individual zebrafish into the swim tunnel (figure 4.6) and enabling them to swim against a current of water, starting at approximately 6.58cm/s. Every five minutes, this current increased by approximately 6.58cm/s, until the zebrafish could no longer swim or until a maximum of 39.47cm/s was established. To quantify endurance, critical swimming speed ($U_{crit}$) was determined by monitoring the ability of the zebrafish to swim against the increasing current over time (Plaut 2000), on the cohorts summarised in table 4.6.
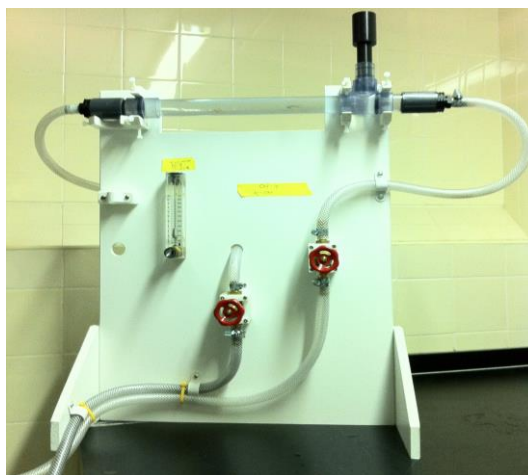


**Figure 4.6 Image of swim tunnel apparatus used to measure swimming endurance.**
The custom-built swim tunnel was used to measure swimming endurance. Zebrafish were placed in the tunnel and a current of water applied. Which they naturally swim against. Every 5 minutes this current was increased until they could no longer swim against it or 30 minutes had passed.

**Table 4.6 Genotype and group sizes of clutches tested through swim tunnel apparatus.** Key words: WT = wild type; HOM = homozygous mutant.

| Line | DOB | Genotype | Number of males | Number of females | Overall sample size |
|---|---|---|---|---|---|
| SH448 clutch 1 | 28.1.15 | WT | 5 | 6 | 11 |
| -- | -- | HOM | 5 | 6 | 11 |
| SH448 clutch 2 | 13.1.16 | WT | 6 | 5 | 11 |
| -- | -- | HOM | 6 | 5 | 11 |
| SH451 clutch 1 | 18.3.15 | WT | 5 | 6 | 11 |
| -- | -- | HOM | 5 | 6 | 11 |
| SH451 clutch 2 | 25.2.16 | WT | 6 | 4 | 10 |
| -- | -- | HOM | 6 | 4 | 10 |
| SH470 | 30.3.16 | WT | 5 | 6 | 11 |
| -- | -- | HOM | 5 | 6 | 11 |

#### 4.3.2.1. SH448 swimming endurance clutch 1 (DOB 28.1.15)

Critical swimming velocity ($U_{crit}$) of C13H9orf72$^{SH448/SH448}$ zebrafish and their wild-type siblings was initially determined at 12, 15, 18, 21 and 24 months (± 7 days). The results demonstrate that $U_{crit}$ is significantly reduced in C13H9orf72$^{SH448/SH448}$ zebrafish at 15 months (p=0.0042, 2-way ANOVA with fisher's LSD test) and 21 months (p=0.0195, 2-way ANOVA with fisher's LSD test), relative to wild-types (figure 4.7). Additionally, a non-significant reduction in $U_{crit}$ is seen at 12, 18 and 24 months in C13H9orf72$^{SH448/SH448}$ zebrafish (figure 4.7). The mean $U_{crit}$ ± SD, plus coefficient of variation is summarised in table 4.7.
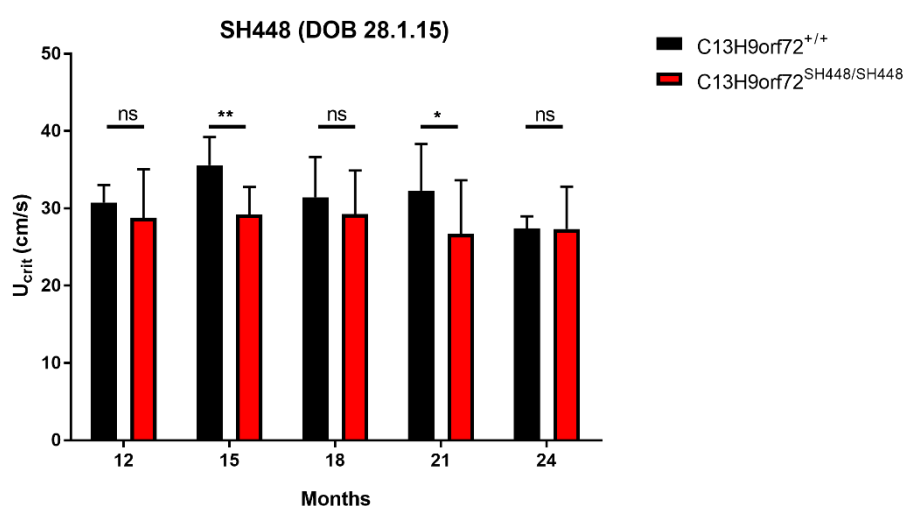


**Figure 4.7 Ucrit values for line SH448 clutch 1 (DOB 28.1.15)** Graph shows mean $U_{crit}$ values ± s.d. for C9orf72$^{SH448/SH448}$ vs wild-type siblings at all the time points tested in the swim tunnel. Significance tested using 2-way ANOVA with Fisher's LSD test, * p<0.05 and ** p<0.01, n = 6-11.

**Table 4.7 Summary of line SH448 clutch 1 (DOB 28.1.15)**

| Genotype | DOB | Age (months) | Mean U$_{crit}$ (cm/s) ± SD | Coefficient of variation |
|---|---|---|---|---|
| C13H9orf72$^{+/+}$ | 28.1.15 | 12 | 30.76 ± 2.24 | 7.28% |
| C13H9orf72$^{SH448/SH448}$ | 28.1.15 | 12 | 28.79 ± 6.25 | 21.70% |
| C13H9orf72$^{+/+}$ | 28.1.15 | 15 | 35.57 ± 3.64 | 10.24% |
| C13H9orf72$^{SH448/SH448}$ | 28.1.15 | 15 | 29.21 ± 3.57 | 12.22% |
| C13H9orf72$^{+/+}$ | 28.1.15 | 18 | 31.43 ± 5.19 | 16.52% |
| C13H9orf72$^{SH448/SH448}$ | 28.1.15 | 18 | 29.25 ± 5.66 | 19.34% |
| C13H9orf72$^{+/+}$ | 28.1.15 | 21 | 32.27 ± 6.06 | 18.78% |
| C13H9orf72$^{SH448/SH448}$ | 28.1.15 | 21 | 26.69 ± 6.96 | 26.06% |
| C13H9orf72$^{+/+}$ | 28.1.15 | 24 | 27.44 ± 1.52 | 5.54% |
| C13H9orf72$^{SH448/SH448}$ | 28.1.15 | 24 | 27.34 ± 5.46 | 19.97% |

#### 4.3.2.2. SH448 swimming endurance clutch 2 (DOB 13.1.16)

Next, the $U_{crit}$ of C13H9orf72$^{SH448/SH448}$ zebrafish and their wild-type siblings was determined in a second clutch at 4, 6, 9 and 12 months ($\pm$ 7 days), to see if the reduction in $U_{crit}$ reported in section 4.3.2.1 was observed earlier than 12 months. The results demonstrate that $U_{crit}$ is reduced in C13H9orf72$^{SH448/SH448}$ zebrafish relative to wild-types at all the time points (figure 4.8). However, this was not statistically significant at any time point tested. The mean $U_{crit} \pm$ SD, plus coefficient of variation is summarised in table 4.8.
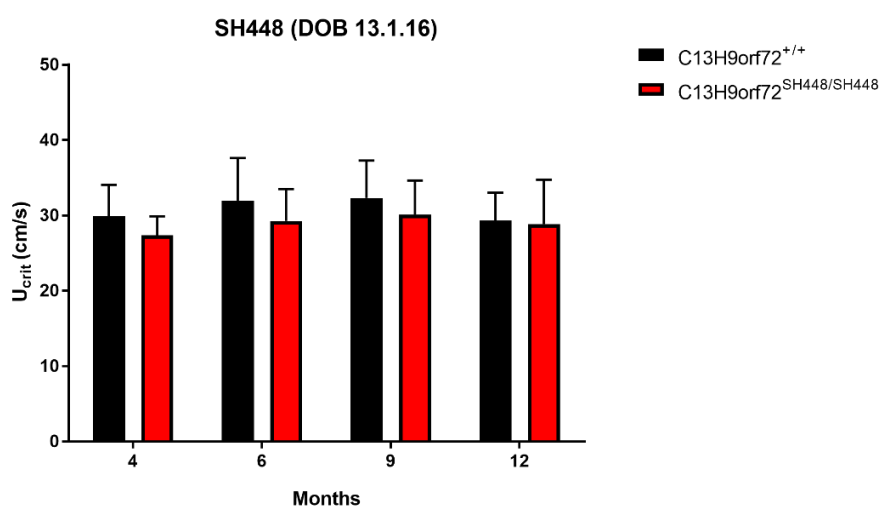


**Figure 4.8 Ucrit values for line SH448 experiment 2 (DOB 13.1.16).** Graph shows mean $U_{crit}$ values $\pm$ s.d. for C9orf72$^{SH448/SH448}$ vs wild-type siblings at all the time points tested in the swim tunnel. Significance tested using 2-way ANOVA with Fisher's LSD test, ns, n=8-11.

**Table 4.8  Summary of line SH448 experiment 2 (DOB 13.1.16)**

| Genotype | DOB | Age (months) | Mean $U_{crit}$ (cm/s) $\pm$ SD | Coefficient of variation |
|---|---|---|---|---|
| C13H9orf72$^{+/+}$ | 13.1.16 | 4 | 29.92 $\pm$ 4.14 | 13.84% |
| C13H9orf72$^{SH448/SH448}$ | 13.1.16 | 4 | 27.38 $\pm$ 2.52 | 9.21% |
| C13H9orf72$^{+/+}$ | 13.1.16 | 6 | 31.95 $\pm$ 5.68 | 17.78% |
| C13H9orf72$^{SH448/SH448}$ | 13.1.16 | 6 | 29.28 $\pm$ 4.23 | 14.45% |
| C13H9orf72$^{+/+}$ | 13.1.16 | 9 | 32.32 $\pm$ 4.96 | 15.36% |
| C13H9orf72$^{SH448/SH448}$ | 13.1.16 | 9 | 30.14 $\pm$ 4.51 | 14.95% |
| C13H9orf72$^{+/+}$ | 13.1.16 | 12 | 29.34 $\pm$ 3.70 | 12.62% |
| C13H9orf72$^{SH448/SH448}$ | 13.1.16 | 12 | 28.87 $\pm$ 5.87 | 20.32% |

### 4.3.2.3. SH451 swimming endurance experiment 1 (DOB 18.3.15)

The $U_{crit}$ of C13H9orf72$^{SH451/SH451}$ zebrafish and their wild-type siblings was initially determined at 9, 12, 15, 18, 21 and 24 months ($\pm$ 7 days). The results demonstrate that $U_{crit}$ is significantly reduced in C13H9orf72$^{SH451/SH451}$ zebrafish at 12 months (p=0.0114, 2-way ANOVA with fisher's LSD test), relative to wild-types (figure 4.9). Additionally, a non-significant reduction in $U_{crit}$ is seen at 9, 15, 18, 21 and 24 months in C13H9orf72$^{SH451/SH451}$ zebrafish (figure 4.9). The mean $U_{crit} \pm$ SD, plus coefficient of variation is summarised in table 4.9.
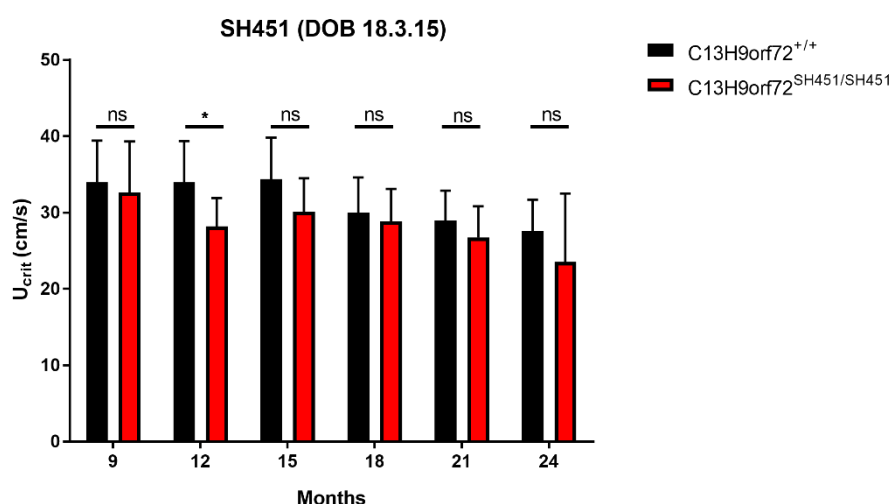


**Figure 4.9 Ucrit values for line SH451 experiment 1 (DOB 18.3.15).** Graph shows mean $U_{crit}$ values $\pm$ s.d. for C9orf72$^{SH451/SH451}$ vs wild-type siblings at all the time points tested in the swim tunnel. Significance tested using 2-way ANOVA with Fisher's LSD test, * p<0.05, n = 9-11.

**Table 4.9 Summary of line SH451 experiment 1 (DOB 18.3.15)**

| Genotype | DOB | Age (months) | Mean U$_{crit}$ (cm/s) ± SD | Coefficient of variation |
|----------|-----|--------------|------------------------------|--------------------------|
| C13H9orf72$^{+/+}$ | 18.3.15 | 9 | 34.00 ± 5.41 | 15.94% |
| C13H9orf72$^{SH451/SH451}$ | 18.3.15 | 9 | 32.68 ± 6.65 | 20.36% |
| C13H9orf72$^{+/+}$ | 18.3.15 | 12 | 33.97 ± 5.42 | 15.35% |
| C13H9orf72$^{SH451/SH451}$ | 18.3.15 | 12 | 28.22 ± 3.68 | 13.04% |
| C13H9orf72$^{+/+}$ | 18.3.15 | 15 | 34.38 ± 5.43 | 15.78% |
| C13H9orf72$^{SH451/SH451}$ | 18.3.15 | 15 | 30.13 ± 4.38 | 14.54% |
| C13H9orf72$^{+/+}$ | 18.3.15 | 18 | 29.98 ± 4.63 | 15.44% |
| C13H9orf72$^{SH451/SH451}$ | 18.3.15 | 18 | 28.87 ± 4.24 | 14.68% |
| C13H9orf72$^{+/+}$ | 18.3.15 | 21 | 28.99 ± 3.89 | 13.40% |
| C13H9orf72$^{SH451/SH451}$ | 18.3.15 | 21 | 26.77 ± 4.07 | 15.94% |
| C13H9orf72$^{+/+}$ | 18.3.15 | 24 | 27.60 ± 4.08 | 14.80% |
| C13H9orf72$^{SH451/SH451}$ | 18.3.15 | 24 | 23.61 ± 9.07 | 38.39% |

#### 4.3.2.4. SH451 swimming endurance experiment 2 (DOB 25.2.16)

Next, the $U_{crit}$ of C13H9orf72$^{SH451/SH451}$ zebrafish and their wild-type siblings was determined in a second clutch at 4, 6, 9 and 12 months ($\pm$ 7 days), to see if the reduction in $U_{crit}$ reported in section 4.3.2.3 was observed earlier than 9 months. The results demonstrate that $U_{crit}$ is reduced in C13H9orf72$^{SH451SH451}$ zebrafish relative to wild-types at all the time points (figure 4.10). However, this was not statistically significant at any time point tested. The mean $U_{crit} \pm$ SD, plus coefficient of variation is summarised in table 4.10.
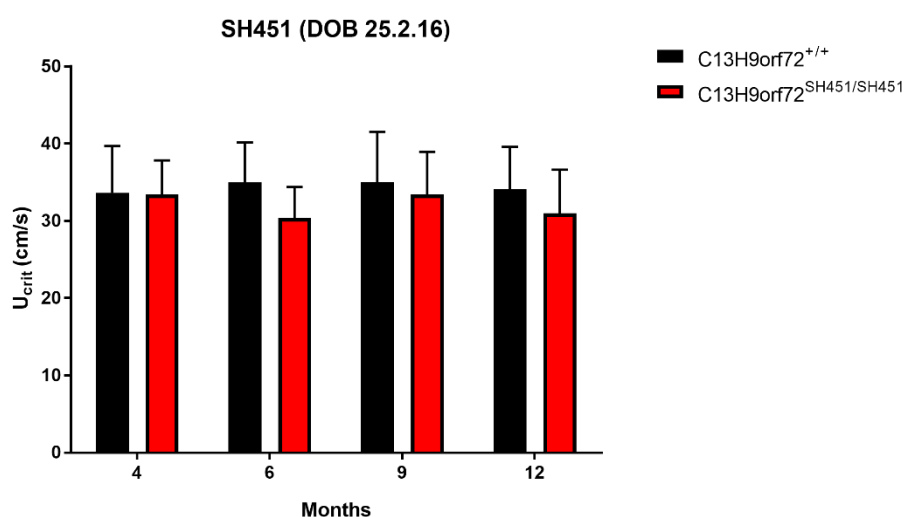


**Figure 4.10 Ucrit values for line SH451 experiment 2 (DOB 25.2.16).** Graph shows mean $U_{crit}$ values $\pm$ s.d. for C9orf72$^{SH451/SH451}$ vs wild-type siblings at all the time points tested in the swim tunnel. Significance tested using 2-way ANOVA with Fisher's LSD test, ns, n = 9-10.

**Table 4.10 Summary of line SH451 experiment 2 (DOB 25.2.16)**

| Genotype | DOB | Age (months) | Mean U$_{crit}$ (cm/s) $\pm$ SD | Coefficient of variation |
|---|---|---|---|---|
| C13H9orf72$^{+/+}$ | 25.2.16 | 4 | 34.16 $\pm$ 6.03 | 17.64% |
| C13H9orf72$^{SH451/SH451}$ | 25.2.16 | 4 | 33.42 $\pm$ 4.40 | 13.17% |
| C13H9orf72$^{+/+}$ | 25.2.16 | 6 | 34.98 $\pm$ 5.18 | 14.80% |
| C13H9orf72$^{SH451/SH451}$ | 25.2.16 | 6 | 30.37 $\pm$ 4.01 | 13.21% |
| C13H9orf72$^{+/+}$ | 25.2.16 | 9 | 35.03 $\pm$ 6.50 | 18.57% |
| C13H9orf72$^{SH451/SH451}$ | 25.2.16 | 9 | 33.42 $\pm$ 5.52 | 16.51% |
| C13H9orf72$^{+/+}$ | 25.2.16 | 12 | 34.14 $\pm$ 5.45 | 15.96% |
| C13H9orf72$^{SH451/SH451}$ | 25.2.16 | 12 | 30.98 $\pm$ 5.64 | 18.22% |

#### 4.3.2.5. Swimming endurance line SH470 (DOB 30.3.16)

The $U_{crit}$ of C13H9orf72$^{SH470/SH470}$ zebrafish and their wild-type siblings was determined at 4, 6, 9 and 12 months ($\pm$ 7 days). The results demonstrate that $U_{crit}$ is significantly reduced in C13H9orf72$^{SH470/SH470}$ zebrafish at 9 months (p=0.0276, 2-way ANOVA with fisher's LSD test), relative to wild-types (figure 4.11). Additionally, a non-significant reduction in $U_{crit}$ is seen at 4, 6 and 12 months in C13H9orf72$^{SH470/SH470}$ zebrafish (figure 4.11). The mean $U_{crit}$ $\pm$ SD, plus coefficient of variation is summarised in table 4.11.
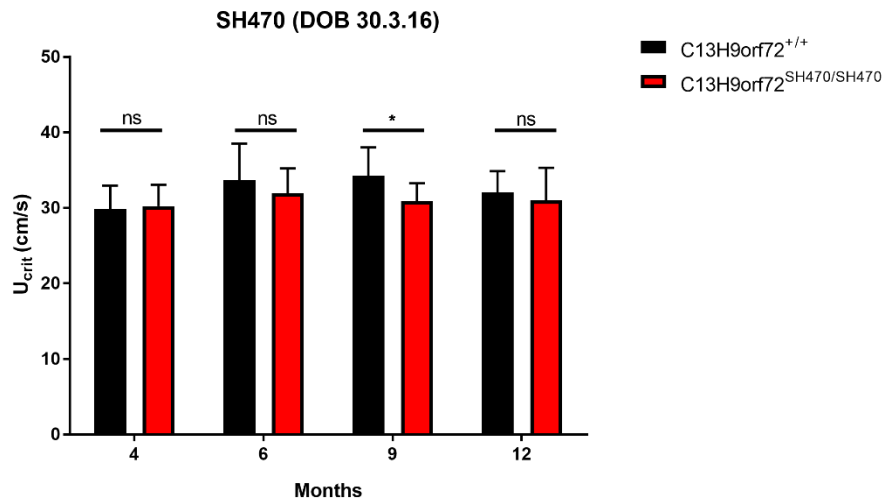


**Figure 4.11 Ucrit values for line SH470.** Graph shows mean $U_{crit}$ values $\pm$ s.d. for C9orf72$^{SH470/SH470}$ vs wild-type siblings at all the time points tested in the swim tunnel. Significance tested using 2-way ANOVA with Fisher's LSD test, * p<0.05, n = 11.

**Table 4.11 Summary of line SH470 experiment (DOB 30.3.16)**

| Genotype | DOB | Age (months) | Mean U$_{crit}$ (cm/s) $\pm$ SD | Coefficient of variation |
|---|---|---|---|---|
| C13H9orf72$^{+/+}$ | 30.3.16 | 4 | 29.85 $\pm$ 3.12 | 10.45% |
| C13H9orf72$^{SH470/SH470}$ | 30.3.16 | 4 | 30.23 $\pm$ 2.83 | 9.36% |
| C13H9orf72$^{+/+}$ | 30.3.16 | 6 | 33.67 $\pm$ 4.83 | 14.33% |
| C13H9orf72$^{SH470/SH470}$ | 30.3.16 | 6 | 31.94 $\pm$ 3.30 | 10.33% |
| C13H9orf72$^{+/+}$ | 30.3.16 | 9 | 34.24 $\pm$ 3.78 | 11.04% |
| C13H9orf72$^{SH470/SH470}$ | 30.3.16 | 9 | 30.88 $\pm$ 2.39 | 7.74% |
| C13H9orf72$^{+/+}$ | 30.3.16 | 12 | 32.06 $\pm$ 2.80 | 8.72% |
| C13H9orf72$^{SH470/SH470}$ | 30.3.16 | 12 | 31.00 $\pm$ 4.30 | 13.86% |

#### 4.3.2.6.  Investigating the correlation between weight and/or length vs $U_{crit}$ value

If possible, zebrafish of a similar weight and length were selected when determining experimental groups for the swim tunnel. To investigate whether the weight and lengths of individuals were influencing swimming performance, the correlation coefficient for weight vs $U_{crit}$ and length vs $U_{crit}$ (n=8-11) was calculated. The correlation coefficient can take a range of values from -1 to +1. A value of 0 indicates that there is no association, a positive value indicates a positive association and a negative value indicates a negative association between the two variables investigated. The magnitude of the correlation coefficient determines the strength of the correlation, summarised in the table below (table 4.12) (Mukaka 2012).

**Table 4.12 Guidelines to determine the strength of the correlation coefficient** Adapted from (Mukaka 2012).

| Strength of association | Size of Correlation |
|---|---|
| Very high positive (negative) correlation | 0.90 to 1.00 (-0.9 to – 1.00) |
| High positive (negative) correlation | 0.70 to 0.90 (-0.70 to -0.90) |
| Moderate positive (negative) correlation | 0.50 to 0.70 (-0.50 to -0.70) |
| Low positive (negative) correlation | 0.30 to 0.50 (-0.30 to -0.50) |
| Negligible correlation | 0.00 to 0.30 (0.00 to -0.30) |

Figures 4.12 and 4.13 show data collated from each line at the 12-month time point for comparison. In most lines tested, there was a negligible correlation between weight and $U_{crit}$ at this time point (values <0.3, figure 4.12, A-C). However, the wild-type siblings for line SH470 showed a low positive correlation between weight and $U_{crit}$ (value >0.3) (figure 4.12 C). Regarding length, line SH448 showed a low positive correlation between length and $U_{crit}$ (value >0.3, figure 4.13 A). However, both lines SH451 and SH470 showed a negligible correlation between length and $U_{crit}$ (values >0.3, figure 4.13 B-C). As no high correlations were observed for this time point, it provides confidence that the weight and lengths of the individuals selected for the experimental groups are not influencing the $U_{crit}$ values obtained from the swim tunnel.
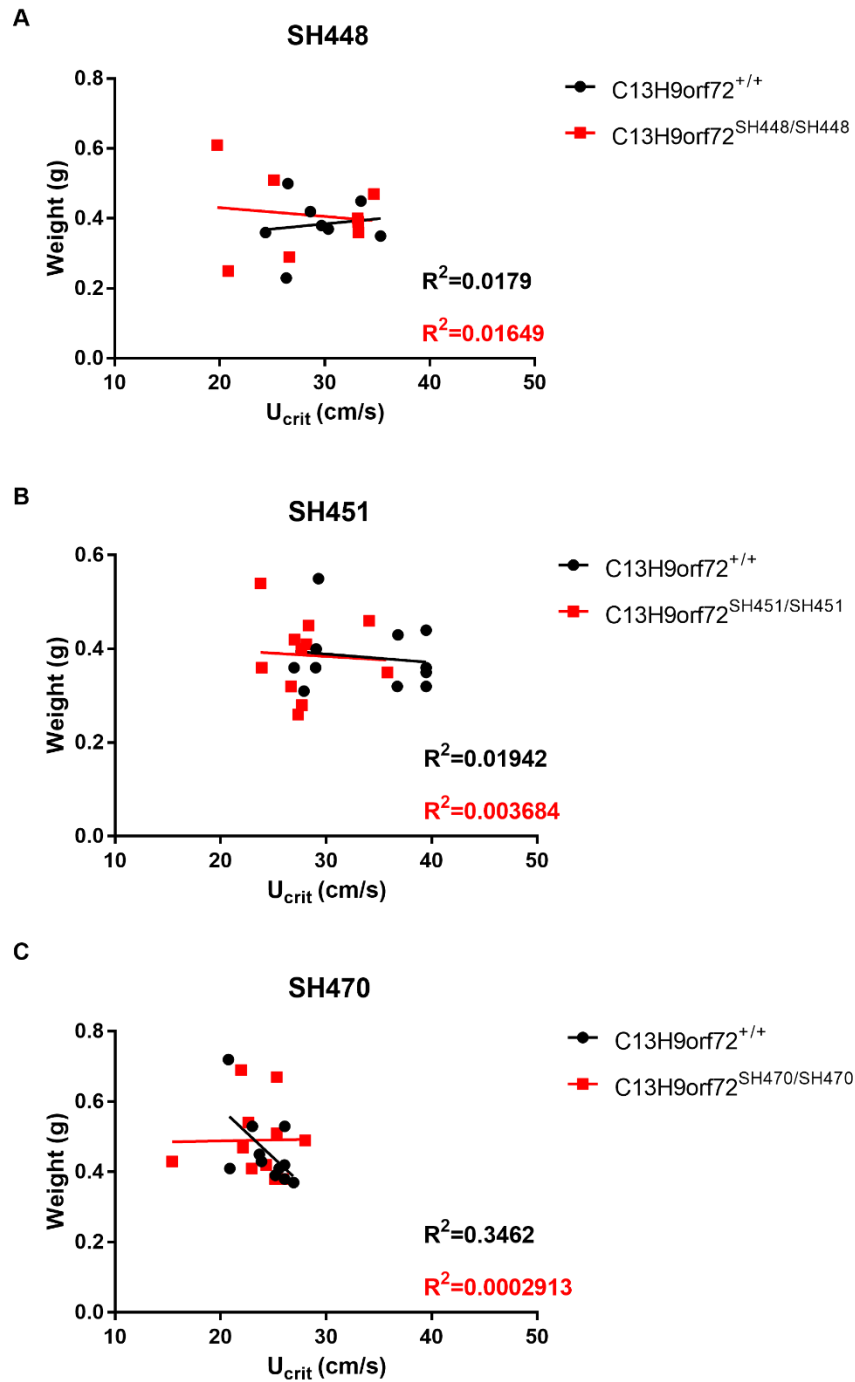
**Figure 4.12 Investigating the correlation between weight vs Ucrit values at 12 months.** Graphs represent correlation coefficients for weight (g) vs $U_{crit}$ (cm/s) for line A) SH448, B) SH451 and C) SH470. $R^2$ values shown on the graphs, with wild-type values in black and homozygous mutant values in red for all alleles. Group sizes n=8-11.
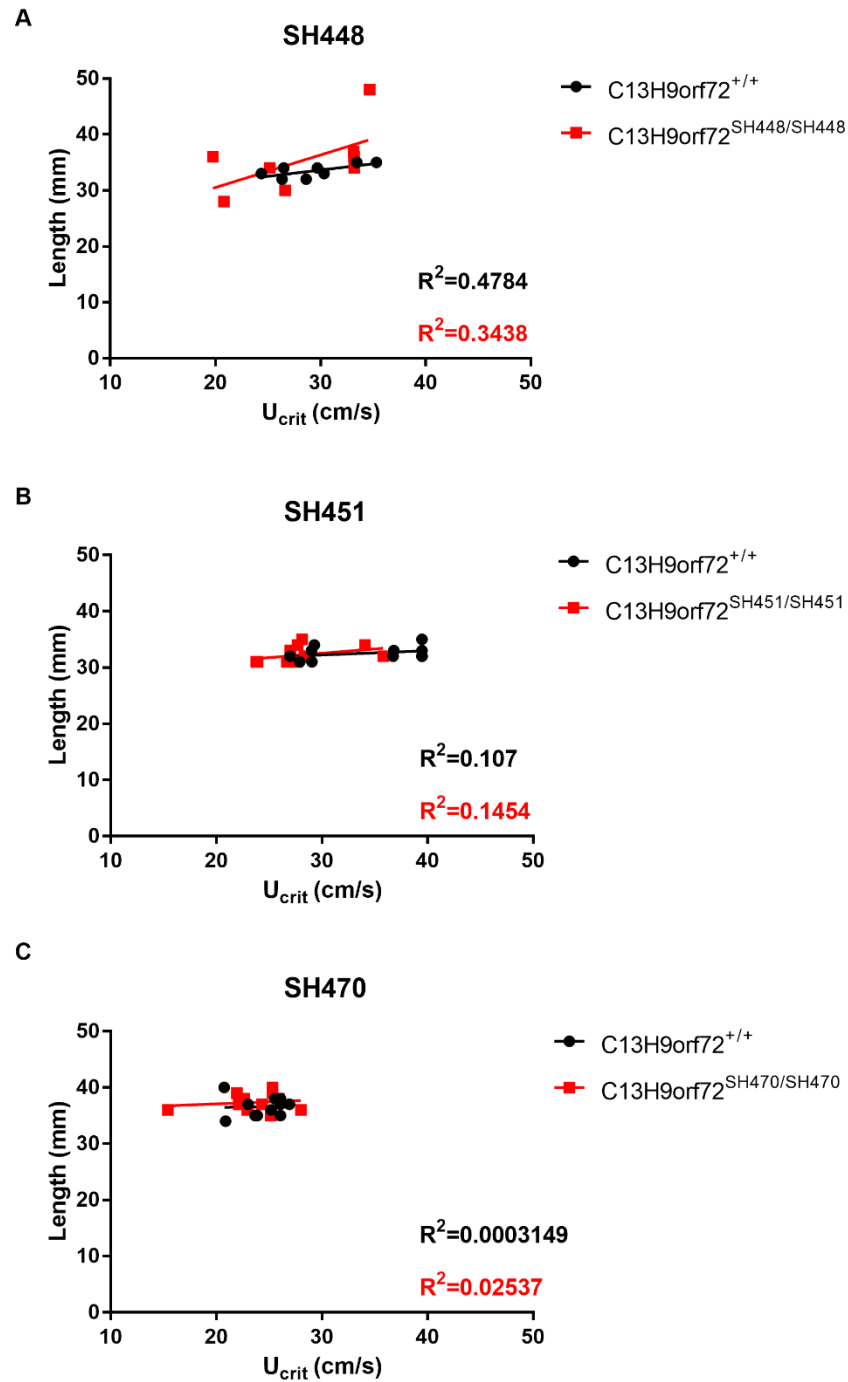
**Figure 4.13 Investigating the correlation between length vs Ucrit values at 12 months.** Graphs represent correlation coefficients for length (mm) vs $U_{crit}$ (cm/s) for line A) SH448, B) SH451 and C) SH470. $R^2$ values shown on the graphs, with wild-type values in black and homozygous mutant values in red for all alleles. Group sizes n=8-11.

#### 4.3.2.7.    Investigating the effect of gender on swimming endurance

To determine whether gender had an effect on the $U_{crit}$ of the zebrafish, the $U_{crit} \pm SD$ for both wild-type and mutant males and females were compared. Figure 4.14 shows data collected from each line at a 9-month time point for all lines tested. In 4.14 A, there is a significant difference between female C13H9orf72$^{SH448/SH448}$ vs male C13H9orf72$^{SH448/SH448}$ (p=0.0070). In 4.14 B, there is a significant difference between male C13H9orf72$^{+/+}$ vs female C13H9orf72$^{+/+}$ (p=0.0030). There is also a significant difference between male C13H9orf72$^{SH451/SH451}$ vs female C13H9orf72$^{SH451/SH451}$ (p=0.0303). Additionally, in 4.14 C, there is a significant difference between male C13H9orf72$^{+/+}$ vs female C13H9orf72$^{+/+}$ (p=0.0144). This data demonstrates that female $U_{crit}$ is lower than male $U_{crit}$ in over half of the 9-month data sets. This is possibly linked to body shape, as observed in figure 4.15, the female zebrafish have a distended belly, as they contain eggs, whereas male zebrafish are generally slimmer.  The females may therefore experience increased hydrodynamic drag when swimming in the tunnel, causing them to tire quicker in comparison to males.
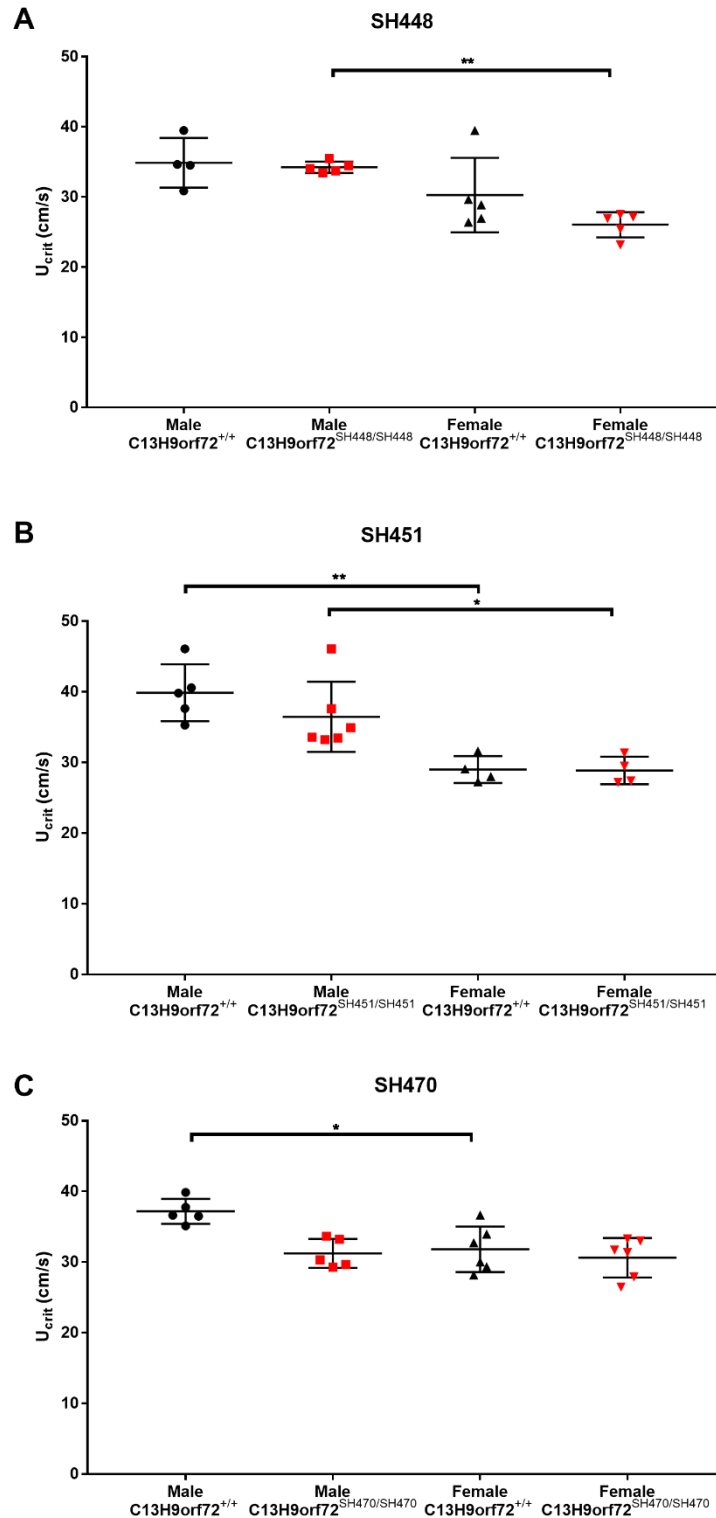
**Figure 4.14 Observing the effect of gender on Ucrit (cm/s) at 9 months.** Graphs show the range of $U_{crit}$ (cm/s) values for males and females, of both genotypes, for lines A) SH448 (n=9-10), B) SH451 (n=9-10) and C) SH470 (n=11). Significance tested using a one-way ANOVA with Tukey's post-test A) $p < 0.01$ B) $p < 0.001$ and C) $p < 0.01$. Multiple comparisons were also made, * = $p < 0.05$ and ** = $p < 0.01$

**Figure 4.15 Comparisons between male and female zebrafish body shape.** Photograph depicts an adult wild-type male (WT, M) and a wild-type female (WT, F) zebrafish, representing the differences in body shape. Scale bar = 1cm.

### 4.3.2.8. Examination of neuromuscular junctions (NMJ) in adult zebrafish

Defects at the neuromuscular junction (NMJ) are apparent in both ALS rodent models and patients well before symptom onset (Fischer et al. 2004, Fischer and Glass 2007). Therefore, it was important to perform pathological characterisation of NMJs in control and homozygous mutant zebrafish. We stained trunk musculature with α-bungarotoxin (a post-synaptic marker of the NMJ) and SV2 (a presynaptic marker that labels motor neurons), and used confocal microscopy to quantify the intensity correlation quotient (ICQ) (Li et al. 2004), size and number of both the pre- and post-synaptic compartments, as has been done in previous studies (Ramesh et al. 2010, Chapman et al. 2013). The ICQ is a statistically testable single-value assessment of the relationship between two staining patterns: colocalising signals have $0<ICQ\leq+0.5$, for random staining $ICQ=0$, and for non-colocalising (segregated) staining $0>ICQ\geq-0.5$ (Li et al. 2004). This was investigated in 11-month old zebrafish from the lines SH448 and SH451, because it was observed that the zebrafish had a moderate reduction in $U_{crit}$ around this time point. If defects at the NMJ are associated with this altered swimming, we would expect to see a reduction in ICQ, as well as the size and number of pre- and post- synaptic compartments, indicative of degeneration of the NMJ.

#### 4.3.2.8.1.　　NMJ analysis in C13H9orf72$^{+/+}$ vs C13H9orf72$^{SH448/SH448}$

In 11-month old C13H9orf72$^{SH448/SH448}$ zebrafish, the SV2 and α-bungarotoxin staining (figure 4.16) showed ICQ values of $0.20 \pm 0.02$, which was not statistically significant from wild-type siblings ICQ value of $0.24 \pm 0.06$ (unpaired t-test, ns, n=4 per genotype, figure 4.17 A). There was no significant difference in the number of pre- or post-synaptic compartments analysed for each section between genotypes (unpaired t-test, ns, n=4 per genotype, figure 4.17 B-C). The sizes of the pre- and post- synaptic compartments were not evenly distributed, thus taking a mean average value for size was not appropriate in this study. Therefore, the relative frequency of pre- and post-synaptic area was elucidated for both wild-type and C13H9orf72$^{SH448/SH448}$ zebrafish (figure 4.17 D-E). There was a significantly lower frequency of pre-synaptic compartments with an area of up to $10\mu m^2$ in the C13H9orf72$^{SH448/SH448}$ zebrafish in comparison to wild-type siblings (two-way ANOVA with Fisher's LSD test, p=<0.0001, n=4 per genotype, see figure 4.17 D). However, there was no significant difference in the frequency of pre-synaptic compartments at any other size (figure 4.17 D). There was a significantly higher frequency of post-synaptic compartments with an area of up to $10\mu m^2$ in the C13H9orf72$^{SH448/SH448}$ zebrafish in comparison to wild-type siblings (two-way ANOVA with Fisher's LSD test, p=<0.01, n=4 per genotype, figure 4.17 E). However, there was no significant difference in the frequency of pre-synaptic compartments at any other size (figure 4.17 E).
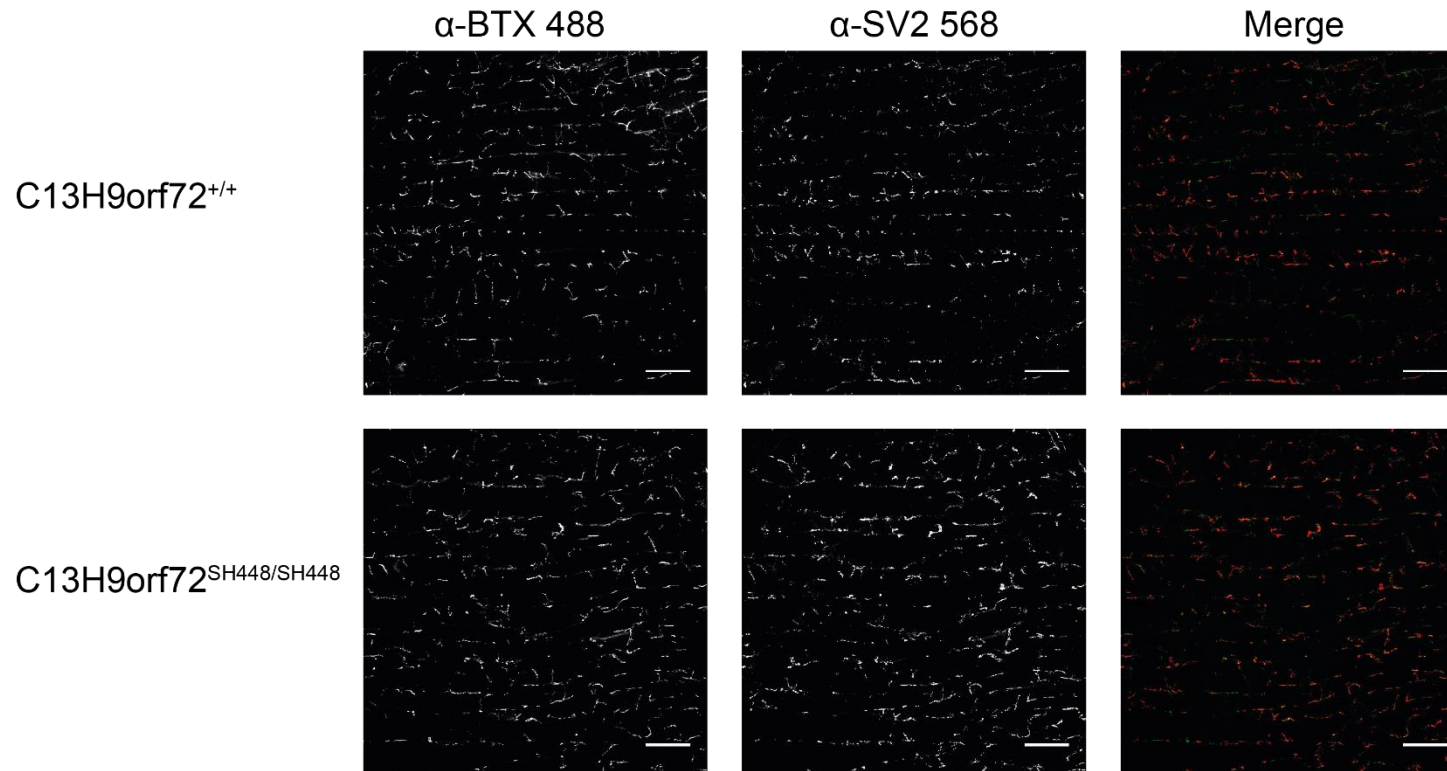
**Figure 4.16 NMJ analysis for SH448 cohort at 11 months.** Representative images of dual immunofluorescence staining of 11-month old adult zebrafish of each genotype for **α**-Bungarotoxin (green) and SV2 (red). Scale bars =100 **µ**m.
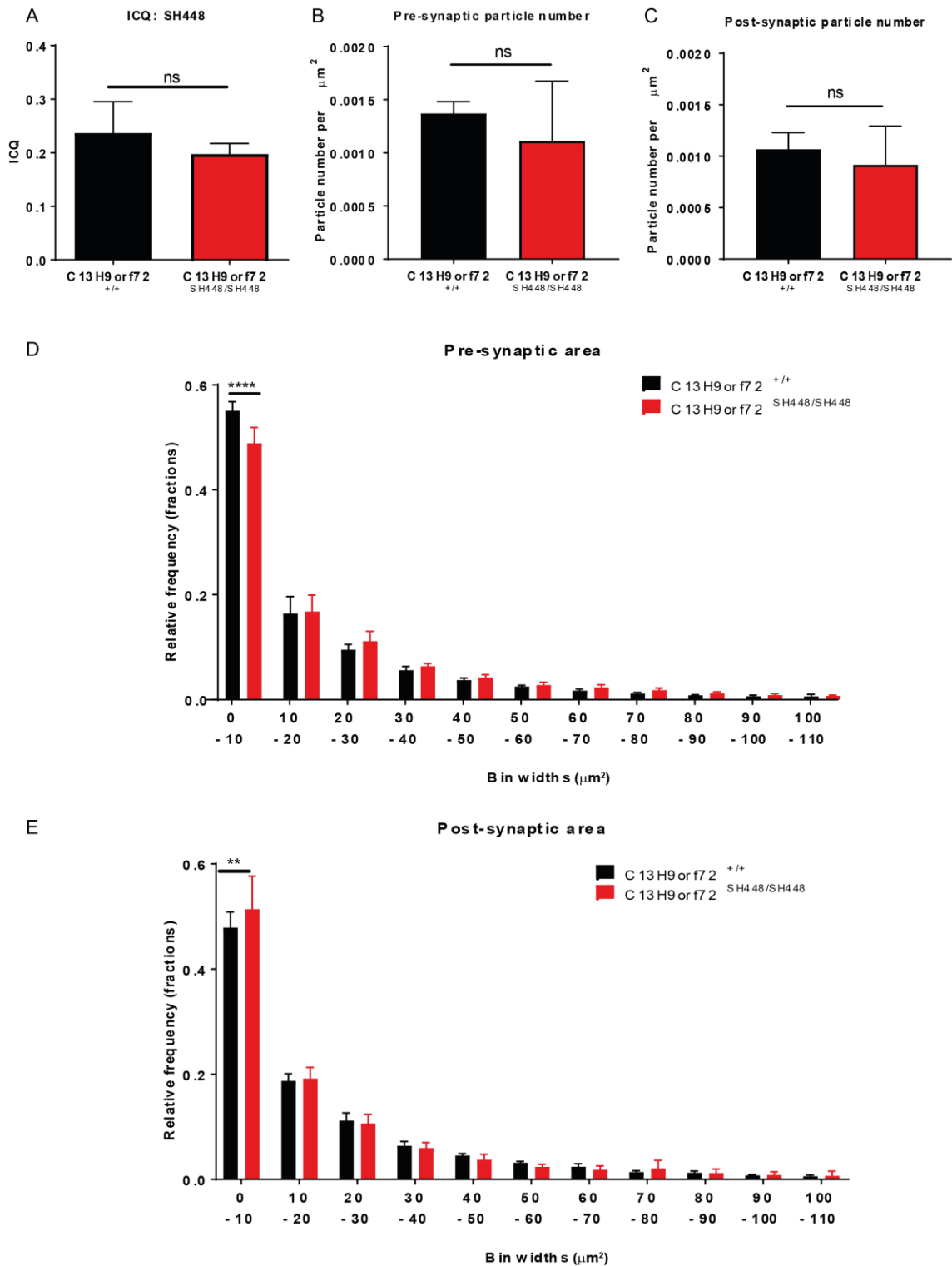
**Figure 4.17 NMJ analysis for SH448 cohort at 11 months.** A) ICQ analysis reveals no alteration of SV2/$\alpha$-Bungarotoxin co-localisation in C13H9orf72$^{+/+}$ or C13H9orf72$^{SH448/SH448}$ zebrafish (unpaired t-test, ns). B-C) There is no difference in pre- and post-synaptic compartment analysed per section (unpaired t-test, ns). D-E) Graphs show frequency distribution of pre- and post-synaptic area (two-way ANOVA, ** p = <0.01, **** p = <0.0001). Graphs show standard deviation. Sample size n=4 per genotype.

#### 4.3.2.8.2. NMJ analysis in C13H9orf72$^{+/+}$ vs C13H9orf72$^{SH451/SH451}$

In 11-month old C13H9orf72$^{SH451/SH451}$ zebrafish, the SV2 and α-bungarotoxin staining (figure 4.18) showed ICQ values of 0.22 ± 0.05, which was not statistically significant from wild-type siblings ICQ values of 0.23 ± 0.04 (unpaired t-test, ns, n=4 per genotype, figure 4.19 A). There was no significant difference in the number of pre-synaptic compartments analysed for each section between genotypes (unpaired t-test, ns, n=4 per genotype, figure 4.19 B). However, there was significant difference in the number of post-synaptic compartments (unpaired t-test, p=<0.05, n=4 per genotype, figure 4.19 C). As seen in line SH448, the sizes of the pre- and post- synaptic compartments were not evenly distributed, thus taking a mean average value for size was not appropriate in this study. Therefore, the relative frequency of pre- and post-synaptic area was elucidated for both wild-type and C13H9orf72$^{SH451/SH451}$ zebrafish (figure 4.19 D-E). There was a significantly lower frequency of pre-synaptic compartments with an area of up to 10μm$^2$ in the C13H9orf72$^{SH451/SH451}$ zebrafish in comparison to wild-type siblings (two-way ANOVA with Fisher's LSD test, p=<0.0001, n=4 per genotype, figure 4.19 D). However, there was no significant difference in the frequency of pre-synaptic compartments at any other size (figure 4.19 D). There was a significantly lower frequency of post-synaptic compartments with an area of up to 10μm$^2$ in the C13H9orf72$^{SH451/SH451}$ zebrafish in comparison to wild-type siblings (two-way ANOVA with Fisher's LSD test, p=<0.0001, n=4 per genotype, figure 4.19 E). However, there was no significant difference in the frequency of pre-synaptic compartments at any other size (figure 4.19 E).
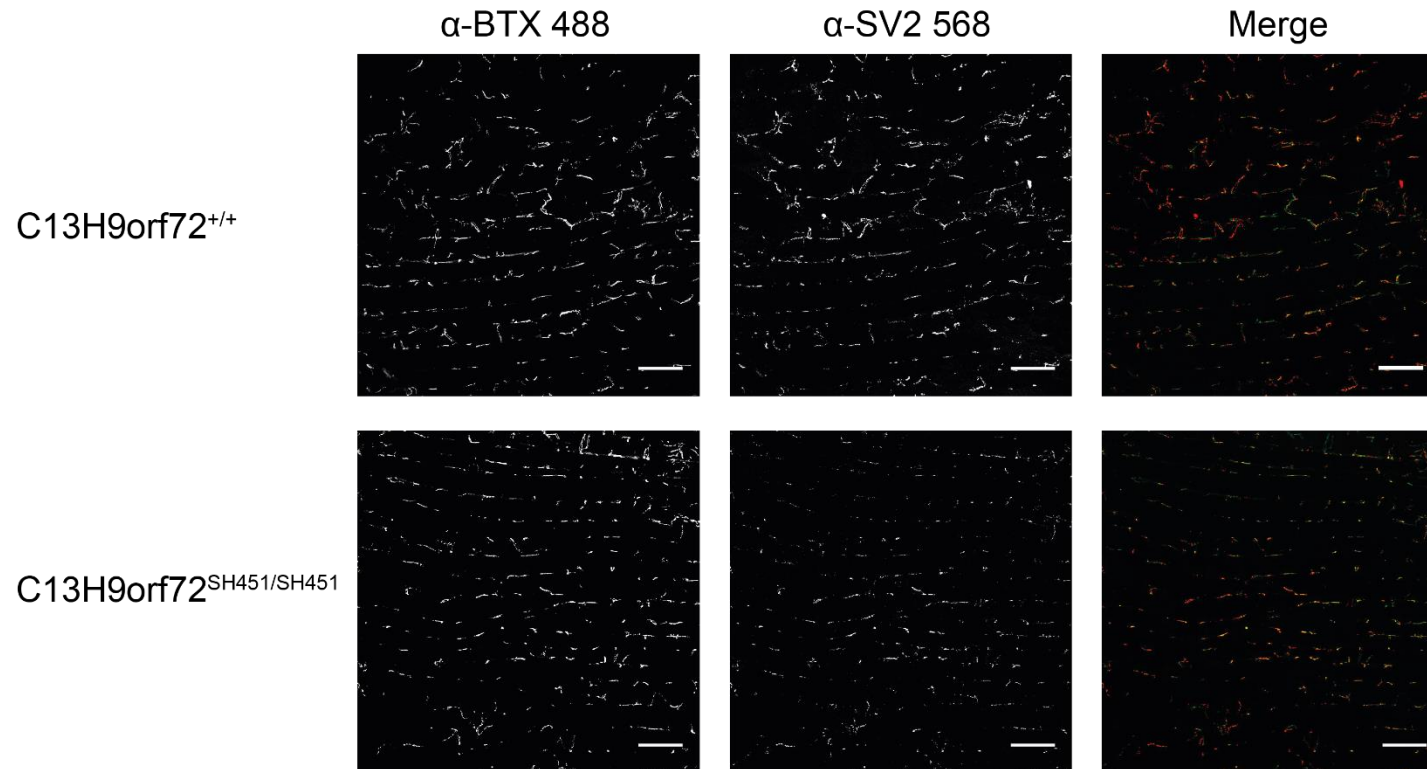
**Figure 4.18 NMJ analysis for SH451 cohort at 11 months.** Representative images of dual immunofluorescence staining of 11-month old adult zebrafish of each genotype for **α**-Bungarotoxin (green) and SV2 (red). Scale bars=100 **μ**m.
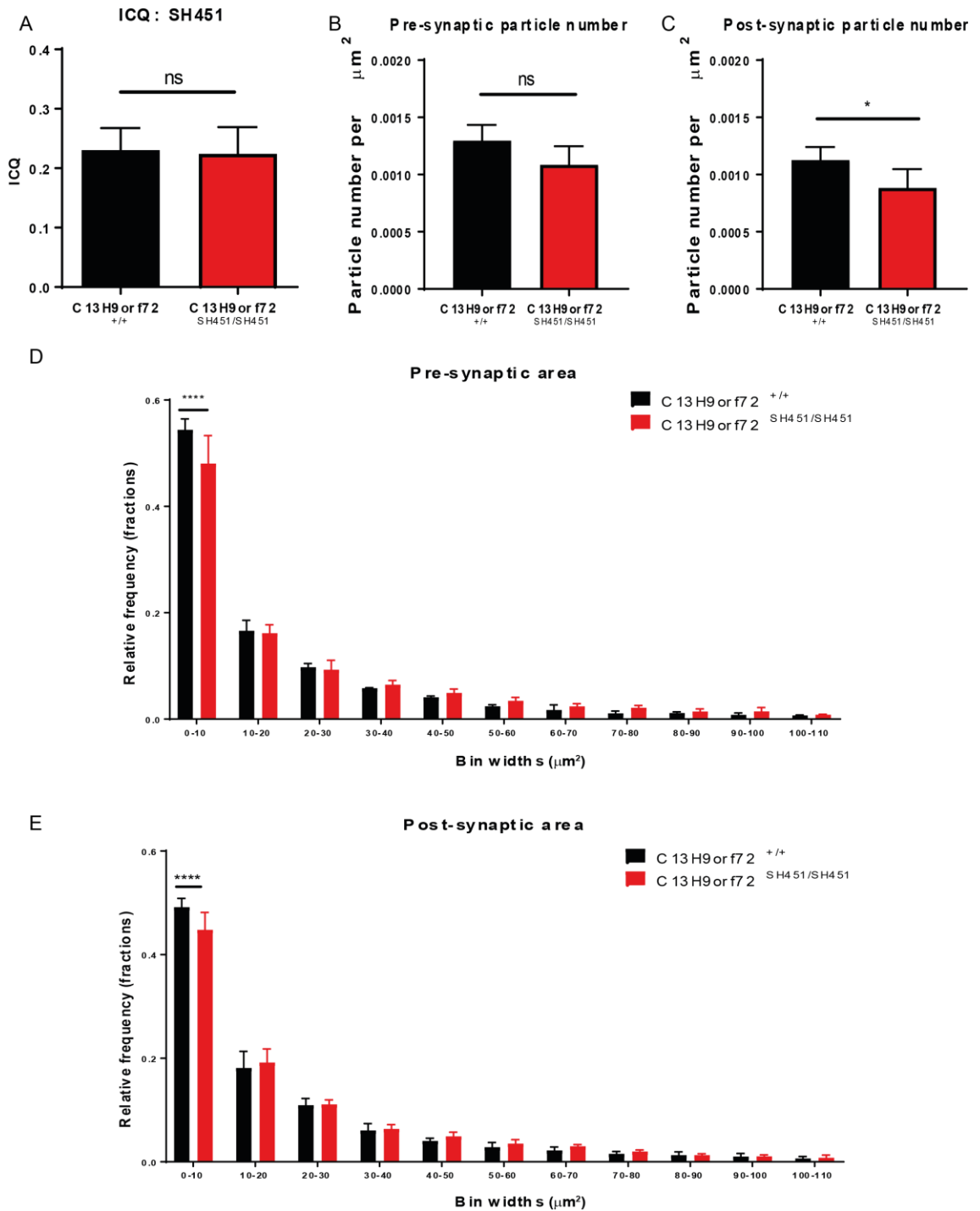
**Figure 4.19 NMJ analysis for SH451 cohort at 11 months.** A) ICQ analysis reveals no alteration of SV2/α-Bungarotoxin co-localisation (unpaired t-test, ns). B-C) There is no difference in pre-synaptic compartments analysed per section, but a significant difference in post-synaptic (unpaired t-test, p = <0.05). D-E) Graphs show frequency distribution of pre- and post-synaptic area (two-way ANOVA, **** p = <0.0001). Graphs show standard deviation. Sample size n=4 per genotype.

## 4.4. Characterisation of behavioural changes in stable *C13H9orf72* loss of function adult zebrafish

It is reported that 50% of ALS patients carrying the repeat expansion in *C9orf72* also show behavioural and/or cognitive impairments (Ringholz et al. 2005). Additionally, a study on a large ALS patient cohort revealed around 15% of these patients met the clinical criteria for FTD, particularly the behavioural variant of FTD (bvFTD) (Ringholz et al. 2005). Patients show symptoms such as: anxiety, disinhibition, apathy, memory loss (Mahoney et al. 2012). As well as this, there is high evidence of psychosis, most commonly featuring hallucinations and delusions (Sha et al. 2012, Snowden et al. 2012, Cooper-Knock et al. 2014a). Adult zebrafish are a powerful tool to model such behaviours. There are now several protocols established to measure behaviours such as anxiety, aggression, social preference, memory and learning in adult zebrafish, which are relevant to the behavioural and/or cognitive changes seen in C9-ALS/FTD (Norton and Bally-Cuif 2010). In order to characterise behaviour in our *C13H9orf72* LOF mutants, we examined anxiety-like behaviour via utilising two tests which robustly measure this behaviour in adult zebrafish; the novel tank diving test and the open field test (Norton and Bally-Cuif 2010).

### 4.4.1. Investigating the impact of frameshift mutations in *C13H9orf72* on anxiety in adult zebrafish using the Novel Tank Diving Test

The novel tank diving test measures anxiety evoked by novelty stress. Zebrafish are known to exhibit a robust behavioural response to this type of stress (Cachat et al. 2010, Parker et al. 2012). When the individual is first placed in the novel environment, their natural instinct is to stay in the bottom of the tank. As the course of exposure to the novel environment continues, they become more exploratory. This behaviour can be investigated by using the novel tank diving test to examine the amount of time a zebrafish spends at the lower half of the tank in comparison to the top, with more time spent in the lower half indicative of anxious behaviour (figure 4.20). The same cohorts used for the swim tunnel were also used for the novel tank diving test (table 4.6), and tested in the same week. Additionally, we show the pilot data (line SH448, DOB 24.09.14). During testing, each individual zebrafish was filmed from the side, with position and locomotion tracked using the equipment and related software included in the ViewPoint analysis suite, as described in section 2.7.3.1 (ViewPoint Life Science, Lyon, France). To analyse any effect a two-way ANOVA with repeated measures was performed, using genotype (wild-type or homozygous mutant) and time (five time intervals: mins 1-5) as independent

variables, with time spent in the lower half of the tank entered as the response. This analysis provided 3 main results, which are summarised in tables 4.13 – 4.18. The measurements 'genotype' and 'time interval' analyse the effect that each independent variable has on time spent in the lower half of the tank, separately. The measurement 'genotype: time interval' analyses the interaction of both variables on the time spent at the lower half. If a significant interaction between 'genotype: time interval' is observed (highlighted in yellow in tables 4.13-4.18), this means that the effect of genotype on time spent in the lower half of the tank is significantly different at different time intervals. If this is the case, results from the analysis of the two independent variables separately can be disregarded, since these variables are interacting, and post-hoc analysis can be performed at different time intervals.
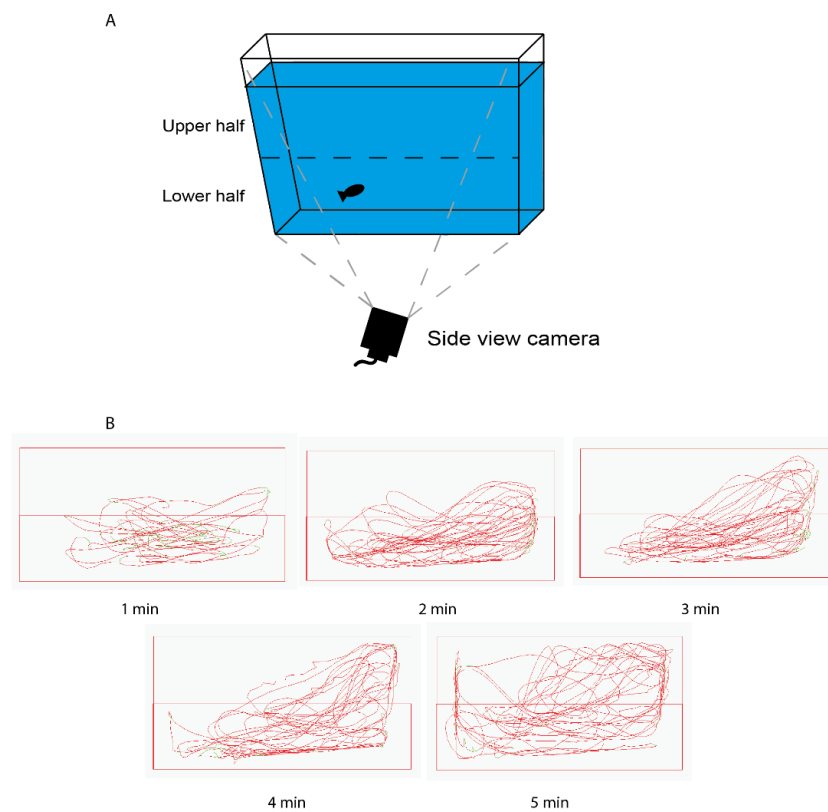


**Figure 4.20 Schematic of Novel Tank Diving Test.** A) Diagram of the novel tank diving test. B) Example traces of a wild-type zebrafish.

#### 4.4.1.1. Line SH448 (pilot study)

Figures 4.21 and 4.22 display the time spent in the lower half (s) during the 5-minute exposure to the novel tank, for months 8-23 (pilot study, line SH448, DOB 24.09.14, n=5-6 per genotype). During the pilot study, the groups were tested once a month. There is a significant main effect of time interval at all of the time points tested (table 4.13), indicating that time spent at the lower half of the tank decreases as a function of time as we expect (figure 4.21 and 4.22). It is also observed that C13H9orf72$^{SH448/SH448}$ zebrafish spend longer in the lower half of the tank over the course of exposure in comparison to wild-type siblings, at all of the time points tested (figure 4.21 and 4.22). This effect was confirmed at months 9-14, 16 and 20, as there was a significant main effect of genotype (table 4.13). There was no significant genotype: time interval interaction at any time point except for at 16 months (table 4.13, highlighted yellow). Post-hoc analysis revealed C13H9orf72$^{SH448/SH448}$ spent significantly longer in the lower half of the tank compared to wild-type siblings at minute 1 and 2 only (figure 4.22, unpaired t-test, minute 1 p=0.0005, minute 2 p=0.0422). Figure 4.23 shows that there were no differences between the two groups in the distances travelled at any time point tested, confirming that any differences seen were due to behaviour and not motor function (2-way ANOVA with Fisher's LSD test, n=5-6).
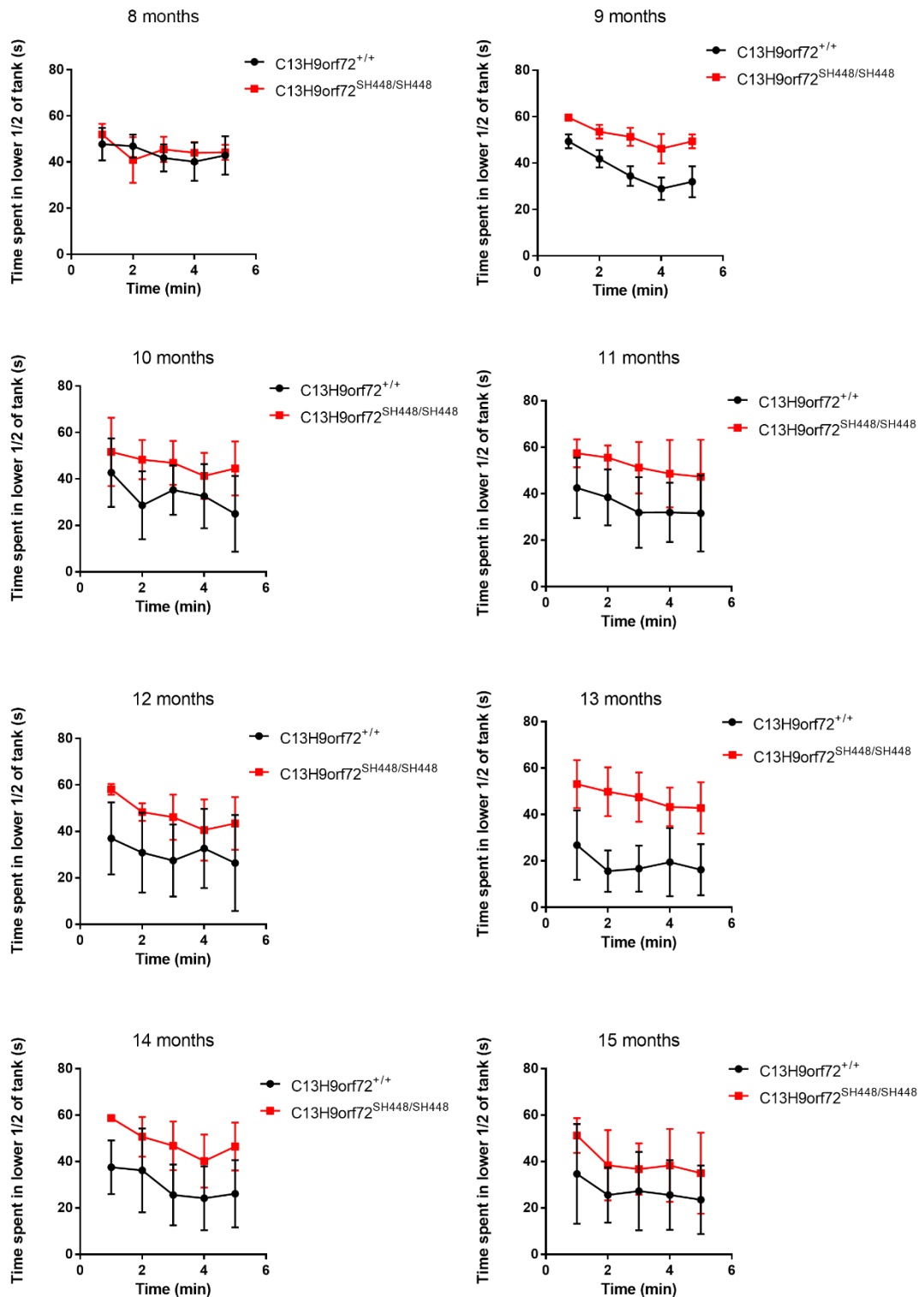
**Figure 4.21 Mean time (s) spent in the lower half of the novel tank during the tank diving test for pilot cohort (8-15m).** Graphs display time spent in lower half of tank during the 5-minute exposure to the novel tank at 8 – 15 months. There was no significant genotype: time interval interaction at any time point (two-way ANOVA with repeated measures). Error bars show standard deviation. Group sizes n=5-6.
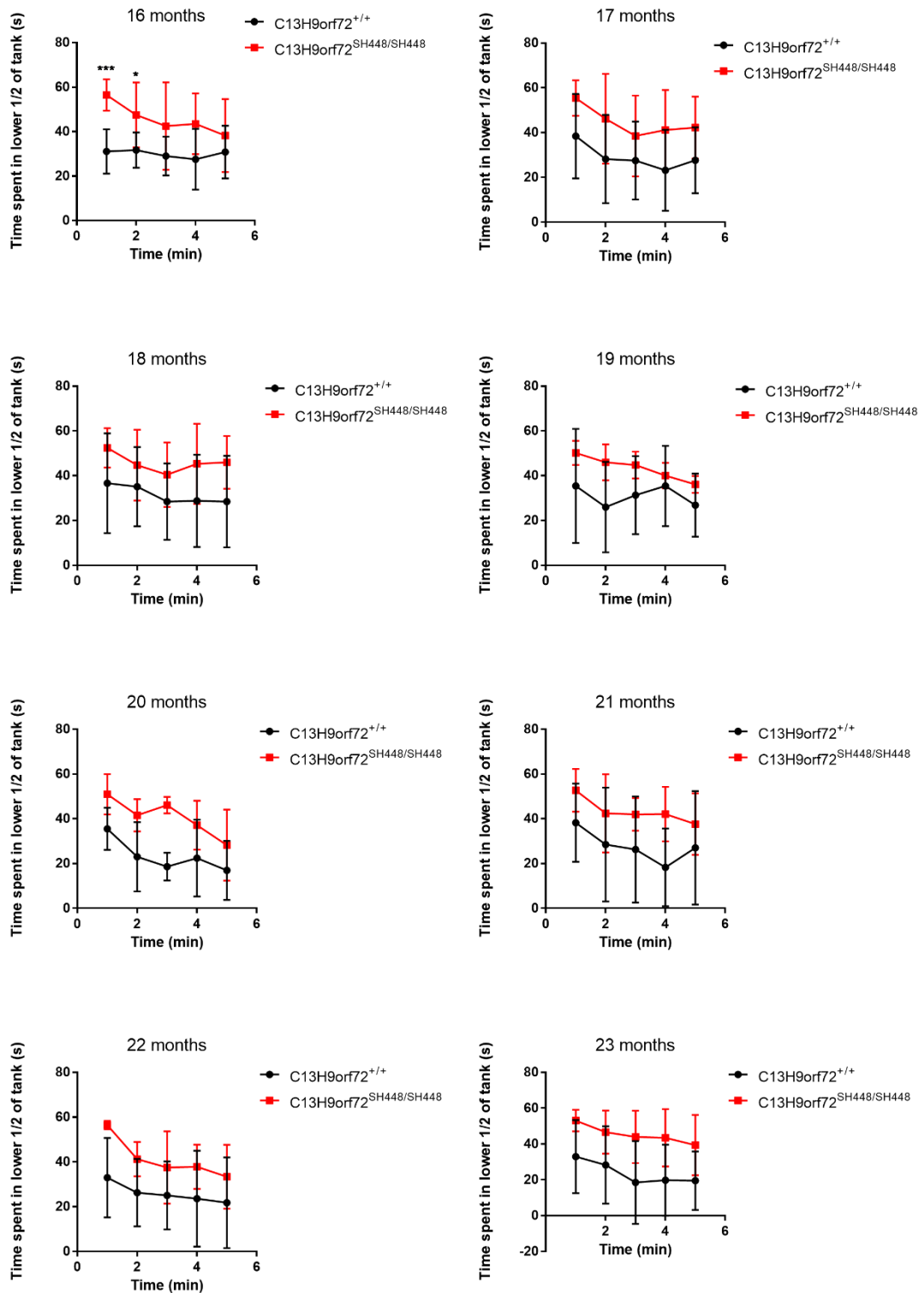
**Figure 4.22 Mean time (s) spent in the lower half of the novel tank during the tank diving test for pilot cohort (16-23m).** Graphs display time spent in lower half of tank during the 5-minute exposure to the novel tank at 16 – 23 months. There was a significant genotype: time interval interaction at 16 months (two-way ANOVA with repeated measures). Post-hoc analysis at 16 months revealed C13H9orf72$^{SH448/SH448}$ spent longer in the lower half of the tank compared to wild-type siblings at minute 1 and 2 only (unpaired t-test, minute 1 p=0.0005, minute 2 p=0.0422). Error bars show standard deviation. Group sizes n=5-6.

**Table 4.13 Result from two-way ANOVA with repeated measures for pilot study line SH448 DOB 24.09.14.** Significance codes: 0 '***'; 0.001 '**';0.01 '*'; 0.05 '.'. Analysis performed on R3.3.2 for Windows.

| Line | Age | Measurement | Df | F Value | Pr (>F) | Sig |
|------|-----|-------------|-----|---------|---------|-----|
| SH448 | 8 | Genotype | 1;9 | 0.029 | 0.869 | ns |
| | | Time Int | 1;42 | 3.442 | 0.0706 | . |
| | | Genotype: Time Int | 1;42 | 0.073 | 0.7876 | ns |
| SH448 | 9 | Genotype | 1;9 | 11.8 | 0.00744 | ** |
| | | Time Int | 1;42 | 23.703 | 1.63e-05 | *** |
| | | Genotype: Time Int | 1;42 | 1.554 | 0.22 | ns |
| SH448 | 10 | Genotype | 1;10 | 6.46 | 0.0293 | * |
| | | Time Int | 1;46 | 8.894 | 0.00457 | ** |
| | | Genotype: Time Int | 1;46 | 0.329 | 0.56910 | ns |
| SH448 | 11 | Genotype | 1;10 | 7.526 | 0.0207 | * |
| | | Time Int | 1;46 | 15.830 | 0.000244 | *** |
| | | Genotype: Time Int | 1;46 | 0.006 | 0.940377 | ns |
| SH448 | 12 | Genotype | 1;10 | 5.673 | 0.0385 | * |
| | | Time Int | 1;46 | 14.990 | 0.00034 | *** |
| | | Genotype: Time Int | 1;46 | 1.461 | 0.23288 | ns |
| SH448 | 13 | Genotype | 1;10 | 27.38 | 0.000383 | *** |
| | | Time Int | 1;46 | 11.933 | 0.0012 | ** |
| | | Genotype: Time Int | 1;46 | 0.581 | 0.4499 | ns |
| SH448 | 14 | Genotype | 1;10 | 9.882 | 0.0104 | * |
| | | Time Int | 1;46 | 25.77 | 6.9e-06 | *** |
| | | Genotype: Time Int | 1;46 | 0.00 | 0.993 | ns |
| SH448 | 15 | Genotype | 1;10 | 3.123 | 0.108 | ns |
| | | Time Int | 1;46 | 9.533 | 0.00342 | ** |
| | | Genotype: Time Int | 1;46 | 0.339 | 0.56331 | ns |
| SH448 | 16 | Genotype | 1;10 | 6.673 | 0.0273 | * |
| | | Time Int | 1;46 | 9.022 | 0.0043 | ** |
| | | Genotype: Time Int | 1;46 | 5.729 | 0.0208 | * |
| SH448 | 17 | Genotype | 1;10 | 3.019 | 0.113 | ns |
| | | Time Int | 1;46 | 15.485 | 0.000279 | *** |
| | | Genotype: Time Int | 1;46 | 0.114 | 0.737675 | ns |
| SH448 | 18 | Genotype | 1;9 | 2.366 | 0.158 | ns |
| | | Time Int | 1;42 | 4.303 | 0.0442 | * |
| | | Genotype: Time Int | 1;42 | 0.353 | 0.5553 | ns |
| SH448 | 19 | Genotype | 1;8 | 2.39 | 0.161 | ns |
| | | Time Int | 1;38 | 7.634 | 0.00878 | ** |
| | | Genotype: Time Int | 1;38 | 3.031 | 0.08980 | . |
| SH448 | 20 | Genotype | 1;8 | 12.04 | 0.00844 | ** |
| | | Time Int | 1;38 | 20.852 | 5.09e-05 | *** |
| | | Genotype: Time Int | 1;38 | 0.401 | 0.53 | ns |
| SH448 | 21 | Genotype | 1;8 | 2.164 | 0.18 | ns |
| | | Time Int | 1;38 | 17.019 | 0.000194 | *** |
| | | Genotype: Time Int | 1;38 | 0.019 | 0.890392 | ns |
| SH448 | 22 | Genotype | 1;8 | 3.487 | 0.0988 | . |
| | | Time Int | 1;38 | 19.566 | 7.89e-05 | *** |
| | | Genotype: Time Int | 1;38 | 2.102 | 0.155 | ns |
| SH448 | 23 | Genotype | 1;8 | 4.534 | 0.0659 | . |
| | | Time Int | 1;38 | 19.338 | 8.54e-05 | *** |
| | | Genotype: Time Int | 1;38 | 0.103 | 0.75 | ns |
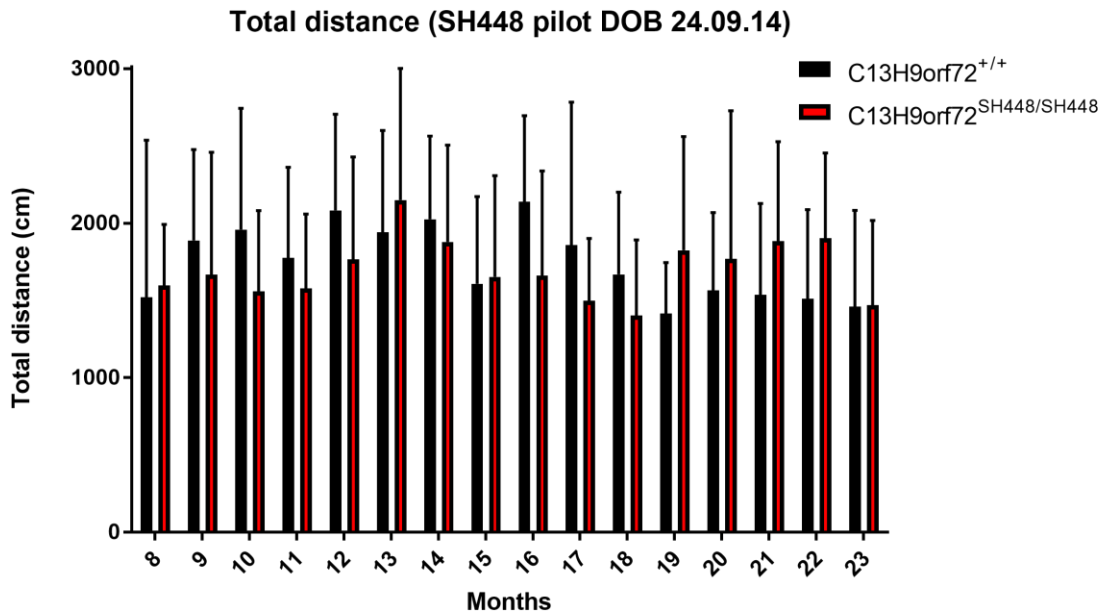
**Figure 4.23 Total distance travelled during pilot novel tank diving.** Displays the total distance travelled in the whole tank during the 5-minute exposure to the novel tank. There is no significant difference in total distance travelled between C13H9orf72$^{+/+}$ zebrafish and C13H9orf72$^{SH448/SH448}$ zebrafish at 8-23 months of age (2-way ANOVA with Fisher's LSD test, n=5-6). Error bars show standard deviation.

153

#### 4.4.1.2. SH448 clutch 1 (DOB 28.1.15)

Figure 4.24 displays the time spent in the lower half (s) during the 5-minute exposure to the novel tank, for months 9-24 (SH448 clutch 1, DOB 28.1.15, n=6-11 per genotype - table 4.6). During the study, the cohort was tested once every 3 months. There is a significant main effect of time interval at months 9 and 15-24, indicating that time spent at the lower half of the tank decreases as a function of time, as we expect (figure 4.24, table 4.14). However, this effect is not observed at month 12 (figure 4.24, table 4.14), which indicates that the zebrafish are not displaying the typical response to a novel environment at this time point. It is also observed that C13H9orf72$^{SH448/SH448}$ zebrafish spend longer in the lower half of the tank over the course of exposure in comparison to wild-type siblings, at 9 months (figure 4.24). This effect was confirmed, as there was a significant main effect of genotype at this time point (table 4.14). However, there was no significant effect of genotype at any other time points tested (table 4.14). Additionally, there was no significant genotype: time interval interaction at any time point except for at 15 and 18 months (table 4.14, highlighted yellow). Post-hoc analysis at 15 months revealed C13H9orf72$^{SH448/SH448}$ spent longer in the lower half of the tank compared to wild-type siblings at minute 1 only (unpaired t-test, minute 1 p=0.0331). Conversely, post-hoc analysis at 18 months revealed C13H9orf72$^{SH448/SH448}$ spent less time in the lower half of the tank compared to wild-type siblings at minute 3 (unpaired t-test, minute 3 p=0.0333), suggesting that at 18 months, C13H9orf72$^{SH448/SH448}$ were less anxious. Figure 4.25 shows that there were no differences between the two groups in the distances travelled at any time point tested, confirming that any differences seen were due to behaviour and not motor function (2-way ANOVA with Fisher's LSD test, n=6-11).
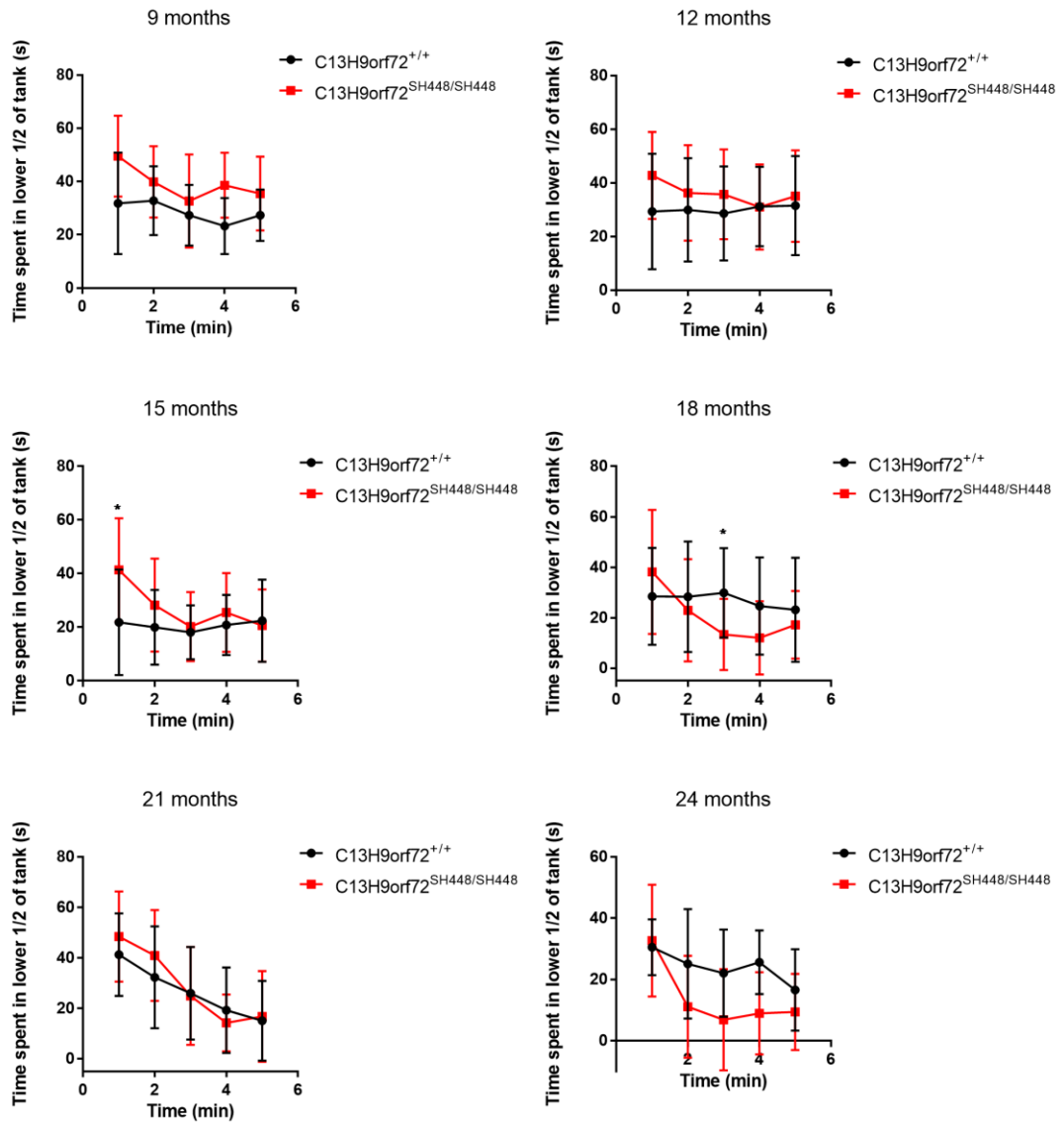
**Figure 4.24 Mean time (s) spent in the lower half of the novel tank during the tank diving test for line SH448 DOB 28.1.15.** Graphs display time spent in lower half of tank during the 5-minute exposure to the novel tank at 9-24 months. There was a significant genotype: time interval interaction at 15 and 18 months (two-way ANOVA with repeated measures). Post-hoc analysis at 15 months revealed C13H9orf72[SH448/SH448] spent longer in the lower half of the tank compared to wild-type siblings at minute 1 only (unpaired t-test, minute 1 p=0.0331). Post-hoc analysis at 18 months revealed C13H9orf72[SH448/SH448] spent less time in the lower half of the tank compared to wild-type siblings at minute 3 (unpaired t-test, minute 3 p=0.0333). Error bars show standard deviation. Group sizes n=6-11.

**Table 4.14 Result from two-way ANOVA with repeated measures for line SH448 DOB 28.01.15.** Significance codes: 0 '***'; 0.001 '**';0.01 '*'; 0.05 '.'. Analysis performed on R3.3.2 for Windows.

| Line | Age | Measurement | Df | F Value | Pr (>F) | Sig |
|------|-----|-------------|-----|---------|---------|-----|
| SH448 | 9 | Genotype | 1;20 | 6.433 | 0.0197 | * |
| | | Time Int | 1;86 | 10.202 | 0.00196 | ** |
| | | Genotype: Time Int | 1;86 | 0.539 | 0.46477 | ns |
| SH448 | 12 | Genotype | 1;20 | 0.997 | 0.33 | ns |
| | | Time Int | 1;86 | 0.934 | 0.3366 | ns |
| | | Genotype: Time Int | 1;86 | 2.911 | 0.0916 | . |
| SH448 | 15 | Genotype | 1;19 | 2.36 | 0.141 | ns |
| | | Time Int | 1;82 | 5.033 | 0.0276 | * |
| | | Genotype: Time Int | 1;82 | 6.759 | 0.0111 | * |
| SH448 | 18 | Genotype | 1;18 | 0.869 | 0.363 | ns |
| | | Time Int | 1;78 | 12.318 | 0.000749 | *** |
| | | Genotype: Time Int | 1;78 | 4.073 | 0.047006 | * |
| SH448 | 21 | Genotype | 1;16 | 0.14 | 0.713 | ns |
| | | Time Int | 1;70 | 66.136 | 1.04e-11 | *** |
| | | Genotype: Time Int | 1;70 | 1.579 | 0.213 | ns |
| SH448 | 24 | Genotype | 1;12 | 2.904 | 0.114 | ns |
| | | Time Int | 1;54 | 15.443 | 0.000244 | *** |
| | | Genotype: Time Int | 1;54 | 1.302 | 0.258967 | ns |
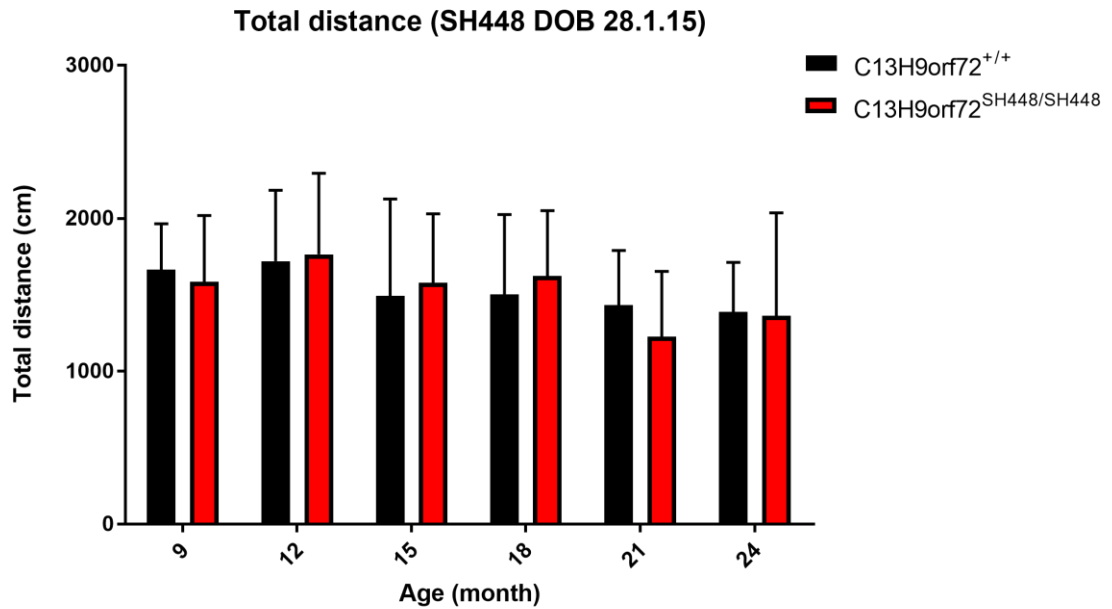
**Figure 4.25 Total distance travelled during novel tank diving test SH448 DOB 28.1.15.** Displays the total distance travelled in the whole tank during the 5-minute exposure to the novel tank. There is no significant difference in total distance travelled between C13H9orf72$^{+/+}$ zebrafish and C13H9orf72$^{SH448/SH448}$ zebrafish at 9-24 months of age (2-way ANOVA with Fisher's LSD test, n=6-11). Error bars show standard deviation.

### 4.4.1.3. SH448 clutch 2 (DOB 13.1.16)

To determine whether anxiety-like behaviour was altered in C13H9orf72$^{\text{SH448/SH448}}$ prior to 9 months, a second clutch (SH448 clutch 2, DOB 13.1.16, n=9-11 per genotype – table 4.6) was run through the novel tank diving test. Figure 4.26 displays the time spent within the lower half (s) during the 5-minute exposure to the novel tank, at months 4-12. During the study, the cohort was tested once every 3 months. There is a significant main effect of time interval at all of the time points tested (table 4.15), indicating that time spent at the lower half of the tank decreases as a function of time as we expect (figure 4.26). It is also observed that wild-types spend longer in the lower half of the tank over the course of exposure in comparison to C13H9orf72$^{\text{SH448/SH448}}$ zebrafish, at 4 and 6 months (figure 4.26). This effect was confirmed, as there was a significant main effect of genotype at this time point (table 4.15), indicating higher anxiety levels in the wild-types. However, there was no significant effect of genotype at any other time points tested (table 4.15), complimentary to SH448 clutch 1 at months 12-24. Additionally, there was no significant genotype: time interval interaction at any time point tested (table 4.14). Figure 4.27 shows that at 4 months C13H9orf72$^{\text{SH448/SH448}}$ zebrafish swim significantly less over the course of exposure in comparison to wild-type siblings (2-way ANOVA with Fisher's LSD test, n=9-11, p = <0.001), however, there were no significant differences at any other time point tested, confirming that any differences seen were due to behaviour and not motor function at these time points.
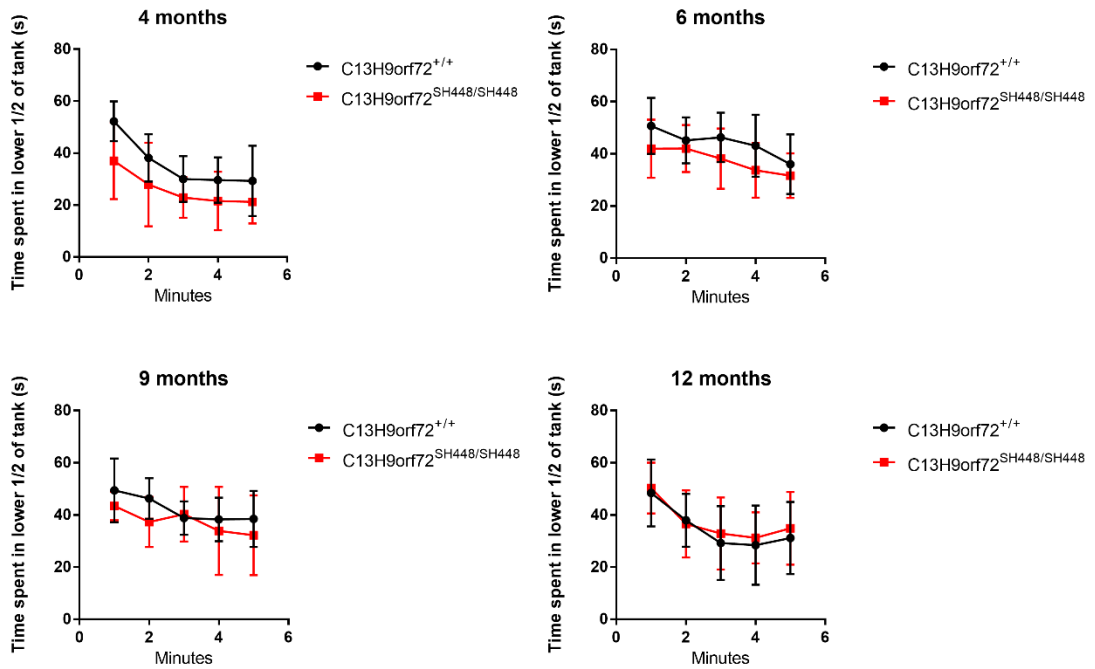
**Figure 4.26 Mean time (s) spent in the lower half of the novel tank during the tank diving test for line SH448 DOB 13.1.16.** Graphs display time spent in lower half of tank during the 5-minute exposure to the novel tank at 4-12 months. There was no significant genotype: time interval interaction at any time point (two-way ANOVA with repeated measures). Error bars show standard deviation. Group sizes n=9-11.

**Table 4.15 Result from two-way ANOVA with repeated measures for line SH448 DOB 13.01.16.** Significance codes: 0 '***'; 0.001 '**';0.01 '*'; 0.05 '.'. Analysis performed on R3.3.2 for Windows.

| Line | Age | Measurement | Df | F Value | Pr (>F) | Sig |
|------|-----|-------------|-----|---------|---------|-----|
| **SH448** | **4** | **Genotype** | 1;20 | 9.567 | 0.00573 | ** |
| | | **Time Int** | 1;86 | 49.890 | 3.97e-10 | *** |
| | | **Genotype: Time Int** | 1;86 | 1.575 | 0.213 | ns |
| **SH448** | **6** | **Genotype** | 1;17 | 7.318 | 0.015 | * |
| | | **Time Int** | 1;74 | 18.735 | 4.64e-05 | *** |
| | | **Genotype: Time Int** | 1;74 | 0.029 | 0.864 | ns |
| **SH448** | **9** | **Genotype** | 1;17 | 1.554 | 0.229 | ns |
| | | **Time Int** | 1;74 | 23.793 | 5.98e-06 | *** |
| | | **Genotype: Time Int** | 1;74 | 0.132 | 0.178 | ns |
| **SH448** | **12** | **Genotype** | 1;17 | 0.219 | 0.646 | ns |
| | | **Time Int** | 1;74 | 31.164 | 3.71e-07 | *** |
| | | **Genotype: Time Int** | 1;74 | 0.304 | 0.583 | ns |
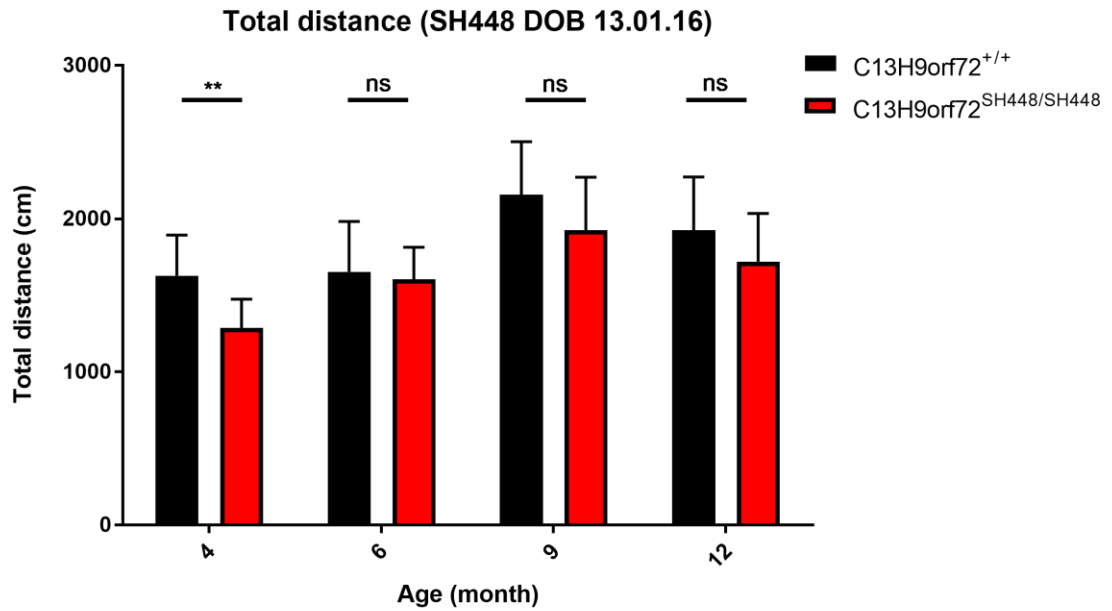
**Figure 4.27 Total distance travelled during novel tank diving test SH448 DOB 13.1.16.** Displays the total distance travelled in the whole tank during the 5-minute exposure to the novel tank. There is no significant difference in total distance travelled between C13H9orf72$^{+/+}$ zebrafish and C13H9orf72$^{SH448/SH448}$ zebrafish at 6-12 months of age (2-way ANOVA with Fisher's LSD test, n=9-11), however there is at 4 months (p=0.0083). Error bars show standard deviation.

#### 4.4.1.4.  SH451 clutch 1 (DOB 18.3.15)

Figure 4.28 displays the time spent within the lower half (s) during the 5-minute exposure to the novel tank, at months 9-24 (SH451 clutch 1, DOB 18.3.15, n=10-11 per genotype – table 4.6). During the study, the cohort was tested once every 3 months. There is a significant main effect of time interval at months 9-15, indicating that time spent at the lower half of the tank decreases as a function of time, as we expect (figure 4.28, table 4.16). However, this effect is not observed at months 18-24 (figure 4.28, table 4.16), which indicates that the zebrafish are not displaying the typical response to a novel environment at these time points. It is also observed that wild-types spend longer in the lower half of the tank over the course of exposure in comparison to C13H9orf72$^{SH448/SH448}$ zebrafish, at 21 months (figure 4.28). This effect was confirmed, as there was a significant main effect of genotype at this time point (see table 4.16), indicating higher anxiety levels in the wild-types. However, there was no significant effect of genotype at any other time points tested (see table 4.16). Additionally, there was no significant genotype: time interval interaction at any time point tested (see table 4.16). Figure 4.29 shows that at 9 months C13H9orf72$^{SH451/SH451}$ zebrafish swim significantly more over the course of exposure in comparison to wild-type siblings (2-way ANOVA with Fisher's LSD test, n=10-11, p = <0.05), however, there were no significant differences at any other time point tested, confirming that any differences seen were due to behaviour and not motor function at these time points.
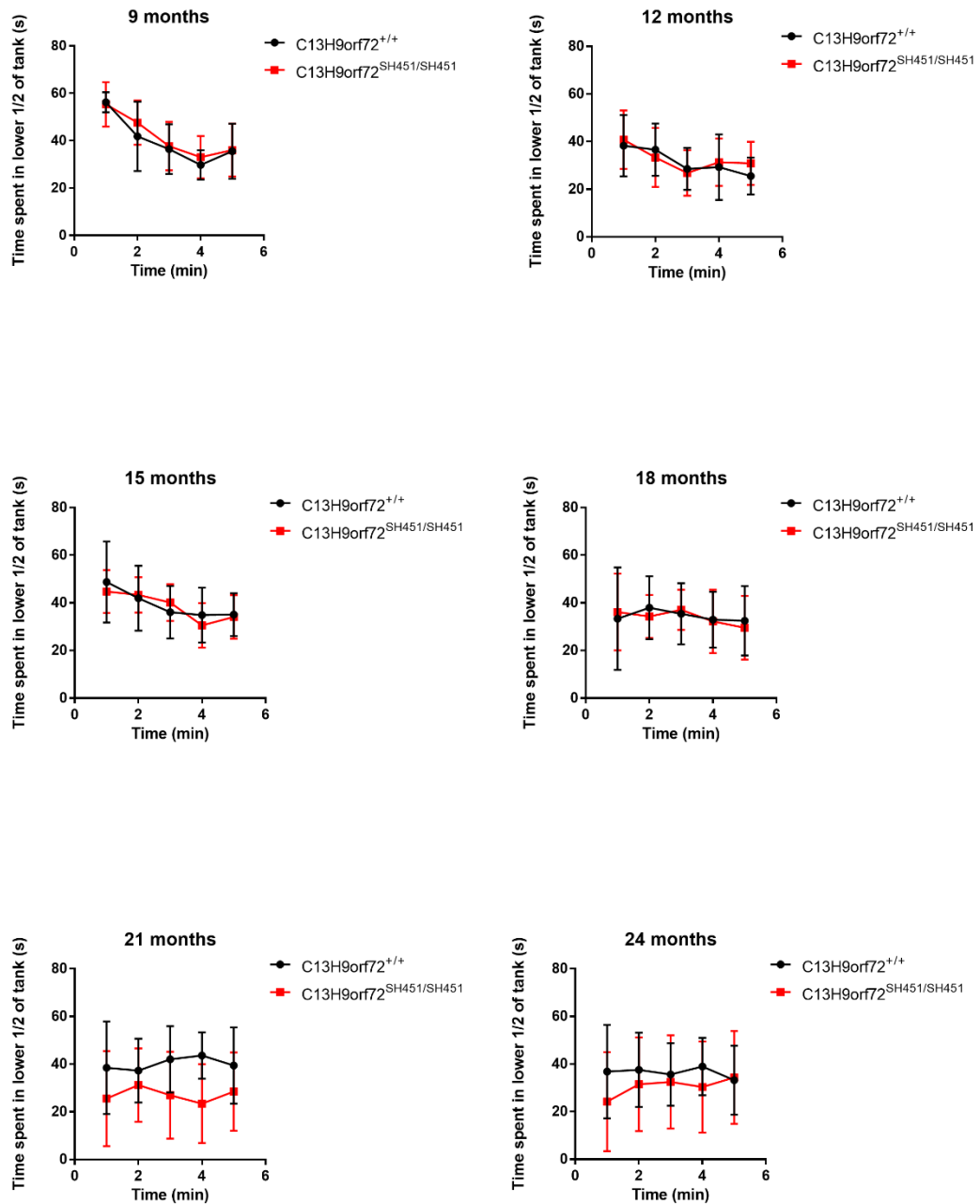
**Figure 4.28 Mean time (s) spent in the lower half of the novel tank during the tank diving test for SH451 DOB 18.3.15.** Graphs display time spent in lower half of tank during the 5-minute exposure to the novel tank at 9-24 months. There was no significant genotype: time interval interaction at any time point (two-way ANOVA with repeated measures). Error bars show standard deviation. Group sizes n=10-11.

**Table 4.16 Result from two-way ANOVA with repeated measures for line SH451 DOB 18.03.15.** Significance codes: 0 '***'; 0.001 '**';0.01 '*'; 0.05 '.'. Analysis performed on R3.3.2 for Windows.

| Line | Age | Measurement | Df | F Value | Pr (>F) | Sig |
|------|-----|-------------|-----|---------|---------|-----|
| **SH451** | **9** | **Genotype** | 1;20 | 0.491 | 0.492 | ns |
| | | **Time Int** | 1;86 | 70.79 | 7.68e-13 | *** |
| | | **Genotype: Time Int** | 1;86 | 0.00 | 0.996 | ns |
| **SH451** | **12** | **Genotype** | 1;20 | 0.126 | 0.727 | ns |
| | | **Time Int** | 1;86 | 16.782 | 9.45e-05 | *** |
| | | **Genotype: Time Int** | 1;86 | 0.673 | 0.414 | ns |
| **SH451** | **15** | **Genotype** | 1;20 | 0.115 | 0.738 | ns |
| | | **Time Int** | 1;86 | 23.21 | 6.17e-06 | *** |
| | | **Genotype: Time Int** | 1;86 | 0.00 | 0.985 | ns |
| **SH451** | **18** | **Genotype** | 1;20 | 0.019 | 0.893 | ns |
| | | **Time Int** | 1;86 | 2.318 | 0.132 | ns |
| | | **Genotype: Time Int** | 1;86 | 0.341 | 0.561 | ns |
| **SH451** | **21** | **Genotype** | 1;19 | 5.452 | 0.0307 | * |
| | | **Time Int** | 1;82 | 0.203 | 0.653 | ns |
| | | **Genotype: Time Int** | 1;82 | 0.467 | 0.496 | ns |
| **SH451** | **24** | **Genotype** | 1;19 | 0.778 | 0.389 | ns |
| | | **Time Int** | 1;82 | 0.830 | 0.3651 | ns |
| | | **Genotype: Time Int** | 1;82 | 3.532 | 0.0638 | . |
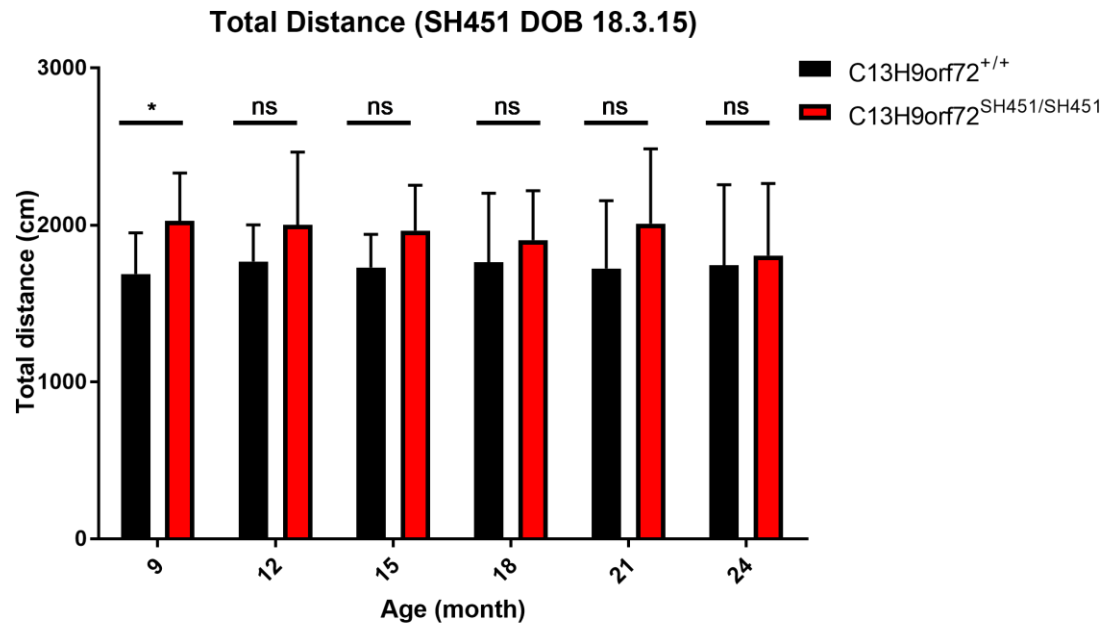
**Figure 4.29 Total distance travelled during novel tank diving test SH451 DOB 18.3.15.** Displays the total distance travelled in the whole tank during the 5-minute exposure to the novel tank. There is no significant difference in total distance travelled between C13H9orf72$^{+/+}$ zebrafish and C13H9orf72$^{SH451/SH451}$ zebrafish at 12-24 months of age (2-way ANOVA with Fisher's LSD test, n=10-11), however there is at 9 months (p= 0.0270). Error bars show standard deviation.

### 4.4.1.5.  SH451 experiment 2 (DOB 25.2.16)

To determine whether anxiety-like behaviour was altered in C13H9orf72$^{SH451/SH451}$ prior to 9 months, a second clutch (SH451 clutch 2, DOB 25.2.16, n=9-10 per genotype – table 4.6) was run through the novel tank diving test. Figure 4.30 displays the time spent within the lower half (s) during the 5-minute exposure to the novel tank, at months 4-12. During the study, the cohort was tested once every 3 months. There is a significant main effect of time interval at all of the time points tested (table 4.17), indicating that time spent at the lower half of the tank decreases as a function of time as we expect (see figure 4.30). It is also observed that wild-types spend longer in the lower half of the tank over the course of exposure in comparison to C13H9orf72$^{SH448/SH448}$ zebrafish, at 6 months (figure 4.30). This effect was confirmed, as there was a significant main effect of genotype at this time point (table 4.17), indicating higher anxiety levels in the wild-types. However, there was no significant effect of genotype at any other time points tested (table 4.17), complimentary to SH451 clutch 1 at months 9-18 and 24. Additionally, there was no significant genotype: time interval interaction at any time point tested (table 4.17). Figure 4.31 shows that at 6 months C13H9orf72$^{SH451/SH451}$ zebrafish swim significantly more over the course of exposure in comparison to wild-type siblings (2-way ANOVA with Fisher's LSD test, n=9-10, p = <0.05), however, there were no significant differences at any other time point tested, confirming that any differences seen were due to behaviour and not motor function.
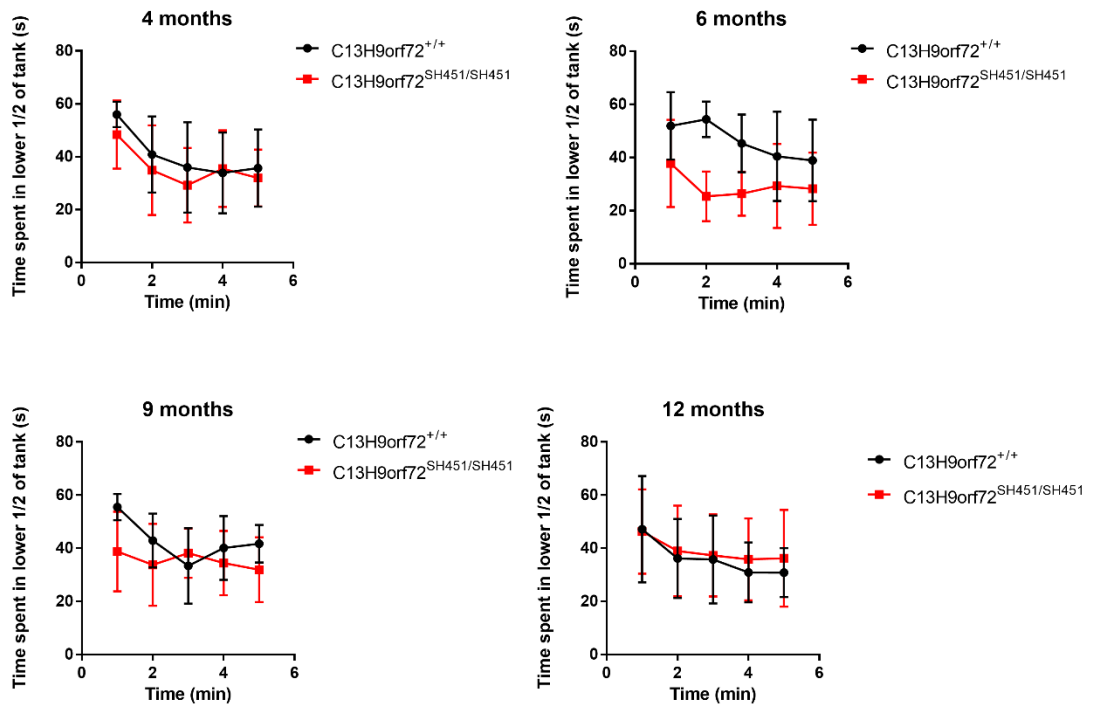
**Figure 4.30 Mean time (s) spent in the lower half of the novel tank during the tank diving test for line SH451 DOB 25.2.16.** Graphs display time spent in lower half of tank during the 5-minute exposure to the novel tank at 4-12 months. There was no significant genotype: time interval interaction at any time point (two-way ANOVA with repeated measures). Error bars show standard deviation. Group sizes n= 9-10.

**Table 4.17 Result from two-way ANOVA with repeated measures for line SH451 DOB 25.02.16.** Significance codes: 0 '***'; 0.001 '**';0.01 '*'; 0.05 '.'. Analysis performed on R3.3.2 for Windows.

| Line | Age | Measurement | Df | F Value | Pr (>F) | Sig |
|------|-----|-------------|-----|---------|---------|-----|
| **SH451** | **4** | **Genotype** | 1;18 | 0.757 | 0.396 | ns |
| | | **Time Int** | 1;78 | 32.085 | 2.37e-07 | *** |
| | | **Genotype: Time Int** | 1;78 | 1.174 | 0.282 | ns |
| **SH451** | **6** | **Genotype** | 1;18 | 21.14 | 0.000223 | *** |
| | | **Time Int** | 1;78 | 11.438 | 0.00113 | ** |
| | | **Genotype: Time Int** | 1;78 | 2.322 | 0.13161 | ns |
| **SH451** | **9** | **Genotype** | 1;17 | 3.13 | 00948 | . |
| | | **Time Int** | 1;74 | 9.690 | 0.00263 | ** |
| | | **Genotype: Time Int** | 1;74 | 1.578 | 0.21304 | ns |
| **SH451** | **12** | **Genotype** | 1;17 | 0.306 | 0.588 | ns |
| | | **Time Int** | 1;74 | 11.132 | 0.00133 | ** |
| | | **Genotype: Time Int** | 1;74 | 0.652 | 0.42208 | ns |
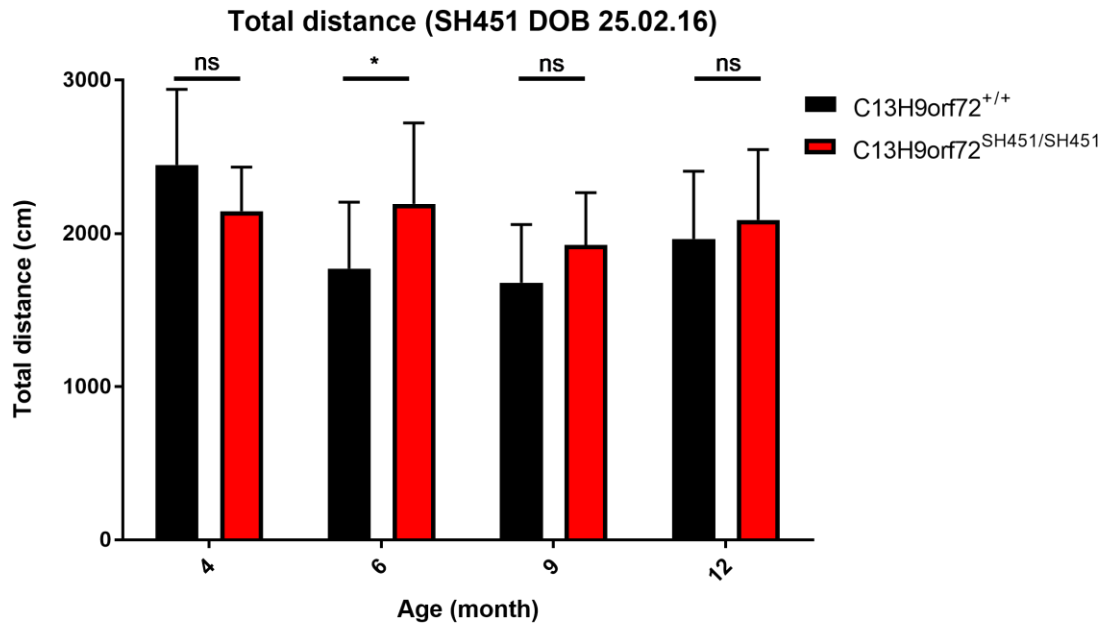
**Figure 4.31 Total distance travelled during novel tank diving test SH451 DOB 25.2.16.** Displays the total distance travelled in the whole tank during the 5-minute exposure to the novel tank. There is no significant difference in total distance travelled between C13H9orf72$^{+/+}$ zebrafish and C13H9orf72$^{SH451/SH451}$ zebrafish at 4, 9 and 12 months of age (2-way ANOVA with Fisher's LSD test, n=9-10), however there is at 6 months (p= 0.0304). Error bars show standard deviation.

#### 4.4.1.6. SH470 (DOB 30.3.16)

Figure 4.32 displays the time spent within the lower half (s) during the 5-minute exposure to the novel tank, at months 4-12 (SH470, DOB 30.3.16, n=11 per genotype – table 4.6). During the study, the cohort was tested once every 3 months. There is not a significant effect of time interval at any time point tested (figure 4.32, table 4.18), which indicates that the zebrafish are not displaying the typical response to a novel environment as we would expect. There was also no significant effect of genotype at any of the time points tested (table 4.18). Additionally, there was no significant genotype: time interval interaction at any time point except for at 12 months (table 4.18, highlighted yellow). Post-hoc analysis at 12 months revealed C13H9orf72$^{SH470/SH470}$ spent longer in the lower half of the tank compared to wild-type siblings at minute 1 only (unpaired t-test, minute 1 p=0.0221). Figure 4.33 shows that there were no differences between the two groups in the distances travelled at any time point tested, confirming that any differences seen were due to behaviour and not motor function (2-way ANOVA with Fisher's LSD test, n=11).
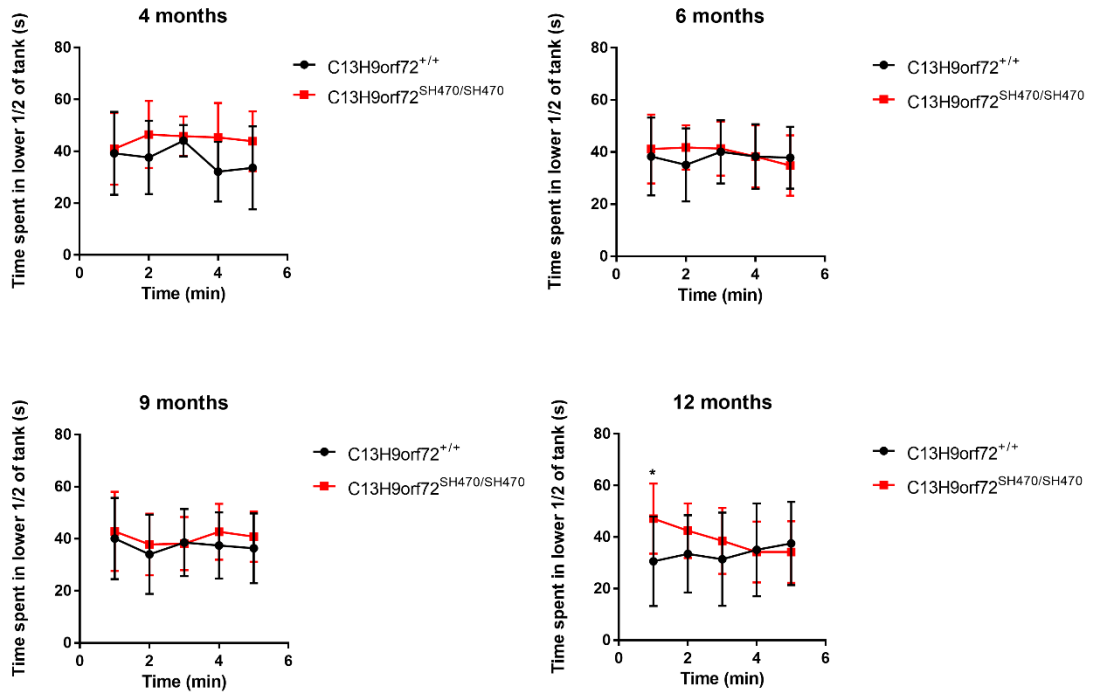
**Figure 4.32 Mean time (s) spent in the lower half of the novel tank during the tank diving test for line SH470 DOB 30.3.16.** Graphs display time spent in lower half of tank during the 5-minute exposure to the novel tank at 9-24 months. There was a significant genotype: time interval interaction at 12 months revealed C13H9orf72$^{SH470/SH470}$ spent longer in the lower half of the tank compared to wild-type siblings at minute 1 only (unpaired t-test, minute 1 p=0.0221). (two-way ANOVA with repeated measures). Post-hoc analysis at 12 months revealed. Error bars show standard deviation. Group sizes n=11.

**Table 4.18 Result from two-way ANOVA with repeated measures for line SH470 DOB 30.3.16.** Significance codes: 0 '***'; 0.001 '**';0.01 '*'; 0.05 '.'. Analysis performed on R3.3.2 for Windows.

| Line | Age | Measurement | Df | F Value | Pr (>F) | Sig |
|---|---|---|---|---|---|---|
| **SH470** | **4** | **Genotype** | 1;20 | 3.285 | 0.0849 | . |
| | | **Time Int** | 1;86 | 0.808 | 0.371 | ns |
| | | **Genotype: Time Int** | 1;86 | 2.563 | 0.113 | ns |
| **SH470** | **6** | **Genotype** | 1;20 | 0.171 | 0.684 | ns |
| | | **Time Int** | 1;86 | 1.237 | 0.269 | ns |
| | | **Genotype: Time Int** | 1;86 | 2.188 | 0.143 | ns |
| **SH470** | **9** | **Genotype** | 1;20 | 0.613 | 0.443 | ns |
| | | **Time Int** | 1;86 | 0.056 | 0.813 | ns |
| | | **Genotype: Time Int** | 1;86 | 0.144 | 0.705 | ns |
| **SH470** | **12** | **Genotype** | 1;20 | 1.668 | 0.211 | ns |
| | | **Time Int** | 1;86 | 1.43 | 0.2350 | ns |
| | | **Genotype: Time Int** | 1;86 | 10.26 | 0.0019 | ** |
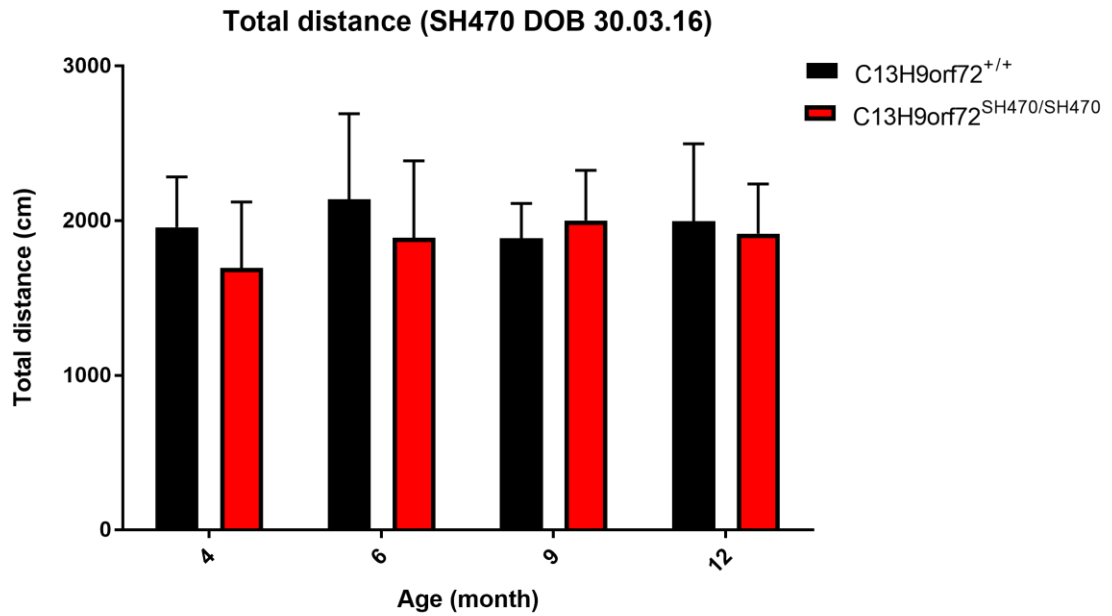
**Figure 4.33 Total distance travelled during novel tank diving test SH470 DOB 30.3.16.** Displays the total distance travelled in the whole tank during the 5-minute exposure to the novel tank. There is no significant difference in total distance travelled between C13H9orf72$^{+/+}$ zebrafish and C13H9orf72$^{SH470/SH470}$ zebrafish at 4-9 months of age (2-way ANOVA with Fisher's LSD test, n=11). Error bars show standard deviation.

### 4.4.2. Pilot study investigating the impact of frameshift mutations in *C13H9orf72* on thigmotaxis using the Open Field test

In addition to the novel tank diving, the open field test was also used to examine anxiety-like behaviour in the *C13H9orf72* LOF mutants. This is a commonly used method to measure anxiety in rodents, via observation of thigmotaxic behaviour (increased amount of time exploring the periphery of an arena compared to the centre). It has been reported that adult zebrafish exhibit thigmotaxic behaviour in an aquatic open field test, thus this test was set up to examine the effect that frameshift mutations in *C13H9orf72* has on thigmotaxic behaviour in adult zebrafish (Schnorr et al. 2012). This was done on the pilot cohort only (line SH448, DOB 24.09.14). Additionally, after placing the zebrafish in the middle of the test arena, each individual was left 60s to acclimatise. This was done to reduce the effects of any differences between zebrafish in the time to be netted, and is a technique that has been reported with zebrafish and other fish species (Burns 2008, Ariyomo and Watt 2012, Ariyomo and Watt 2015). Therefore, this means that unlike the novel tank test, anxiety behaviour is observed under a lower stress environment.

Initially, this test was performed in a rectangular tank and the bottom of the tank was divided into two virtual zones – the centre and the periphery (the area within 6 cm of the walls). Each individual was filmed from above for 6 minutes in total (including acclimatisation) (figure 4.34, A-B), with time spent in each zone (s) and overall distance travelled (cm) recorded using the equipment and related software included in the ViewPoint analysis suite (ViewPoint Life Science, Lyon, France). Thigmotaxis was defined as the percentage of time spent in the periphery, as described in section 2.7.3.2. Figure 4.34 C shows that there was no significant difference between the groups in percentage time spent in the periphery of the tank during the time points 8-12 months (2-way ANOVA with Fisher's LSD test, ns, n = 5-6). Additionally, figure 4.34 D shows that there was no significant difference between the groups in total distance travelled during the test at 8-12 months (2-way ANOVA with Fisher's LSD test, ns, n = 5-6).
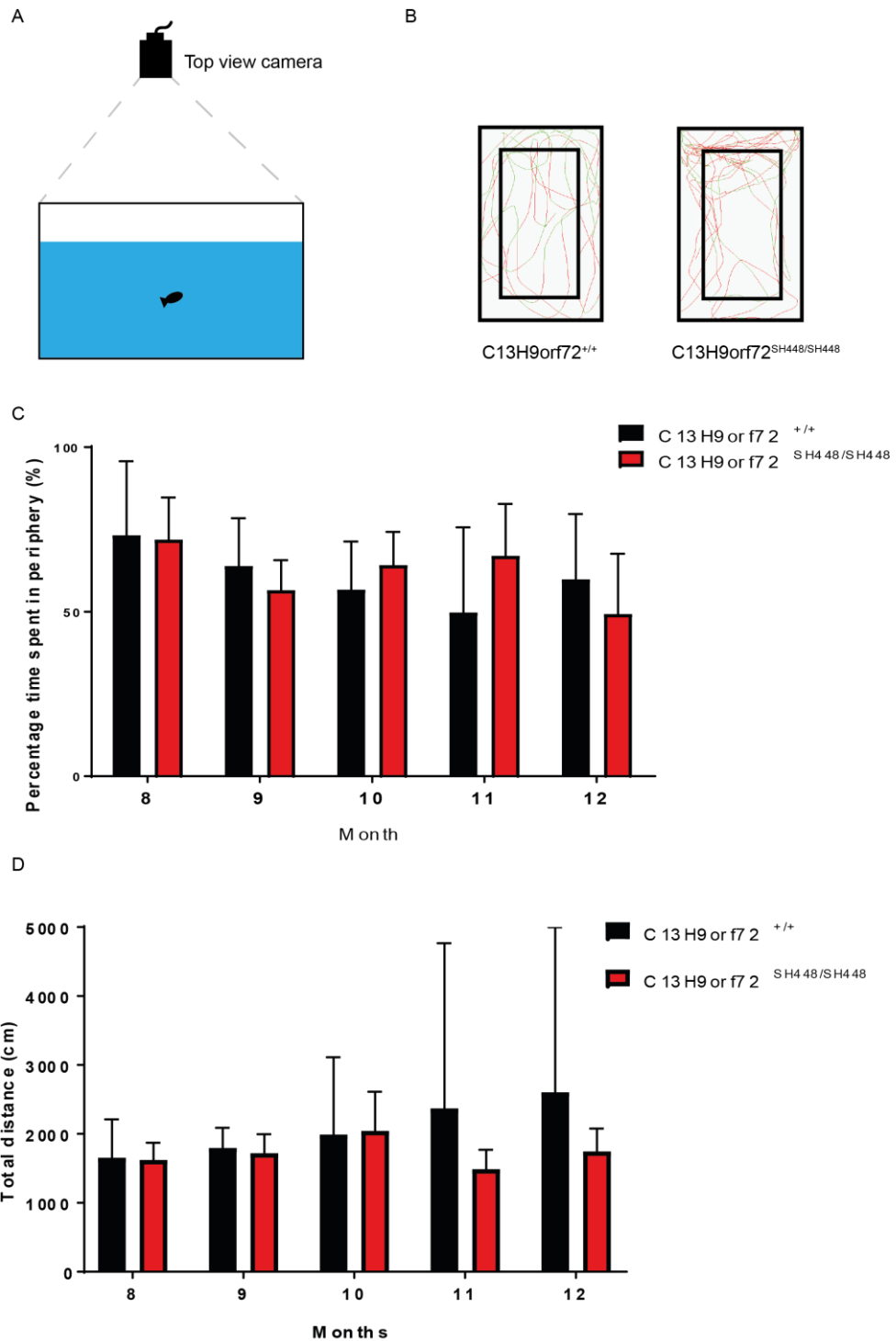
**Figure 4.34 Frameshift mutations in C13H9orf72 do not lead to changes in thigmotaxis age 8-12 months.** A) Original rectangular, transparent arena used for the Open Field test. B) Shows example traces produced from the ViewPoint system during the test from a C13H9orf72^{+/+} and C13H9orf72[SH448/SH448] fish. C) Bar graph representing the mean percentage time spent in the periphery (thigmotaxis) of each group (2-way ANOVA with Fisher's LSD test, ns, n = 5-6 fish per group). D) Bar graph representing total distance travelled of each group (2-way ANOVA with Fisher's LSD test, ns, n = 5-6 fish per group). Error bars represent standard deviation.

During months 8-12, we had consistent problems with the ViewPoint analysis suite being sensitive to reflections on the side of the tank during the experiment. Despite the addition of several non-reflective materials surrounding the tank, it was difficult to prevent this in the initial arena used. Following personal communication with Dr Caroline Brennan, the arena was changed to an opaque, white cylinder from 13 months onwards as described in section 2.7.3.2 (figure 4.35, A). The change of arena prevented issues with reflection in future tests. As before, the bottom of the tank was divided into two virtual zones – the centre and the periphery (the area within 5 cm of the walls). Each individual was filmed from above for 6 minutes in total (including acclimatisation) (figure 4.35, A-B), with time spent in each zone (s) and overall distance travelled (cm) recorded using the equipment and related software included in the ViewPoint analysis suite (ViewPoint Life Science, Lyon, France). Thigmotaxis was defined as the percentage of time spent in the periphery, as described in section 2.7.3.2. Figure 4.35 C shows that there was no significant difference between the groups in percentage time spent in the periphery of the tank during the time points 13-23 months (2-way ANOVA with Fisher's LSD test, ns, n = 5-6). Additionally, figure 4.35 D shows that there was no significant difference between the groups in total distance travelled during the test at 13-23 months (2-way ANOVA with Fisher's LSD test, ns, n = 5-6). Overall, the observed results indicate that there was no change in anxiety-like behaviour in either group in the open field test, thus other experimental groups were not tested.
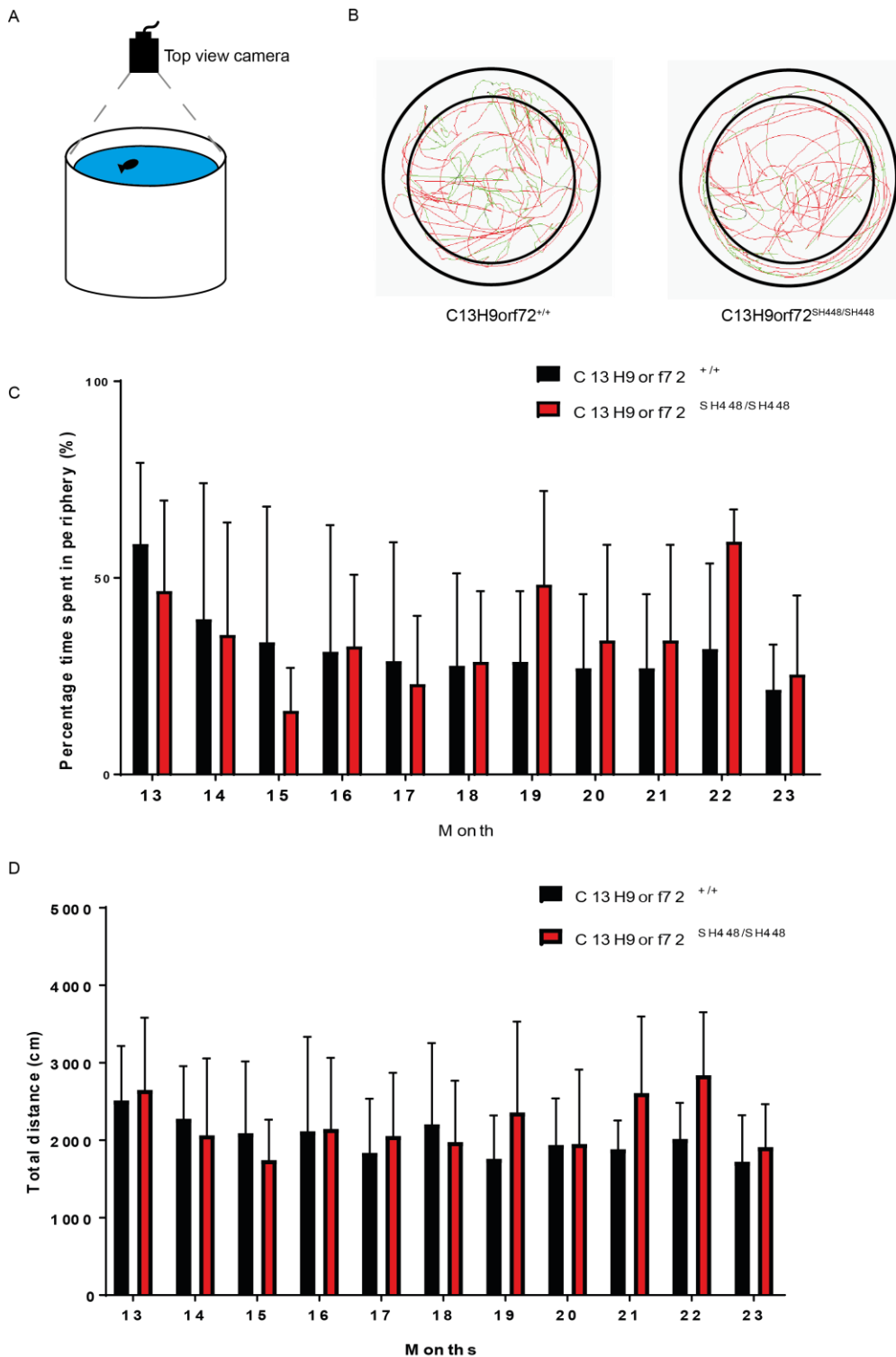
**Figure 4.35 Frameshift mutations in C13H9orf72 do not lead to changes in thigmotaxis age 13-23 months.** A) Schematic representation of the white, circular arena used for the Open Field test. B) Shows example traces produced from the ViewPoint system during the test from a C13H9orf72$^{+/+}$ and C13H9orf72$^{SH448/SH448}$ fish. C) Bar graph representing the mean percentage time spent in the periphery (thigmotaxis) of each group (2-way ANOVA with Fisher's LSD test, ns, n = 5-6 fish per group). D) Bar graph representing total distance travelled for each group (2-way ANOVA with Fisher's LSD test, ns, n = 5-6 fish per group). Error bars represent standard deviation.

## 4.5. Discussion

Following the generation of several *C13H9orf72* LOF zebrafish lines, as discussed in chapter 3, this study focussed on investigating whether loss of *C13H9orf72* results in ALS- and/or FTD-like phenotypes. Previously, no stable *in vivo* model of C9-ALS/FTD in zebrafish has been characterised, highlighting the importance of phenotypic characterisation during this project. As mentioned, phenotypes such as survival, motor function and NMJ pathology were investigated, as has been done in other models of ALS in zebrafish (Ramesh et al. 2010, Hewamadduma et al. 2013). In addition, due to the link between ALS and FTD in *C9orf72*-related disease, zebrafish were investigated for any behavioural changes. Characterisation of these zebrafish has allowed further understanding in to the role that haploinsufficiency of *C9orf72* may play in C9-ALS/FTD.

### 4.5.1. Characterisation of survival in *C13H9orf72* loss-of-function zebrafish

As mentioned previously, AMO experiments suggest that transient KD of *C13H9orf72* in zebrafish produce viable embryos (Ciura et al. 2013). However, a previous AMO experiment which transiently KD *tardbp* in zebrafish reported viable embryos (Kabashi et al. 2010b), but when both orthologues were knocked out, homozygous mutants only survived up to 10dpf (Hewamadduma et al. 2013, Schmid et al. 2013). Therefore, early viability of *C13H9orf72* LOF zebrafish was characterised during this project, as it was unknown whether complete loss of the gene would result in embryonic or larval lethality. To determine this, zebrafish heterozygous carriers for all identified frameshift mutations were in-crossed and the resulting progeny monitored twice per day, removing dead larvae for genotyping, as previously done (Chapman et al. 2013). As discussed in sections 4.2.1.1 and 4.2.2.1, the majority of the lines investigated showed no significant difference in early survival of all three genotypes. This supports the previous study which showed transient knockdown of *C13H9orf72* did not result in embryonic lethality (Ciura et al. 2013). However, it was observed that two lines investigated showed a significant difference in early survival of the three genotypes.

Initial survival characterisation of line SH470 showed that only 41% of *C13H9orf72*$^{SH470/SH470}$ embryos survived up to day 21, in comparison to 68% *C13H9orf72*$^{+/+}$ and 74% *C13H9orf72*$^{SH470/+}$ embryos (figure 4.2). Additionally, in a separate batch raised to adulthood, although survival rates were improved for all three genotypes, there was still a decrease in survival of homozygous mutants. The decreased viability of the homozygous mutants in this line could be due to a genetically linked

mutation, causing a proportion of the embryos to be non-viable. This could be examined further via exome sequencing. However, when the aforementioned clutch was genotyped at 90dpf, there was no significant difference between the observed and expected Mendelian ratios (section 4.2.1.2, table 4.1), suggesting further analysis into this line may not be necessary. The line SH470 was the only one raised to adulthood for phenotypic characterisation, because the heterozygous carriers obtained for line SH471 showed a sex skew bias towards males, therefore it was not possible to raise F3 offspring to characterise before the end of this project. Additionally, as described previously, line SH472 did not show a significant reduction in *C13H9orf72* mRNA levels and was therefore not taken forward for further studies.

In addition, a significant difference in survival was observed for line SH448, with 37% survival for *C13H9orf72$^{SH448/SH448}$*, 48% for *C13H9orf72$^{SH448/+}$* and 55% for *C13H9orf72$^{+/+}$* embryos reported. However, although viability of *C13H9orf72$^{SH448/SH448}$* embryos was low, survival overall was low for all genotypes (see figure 4.2). This was also seen for lines SH449 and SH450 (see figure 4.2). This was due to a high rate of failed PCRs when genotyping, as some of the larvae collected were degrading thus the extracted DNA failed to amplify. Despite this, when the line SH448 was genotyped at 90dpf, there was no significant difference between the observed and expected Mendelian ratios (see section 4.2.2.2, table 4.3), suggesting there is no difference between genotypes and viability is normal.

To determine if *C13H9orf72* is important for viability in adult life we also monitored survival until end stage. This would better reflect human disease, as disease onset and death occurs in adulthood. This would also compare well with other zebrafish models of ALS, such as the transgenic zebrafish overexpressing sod1, where survival has been reported to decrease in adulthood but not during larval stages (Ramesh et al. 2010). As discussed, there was no significant difference between original and end-stage group sizes in any line (tables 4.2 and 4.4). This data suggests that the frameshift mutations identified in *C13H9orf72* do not impact survival at any stage throughout the lifetime of the zebrafish. These findings do not recapitulate what has been shown in some *C9orf72* LOF mouse models, who report a decrease in survival of homozygous mutants during adulthood in comparison to wild-type controls (Burberry et al. 2016, Sudria-Lopez et al. 2016). However, the reduction in survival observed in the *C9orf72* LOF mice may be linked to an immune defect and not neurodegeneration, and we go on to investigate

whether our model recapitulates any of the immune defect symptoms found in the next chapter (O'Rourke et al. 2016, Sudria-Lopez et al. 2016, Koppers et al. 2015).

### 4.5.2. Characterisation of motor function in *C13H9orf72* loss-of-function zebrafish

As loss of muscle strength is a characteristic phenotype of C9-ALS/FTD, the next aim of the project was to examine motor function of the zebrafish carrying frameshift mutations in *C13H9orf72*. The Spinning Task and the Swim tunnel were utilised in order to do this. It was expected that if loss of *C13H9orf72* results ALS/FTD-like phenotypes in these zebrafish, a reduction in swimming endurance would be observed during the aforementioned tests.

### 4.5.2.1. The spinning task as a measure of swimming endurance

As discussed, one of the main disadvantages of using the swim tunnel was that it took a long time to test motor function in large clutches of zebrafish, taking up to 30 minutes per individual. Therefore, we initially used a novel method called the Spinning Task, due to the protocols ability to test the swimming endurance of an individual zebrafish in only a few minutes (Blazina et al. 2013). However, we demonstrated that the coefficient of variation (which is the standard deviation as a percentage of the mean) was high for this test, reflecting the variability of this method in measuring motor function. For example, an average coefficient of variation of wild-types in the swim tunnel was 11.67%, whereas the average for wild-types in the Spinning Task was 95.68% at 400rpm and 80.34% at 500rpm (section 4.3.1). A reason for this variability may be due to the subjective nature of determining the latency of individuals to be 'swept in' to the whirlpool. This observation meant that the suggested recording time of 180s was not suitable, thus we increased recording time up to 300 seconds from 7 months onwards, in order to fully determine when the individual was 'swept in' (Blazina et al. 2013). There were no other major differences in the overall protocol used minus recording time, with similar speeds and age of zebrafish used.

It was reported in the original publication that the time spent swimming during the test increases with the size of the individual, with fish of 3-4cm in length able to swim longer than smaller fish (Blazina et al. 2013). There is a trend that individuals are able to swim longer as time goes on (see table 4.5), which may be due to increasing size over time. However, as there is no data on length of this cohort it cannot be determined size of the individuals cause this. It may be that as the recording time was increased at 7 months,

they were recorded to swim for longer due to the subjective nature of the test as discussed. Alternatively, they may get used to the test over time. Additionally, there is a trend (table 4.5) that the fish swim for less time at 500rpm. This also agrees which the original publication, which showed that at lower speeds the fish could swim for longer (Blazina et al. 2013). Therefore, if this test would be utilised in the future, higher speeds should be used. However, overall due to the high level of variation observed during this test, it suggests that this protocol is not a reliable method to measure swimming endurance. As a result, it was decided to primarily use the swim tunnel in order to investigate motor function for this project going forward.

### 4.5.2.2. The swim tunnel as a measure of swimming endurance

The swim tunnel is an established method used to determine the critical swimming velocity ($U_{crit}$) of individual zebrafish, which is the maximum flow rate a fish can swim against for a sustained period (Plaut 2000, Brett 1964). This method has previously been used to characterise motor function in several zebrafish models of neuromuscular degeneration (Ramesh et al. 2010, Chapman et al. 2013), and is similar in nature to the rotarod test used to measure motor function in mouse models. As described in section 4.3.2, for each line tested there was a mild reduction in $U_{crit}$ observed for homozygous mutant zebrafish in relation to wild-type siblings, which was statistically significant at some time points. The mild motor deficit observed in this current study is in keeping with a *C9orf72* LOF mouse model, which demonstrated mild motor deficits in open field observations and CatWalk gait analysis (Atanasio et al. 2016). Interestingly, they did not report a difference in time spent on the rotarod (Atanasio et al. 2016). Conversely, neither the stable zebrafish or the mouse model of *C9orf72* LOF agree with the more severe locomotor deficits reported at larval stages following transient KD of *C13H9orf72* in zebrafish (Ciura et al. 2013), suggesting that this phenotype may have been an off-target mediated effect. To investigate this in the future, we would microinject the same AMOs used in the KD study into both wild-types and our stable *C13H9orf72* KO mutants. We would expect to see the same effect in wild-types as reported in the paper, but not in the stable knockout zebrafish, as these should not have endogenous *C13H9orf72*. However, if we did see the same effects in our mutants, it would suggest the AMOs used in the aforementioned study had off-target effects. A similar method has been used to show that an AMO used to KD *Tardbp* in zebrafish also had off-target effects (Kabashi et al. 2010b, Hewamadduma et al. 2013).

Initial characterisation suggests a mild swimming defect in the *C13H9orf72* LOF zebrafish, however the model needs further development to see if it will be useful as a model of motor dysfunction in the future. Firstly, the coefficient of variation was relatively high at some time points, ranging from 5.54% to 18.78% in controls and 7.74% to 38.39% in mutants. Although overall this is lower in comparison to the Spinning Task, it indicates that there is still variation within the groups. High variation may be attributable to the fact that unlike rodents, zebrafish are not maintained as inbred strains in the laboratory. This is because it can lead to a phenomena called inbreeding depression, resulting in loss of fitness due to increased homozygosity (Monson and Sadler 2010). Inbreeding depression has been reported to result in fewer successful matings and smaller clutch sizes in common wild-type zebrafish strains, including AB which is the strain used in this project (Monson and Sadler 2010). As a result, the zebrafish used in this project are genetically diverse due to outcrossing, therefore resulting in possible heterogeneity within the different lines.

Secondly, the original swim tunnel utilised for characterisation was used to detect the motor dysfunction of the Mitofusin 2 (Mfn2) zebrafish model (Chapman et al. 2013), and could reach a maximum flow rate of 18.04 cm/s. However, as the phenotype displayed by the *C13H9orf72* LOF zebrafish was less severe than that of the *Mfn2* zebrafish, this original tunnel was unable to exhaust both the wild-type and mutant zebrafish in the current study. Therefore, this tunnel was modified in order to reach a maximum flow rate of 39.47cm/s, whilst the studies were ongoing. This meant that data was only obtained from 9 or 12 months onwards for line SH451 clutch 1 and SH448 clutch 1, respectively (section 4.3.2.1 and 4.3.2.3). As a result, a second clutch was raised for these lines, in order to obtain data at earlier time points (section 4.3.2.2 and 4.3.2.4). The modified swim tunnel had already been established by the time the clutch for line SH470 had been raised to adulthood (section 4.3.2.5).

Thirdly, it is important to consider when analysing these data that we may only see a mild motor dysfunction in our *C13H9orf72* LOF zebrafish, as individual muscle fibres are polyneuronally innervated throughout the zebrafish lifetime, unlike in rodents and humans (Westerfield et al. 1986). Additionally, it has been reported that adult zebrafish have the capability to regenerate motor neurons (Reimer et al. 2008), which rodents and humans cannot do. Therefore, it is possible that compensatory mechanisms such as polyneuronal innervation and motor neuron regeneration that occur in zebrafish may

affect the observed phenotype. Thus, possible degeneration or death of a few motor neurons may not have much of an effect on movement overall. However, NMJs were investigated via immunohistochemical analysis to look into this further, which will be discussed in section 4.5.2.3.

Finally, power analysis using G*Power Version 3.0.3, based on $U_{crit}$ values obtained from a transgenic SOD-1 zebrafish model of ALS (Ramesh et al. 2010), indicated a sample of 11 zebrafish per group would provide 80% power to detect a 20% reduction in $U_{crit}$ (student's t-test, two-tailed, $\alpha = 0.05$, $\beta = 0.8$). This was then applied to the other characterisation tests. However, due to variability and the mild phenotype observed in the *C13H9orf72* LOF zebrafish, the study was underpowered. Retrospective power calculations using G*Power Version 3.0.10, based on $U_{crit}$ values obtained in this study, revealed a sample of 25 zebrafish per group would provide 80% power to detect a 20% reduction in $U_{crit}$ (student's t-test, two-tailed, $\alpha = 0.05$, $\beta = 0.8$). Based on these calculations, a cohort of this size has been raised, with motor function analysis ongoing. As we know that there is most likely genetic heterogeneity within these lines due to outcrossing, resulting in an increase in the coefficient of variation. Therefore, larger group sizes will increase sensitivity of the swim tunnel test and allow us to address these issues. However, such large group sizes are not ideal for this type of analysis, due to the length of time it takes to obtain data.

### 4.5.2.2.1.    Impact of body size on swimming endurance

It is important to account for body size when using the swim tunnel apparatus, as previous research has linked body shape and size to swimming ability in a variety of fish species (Domenici 2003, Langerhans 2009, Gordon et al. 2015). As discussed in section 4.3.2.6, when experimental groups for the swim tunnel were determined, zebrafish of a similar weight and length were selected when available numbers permitted. At each time point, the weight and length of each individual zebrafish was recorded, alongside its $U_{crit}$ value. The data revealed that there were no strong correlations between recorded weights and/or lengths vs $U_{crit}$ values in all lines tested. Therefore, it can be concluded that the weights and lengths of the chosen individuals did not have a significant influence on the swimming performance of the fish.

In order to maintain consistency in the future, it would be advisable to ensure that experimental groups are of a similar weight and length, in order to limit variation. This can be difficult if there is only a limited number of zebrafish of the correct genotype.

Additionally, it is known that the rate of zebrafish growth is influenced by many factors, including water quality, temperature, food quality and availability, and population density of the tank (Singleman and Holtzman 2014). Thus, it is suggested that husbandry is standardised and zebrafish are not raised in high density tanks before genotyping to prevent variation in growth. This would ensure that individuals in the tank have an increased access to food and develop at a similar rate. However, even when grown in standardized conditions, zebrafish can still develop into a range of sizes (Singleman and Holtzman 2014). Thus, as well as standardising conditions, raising large clutches to ensure you can obtain an experimental group of similarly sized zebrafish would be essential. This is also something to consider with regards to gender, discussed in section 4.5.2.2.2.

### 4.5.2.2.2.    Impact of gender on swimming endurance

Interestingly, it was observed that gender had a significant impact on the swimming endurance of zebrafish in the swim tunnel. In all lines tested, there was evidence that female $U_{crit}$ was significantly lower than male $U_{crit}$, but there were some notable exceptions. Firstly, in line SH448, there was no significant decrease in $U_{crit}$ between male $C13H9orf72^{+/+}$ and female $C13H9orf72^{+/+}$. However, this could be explained by an outlier in the female group, who had a much higher Ucrit value compared to the rest of the group (figure 4.14A). Additionally, in line SH470, there was no significant decrease in $U_{crit}$ between male $C13H9orf72^{SH470/SH470}$ and female $C13H9orf72^{SH470/SH470}$ (figure 4.14C). In this case, there was a significant difference between male $C13H9orf72^{+/+}$ and male $C13H9orf72^{SH470/SH470}$ (p=0.0092), but no difference between the female genotypes. This suggests that the mutation, which is located in exon 1 in comparison to lines SH448 and SH451 which are located in exon 7, may have a greater effect on male $U_{crit}$.

As discussed, the evidence that female $U_{crit}$ was significantly lower than male $U_{crit}$ may be linked to body shape. Female zebrafish typically have a distended belly which contains eggs, which means that they will have an increased maximum cross-section area in comparison to males. This increase in cross-section area may lead to increased hydrodynamic drag when swimming in the tunnel, which in turn may result in the decrease in maximum $U_{crit}$ observed in females. Interestingly, other groups have previously published that there is not a difference in $U_{crit}$ between the sexes in zebrafish, at a range of ages (8-30 months) (Marit and Weber 2011, Gilbert, Zerulla and Tierney 2014). However, the effect of gender on swimming ability has been extensively observed

in other fish species, and has revealed some differences. Converse to the present study, investigation into the effect of gender on $U_{crit}$ in Trinidadian guppies revealed that on average males had much lower $U_{crit}$ values than females (Gordon et al. 2015). However, this same study did report that pregnant females had lower $U_{crit}$ in comparison to non-pregnant females. This in part was attributed to a large distension of the body due to pregnancy. This caused females to have rounder bodies, resulting in increased hydrodynamic drag. Previous studies have also shown that in various fish systems, rounder bodies result in a decrease in $U_{crit}$ due to increased drag (Webb 1994, Plaut 2002). This complements our explanation as to why female zebrafish have decreased swimming endurance on average in comparison to males in the present study.

Overall, gender should be matched between experimental groups for swim tunnel studies, as it is clear that bias towards one gender in either group could skew data. However, sex ratios in groups of zebrafish can be problematic. In many species, gender is determined by a chromosomal background, but no distinct genetic mechanism has been identified in zebrafish thus far. Several candidate genes have now been implicated in the process, which suggests that sex determination it is likely to be a complex interaction between several loci interacting with environmental factors (Wilson 2012). All zebrafish initially have undifferentiated, ovary-like gonads but by 30dpf all oocytes disappear from male gonads, and males undergo testicular differentiation (Watts, Powell and D'Abramo 2012, Takahashi 1977). However, the point at which spermatogenesis is determined in zebrafish that go on to develop into males is not known (Wilson 2012, Orban, Sreenivasan and Olsson 2009). Interestingly, one study found that somatic genes were expressed indifferently at 10 to 17dpf, but became sexually dimorphic after 3 weeks (Wilson 2012, Tong, Hsu and Chung 2010). This suggests that if there is an environmental effect on sex determination, husbandry during larval rearing is likely to affect it (Wilson 2012). Anecdotally, it has been observed that high stocking densities and limited food resources may produce more males, and vice versa (Wilson 2012). Additionally, other environmental factors such as hypoxia, temperature, nutrition, exposure to hormones have been shown to have an effect on sex determination (Nagabhushana and Mishra 2016). Due to the unpredictable nature of sex determination, raising larger clutches could help to ensure experimental groups can be sex matched in the future.

### 4.5.2.3. Immunohistochemical analysis of neuromuscular junctions

In order to further investigate the basis for the subtle alteration in motor function that was observed, quantitative assessment of NMJs was performed (see section 4.3.2.8). As described, we stained trunk musculature with α-bungarotoxin (a post-synaptic marker of the NMJ) and SV2 (a presynaptic marker that labels motor neurons), and used confocal microscopy to quantify the intensity correlation quotient (ICQ) (Li et al. 2004), size and number of both the pre- and post-synaptic compartments. This was investigated in 11-month old zebrafish from the lines SH448 and SH451, because it was observed that the zebrafish had a moderate reduction in $U_{crit}$ around this time point. If defects at the NMJ are associated with this altered swimming, we would have expected to have seen a reduction in ICQ, as well as the size and number, of pre- and post- synaptic compartments, indicative of NMJ degeneration.

Firstly, the number of pre- and post-synaptic compartments per section was analysed, to determine if there was a loss of NMJs. There is a trend that the number of pre- and post-synaptic compartments is decreased in homozygous mutants in comparison to wild-type siblings, in both lines tested. However, this is only significantly reduced for post-synaptic compartments in C13H9orf72$^{SH451/SH451}$ trunk musculature in comparison to wild-type siblings. These observations may indicate that there is a loss of NMJs, but further work would need to be done to explore this. Secondly, to look at co-localisation between SV2 and α-bungarotoxin the ICQ value was quantified, as this method has been published in relation to examining the integrity of NMJs in zebrafish previously (Chapman et al. 2013). We found that there was no difference in ICQ values between homozygous mutants (C13H9orf72$^{SH448/SH448}$ and C13H9orf72$^{SH451/SH451}$) and wild-type siblings in both lines tested, indicative of intact NMJs in both genotypes. Finally, the frequency distribution of pre- and post-synaptic area was observed and compared between genotypes. This was done, as the sizes of the pre- and post-synaptic compartments were not normally distributed, therefore taking a mean value for comparison would not have been an appropriate method. It was observed in both lines that there was a high frequency of small (up to 10μm$^2$) pre- and post-synaptic compartments. There may be several reasons for this. For example, zebrafish have striated skeletal muscle, therefore it could be that when processing the sections, they were not cut longitudinally along the muscle, resulting in some NMJs being cut at an angle, affecting the size of pre- or post-synaptic compartment observed. Alternatively, this could be an artefact of the microscope settings used.

Interestingly, a significant difference was only observed between pre- and post-synaptic compartments up to $10\mu m^2$ in both lines. However, the differences between the mean frequencies are actually very small therefore calling in to question the biological relevance of this observation.

Overall, despite the observation that homozygous mutants have a moderate decrease in swimming endurance in comparison to wild-type siblings, quantitative assessment did not reveal any significant abnormalities relating to NMJs. It is possible that compensatory mechanisms such as polyneuronal innervation of zebrafish muscle (Westerfield et al. 1986) and the capacity for motor neurons to regenerate (Reimer et al. 2008), affects the phenotype observed. Additionally, we are limited in this study as only a single time point was tested. Based on these results, it is unlikely there would be any difference at earlier time points but examination of NMJs at later time points would be interesting.

### 4.5.3. Characterisation of behaviour in *C13H9orf72* loss-of-function zebrafish

It is reported that 50% of ALS patients carrying the repeat expansion in *C9orf72* also show behavioural and/or cognitive impairments (Ringholz et al. 2005). Additionally, a study on a large ALS patient cohort revealed around 15% of these patients met the clinical criteria for FTD, particularly the behavioural variant of FTD (bvFTD) (Ringholz et al. 2005). Patients show symptoms such as: anxiety, disinhibition, apathy, memory loss (Mahoney et al. 2012). As well as this, there is high evidence of psychosis, most commonly featuring hallucinations and delusions (Sha et al. 2012, Snowden et al. 2012, Cooper-Knock et al. 2014a). As gene function is widely conserved between zebrafish and humans, there is homology between their nervous systems and behaviours (Lieschke and Currie 2007). As a result, zebrafish are now widely used in behavioural neuroscience (Champagne et al. 2010, Norton and Bally-Cuif 2010). There are now several protocols established to measure behaviours such as anxiety, aggression, social preference, memory and learning in adult zebrafish (Norton and Bally-Cuif 2010). As discussed in section 4.4, the following tests were performed in order to establish whether *C13H9orf72* LOF in the zebrafish resulted any behavioural changes: novel tank diving and open field analysis, both of which are tests to examine anxiety.

#### 4.5.3.1. Novel tank diving test

Increased anxiety has been observed in patients carrying the repeat expansion in *C9orf72* (Mahoney et al. 2012). This may be directly linked to *C9orf72*-linked disease, but it is

important to consider that this may be a consequence of the patient understanding they have a terminal illness. However, it has been reported that these symptoms are present in FTD patients carrying the repeat expansion in *C9orf72,* before being in contact with psychiatric services, suggesting this is an important behavioural change in patients (Mahoney et al. 2012). To examine this behavioural trait in *C13H9orf72* LOF adult zebrafish, the novel tank diving test was performed (section 4.4.1). The test measures anxiety evoked by novelty stress. Adult zebrafish have been reported to exhibit a robust behavioural response to this stress (Cachat et al. 2010, Parker et al. 2012). When the individual is first placed in the novel environment, their natural instinct is to stay in the bottom of the tank. As the course of exposure to the novel environment continues, they become more exploratory. As a result, the amount of time spent in the lower half of the tank should decrease over the time course of the experiment, which is response we expect to see in controls. The novel tank diving test can quantify this behaviour by examining the amount of time a zebrafish spends at the lower half of the tank in comparison to the top, with more time spent in the lower half indicative of anxious behaviour (Cachat et al. 2010). It has been reported that use of anxiolytic treatments significantly decrease the amount of time spent in the lower half of the tank (Cachat et al. 2010, Parker et al. 2014, Bencan, Sledge and Levin 2009, Levin, Bencan and Cerutti 2007), further supporting this protocols ability to measure anxiety.

The pilot cohort displayed the typical diving response at each time point, meaning that they gradually spent less time in the lower half over the course of exposure to the novel tank. This observation is supported as there was a significant main effect of time interval at all of the time points tested (table 4.13). *C13H9orf72*$^{SH448/SH448}$ zebrafish spent more time in the lower half of the tank over the course of exposure in comparison to their wild-type siblings, indicative of increased anxiety (section 4.4.1.1). Again**,** this effect was confirmed at months 9-14, 16 and 20, as there was a significant main effect of genotype (table 4.13). Additionally, no significant difference in distance travelled during the course of exposure was noted between the two genotypes, allowing further confidence that the result seen was due to behaviour and not because the motor function of the *C13H9orf72* LOF zebrafish was impaired. Due to the consistency of the pilot study, characterisation of behaviour was carried out in three separate lines using the novel tank diving test. The lines tested included SH448, which carried the same mutation in exon 7 as the pilot cohort, SH451 (another exon 7 mutant) and SH470 (an exon 1 mutant) (details for all

mutants generated in chapter 3). As discussed earlier, a second clutch was raised for line SH448 and SH451, in order to obtain data for earlier time points (which was also necessary for the swim tunnel, as discussed previously). Overall, it was observed that *C13H9orf72* LOF adult zebrafish showed no evidence for increased anxiety under stressed conditions in lines SH448, SH451 and SH470, converse to the pilot data. However, these findings are consistent with recently published *C9orf72* LOF mouse models, which do not report on any observed behavioural phenotype, such as anxiety (Atanasio et al. 2016, Burberry et al. 2016, Koppers et al. 2015, O'Rourke et al. 2016, Sudria-Lopez et al. 2016).

The typical diving response in the novel tank diving test, for both homozygous mutants and wild-types, can be represented by line SH448 clutch 2 (figure 4.26), which show a clear decrease in the amount of time spent in the lower half over time. However, it was found that the typical diving response we expect to see was not observed in homozygous mutants nor wild-types in some of the lines. For example, line SH470 did not show the typical diving response at any time point tested, supported as there was not a significant effect of time interval (see figure 4.32 and table 4.17). Interestingly for SH451 clutch 1 there was not a significant effect of time interval at months 18-24, but there was at the earlier time points of 9-15 (see figure 4.28 and table 4.15). This suggests that the zebrafish may acclimatise to the test over time, thus are no longer susceptible to novelty stress. If this is the case, it would suggest that it is not advisable to perform this test over an extended period of time. However, most of the lines tested did show the expected diving response at all of the time points, including SH448 clutch 2 and SH451 clutch 2 (see section 4.4.1.3 and 4.4.1.5). Additionally, the pilot cohort, which was tested once a month compared to once every three months, also showed the expected diving response at all of the time points. Therefore, this does not support the fact that the zebrafish acclimatise to the test over time. Anecdotally, it was noted that when zebrafish showed signs of aging (at later time points) they spent most their time at the top of the tank. Thus, as the analysis is done on the group as a whole, this may have affected the diving response seen overall. In the future, it may be suggested to exclude zebrafish which have aged and are therefore not behaving as expected. However, this observation does not explain why the typical diving response wasn't see at earlier time points for line SH470, as mentioned previously. There was no difference in housing conditions of any of the lines, which is known to effect the diving response seen in the novel tank diving test (Parker et al. 2012). In

summary, we found that some clutches did not show the typical diving response. As wild-type controls were among this group, it is difficult to draw conclusions on the behaviour of mutants.

### 4.5.3.2. Open field test

In addition to the novel tank diving test, the open field test was performed to observe anxiety. The open field test is a commonly used method to measure anxiety in rodents, via observing thigmotaxic behaviour and it is now understood that zebrafish exhibit this same behaviour (Schnorr et al. 2012). Increase in thigmotaxic behaviour is known to be indicative of anxious behaviour (Schnorr et al. 2012). Additionally, it has been reported that use of anxiolytic treatments such as diazepam and ethanol decreases thigmotaxic behaviour, further supporting this tests ability to measure anxiety (Baiamonte et al. 2016). During this project, after placing the individual zebrafish in the middle of the test arena, they were left 60s to acclimatise. This was done to reduce the effects of any differences between zebrafish in the time to be netted, and is a technique that has been reported with zebrafish and other fish species (Burns 2008, Ariyomo and Watt 2012, Ariyomo and Watt 2015). Therefore, this means that unlike the novel tank test, anxiety behaviour is observed under a standard, low stress environment.

The open field analysis was performed on the pilot cohort only. As the results observed for the novel tank diving test were indicative of anxiety, it was expected that increased thigmotaxic behaviour would be observed in the *C13H9orf72* LOF zebrafish during the open field analysis. As discussed in section 4.4.2, no significant difference in thigmotaxic behaviour was observed between the two genotypes at any time point, suggesting the pilot cohort was not anxious under these conditions. One reason for this may be that this cohort only exhibits a difference in anxious behaviour under a more stressful stimulus. Overall, this result again complements observations made in *C9orf72* LOF mouse models, where behavioural changes were not reported (Atanasio et al. 2016, Burberry et al. 2016, Koppers et al. 2015, O'Rourke et al. 2016, Sudria-Lopez et al. 2016).

### 4.5.4. Conclusion

Overall, it can be concluded from this study that *C13H9orf72* LOF does not have an effect on early or late viability of the zebrafish. There is evidence of a subtle motor defect with no corresponding NMJ abnormalities at 11 months. However, a more highly statistically powered study is being undertaken in order to understand if it will be useful as a model of motor dysfunction. Additionally, there is not a significant difference in anxiety

behaviour between the *C13H9orf72* LOF mutants and wild-types, which has been observed in two separate tests of anxiety. These findings conclude that haploinsufficiency of *C13H9orf72* may not be enough to cause C9-ALS/FTD alone, which complements what has been reported in *C9orf72* LOF mouse models (Atanasio et al. 2016, Burberry et al. 2016, Koppers et al. 2015, O'Rourke et al. 2016, Sudria-Lopez et al. 2016). However, these findings do not rule out that *C13H9orf72* LOF may modulate disease onset and progression in C9-ALS/FTD patients, alongside other proposed gain-of-function mechanisms. Further characterisation will be necessary to determine the full potential of this model.

## 5. Investigating the function of C9orf72 *in vivo*

### 5.1. Introduction

*C9orf72* is alternatively spliced into three transcript variants, which are predicted to encode two protein isoforms, namely a 481aa isoform of approximately 50 kDa, referred to as C9orf72 long or C9orf72-L, and a 222aa isoform of approximately 25 kDa, referred to as C9orf72 short or C9orf72-S (Xiao et al. 2015, DeJesus-Hernandez et al. 2011)(Figure 1.2). Due to the lack of reliable, commercially available anti-C9orf72 antibodies, it is difficult to detect endogenous protein expression. However, one group has reported the development of antibodies which are able to detect C9orf72-L and C9orf72-S individually (Xiao et al. 2015). Using these antibodies, they showed that C9orf72-L exhibited diffuse cytoplasmic staining in neurons and labelled large speckles in cerebellar Purkinje cells (Xiao et al. 2015). Additionally, they showed that C9orf72-S exhibited specific staining of the nuclear membrane in healthy neurons, with relocalisation to the plasma membrane in diseased motor neurons in ALS (Xiao et al. 2015). Overall, the protein itself does not show any obvious homology to other proteins, however bioinformatic analysis by two groups have identified that C9orf72 is structurally related to Differentially Expressed in Normal and Neoplasia (DENN) domain-containing proteins (Zhang et al. 2012, Levine et al. 2013). DENN domain-containing proteins function as GDP/GTP exchange factors (GEFs) for Rab GTPases, which are involved in regulating a number of cellular trafficking events, including autophagy (Ao, Zou and Wu 2014).

Autophagy is a conserved lysosomal degradation pathway, involving the degradation of cytoplasmic components within an autophagolysosome. Defects in the autophagy pathway have previously been linked to several neurodegenerative diseases, including ALS (Harris and Rubinsztein 2012). C9-ALS/FTD patients characteristically have p62/SQSTM1 positive, TDP-43 negative inclusions in the cerebellum, hippocampus and neocortex (Cooper-Knock et al. 2012, Al-Sarraj et al. 2011). p62/SQSTM1 binds ubiquitinated cargoes and delivers them to the phagosome (Pankiv et al. 2007)(figure 5.4). As p62/SQSTM1 is degraded by autophagy in the process of delivering ubiquitinated cargo, accumulations of this protein indicate defective autophagy (Pankiv et al. 2007). Thus, the presence of these inclusions, together with evidence of *C9orf72* haploinsufficiency, first suggested the possibility that defective autophagy via loss of C9orf72 function contributed to C9-ALS/FTD. Recent studies revealed that disruption of

C9orf72 function, in both cell lines and primary neurons, results in an inhibition of autophagy initiation and accumulation of p62/SQSTM1, similar to the pathology seen in C9-ALS/FTD patients (Farg et al. 2014, Yang et al. 2016, Sellier et al. 2016, Sullivan et al. 2016a, Webster et al. 2016a). These findings further suggest that defects in autophagy via C9orf72 haploinsufficiency may be involved in C9-ALS/FTD pathogenesis. Therefore, it is important as part of this project to investigate the role of C9orf72 further *in vivo*, using the *C9orf72* LOF zebrafish. This not only will allow further investigation into the function of C9orf72 *in vivo*, but will also allow investigation into the possible role of autophagy deficits in disease progression.

Loss of the mouse orthologue of *C9orf72* (3110043021Rik), in either a tissue-specific or ubiquitous manner, has also been linked to defects in the immune system *in vivo* (O'Rourke et al. 2016, Sudria-Lopez et al. 2016, Koppers et al. 2015). For example, these models have consistently reported symptoms such as enlarged spleens and lymph nodes, microglia activation with abnormal lysosomal activity, altered cytokine production and impaired autophagy function (Atanasio et al. 2016, O'Rourke et al. 2016, Sudria-Lopez et al. 2016). Interestingly, these studies do not report any neurodegeneration in response to partial or complete loss of *C9orf72*. Therefore, it will be interesting to use the generated *C9orf72* LOF zebrafish to study whether defects to the immune system are evident, in particular we will observe for signs of splenomegaly.

### 5.2. Generating the pCI-neo-Myc-C13H9orf72 construct

To be able to explore the function of C13H9orf72 *in vitro* as well as *in vivo*, we first aimed to generate a C13H9orf72 expression construct. In order to achieve this, the C13H9orf72 cDNA reference sequence (ensembl: ENSDART00000015127.6) was BLAST searched against the NCBI expressed sequence tag (EST) database to identify a full length cDNA clone. As a result, complementary sequencing data for both the 5' and 3' ends were identified for cDNA clone ID FDR306-p00004_BR_K14 (accession number EH579768.1 and EH597144.1, respectively), suggesting this would be a full-length cDNA clone. The identified cDNA clone was purchased from GE Healthcare Life Sciences (corresponding ID: MDR-1734-202835311). Primers were designed to fully sequence the purchased cDNA clone, to ensure it was full length and had no sequence variations from the reference. Sequencing data revealed the cDNA clone was full length, but had a number of sequence variants throughout the cDNA clone when aligned to the C13H9orf72 reference sequence (ensembl: ENSDART00000015127.6), as detailed in table 5.1.

**Table 5.1 Sequence variants identified in the C13H9orf72 sequence.**

| Sequence variants locus | Effect of sequence variants |
|---|---|
| *ZGC_100846:c.66 T>G* | Codon change TGT>TGG, resulting in an amino acid change of cysteine to tryptophan. Known missense variant, rs40965738. Position 66, within coding exon 1. Found previously, see section 3.3.1 |
| *ZGC_100846:c.634 T>C* | Codon change TGC>CGC, resulting in an amino acid change of cysteine to arginine. Novel variant. Position 634, within coding exon 4. In a conserved region. |
| *ZGC_100846:c.687 T>G* | Codon change GTT>GTG, synonymous mutation encoding the amino acid valine. Known variant, rs179848938. Position 687, within coding exon 5. |
| *ZGC_100846:c.813 T>C* | Codon change AGT>AGC, synonymous mutation encoding the amino acid serine. Novel variant. Position 813, within coding exon 6. |
| *ZGC_100846:c.916_917del* | Deletion of two base pairs (AC) at position 916-17, within coding exon 6. This polymorphism causes a frameshift, resulting in a premature stop codon within coding exon 6. Translated sequence: MSSACPPQSPAVAKTEVLVDDCCPVLAATFA YWDNILGPRVRHIWAPKSQGLLLLLSDGEVTF LANHTLNGEILRSAESGAVDVKFFVLAEKGV IIVSLIFDGELKGDKNTCALSIILPQSELSFYLP LHAVCVERLKHVIRKGRICMQKGYNIISMLS SEIVPIMELLTSMKKHSVPEEVDLKDTVLND DDIGDSCHEDFLHKAISSHLQTCGCSMVVGS NPEKVNKIVLTLCLFLTPAERKCSRLCHPDG SFKYDTGLFVQGLLKDSTGSFVFPYRQVLY SPYPTTHIDVDINTVKQMPPCHEHVSSAAL HACGAQCPLEGGQRG* |

A novel sequence variant ZGC_100846:c.634 T>C was identified (figure 5.1), resulting in a codon change of TGC>CGC. This resulted in non-synonymous change in the corresponding amino acid sequence, which was located in a conserved region (table 5.1). In order to correct this sequence, we used site directed mutagenesis to change the C>T, see section 2.4.2 for details (figure 5.1).
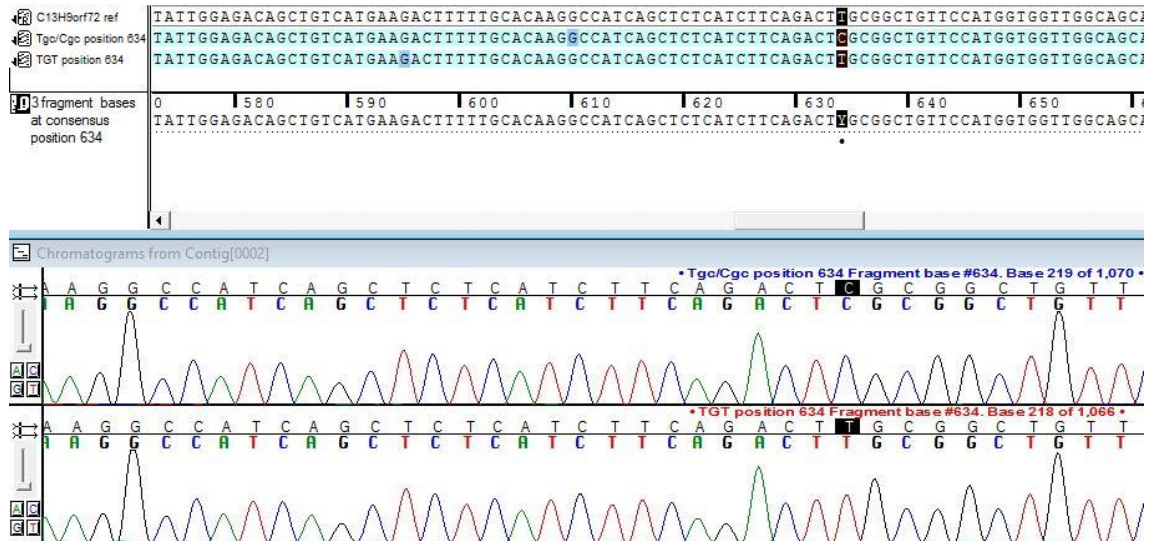


**Figure 5.1 Chromatographs following site-directed mutagenesis on ZGC_100846:c.634 T>C.** Chromatographs, produced by Sequencher v5.4.5, highlight the site variant ZGC_100846:c.634 T>C before site-directed mutagenesis (*Tgc/Cgc position 634*) and after site-directed mutagenesis (*TGT position 634*). Both sequences are aligned to the C13H9orf72 reference sequence from ensembl (*ENSDART00000015127.6*).

Another novel sequence variant ZGC_100846:c.916_917del was identified (figure 5.2), resulting in the deletion of two base pairs (AC) and causing a frameshift. This variant was predicted to result in a premature stop codon in the translated protein sequence (table 5.1 for details). In order to correct this sequence, we used site directed mutagenesis to insert the two base pairs (AC), see section 2.4.2 for details (figure 5.2).



**Figure 5.2 Chromatographs following site-directed mutagenesis on ZGC_100846:c.916_917del.** Chromatographs, produced by Sequencher v5.4.5, highlight the ZGC_100846:c.916_917del before site-directed mutagenesis (*2bp deletion*) and after site-directed mutagenesis (*AC insert position 916-917*). Both sequences are aligned to the C13H9orf72 reference sequence from ensembl (*ENSDART00000015127.6*).

The sequence variant ZGC_100846:c.66 T>G corresponded to a known missense variant, rs40965738 (table 5.1). This variant had previously been identified when sequencing the region surrounding the CRISPR gRNA target site (section 3.1.1) and was revealed to be in a non-conserved area. Additionally, a known sequence variant ZGC_100846:c.687 T>G and a novel sequence variant ZGC_100846:c.813 T>C, were identified. These both resulted in synonymous changes in the corresponding amino acid sequence (table 5.1). The aforementioned sequence variants were therefore not corrected by site-directed mutagenesis, as did not affect the protein sequence.

Following correction by site-directed mutagenesis, the C13H9orf72 cDNA construct was subcloned from pDNR-LIB into the mammalian expression vector pCI-neo-Myc (detailed in section 2.4.3). C13H9orf72 was amplified using PCR, introducing 5' NotI and 3' XhoI restriction sites, and the PCR DNA fragment was sent for sequencing, confirming restriction sites were in-frame. The PCR DNA fragment was subsequently inserted in pCI-neo-Myc vector via complementary restriction digest using NotI/XhoI, followed by ligation and transformation into competent cells. Following screening of single colonies, the cloned plasmid was then isolated from the transformed cells and sequenced.

### 5.3. Investigating whether the function of C9orf72 is conserved in zebrafish
#### 5.3.1. C13H9orf72 interacts with human ATG13

There is 68.55% nucleotide identity and 76.14% amino acid identity between human C9orf72 (hC9orf72) and the zebrafish orthologue (C13H9orf72; zgc: 100846). This high sequence similarity suggests a conservation of C9orf72 protein function between species. hC9orf72 has been reported to play a role in the autophagy pathway (Amick et al. 2016, Sellier et al. 2016, Sullivan et al. 2016a, Webster et al. 2016b, Webster et al. 2016a, Yang et al. 2016). Autophagy is initiated by the ULK-1 complex, consisting of Unc-51-like kinase 1 (ULK-1), FAK family kinase-interacting protein of 200 kDa (FIP200), autophagy-related 13 (ATG13) and ATG101 (Klionsky et al. 2012). Published data from our lab reported that C9orf72 interacts with components of the ULK-1 complex, including ULK-1, ATG13 and FIP200 (Webster et al. 2016a). Overall amino acid identity between human and zebrafish core autophagy proteins range from 40-96%, with zebrafish orthologues of the ULK-1 initiation complex sharing 50-87% amino acid identity with their human counterpart (Mathai et al. 2017). Assuming functional conservation, zebrafish C9orf72 would be expected to also bind and interact with members of the ULK-1 initiation complex. To determine whether C13H9orf72 interacts with the ULK-1 initiation complex, the interaction between C13H9orf72 and human ATG13 (hATG13) was investigated. hATG13 showed a strong interaction with hC9orf72 *in vitro* (Webster et al. 2016a). Furthermore, the high conservation with the zebrafish atg13 orthologue (>70% identity) made hATG13 a promising candidate to study the interaction C13H9orf72 with the autophagy initiation complex.

To investigate whether C13H9orf72 was directly interacting with hATG13, we performed an *in vitro* binding assay (section 2.9.5). Firstly, C13H9orf72 was cloned into the pGEX6p1 vector to allow bacterial expression and recombinant protein production (section 2.4.8). Recombinant GST-tagged C13H9orf72 and hC9orf72 protein, produced in bacteria, was incubated with *in vitro* translated $^{35}$S-labelled hATG13. Following this, GST-tagged C13H9orf72 and hC9orf72, plus a GST control, were pulled down using Glutathione Sepharose High performance (GSH) beads and proteins eluted using excess glutathione. Samples were analysed by SDS-PAGE and $^{35}$S-labelled protein detected using a phosphoimager (figure 5.3 B). It was shown that hATG13 directly interacts with both C13H9orf72 and hC9orf72, but not with the GST control (figure 5.3 B). This data reproduces the interaction between hC9orf72 and hATG13 as previously reported (Webster et al. 2016a). It also shows that C13H9orf72 is capable of interacting with

hATG13, therefore supporting the idea that there is conservation of protein function and that C13H9orf72 likely interacts with zebrafish atg13.
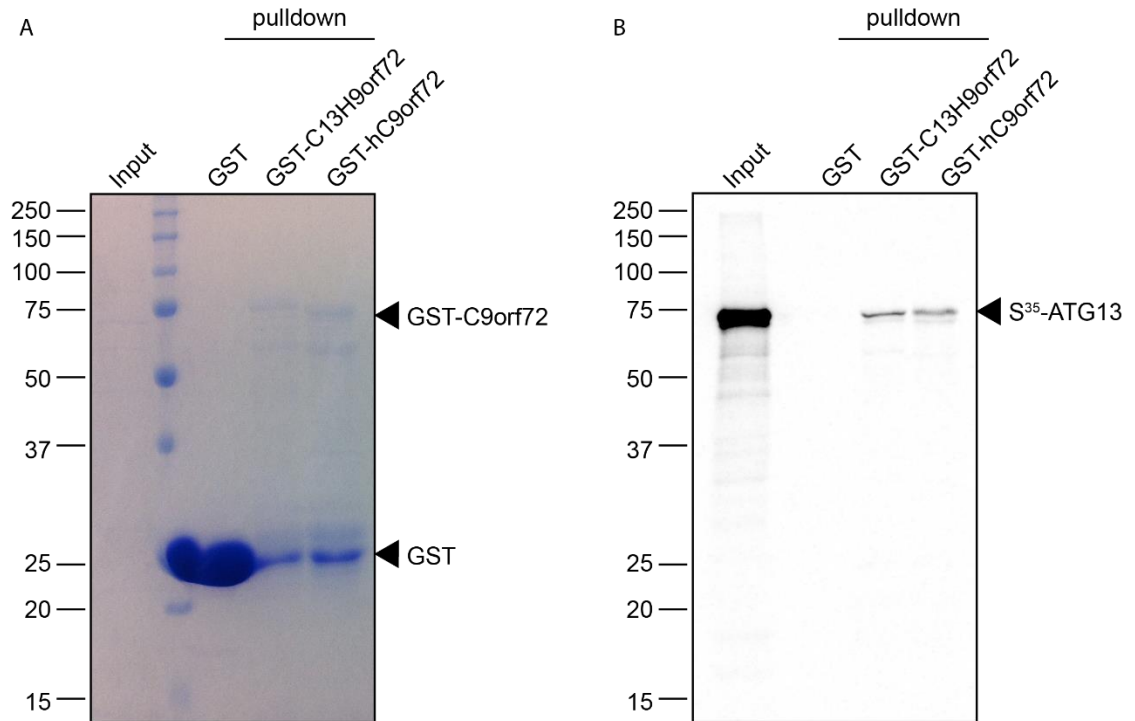


**Figure 5.3 C13H9orf72 directly interacts with hATG13.**[35]S-labelled recombinant ATG13 was added to GST, GST-C13H9orf72 and GST-hC9orf72 immobilized on glutathione-coated beads. Samples were analysed by SDS-PAGE and ^{35}S-labelled detected using a phosphoimager. Coomassie-stained GST, GST-C13H9orf72 and GST-hC9orf72 from the pull-down samples are shown (A). [35]-S labelled ATG13 was visualised using a phosphoimager, showing hATG13 directly interacts with GST-C13H9orf72 and GST-hC9orf72 *in vitro*, but not the GST control (B).

### 5.3.2. Further investigating the role of C13H9orf72 in the autophagy pathway *in vivo*

Publications from our lab and others have shown that hC9orf72 plays a role upstream in autophagy, regulating initiation of the pathway (Webster et al. 2016a, Sellier et al. 2016). As C13H9orf72 binds hATG13, supporting the idea that there is conservation of protein function between C13H9orf72 and hC9orf72, we reasoned that it would also regulate the initiation of autophagy in zebrafish. To investigate this, we utilised two different strategies. Firstly, we aimed to examine autophagic flux in the *C9orf72* LOF zebrafish, as recent studies have shown that depletion of C9orf72 expression, in both cell lines and primary neurons, results in defective autophagy initiation (section 5.3.2.1-5.3.2.2)(Webster et al. 2016a, Sellier et al. 2016). Secondly, we aimed to examine the levels of p62/SQSTM1 in the *C9orf72* LOF zebrafish, as depletion of C9orf72 expression, in cell lines and primary neurons, has also resulted in accumulation of p62/SQSTM1 levels, reflective of the p62/SQSTM1 positive, TDP-43 negative inclusions observed in C9-ALS/FTD patients (section 5.3.2.3)(Webster et al. 2016a, Sellier et al. 2016, Cooper-Knock et al. 2012, Al-Sarraj et al. 2011).

### 5.3.2.1. Examining autophagic flux *in vivo*

The most widely used marker to measure autophagic flux is microtubule-associated protein 1A/1B light chain 3 (LC3). During autophagy, cytosolic LC3-I is lipidated to form LC3-II, which is then recruited to the autophagosome membrane (Klionsky et al. 2012). LC3-II remains associated with the autophagosome until it is eventually degraded downstream within the autophagolysosome. Thus, turnover of LC3-II reflects the progression of autophagy (Klionsky et al. 2016). LC3-II can be visualised as cytoplasmic puncta by immunofluorescence microscopy or by an apparent shift in molecular weight when analysed via SDS-PAGE. The latter method was used in this study and this method has been used to measure levels of autophagy in several zebrafish autophagy studies (He et al. 2009, Benato et al. 2013, Underwood et al. 2010, Renna et al. 2013).

To achieve this, zebrafish embryos were treated with autophagy initiating drugs (such as mTOR inhibitors), autophagy inhibiting drugs (such as lysosomotrophic reagents), or both (table 2.8 and figure 5.4). In the presence of mTOR inhibitors only, biogenesis of autophagosomes is increased which in turn will increase LC3-II levels (Klionsky et al. 2012). However, this increase may not be detectable on immunoblot due to rapid degradation in lysosomes under these conditions. In the presence of lysosomotrophic reagents only, autophagosomes-lysosome fusion is prevented, resulting in an

accumulation of autophagosomes and subsequent stabilisation of LC3-II, as lysosomal degradation is blocked (Klionsky et al. 2012). This results in an increase of LC3-II levels on immunoblot. When embryos are treated with both drug types in combination, specific quantification of autophagy induction can be determined. In wild-type embryos, we would expect a further increase in LC3-II levels on immunoblot, as biogenesis of autophagosomes is increased, but lysosomal degradation is simultaneously blocked. However, if initiation is impaired, for example due to loss of C9orf72 as has been shown previously, we would not expect to see an increase in LC3-II levels under these conditions (Klionsky et al. 2012, Webster et al. 2016a).
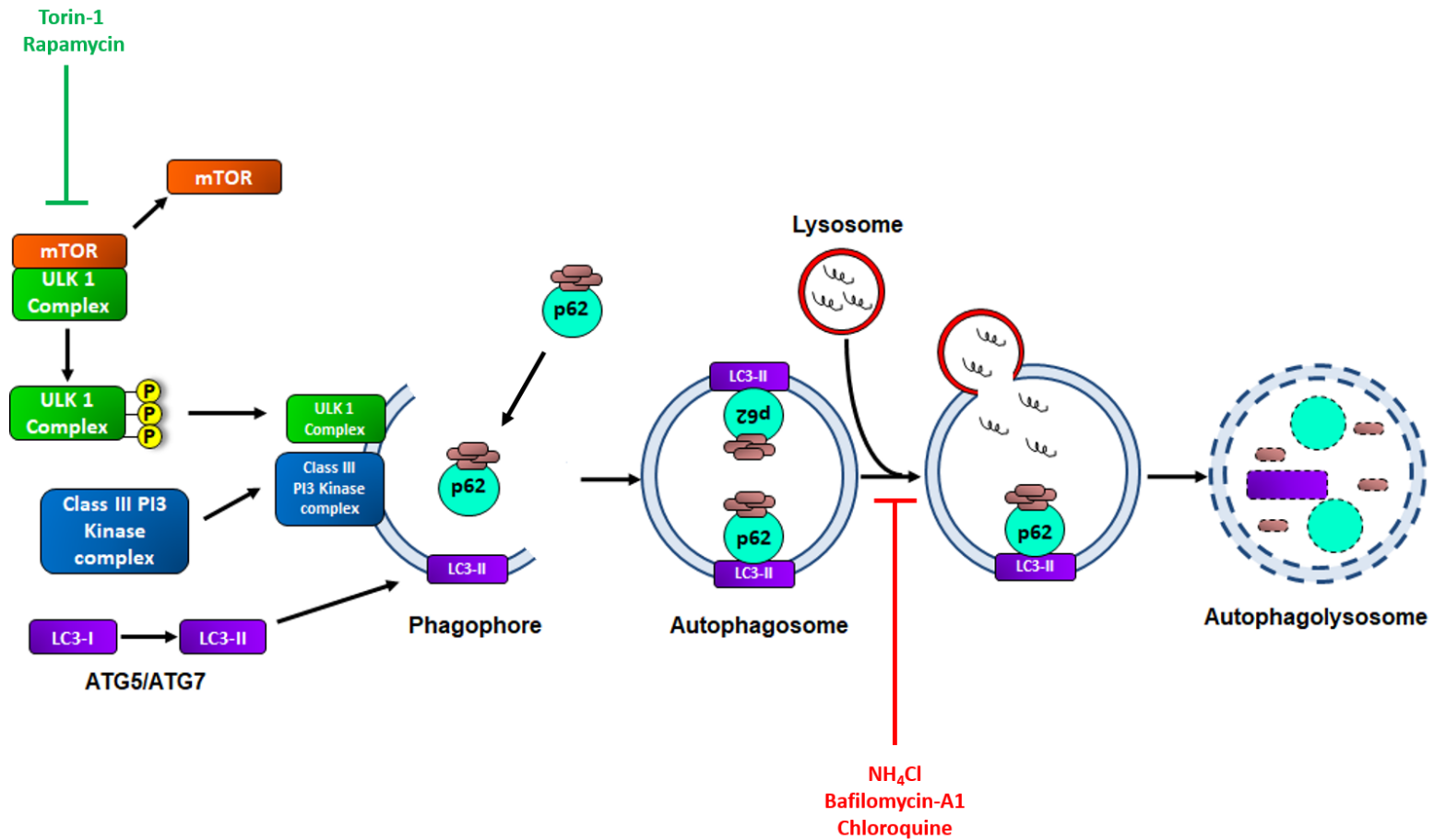
**Figure 5.4 Autophagy initiating and inhibiting drugs.** Schematic overview of the autophagy, as described in figure 1.3, and a non-exhaustive list of reagents that can initiate or inhibit autophagy. mTOR inhibitors, such as torin-1 and rapamycin (shown in green), activate the autophagy pathway. Conversely, lysosomotrophic reagents, such as ammonium chloride ($NH_4Cl$), Bafilomycin-A1 and Chloroquine (shown in red), prevent autophagosome-lysosome fusion. A detailed description of treatments used can be found in table 2.8.

### 5.3.2.1.1. Optimisation of the autophagic flux assay

We first optimised the assay using wild-type AB zebrafish, which is the same wild-type strain used to generate the *C13H9orf72* LOF zebrafish. Initially, to determine whether zebrafish LC3-I and LC3-II could be visualised by immunoblotting, wild-type embryos were incubated for 6-hours at 24 hpf with the following treatments; 2% DMSO (as a control), 1 μM torin-1 (an mTOR inhibitor, figure 5.4), 100 nM bafilomycin-A1 (a lysosomotrophic reagent, figure 5.4) or both 1 μM torin-1 and 100 nM bafilomycin-A1. These treatments have been used previously to show C9orf72 KD results in a disruption of autophagy induction in cells and primary neurons (Webster et al. 2016a). Following incubation, embryos were homogenised and lysed in BRB80 lysis buffer (Webster et al. 2016a) and the total protein concentration of each sample was quantified. Samples were subjected to SDS-PAGE and immunoblot analysis alongside a lysate of HEK-293 cells treated with torin-1 + bafilomycin-A1 (baf-A1), which was used as a control for the LC3 antibody.

For the HEK-293 torin-1 + baf-A1 treated cells, two strong bands were evident around 17 kDa and 14 kDa, which correspond to the expected molecular weight (MW) for LC3-I and LC3-II respectively (figure 5.5). This indicates the antibody can detect endogenous human LC3. The treated embryo samples gave a single band was visible around 14kDa, which is the expected MW for zebrafish LC3-II, but we did not observe a 16kDa band, which is the expected MW of LC3-I (He et al. 2009). Additionally, inhibition of mTOR using torin-1 in the presence of baf-A1 did not result in a marked increase in LC3-II levels compared to baf-A1 alone (figure 5.5). This indicates torin-1 did not efficiently induce autophagy in the zebrafish in this experiment. Overall, these results indicated that using this antibody, we could detect zebrafish LC3-II on immunoblot, but not zebrafish LC3-I.
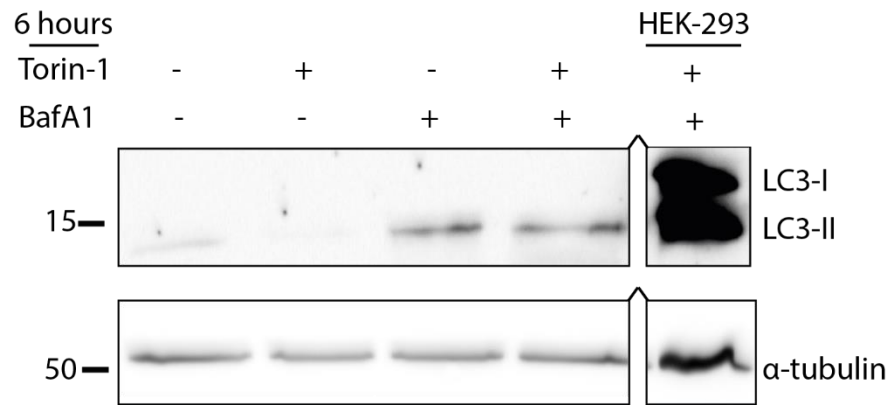
**Figure 5.5 LC3-II is observed in zebrafish lysates.** 24hpf embryos were treated with the indicated chemicals for 6 hours. Protein extracts were analysed by SDS-PAGE and detected using anti-LC3 or anti-α-tubulin as a loading control. Samples were run alongside lysates of HEK-293 cells treated with bafilomycin-A1+ torin-1, acting as a control (n=1).

In an attempt to detect endogenous LC3-I on immunoblot, we optimised several steps in the protocol. Firstly, as homogenisation and lysis of embryos in BRB80 involves sequential steps (section 2.9.3), we reasoned that LC3-I might not be detectable via immunoblot due to loss of protein during this sample preparation process. Therefore, we optimised the protein extraction method. To do this, we compared the original method (method 1) with an alternate lysis protocol which contained less steps and involved the transfer of treated, deyolked embryos straight into laemmli loading buffer (method 2) (figure 5.6). Secondly, although nitrocellulose membrane was used previously (figure 5.5), it is known that Polyvinylidene Difluoride (PVDF) membranes have a higher protein binding capacity than nitrocellulose (Klionsky et al. 2016). Therefore, we reasoned that use of PVDF membrane, may result in a higher retention of LC3-I and allow us to visualise this protein on immunoblot. To investigate this in the same experiment, we also compared the transfer of both LC3-I and –II on nitrocellulose membrane to PVDF.

As before, wild-type zebrafish were incubated for 6-hours at 24 hpf with the following treatments; 2% DMSO, 1 μM torin-1, 100 nM baf-A1 or both 1 μM torin-1 and 100nM baf-A1. Following incubation, protein was extracted as described. Samples were subjected to SDS-PAGE and immunoblot analysis. For all samples, a band was visible around 14kDa, the expected MW for zebrafish LC3-II, but we did not observe a 16kDa band, the expected MW of LC3-I (figure 5.6). This indicated that the method of protein extraction did not impact the ability to visualise endogenous LC3-I on immunoblot, thus the original method of protein extraction was used in future experiments. In comparison to PVDF, transfer of LC3-II appeared weaker on nitrocellulose. Therefore, PVDF membrane was used for transfer in all future experiments. Additionally, treatment with baf-A1 did not markedly increase LC3-II levels compared to torin-1 treatment alone, indicating that baf-A1 did not efficiently block autophagy in the zebrafish in this experiment (figure 5.6). Overall, these results indicate that we can visualise endogenous zebrafish LC3-II on immunoblot, but not LC3-I, consistent with a previous publication (Benato et al. 2013).
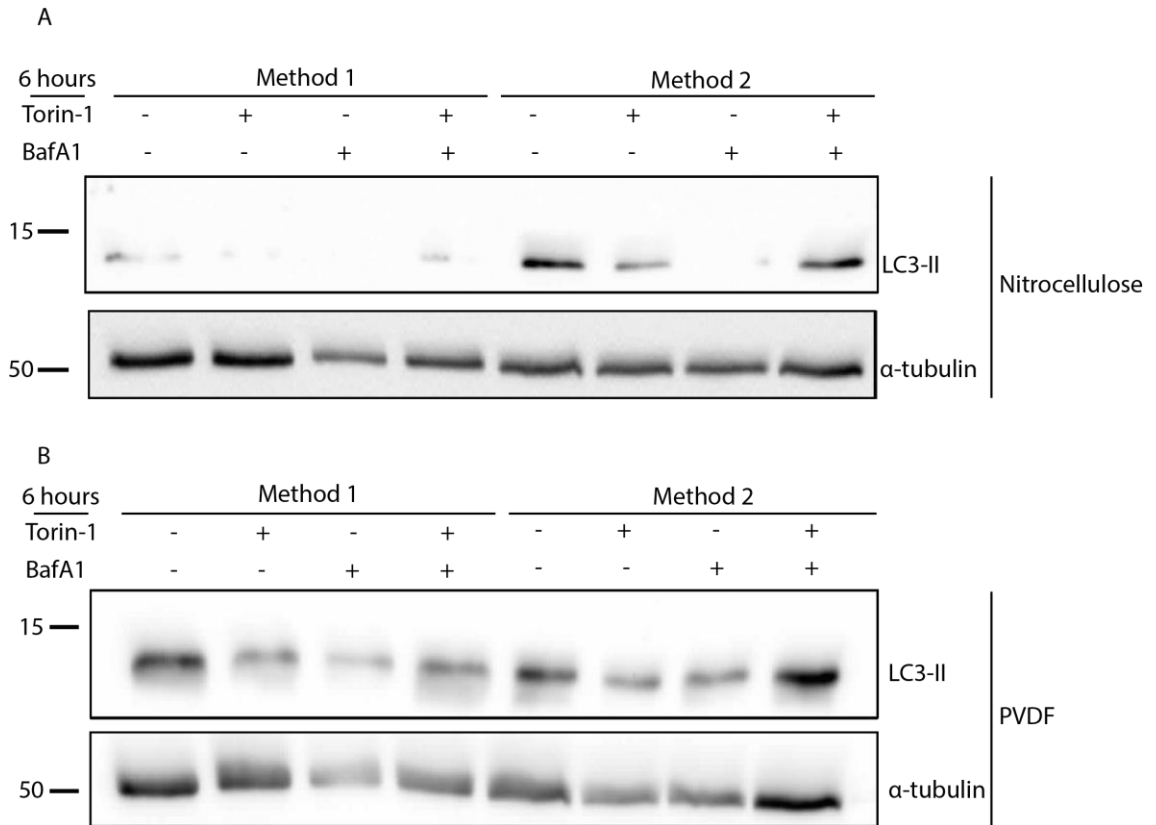
**Figure 5.6 Optimisation of protein extraction and transfer method.** 24hpf embryos were treated with the indicated chemicals for 6 hours. Protein lysates were prepared in two ways. Method 1: embryos from each treatment were homogenised then lysed in BRB80 lysis buffer and the total protein concentration of each sample was quantified. Method 2: Embryos were transferred straight into laemmli buffer. Protein extracts were analysed by SDS-PAGE and transferred onto either A) Nitrocellulose or B) PVDF membrane. Protein was detected using anti-LC3 or anti-α-tubulin as a loading control (n=1).

We found that baf-A1 does not efficiently block autophagy in zebrafish (figure 5.6). Other groups have shown that lysosomotrophic reagents such as ammonium chloride ($NH_4Cl$) and chloroquine, which increase lysosomal pH preventing autophagosome-lysosome fusion like baf-A1, were effective in blocking autophagy in zebrafish at 48hpf (He et al. 2009, Underwood et al. 2010, Renna et al. 2013, Benato et al. 2013). Therefore, in order to confirm optimal lysosomotrophic reagents, wild-type AB zebrafish embryos were treated at 48hpf with either baf-A1, chloroquine or $NH_4Cl$. These treatments were tested with or without the addition of torin-1 and incubated for a total of 24 hours.

Treatment with 100 nM baf-A1 and 50 µM chloroquine for 24 hours resulted in high level of toxicity (data not shown). Treatment with 100 mM $NH_4Cl$ markedly increased LC3-II levels compared to 1µM torin-1 treatment alone, indicating $NH_4Cl$ efficiently blocked autophagy in the zebrafish under these conditions (figure 5.7). However, treatment with torin-1 and $NH_4Cl$ did not markedly increase LC3-II levels compared to $NH_4Cl$ treatment alone, indicating that torin-1 did not efficiently induce autophagy in the zebrafish in this experiment, as shown previously (figure 5.5 and 5.7). Overall, it was concluded that $NH_4Cl$ is the optimal lysosomotrophic reagent to treat embryos at 48 hpf for future experiments.
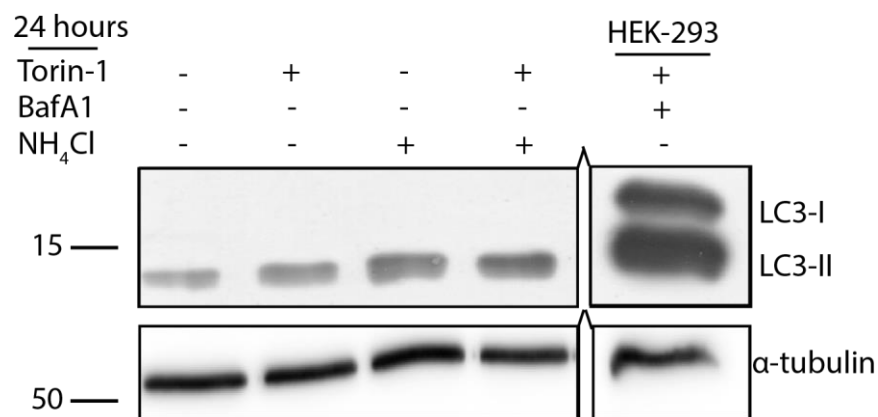


**Figure 5.7 Ammonium chloride treatment results in LC3-II accumulation after a 24-hour incubation.** 2dpf embryos were treated with the indicated chemicals for 24 hours. Embryos were homogenised and lysed in BRB80. Samples were analysed by SDS-PAGE and detected using anti-LC3 or anti-α-tubulin as a loading control. Samples were run alongside lysates of HEK-293 cells treated with bafilomycin-A1+ torin-1, acting as a control. (n=1).

Previously, torin-1 was used as it has been shown to be effective in inducing autophagy in mammalian cells (Klionsky et al. 2016). However, we found that its effect was marginal in zebrafish (figures 5.5 and 5.7). Therefore, as well as optimising the lysosomotrophic reagent used, it was essential to optimise the mTOR inhibitor used. Another mTOR inhibitor, rapamycin, is commonly used to initiate autophagy in zebrafish, therefore this was tested (He et al. 2009). Additionally, a number of rapalogs, which have the same molecular scaffold but different physiochemical properties (Meng and Zheng 2015), were tested alongside. We reasoned that if C13H9orf72 LOF does result in a defect in autophagy initiation, the improved pharmacokinetics of rapalogs would be beneficial to test as a future treatment, if they are shown to initiate autophagy in zebrafish effectively. As well as this, we tested an mTOR-independent autophagy initiating drug, trehalose, as another potential drug treatment.

To confirm the optimal mTOR inhibitor to use, wild-type AB zebrafish embryos were treated at 48hpf with varying concentrations of the treatments detailed in figure 5.8 A-C. These treatments were tested with or without the addition of 100 mM $NH_4Cl$ and incubated for a total of 24 hours. Overall, it was observed that incubation with rapamycin at 250 nM in the presence of $NH_4Cl$ caused a marked increase in LC3-II levels, indicating induction of autophagy (see figure 5.8 A). This effect was also observed for all of the rapalogs (see figure 5.8 A-B), except AZD8055 (see figure 5.8 C). Additionally, incubation with torin-1 or trehalose, in the presence of $NH_4Cl$, did not consistently increase LC3-II levels in comparison to $NH_4Cl$ treatment alone (see figure 5.8 A-C), indicating these treatments do not efficiently induce autophagy in zebrafish. It was decided to further optimise rapamycin concentration for future experiments, as this had previously been used to monitor autophagic flux in zebrafish (He et al. 2009).
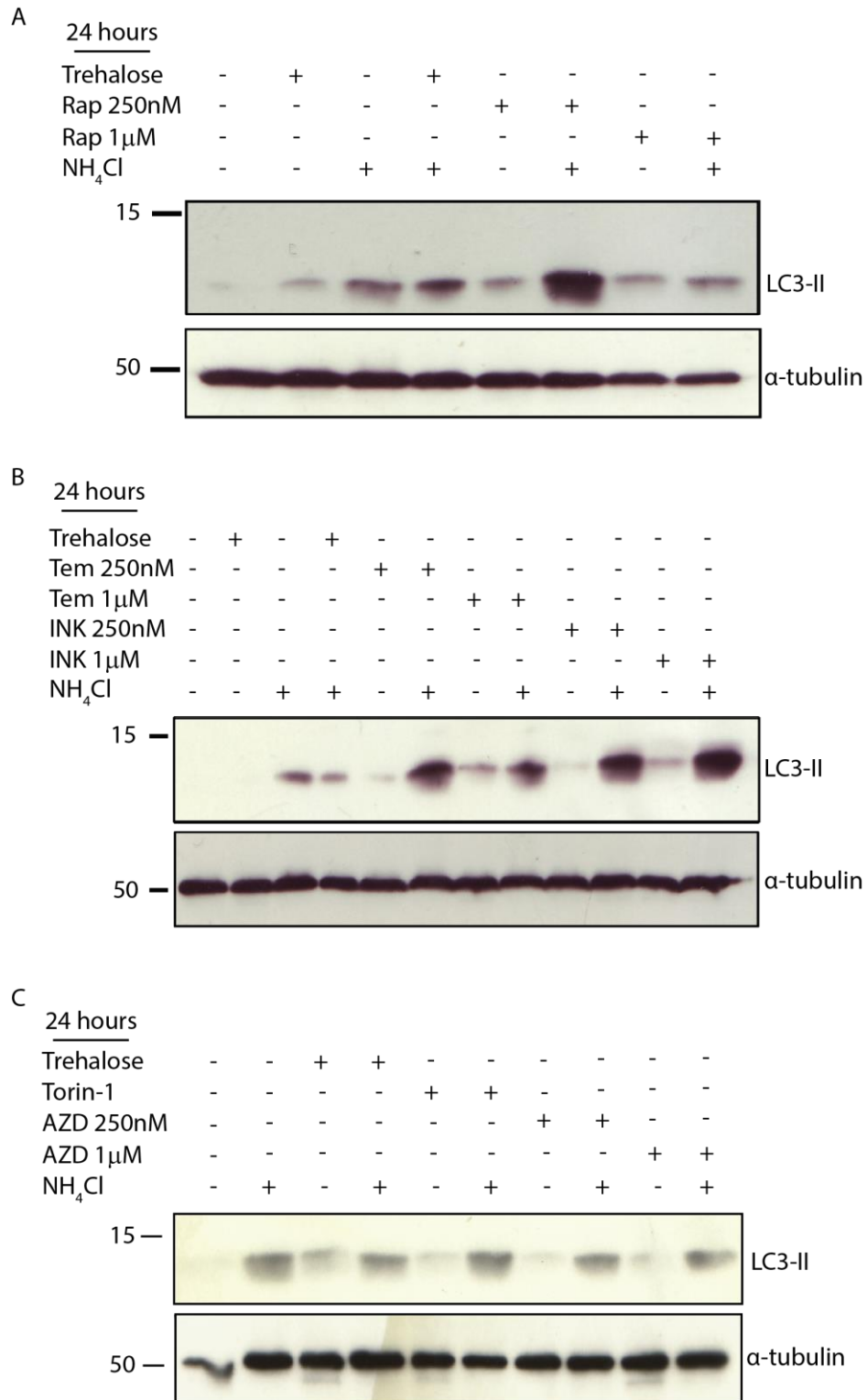
**Figure 5.8 Optimisation of autophagy initiating drug treatments.** LC3-II levels were observed in response to various autophagy initiating compounds, as well as the lysosomal inhibitor treatment NH4Cl. In A, B and C 2dpf embryos were treated with the indicated chemicals in 2% DMSO for 24 hours. Protein extracts were analysed by SDS-PAGE and detected using anti-LC3 or anti-α-tubulin as a loading control. NH4Cl: Ammonium Chloride; Rap: Rapamycin; Tem: Temsirolimus; INK: INK128; AZD: AZD8055. (n=1).

As rapamycin was shown to efficiently induce autophagy, we further optimised the concentration of rapamycin to use in future experiments. To achieve this, wild-type AB zebrafish were incubated for 24-hours at 48 hpf with the following treatments; 2% DMSO, 100 nM or 500 nM rapamycin, 100mM NH4Cl or both. Overall it was observed that incubation with rapamycin at 100 nM, but not 500 nM, in the presence of NH4Cl caused a marked increase in LC3-II levels, indicating induction of autophagy (see figure 5.9 A-B). As efficient autophagy induction was observed following incubation with 100 nM rapamycin, this concentration was used for future experiments.
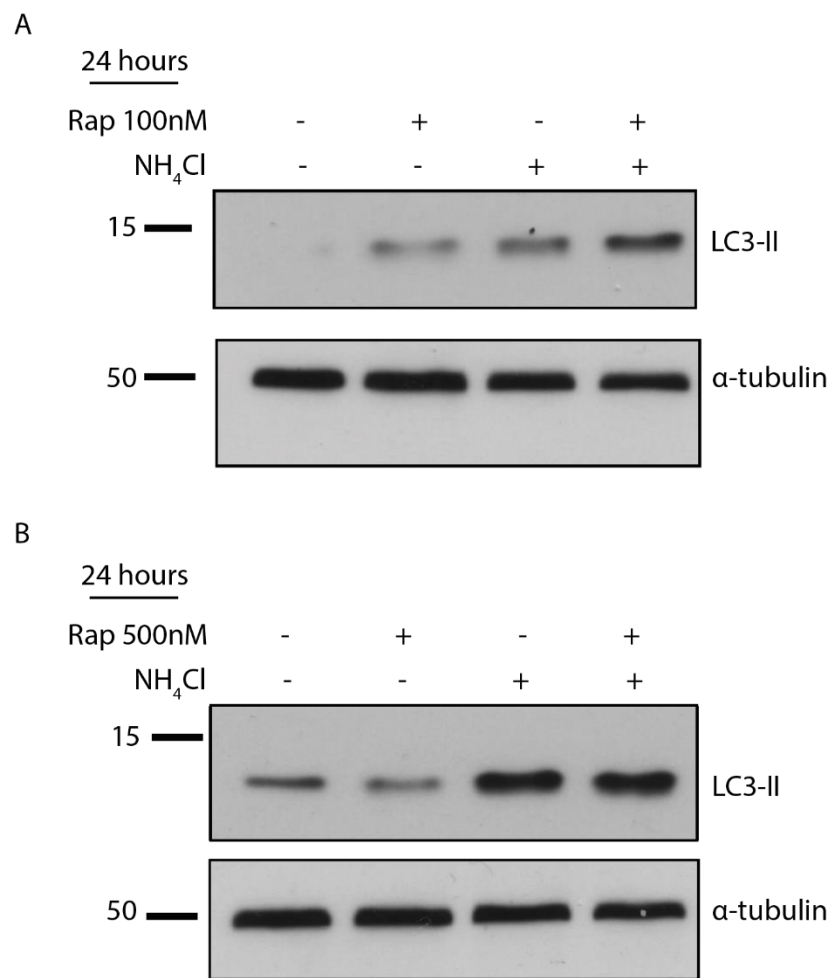


**Figure 5.9 Optimisation of rapamycin treatment.** 2dpf embryos were treated with A) DMSO, 100nM Rapamycin, 100mM NH4Cl or both and B) DMSO, 500nM Rapamycin, 100mM NH4Cl or both, for 24 hours. Embryos were homogenised and lysed in BRB80. Samples were analysed by SDS-PAGE and detected using anti-LC3 or anti-α-tubulin as a loading control. (n=1).

### 5.3.2.1.2. Examining autophagic flux in *C13H9orf72* loss-of-function mutants

To investigate the effect of loss of C13H9orf72 expression on autophagy, optimised autophagic flux assays were performed on *C13H9orf72* LOF mutants and wild-type controls. Autophagic flux experiments were only performed on lines SH448 and SH451, which carry frameshift mutations in exon 7, as these were generated first and embryos were available. If zebrafish C9orf72 encodes both protein isoforms as predicted, this means that we can only observe the effect of loss of C9orf72-L on autophagy function in these lines.

### 5.3.2.1.2.1. Examining autophagic flux in C13H9orf72$^{SH451/SH451}$ mutants

To investigate the effect of loss of C13H9orf72 expression on autophagy initiation in zebrafish, we performed the autophagic flux assay on *C13H9orf72*$^{SH451/SH451}$ embryos and wild-type controls. In 48 hpf wild-type embryos, inhibition of mTOR with 100 nM rapamycin in the presence of 100 mM NH$_4$Cl resulted in a non-significant increase in LC3-II levels, compared to 100 mM NH$_4$Cl treatment alone, indicating induction of autophagy (Figure 5.10 A-B). The same effect was also seen in 48hpf *C13H9orf72*$^{SH451/SH451}$ embryos, indicating that mTOR-dependent autophagy induction is not impaired in *C13H9orf72*$^{SH451/SH451}$ embryos under these conditions (Figure 5.10 A-B).

Interestingly, others have reported that C9orf72 depletion results in an increase, not decrease, of basal LC3-II levels, which could be a result of increased autophagic flux or accumulation of autophagosomes due to a defect in lysosome function (Farg et al. 2014, O'Rourke et al. 2016). Therefore, we quantified basal levels of LC3-II in 2% DMSO treated *C13H9orf72*$^{+/+}$ and *C13H9orf72*$^{SH451/SH451}$ embryos from previous autophagic flux assays. As seen in figure 5.10 C, there was a non-significant increase in basal LC3-II in *C13H9orf72*$^{SH451/SH451}$ embryos in comparison to wild-type controls (Figure 5.10 C).
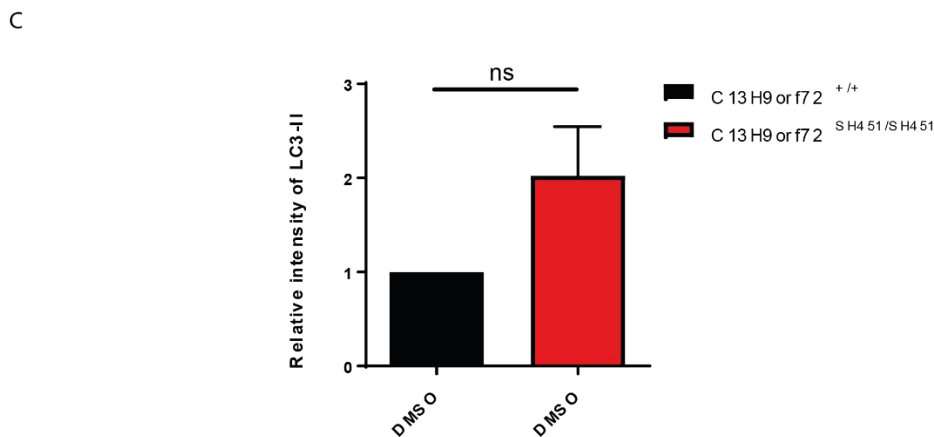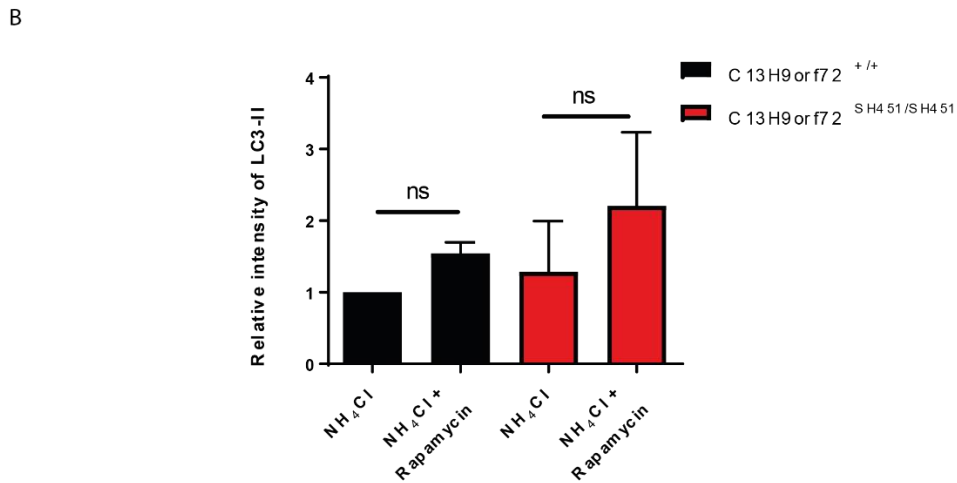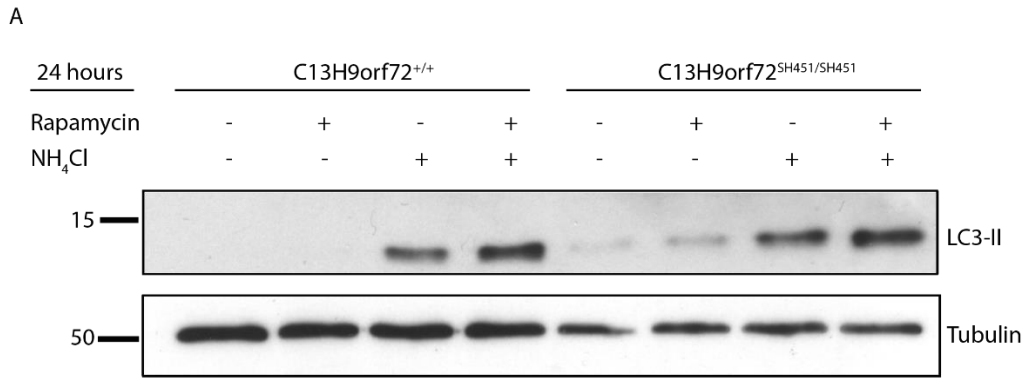
**Figure 5.10 Examining autophagy in C13H9orf72SH451/SH451 zebrafish.** A) 2dpf embryos were treated with the indicated chemicals for 24 hours. Protein extracts were analysed by SDS-PAGE and detected using anti-LC3 and anti-α-tubulin as a loading control. B) Relative levels of LC3-II quantified using ImageJ software. Levels of LC3-II were normalised against α-tubulin and are shown relative to the $NH_4Cl$ treated control sample, which is set to 1.0 (mean ± SEM; one-way ANOVA with fisher's LSD test; ns, not significant, n=3). C) Indicates levels of LC3-II in zebrafish treated with DMSO (2%) only. LC3-II levels were normalised against α-tubulin loading control and are shown relative to the DMSO treated control sample, which is set to 1.0 (mean ± SEM, unpaired t-test, ns = non-significant, n=8).

### 5.3.2.1.2.2. Examining autophagic flux in C13H9orf72$^{SH448/SH448}$ mutants

We investigated the effect of loss of C13H9orf72 expression on autophagy initiation in *C13H9orf72$^{SH448/SH448}$* embryos and wild-type controls, to understand whether the results reported for line SH451 were line specific or observed in other C13H9orf72 LOF mutants. In 48 hpf *C13H9orf72$^{+/+}$* zebrafish embryos, inhibition of mTOR with 100 nM rapamycin in the presence of 100 mM NH$_4$Cl resulted in a non-significant increase in LC3-II levels, compared to 100 mM NH$_4$Cl treatment alone (figure 5.11 A-B), consistent with induction of autophagy. The same effect was also seen in 48 hpf *C13H9orf72$^{SH448/SH4448}$* embryos (figure 5.11 A-B). Again, this indicates that autophagy induction is not impaired in *C13H9orf72$^{SH448/SH448}$* embryos under these conditions, as seen in the *C13H9orf72$^{SH451/SH451}$* embryos (section 5.3.2.1.2.1).

Due to reports that C9orf72 depletion results in an increase, not decrease, of basal LC3-II levels (Farg et al. 2014, O'Rourke et al. 2016), we quantified basal levels of LC3-II in DMSO treated *C13H9orf72$^{+/+}$* and *C13H9orf72$^{SH448/SH448}$* embryos from previous autophagic flux assays. As seen in figure 5.11 C, there was no significant difference between basal LC3-II in *C13H9orf72$^{SH448/SH448}$* embryos in comparison to wild-type controls.

A



B



C
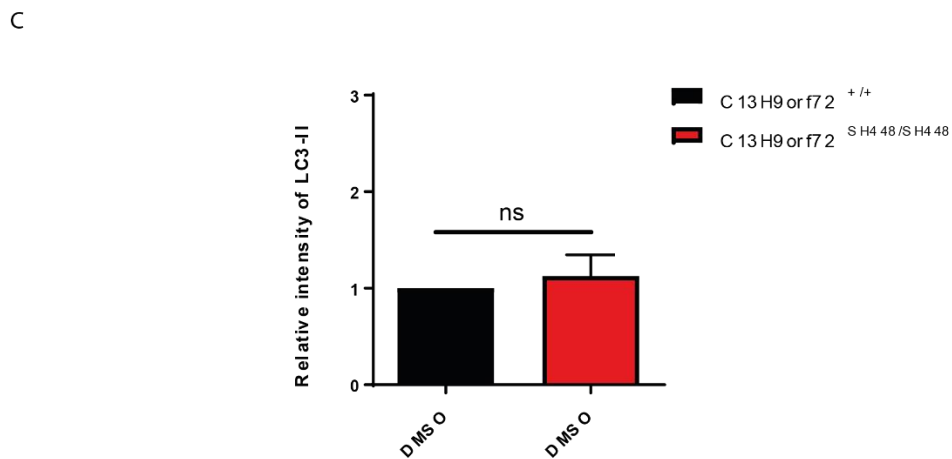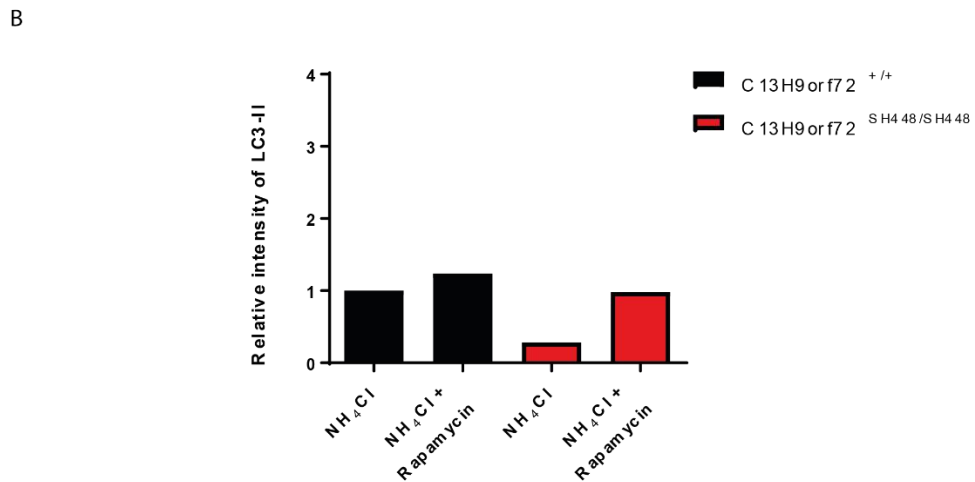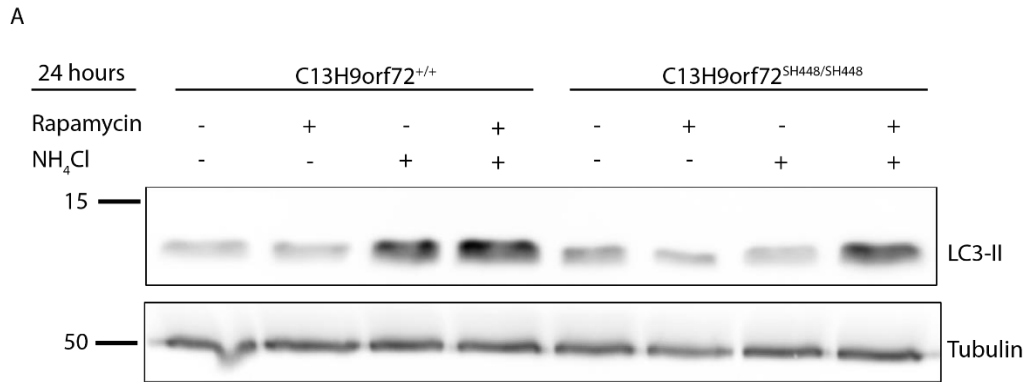


**Figure 5.11 Examining autophagy in C13H9orf72<sup>SH448/SH448</sup> zebrafish.** A) 2dpf embryos were treated with the indicated chemicals for 24 hours. Protein extracts were analysed by SDS-PAGE and detected using anti-LC3 and anti-α-tubulin as a loading control. B) Relative levels of LC3-II quantified using ImageJ software. Levels of LC3-II were normalised against α-tubulin and are shown relative to the NH$_4$Cl treated control sample, which is set to 1 (n=3). C) Indicates levels of LC3-II in zebrafish treated with DMSO (2%) only. LC3-II levels were normalised against α-tubulin loading control and are shown relative to the DMSO treated control sample, which is set to 1.0 (mean ± SEM, unpaired t-test, ns = non-significant, n=3).

### 5.3.2.2.    Investigating p62/SQSTM1 protein levels *in vivo*

A characteristic phenotype of C9-ALS/FTD patients is the presence of p62/SQSTM1 positive, TDP-43 negative inclusions (Cooper-Knock et al. 2012, Al-Sarraj et al. 2011). p62/SQSTM1 is important for targeting ubiquitinated proteins to the autophagy pathway for degradation and accumulation of this protein has been associated with inhibition of autophagy (Hara et al. 2006). There is evidence from our lab that disruption of C9orf72 function in cell lines and primary neurons, results in accumulation of p62/SQSTM1(Webster et al. 2016a). Therefore, we reasoned that if C13H9orf72 is involved in the regulation of autophagy in zebrafish, loss of C13H9orf72 expression would also result in defective autophagy and accumulation of autophagy substrates such as p62/SQSTM1. However, based on the LC3 results discussed in the previous section, we expected that we would not see a difference in p62/SQSTM1 levels between wild-type and *C9orf72* LOF zebrafish.

In order to see whether we could detect endogenous p62/SQSTM1 protein levels by western blot, a commercially available antibody was optimised (see table 2.9). A previous report performing western blots on zebrafish embryo lysates has demonstrated a clear band at 50kDa for the endogenous wild-type p62/SQSTM1 protein using this antibody (Mostowy et al. 2013). Initially, we homogenised and lysed wild-type AB zebrafish embryos at 2dpf in BRB80 lysis buffer and the total protein concentration of each sample was quantified. Samples were subject to SDS-PAGE and western blot analysis. Although a band was observed at 50kDa (see figure 5.12) as previously reported, there were many non-specific bands which were not present in the previous publication, therefore it was unclear which band was specific to the protein of interest.
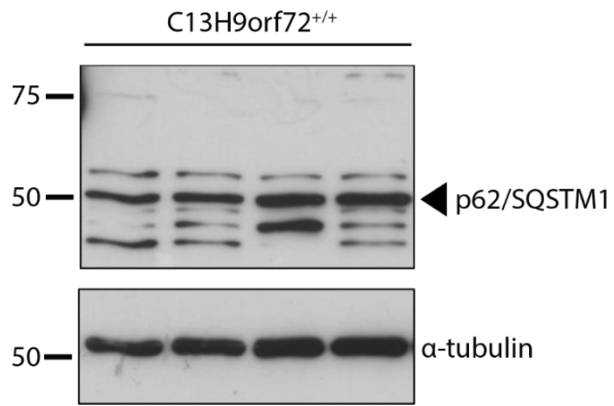
**Figure 5.12 Examining p62/SQSTM1 protein levels in wild-type zebrafish.** Protein was extracted from 2dpf wild-type AB. Protein extracts were analysed by SDS-PAGE and detected using anti-p62/SQSTM1 or anti-α-tubulin as a loading control.

To establish which of these bands was specific to p62/SQSTM1, we utilised three p62/SQSTM1 deletion zebrafish lines that were generated in our laboratory. These lines carry nonsense mutations in the final exon of p62/SQSTM1 and are predicted to truncate the C-terminus of the p62/SQSTM1 protein, resulting in the deletion of the UBA domain, which binds to ubiquitinated proteins (Seibenhener et al. 2004). The heads of three 21 dpf wild-type, heterozygous carriers and homozygous mutants from each of these lines were homogenised and lysed in RIPA buffer and the total protein concentration of each sample was quantified (see section 2.9.2 and 2.9.3). Samples were subject to SDS-PAGE and western blot analysis. It was expected that the mutant protein would either not be visible on immunoblot if the truncated protein is not expressed, or, if the truncated protein is expressed, produce bands at a lower MW, as detailed in table 5.2.

**Table 5.2 Summary of wild-type and mutant p62/SQSTM1 protein length.**

| Line | Detail of deletion | Predicted protein length | Predicted molecular weight (kDa) |
|------|--------------------|--------------------------|----------------------------------|
| Wild-type | N/A | 452aa | 49.21 |
| A | ZGC_85784:c.1211_1221del | 420aa | 45.63 |
| C | ZGC_85784:c.1211_1216del | 417aa | 45.19 |
| D | ZGC_85784:c.1212_1216del | 422aa | 45.98 |

As before, immunoblotting revealed a band at approximately 50kDa for all samples, which is the same MW that has been published for wild-type endogenous p62/SQSTM1 (Figure 5.13 A-C). However, again there were several non-specific bands (Figure 5.13). None of the bands showed altered size or intensity in p62/SQSTM1 C-terminal deletion zebrafish, suggesting that the antibody did not detect endogenous zebrafish p62/SQSTM1. Therefore, we were unable to determine which bands represented wild-type or mutant p62/SQSTM1 protein with this antibody.
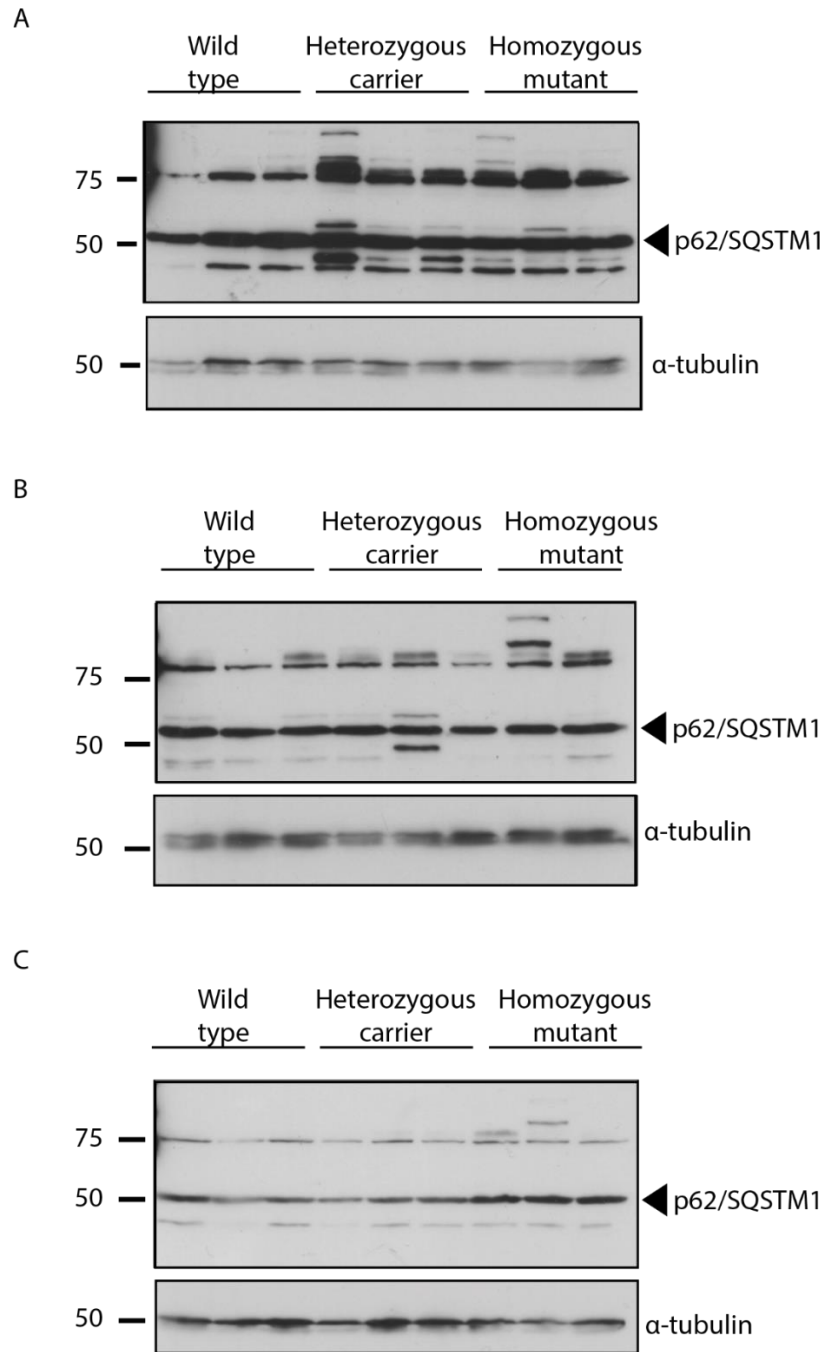
**Figure 5.13 Examining p62/SQSTM1 protein levels in p62/SQSTM1 loss-of-function zebrafish.** Protein was extracted from heads of 21dpf zebrafish from the following lines A) Line A, B) Line C, C) Line D. Protein extracts were analysed by SDS-PAGE and detected using anti-p62/SQSTM1 or anti-α-tubulin as a loading control.

### 5.4. Investigating the link between *C9orf72* LOF and splenomegaly

Complete or partial loss of the mouse orthologue of *C9orf72* (3110043021Rik) has not been reported to result in neurodegeneration in mice, but has been linked to defects in the immune system (O'Rourke et al. 2016, Sudria-Lopez et al. 2016, Koppers et al. 2015, Atanasio et al. 2016). In C9orf72 knockout (KO) mice, splenomegaly, enlargement of the spleen, was evident as early as at 1 month of age (Atanasio et al. 2016, O'Rourke et al. 2016, Sudria-Lopez et al. 2016). Additionally, disrupted tissue structure and infiltration of immune cells such as macrophages in splenic tissue were reported (Sudria-Lopez et al. 2016, O'Rourke et al. 2016, Atanasio et al. 2016). Therefore, we reasoned that similar changes might be detected in the *C13H9orf72* LOF zebrafish.

### 5.4.1. Investigating splenomegaly in *C13H9orf72*<sup>SH448/SH448</sup> adult zebrafish

Spleens were dissected from *C13H9orf72*<sup>SH448/SH448</sup> adult zebrafish and their wild-type siblings at 24 months (Figure 5.14 A). To estimate the size of the spleens, we imaged dissected spleens by light microscopy and the area of the spleen was subsequently calculated. *C13H9orf72* LOF spleens were larger than wild-type siblings by 35%, but this was not significant, given the small sample size (figure 5.14 B).
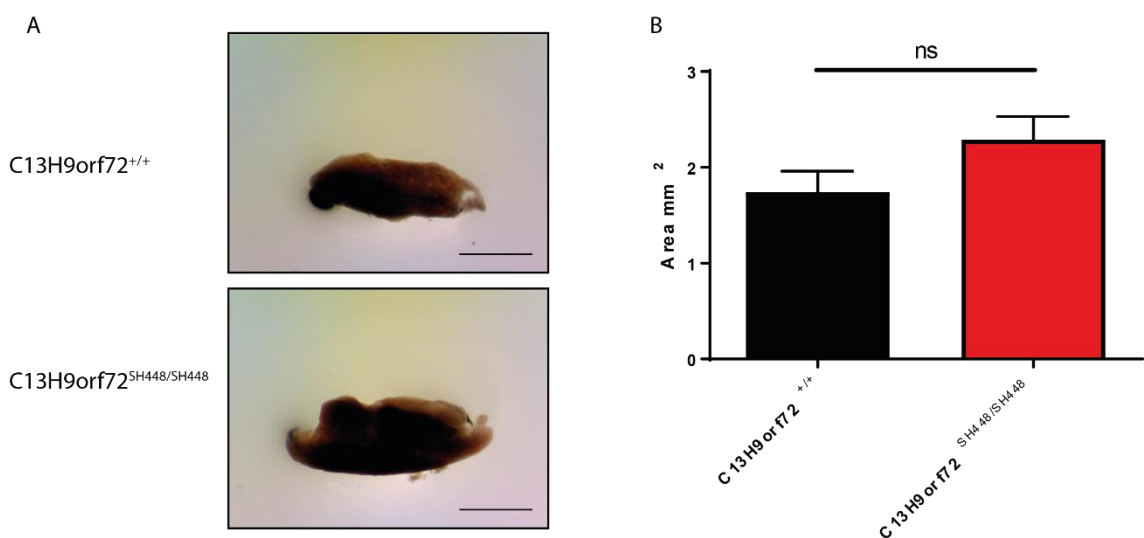


**Figure 5.14 C13H9orf72<sup>SH448/SH448</sup> zebrafish show no signs of splenomegaly.** Images of spleens from 24-month old C13H9orf72<sup>SH448/SH448</sup> zebrafish and their wild-type siblings. Scale bar = 1.0 mm B) Quantification of spleen surface area ($mm^2$), was carried out using ImageJ following dissection of the spleens (n=4 C13H9orf72<sup>+/+</sup> and n=3 C13H9orf72<sup>SH448/SH448</sup>). Mean ± SEM, unpaired t-test, ns = non-significant.

## 5.5. Discussion

There is evidence that *C9orf72* LOF via haploinsufficiency may be a pathogenic mechanism in C9-ALS/FTD. In order to fully understand how haploinsufficiency of *C9orf72* may result in disease, it is essential to unravel the protein functions of C9orf72. There is high conservation between human *C9orf72* and the zebrafish orthologue, *C13H9orf72*, which indicates there may be functional conservation. This project focuses mainly on exploring the role of C13H9orf72 in autophagy, as reports from our laboratory and from others have shown that C9orf72 is involved in this process (Sellier et al. 2016, Sullivan et al. 2016a, Webster et al. 2016a, Farg et al. 2014, Yang et al. 2016, Ugolino et al. 2016). Additionally, due to reports that loss of the mouse orthologue of *C9orf72* (3110043021Rik) results in defects in the immune system *in vivo*, resulting in symptoms such as splenomegaly, we examined whether this was present in the *C13H9orf72* LOF zebrafish (O'Rourke et al. 2016, Sudria-Lopez et al. 2016, Atanasio et al. 2016, Koppers et al. 2015).

### 5.5.1. Generation of the pCI-neo-Myc-C13H9orf72 construct

We successfully generated a pCI-neo-Myc-C13H9orf72 construct, to allow for examination of C13H9orf72 function *in vitro* (section 5.2). To achieve this, the C13H9orf72 cDNA reference sequence (ensembl: ENSDART00000015127.6) was BLAST searched against the NCBI EST database, identifying a full length cDNA clone FDR306-p00004_BR_K14 which was subsequently purchased from GE Healthcare Life Sciences. ESTs are short sub-sequences of transcripts, important for evaluating gene expression, annotating genes and identifying potential variation (Lindlof 2003). A limitation to using the NCBI EST database to identify a full length cDNA clone, is that the way that ESTs are produced means that they are often of low quality and have a high error rate (Lindlof 2003). For example, ESTs are sequenced only once, and are not verified. This means that they can contain a number of unidentified errors, which can result in site variations. These errors may come from the original mRNA sequence or from the experimental procedure itself (Lindlof 2003). Therefore, it was essential to sequence the clone we identified to ensure that any site variation would not affect the overall protein sequence, as this may result in aberrant functions and we wanted to identify a wild-type C13H9orf72 construct to examine normal function. It was identified that the cDNA clone FDR306-p00004_BR_K14 contained a number of variants that would potentially affect protein function (table 5.1). These were successfully reverted back to the reference sequence using site-directed mutagenesis (figure 5.1 and 5.2).

### 5.5.2. Investigating the role of C13H9orf72 in autophagy *in vivo*

Autophagy is a conserved lysosomal degradation pathway which involves the degradation of cytoplasmic components, such as misfolded proteins and damaged organelles, within an autophagolysosome, for bulk degradation or recycling (Klionsky et al. 2012). The process consists of several sequential steps, including: the sequestration of cytoplasmic components, transport of these to lysosomes, degradation via lysosomal hydrolases and utilization of the degradation products. A characteristic phenotype of C9-ALS/FTD is the presence of p62/SQSTM1 positive, TDP-43 negative inclusions found in the cerebellum, hippocampus and the neocortex (Cooper-Knock et al. 2012, Al-Sarraj et al. 2011). Accumulation of p62/SQSTM1 has been shown to occur when autophagy is blocked, therefore suggesting that C9orf72 may function in autophagy (Hara et al. 2006). In this project we further investigated the role of C9orf72 *in vivo*, using the *C13H9orf72* LOF zebrafish generated. Proteins involved in autophagy in zebrafish are highly conserved with their human counterparts, with amino acid identity ranging from 40-96% (Mathai et al. 2017). The similarity between autophagy components alongside the advantages of this vertebrate model system, as previously discussed, has led to several assays being established in order to examine this pathway in zebrafish, some of which have been used in this project as described below.

### 5.5.2.1. C13H9orf72 interacts with human ATG13

Autophagy is activated by the ULK-1 complex, which consists of ULK-1, FIP200, ATG13 and ATG101. This complex is kept inactive via the phosphorylation of ULK-1 by mTOR. Inactivation of mTOR, for example in nutrient poor conditions, results in the release of the ULK-1 initiation complex. ULK-1 is then able to phosphorylate FIP200 and ATG13, activating the complex and initiating autophagy (Jung et al. 2009, Ganley et al. 2009). Various reports have suggested C9orf72 interacts with the ULK-1 initiation complex. Overexpression of C9orf72 has been reported to activate autophagy (Webster et al. 2016a). However, when the ULK-1 complex was disrupted, via depletion of the component FIP200, overexpression of C9orf72 no longer activated the pathway, indicating that C9orf72 functions at the level of the ULK-1 complex (Webster et al. 2016a). Strengthening this association, it was reported that C9orf72 directly interacts with ULK-1, FIP200 and ATG13 via co-immunoprecipitation, proximity ligation assay (PLA) and *in vitro* binding assays (Webster et al. 2016a). This data agrees with a previous report that C9orf72 interacts with FIP200 (Behrends et al. 2010). Additionally, it has also been

reported that C9orf72, in complex with SMCR8 and WDR41, interacts with the ULK-1 initiation complex (Sullivan et al. 2016b).

If C9orf72 is functionally conserved in zebrafish and humans, then we predict that zebrafish C9orf72 will interact with the ULK-1 initiation complex. To test this, we chose human ATG13. This member of the ULK-1 initiation complex was chosen first, due to its strong interaction with human C9orf72 *in vitro* (Webster et al. 2016a). Additionally, human ATG13 shares >70% identity with the zebrafish orthologue (ensembl: ENSDARG00000036040). As shown via an *in vitro* binding assay in section 5.3.1, zebrafish C9orf72 interacts with human ATG13. As there is an interaction between these two proteins, it supports the idea that there is functional conservation between zebrafish and human C9orf72. It would be of interest in the future to investigate whether zebrafish C9orf72 interacts with the other members of the ULK-1 initiation complex *in vitro*, such as ULK-1 and FIP200, as it has been shown in humans (Webster et al. 2016a). Human ULK1 and FIP200 both share >60% identity with the corresponding zebrafish orthologues. Thus, as with ATG13, it is predicted that these proteins should interact due to high conservation. In addition to the initiation complex, there are reports that C9orf72 forms a complex alongside SMCR8 and WDR41 (Sullivan et al. 2016a, Sellier et al. 2016, Amick et al. 2016, Yang et al. 2016). Therefore, it would also be interesting to see whether zebrafish C9orf72 interacts with these proteins as well.

Due to time constraints, we were unable to investigate whether there is a direct interaction between zebrafish C9orf72 and zebrafish ATG13, which is a limitation to this study. We have previously identified a potential full length cDNA clone of zebrafish ATG13 via a BLAST search of the zebrafish ATG13 reference sequence against the NCBI expressed sequence tag (EST), as we have done previously for C13H9orf72 (section 5.2). By obtaining a full length zebrafish ATG13 cDNA clone, we would have the potential to look at its interaction with zebrafish C9orf72 using several assays including co-immunoprecipitation, proximal ligation assay and an *in vitro* binding assay.

### 5.5.2.2.    Understanding the role of C13H9orf72 in autophagy *in vivo*

As well as interacting with components of the ULK-1 initiation complex, as stated above, it has been reported that there is a dysfunction in autophagy induction when C9orf72 expression is depleted in cell lines, primary neurons and *in vivo* (Webster et al. 2016a, Sellier et al. 2016, Sullivan et al. 2016a). This indicates that the protein may regulate the function of the ULK-1 initiation complex. Further analysis from our lab has shown that

depletion of C9orf72 in cell lines prevented the translocation of the ULK-1 initiation complex to the phagophore, which is essential for the formation of the autophagosome (Webster et al. 2016a). As we showed that C13H9orf72 binds hATG13, further supporting the idea that there is conservation of protein function between C13H9orf72 and hC9orf72, we investigated whether C13H9orf72 regulated the initiation of autophagy, as has been reported with hC9orf72 previously (Webster et al. 2016a). This was initially examined via an autophagic flux assay, using LC3-II levels as a readout. Several studies have used zebrafish embryos to monitor LC3-II levels in this way via immunoblotting using commercially available anti-LC3 antibodies (He et al. 2009, He and Klionsky 2010, Underwood et al. 2010, Renna et al. 2013, Benato et al. 2013). However, there is still not a standardised procedure for this experiment in zebrafish. Therefore, it was essential to optimise several conditions in wild-type zebrafish before performing it in the *C13H9orf72* LOF mutants.

Several conditions were optimised for the autophagic flux assay during the project. Firstly, it was established that incubation of embryos in multiple autophagy inducers and blockers was optimal at 48 hpf (see section 5.3.2). We initially found that LC3-II protein levels were very low when treated at 24 hpf and were difficult to observe via immunoblot (Figure 5.5). This agrees with a previous report which stated that although transcripts of autophagy genes such as LC3 are present at 0 hpf, others such as ULK1 are not expressed until around 23 hpf (He et al. 2009). Thus, they report that LC3-II is only detectable via western blot analysis at around 32 hpf onwards (He et al. 2009). However, in contrast to this report we show evidence of LC3-II at around 30 hpf (Figure 5.5), as these 24 hpf embryos were treated for 6 hours although it is clear that expression of LC3-II was higher at the later time points (Figure 5.7). Other groups have also reported treating embryos at 48 hpf when performing autophagic flux assays, which suggests this is a suitable minimum age to study autophagic flux in zebrafish (He et al. 2009, Benato et al. 2013, Underwood et al. 2010, Renna et al. 2013). Secondly, we optimised treatments over a 24-hour incubation time. It was identified that rapamycin and $NH_4Cl$ were most effective in inducing or blocking autophagy, respectively. These treatments have also been used by other groups (He et al. 2009, Underwood et al. 2010). As shown in Figure 5.8, we incubated 48 hpf zebrafish embryos in a variety of autophagy inducing drugs. If there is a link between defective autophagy and the causation of C9-ALS/FTD, this class of drug could be a potential therapy to investigate in the future using zebrafish. It has been

previously reported that daily intake of 2% (w/v) trehalose significantly reduced levels of mutant SOD1 and p62, as well as increased LC3-II levels in the spinal cords of SOD1-G93A mice in early-stage ALS (Li et al. 2015). Additionally, trehalose treatment postponed disease onset and preserved motor function at this stage (Li et al. 2015). Although trehalose did not efficiently induce autophagy in zebrafish (Figure 5.8) many of the different rapalogs tested did. For example, Temsirolimus treatment showed a marked increase in LC3-II levels in combination with $NH_4Cl$, in comparison to $NH_4Cl$ treatment alone (figure 5.8). As this drug is water soluble, its therapeutic potential in C9-ALS/FTD could easily be tested in larval and/or adult zebrafish. Additionally, use of rapalogs such as Temsirolimus could also be translatable to C9-ALS/FTD patients as it is FDA-approved. Finally, transfer of LC3-II protein onto PVDF membrane was optimal over nitrocellulose (see figure 5.6). Although it has been reported that nitrocellulose has a higher affinity for LC3-I, we were unable to visualise LC3-I when transferred onto either membrane (Mathai et al. 2017). However, it has been suggested that using PVDF may result in higher retention of LC3-II, because it has a higher affinity for hydrophobic proteins (Klionsky et al. 2012).

It was consistently reported during this project that LC3-I, the cytosolic form of LC3, was not observed via immunoblot. This phenomenon is something that has been reported by another group (Benato et al. 2013). LC3-I may be less sensitive to detection by some anti-LC3 antibodies in comparison to LC3-II (Klionsky et al. 2012). We did test a different anti-LC3 antibody, which had been published to show immunoreactivity for both LC3-I and LC3-II in zebrafish (He et al. 2009). However, no LC3 was observed for any sample when this was used (data not shown). Despite this, we are confident that the band we are observing is LC3-II, as the protein responds in the way that we would expect to the autophagy inducing and blocking treatments, as shown in section 5.3.2. The fact that LC3-II responds in the expected way to multiple mTOR inhibitors, further supports conservation of mTOR-dependent autophagy induction in zebrafish, which has been previously reported (Makky, Tekiela and Mayer 2007).

The optimised autophagic flux assay was performed on *C13H9orf72* LOF zebrafish and wild-type controls from lines SH448 and SH451, which carry frameshift mutations in exon 7, as these were generated first and embryos were available. If zebrafish C9orf72 encodes both protein isoforms as predicted, this means that we can only observe the effect of loss of C9orf72-L on autophagy function in these lines. These lines were used to

investigate the effect of loss of C13H9orf72 expression on autophagy, and primarily to observe whether the dysfunction in autophagy induction previously reported (Webster et al. 2016a, Sellier et al. 2016, Sullivan et al. 2016a) recapitulated in our model. We performed the autophagic flux assay in two lines to establish that any effect seen was not line specific. We did not observe that loss of C13H9orf72 expression resulted in a defect in autophagy. This is surprising, as it is clear from results in this project that C13H9orf72 does interact with members of the ULK-1 initiation complex, suggesting conservation of protein function between C13H9orf72 and hC9orf72. Interestingly, there are an increasing number of studies reporting an increase, not a decrease, in LC3-II levels in response to reduced C9orf72 expression (Farg et al. 2014, O'Rourke et al. 2016). This increase in basal LC3-II levels could be a result of increased autophagic flux or defective clearance of autophagosomes via the lysosome. Therefore, we investigated basal LC3-II levels in our zebrafish, but no statistically significant difference was observed between genotypes in two mutant lines. However, a major limitation to this analysis was that in most of the immunoblots analysed, LC3-II was below the level of detection in DMSO treated wild-types embryos, which therefore limited the analysis of control samples (Figure 5.10).

Overall, disparity in results between our *C13H9orf72* LOF zebrafish and functional analysis completed in cell culture could be because C13H9orf72 is not ubiquitously expressed in zebrafish, with expression of *C13H9orf72* mRNA reported in a subset of tissues, including regions of the CNS, such as the forebrain, midbrain, hindbrain and spinal cord (Ciura et al. 2013). Therefore, the effect of loss of C13H9orf72 expression on autophagy may be harder to observe via immunoblotting, as we are using the whole fish embryo in comparison to a homogenous population of cells, as used previously (Webster et al. 2016a). In the future, we could extend our *in vivo* study of autophagy into live embryos via injecting mCherry-LC3-EGFP into wild-type and *C13H9orf72* mutant zebrafish embryos to avoid the limitations experienced via immunoblot (Pankiv et al. 2007). The fusion of acid-sensitive GFP and acid-insensitive mCherry to LC3 results in a pH-sensitive sensor to measure autophagy in live cells. This will allow us to probe delivery of autophagy substrates to the lysosome, as we will be able to distinguish autophagosomes (red and green fluorescence) from the acidic autolysosomes (red fluorescence only) in individual cells (Pankiv et al. 2007). Utilising this technique would allow us to detect cell-specific defects, which is not possible using the western blot-based

approach taken in this project. Additionally, there could be a compensatory mechanism *in vivo* which activates autophagy in an mTOR-independent manner, protecting the zebrafish from a defect in the autophagy pathway caused by loss of C13H9orf72 expression. As well as this, the difference in conservation between zebrafish C13H9orf72 and human C9orf72 may explain why we do not see a defect in autophagy. However, we reported C13H9orf72 binds hATG13, supporting the idea that there is conservation of protein function between C13H9orf72 and hC9orf72, which does not support this theory.

### 5.5.2.3. Examining p62/SQSTM1 protein levels in zebrafish

C9-ALS/FTD patients harbour pathognomonic p62/SQSTM1 positive, TDP-43 negative inclusions in several brain regions (Cooper-Knock et al. 2012, Al-Sarraj et al. 2011). p62/SQSTM1 targets ubiquitinated proteins to the autophagy pathway for degradation within the autophagolysosome (Pankiv et al. 2007). The p62/SQSTM1 protein remains bound to its cargo and is eventually degraded within the autophagolysosome. Thus, an impairment either upstream at the initiation complex, or downstream at the lysosome, would prevent its degradation resulting in accumulation of p62/SQSTM1. In support of this theory, it has been shown that blocking autophagy, for example in FIP200$^{-/-}$ MEFs, lead to p62 accumulation (Hara et al. 2008). Additionally, there is published evidence from our laboratory and others that depletion of C9orf72 expression in cell lines and/or primary neurons, results in accumulation of p62/SQSTM1 (Webster et al. 2016a, Sellier et al. 2016).

We reasoned that if C13H9orf72 was involved in the regulation of autophagy in zebrafish, loss of C13H9orf72 expression would also result in defective autophagy and accumulation of p62/SQSTM1, as has been shown in mammalian cells (Webster et al. 2016a, Sellier et al. 2016). In order to see whether we could detect endogenous p62/SQSTM1 protein levels by western blot, a commercially available antibody was used (see table 2.9), which was previously reported to show a specific band at 50kDa for the endogenous wild-type p62/SQSTM1 protein in zebrafish embryo lysates (Mostowy et al. 2013). However, we found that although a band was observed at 50 kDa, there were many non-specific bands that were not present in the previous publication. Therefore, we cannot be certain that the band at 50 kDa is specific for endogenous p62/SQSTM1.

In the future, alternative antibodies need to be tested. Several publications have shown alternative antibodies that are immunoreactive for p62/SQSTM1, but due to time constraints we were unable to test these during this project (Zhang et al. 2017, Zhu et al.

2017, Buhler et al. 2016). Additionally, as the p62/SQSTM1 antibody used was polyclonal, it may be better to use a monoclonal antibody specific for this protein to decrease background and cross-reactivity in the future, which may have confounded results in this study. As well as testing alternative anti-p62/SQSTM1 antibodies to detect protein levels on immunoblot, it would be interesting to use these to examine p62/SQSTM1 positive, TDP-43 negative pathology in the brains of zebrafish. This would be useful as it may be that accumulation of p62/SQSTM1 protein is not detectable on immunoblot, as levels overall do not increase, but rather mislocalise. However, it may be that we do not see such pathology, as we do not report a defect in autophagy in the *C13H9orf72* LOF zebrafish and none of the C9orf72 LOF mice have reported evidence of these characteristic inclusions.

### 5.5.3. Investigating whether *C13H9orf72* loss-of-function results in splenomegaly

It has been reported that when the mouse orthologue of *C9orf72* (3110043021Rik) is either completely or partially lost, there is no evidence of neurodegeneration in the mice, but there is evidence of defects in the immune system (O'Rourke et al. 2016, Sudria-Lopez et al. 2016, Koppers et al. 2015, Atanasio et al. 2016, Burberry et al. 2016). In particular, a major phenotype reported in these mice is splenomegaly, which may be caused by neoplastic events or immune dysregulation (O'Rourke et al. 2016, Atanasio et al. 2016, Sudria-Lopez et al. 2016, Burberry et al. 2016). Several groups have reported large infiltrations of immune cells, such as macrophages, in multiple organs including the spleen (O'Rourke et al. 2016, Atanasio et al. 2016, Sudria-Lopez et al. 2016). This suggests defects in the immune system cause this phenotype. Interestingly, autophagy plays a role in both innate and adaptive immunity (Deretic, Saitoh and Akira 2013). Several studies have now revealed the importance of C9orf72 function in autophagy, thus suggesting the immune phenotypes observed in these mice may be a result of compromised autophagy due to loss of C9orf72 expression. Supporting this, ULK-1 knockout mice also exhibit splenomegaly as seen in the *C9orf72* KO mice (Honda et al. 2014).

We decided to investigate whether the *C13H9orf72* LOF zebrafish harboured defects in the immune system, in particular splenomegaly. As discussed in section 5.4, there was a trend that *C13H9orf72* LOF zebrafish spleens were larger compared to wild-types, but this was not significant. A limiting factor to this analysis is that we could only analyse

four wild type and three mutant spleens. In the future, we would need to analyse more spleens to see if there is a true difference in size. Retrospective power calculation were performed using G*Power Version 3.0.10, based on the spleen areas obtained from SH448 mutants and wild-type siblings analysed during this project. This indicated a sample of 11 spleens per group would provide 80% power to detect a 20% increase in spleen size (student's t-test, two-tailed, $\alpha = 0.05$, $\beta = 0.8$). Another issue with this quantification is that size was measured from a 2-D image. Although measuring area in this way is often used for organelles such as mitochondria, which are also 3-D, it would be beneficial to measure the 3-D area of the spleens in the future, so that sizes can be more accurately compared. Additionally, due to the small size of the spleens in general, it was impossible to weigh them accurately as has been done in the mouse papers (O'Rourke et al. 2016, Burberry et al. 2016). Despite the limitations discussed, in contrast to the mouse models, there was no significant difference in spleen size in the *C13H9orf72* LOF zebrafish. In some cases, homozygote spleens were reported to be two-times bigger than the wild-type controls (O'Rourke et al. 2016, Atanasio et al. 2016). As well as this, others have reported an increase in spleen size from as early as one month (O'Rourke et al. 2016). The fact that even at the late time points examined in the present study revealed no significant difference in size or tissue structure, may indicate splenomegaly is not present.

Additionally, although the immune system in zebrafish and other teleosts is physiologically similar to higher vertebrates like mice, there are some differences. For example, teleosts do not have lymph nodes and *C9orf72* LOF mice reportedly exhibit lymphadenopathy, enlarged lymph nodes, as well as splenomegaly (Uribe et al. 2011, O'Rourke et al. 2016, Atanasio et al. 2016, Sudria-Lopez et al. 2016). It has also been reported in the *C9orf72* LOF mouse model that *Trem2* expression is significantly upregulated in spleen tissue, but zebrafish do not harbour an orthologue for this gene (O'Rourke et al. 2016). Thus, despite the similarities, these differences may be why we do not see symptoms such as splenomegaly in the *C13H9orf72* LOF zebrafish. Further work will need to be done to understand whether these zebrafish have a defective immune response. For example, we could section the spleen tissue and perform Haemotoxylin and Eosin (H&E) staining. This has been done for the *C9orf72* LOF mice and has shown disrupted tissue structure (Atanasio et al. 2016, O'Rourke et al. 2016). Additionally, we could look at the levels of macrophages in the zebrafish spleen, as two groups found

evidence of an increase in macrophage number in the spleens of *C9orf72* LOF mice (Atanasio et al. 2016, O'Rourke et al. 2016)**.** Also, we could examine the expression levels of inflammatory cytokines found in zebrafish, such as IL-1β, IL-6 and IL-10, which have been reported to be upregulated in *C9orf72* LOF mouse models splenic tissue (O'Rourke et al. 2016).

### 5.5.4. Conclusion

We have shown that C13H9orf72 interacts with hATG13, as has been demonstrated previously with the human orthologue. In spite of this, using western blot analysis no defect in autophagy induction was observed in the *C13H9orf72* LOF zebrafish. In addition, no significant difference in the basal levels of autophagy substrates such as LC3-II were observed between *C13H9orf72* LOF zebrafish and wild-type controls. There is also no clear evidence of splenomegaly in these zebrafish, contradictory to recent reports in *C9orf72* LOF rodent models. Overall, we have generated an important tool to be able to further study the function of C9orf72 *in vivo*, which is essential to both further understanding disease processes and identifying novel targets for future therapies.

# 6. Discussion and future work

This project aimed to test the hypothesis that loss-of-function (LOF) mutations in *C9orf72* contribute to ALS/FTD by disruption of the autophagy pathway. In order to achieve this, we generated stable zebrafish *C13H9orf72* LOF models using targeted genome editing techniques (chapter 3) and subsequently characterised them in adulthood to determine whether loss of *C13H9orf72* resulted in any ALS/FTD-like phenotypes, such as changes in survival, motor function or behaviour (chapter 4). Additionally, we investigated the function of the C13H9orf72 protein *in vivo*, with a focus on autophagy (chapter 5).

## 6.1. Animal Models of ALS
### 6.1.1. Mouse

Developing *in vivo* models of ALS is essential in order to further elucidate the pathomechanisms underlying this disorder and aid in evaluating the potential efficacy of novel therapies. Mutations in SOD1 were discovered to cause ALS twenty years ago (Rosen et al. 1993) and this subsequently led to the development of the first transgenic animal model of ALS, the SOD1-G93A mouse (Gurney et al. 1994). In particular, mutant SOD1 transgenic mouse models have been successful in recapitulating characteristic phenotypes of ALS and thus have been used extensively to study the disorder. Unfortunately, translation of findings from these models into the clinic has largely been unsuccessful, with repeated failure of phase 2 and 3 clinical trials based on such studies (Turner et al. 2013). Possible explanations for this failure may be that some mouse lines express high levels of mutant protein, which are not reflective of the human disease state, and that mice are highly inbred, which may in turn affect the disease phenotype. Another major limitation is poor study design, including determining dosing, timing of treatments, number of patients included and the overall selection of patients. For example, the success rate of these clinical trials may significantly increase if they were restricted to patients with SOD1 mutations only. However, this in itself is challenging, as only 2% of ALS patients harbour mutations in SOD1. In addition, the genetic and clinical heterogeneity of ALS may be a key factor. For example, it has been reported TDP-43 positive inclusions are characteristic of around 80-90% of ALS cases (Neumann et al. 2006) but these are not found in SOD1- and FUS-linked ALS, indicating the possibility of distinct pathomechanisms. This shared pathology between the majority of ALS patients resulted in a surge of TDP-43 transgenic rodent models in recent years, as creating a model which had TDP-43 pathology had a high translational potential in comparison to previous SOD1 models. Despite variation in the design of these models, they share common phenotypes

including ubiquitin accumulation, TDP-43 fragmentation, astrogliosis, neuronal loss, defects in motor function and shortened lifespans (Gendron and Petrucelli 2011, Philips and Rothstein 2015). However, none of the TDP-43 models so far develop full blown ALS-disease symptoms as seen in humans. In addition to TDP-43, several mouse models have been developed to understand how a noncoding $(G_4C_2)_n$ hexanucleotide repeat expansion in *C9orf72* results in ALS. As the most prevalent ALS-causing gene identified to date, such models also have a high translational potential. To date, it has been reported that *C9orf72* LOF mouse models do not show signs of neurodegeneration, but show evidence of immune dysregulation (table 6.1). Additionally, *C9orf72* gain-of-function (GOF) mouse models have reported contradictory results, with some models showing no signs of neurodegeneration (O'Rourke et al. 2015, Peters et al. 2015a) and others which do (Chew et al. 2015). As well as *SOD1, TARDBP* and *C9orf72*, multiple other genes have also been identified in rare fALS cases, but mouse models have only been generated for some of these, including *FUS* (Hicks et al. 2000, Mitchell et al. 2013, Sephton et al. 2014), *Ubiquillin-2* (Gorrie et al. 2014, Ceballos-Diaz et al. 2015) and *Optineurin* (Gleason et al. 2011). Generating multiple genetic models is important, as amalgamation of data from several genetically heterogeneous models could produce more powerful results than those obtained from a single model alone. Overall, despite their positives attributes, many of the mouse models that exist so far have a number of pitfalls, including only modelling certain aspects of disease, developing non-ALS/FTD phenotypes and/or lack of translation from lab to clinic. For now, the SOD1 mutant mice are still the only models that develop a phenotype reminiscent of human ALS.

### 6.1.2. Zebrafish

Although rodents remain to be the gold standard for ALS model organisms, they are expensive to maintain and it is time consuming to generate the multiple genetic models that are necessary to study this heterogeneous disease. However, this could be achieved effectively in zebrafish, as they hold several characteristics which make it an advantageous model to use in the study of neurodegenerative disorders such as ALS, due to their reduced cost and ability to produce hundreds of eggs at weekly intervals. In addition, all of the ALS-causing genes are conserved in the zebrafish genome and these genes can be easily manipulated by LOF or GOF approaches in simple, transient assays of gene function and by creation of stable disease models using targeted genome editing techniques. Regarding stable genetic models, several previous reports have exhibited the

effectiveness of using zebrafish models of ALS to investigate the pathogenesis underlying the disorder. Transgenic zebrafish overexpressing mutant sod1 have been reported to display several hallmarks of ALS pathology, including: loss of motor neurons, muscle atrophy, defective motor performance, loss of neuromuscular connectivity and premature death (Ramesh et al. 2010, Sakowski et al. 2012, McGown et al. 2013). Two other studies have demonstrated that stable loss of *tardbp* is fully compensated by alternative splicing of a second *tardbp* orthologue, *tardbpl,* contradictory to previous knockdown studies of this gene in zebrafish (Hewamadduma et al. 2013, Schmid et al. 2013). Additionally, they report that double-homozygous null mutants of *tardbp* and *tardbpl* resulted in muscle degeneration, impaired spinal motor neuron outgrowth and decreased survival (Hewamadduma et al. 2013, Schmid et al. 2013).

As well as their ability to recapitulate phenotypes reminiscent of ALS in humans, due to their small size, the zebrafish is recognised as a powerful model organism amenable to high-throughput drug screening *in vivo* at embryonic and larval stages. The potential of zebrafish as a model system for drug screening for neurodegeneration has been reported, using a SOD1 transgenic zebrafish line (McGown et al. 2013). A neuronal-stress reporter line has previously been utilised to validate the effectiveness of riluzole (McGown et al. 2013). Additionally, this line has been used to develop a high-throughput screening assay, ZNStress, screening over 2000 compounds to identify modulators of neuronal stress (McGown, Shaw and Ramesh 2016). Interestingly, many of the compounds that emerged from murine preclinical studies and failed to show efficacy in human ALS clinical trials also showed no efficacy in the ZNStress assay (McGown et al. 2016). In general, it is important to acknowledge that despite similarities, no model organism can reproduce and accurately model all aspects of human neurodegenerative diseases, including zebrafish. However, the aforementioned studies indicate that zebrafish models of ALS can be used to complement existing rodent models, particularly by revealing novel therapies targets ready for validation in more complex, but low-throughput, mouse models.

### 6.2. Zebrafish models of C9-ALS/FTD

A noncoding $(G_4C_2)_n$ hexanucleotide repeat expansion in *C9orf72* is the most common cause of ALS/FTD, however it is not fully understood how this causes disease. Three pathomechanisms have gained particular attention, including; haploinsufficiency, RNA toxicity and repeat-associated, non-ATG (RAN) translation. It is likely that these pathomechanisms are not mutually exclusive and act in combination. A zebrafish model

recapitulating C9-ALS/FTD would aid in elucidating the unknown function of this novel gene and evidence gathered from such models have the potential to influence future treatments for the largest proportion of ALS patients. Both LOF and GOF models of C9-ALS/FTD have previously been generated in zebrafish. Regarding LOF mechanisms, a group generated a genetic model of *C9orf72* haploinsufficiency via transient knockdown (KD) of *C13H9orf72* transcripts in zebrafish using antisense morpholino oligonucleotides (AMOs), which resulted in disrupted aborisation and shortening of the motor neuron axons, as well as an impaired touch-evoked escape response (Ciura et al. 2013). Regarding GOF mechanisms, RNA injections of 8x, 38x and 72x $G_4C_2$ repeats has previously been reported to result in RNA foci and cell death by apoptosis in zebrafish at 24 hpf, in a repeat length-dependent manner, although no C9-ALS/FTD-like motor or behavioural phenotypes were reported (Lee et al. 2013). Additionally, another group reported generation of two transgenic lines expressing $(G_4C_2)_{80}$ repeats and two lines with the translation initiation codon ATG in front of the $(G_4C_2)_{80}$ repeat sequence, driving expression of poly-GA (Ohki et al. 2017). The transgenic zebrafish with $(G_4C_2)_{80}$ repeats were reported to have key pathological features of ALS/FTD, such as RNA foci, but no RAN translation was detectable and they only showed minor toxicity (mild pericardial oedema) (Ohki et al. 2017). However, toxicity was greatly increased following expression of poly-GA, resulting in severe pericardial oedema, circulatory defects and decreased survival (Ohki et al. 2017).

The focus of this thesis was to study whether LOF mutations in *C9orf72* contribute to ALS/FTD. In order to investigate this, methods leading to both transient and stable loss of C9orf72 can be utilised. A transient KD of both isoforms of *C13H9orf72* using AMOs in zebrafish embryos has already been published (Ciura et al. 2013). However, we successfully generated stable *C13H9orf72* LOF zebrafish using two different targeted genome editing techniques; TALENs to target exon 7 and CRISPR/Cas9 to target exon 1. Generation of these stable models was essential for several reasons. Firstly, there is currently no publication characterising a stable C13H9orf72 LOF zebrafish, thus the generation and subsequent characterisation of our zebrafish is novel and essential for the C9-ALS/FTD field. Secondly, AMOs are only transient and as ALS is mainly an adult onset disorder, the generation of a stable model allowed us to study the long term phenotypic effects of loss of C13H9orf72 expression. Finally, off-target effects can confound AMO-mediated knockdown studies. For example, KD of *Tardbp* orthologue in

zebrafish using AMOs was reported to cause shorter, disorganised motor neuron axons (Kabashi et al. 2010b). However, two independent studies demonstrated that stable loss of *Tardbp* was fully compensated by alternative splicing of a second *Tardbp* orthologue in the zebrafish, *Tardbpl*, thus the *Tardbp* KD-induced phenotype was not observed in these stable *Tardbp* mutants, suggesting the AMO produced off-target effects (Schmid et al. 2013, Hewamadduma et al. 2013). As the same group published the KD of *C13H9orf72* in zebrafish using AMOs, it was essential to generate a stable C13H9orf72 LOF zebrafish to determine whether these phenotypes were real. It is important not to disregard these off-target issues, as it may result in others unintentionally classifying these side effects as genuine phenotypes, which will not aid advancement of the field. In the future, methods such as CRISPRi, which involve co-expressing a catalytically inactive Cas9 protein (dCas9) along with a customizable gRNA, may be used as an alternative to AMOs (Larson et al. 2013). This method has demonstrated specific silencing of genes by blocking transcription (via interfering with transcriptional elongation, RNA polymerase binding or transcription factor binding), without off-target effects (Larson et al. 2013). In addition, multiple gRNAs can be used, silencing multiple genes simultaneously (Larson et al. 2013). This technique is reversible, has high specificity and has been used successfully in model organisms such as the zebrafish (Long et al. 2015).

As well as the limitations surrounding the use of AMOs, it is important to consider limitations, for example the potential for off-target effects, associated with the targeted genome editing techniques used in this study. In comparison to CRISPR/Cas9, off-target effects using TALENs are rare, as the DNA binding site is very long (approx. 36 base pairs) therefore rarely, if ever, is this found elsewhere in the genome (Mussolino et al. 2011, Miller et al. 2011). Additionally, several publications, using genome-wide studies for example, have reported that TALEN-mediated genome modifications are rarely accompanied by off-target effects (Pattanayak, Guilinger and Liu 2014). Thus, we could assume that our TALEN lines are unlikely to be confounded by such effects. Conversely, the CRISPR/Cas9 technique has the potential to deliver unwanted, off-target effects due to the ability of the gRNA to tolerate up to five mismatches (non-Watson-Crick base pairing) (Fu et al. 2013). A simple way of detecting off-target effects is amplification of pre-selected potential off-target sites, followed by sequencing of PCR products using sanger or next generation sequencing methods (Hruscha et al. 2013). This was performed

in the original paper which published the CRISPR/Cas9 target site that we used in the current study, reporting mutation rates at potential off-target sites are only 1.1-2.5% (Hruscha et al. 2013). As we used the same target site and same wild-type strain (AB) as the original paper, it is likely we would have similar low rates of off-target effects in those regions. However, a drawback of this method of screening pre-selected sites is the biased nature of the technique and the risk of overlooking mutations at alternative loci. Recently, several methods have been developed to help reduce the off-target activity of CRISPR/Cas9 system in the future. For example, in one approach two closely-spaced gRNAs are combined with a Cas9 nickase mutant, introducing staggered DSBs by nicking the DNA in two positions, inspired by the dimeric nature of TALENs which are not plagued by off-target effects (Ran et al. 2013). Reduction of off-target effects is not only important with regards to making models of human disease. As the topic of utilising CRISPR/Cas9 to treat and even cure certain human diseases is at the forefront of the media, it is essential that we develop methods to reduce the potential for off-target effects before using them in patients. One consideration is that no two people's genomes are identical, thus identifying off-target sites from a 'reference' human genome would not be suitable. Therefore, reducing or even abolishing the off-target capability the gRNA or nuclease seems the most logical approach to focus on in the future.

## 6.3. Characterisation of the *C13H9orf72* loss-of-function zebrafish generated in this project

We reported that a total of four TALEN-generated lines (SH448, SH449, SH450 and SH451) and two CRISPR/Cas9-generated lines (SH470 and SH471) had a significant reduction in *C13H9orf72* transcript levels, indicating that the predicted truncated transcripts are degraded by nonsense mediated decay before they are able to be translated into protein. We were not able to further confirm this by examining endogenous C13H9orf72 protein levels due to the lack of reliable antibodies available. Further investment in developing reliable anti-C9orf72 antibodies is necessary for investigating *C9orf72* haploinsufficiency and the function of the corresponding protein. Currently, several commercially available antibodies are able to robustly detect overexpression of C9orf72, but are not sufficient to detect endogenous protein or distinguish between the two protein isoforms. As discussed, there has been development of antibodies which are able to detect C9orf72-S and C9orf72-L, individually (Xiao et al. 2015). However, it is uncertain whether these will work in zebrafish models, thus future work would have to involve testing these in the future. It is essential to produce anti-C9orf72 antibodies which

can detect endogenous levels of the two protein isoforms in a variety of species. This will allow us to be certain that C9orf72 is definitely reduced or abolished in previous models of haploinsufficiency and help to advance the field in understanding C9orf72 function.

Characterisation studies were performed on two TALEN-generated lines (SH448 and SH451), as well as one CRISPR/Cas9-generated line (SH470). We were able to characterise the lines SH448 and SH451 up to 24 months, but due to time constraints we were only able to characterise line SH470 up to 12 months. Initially, we expected to see changes in phenotypes such as survival, motor function and pathology, as has been shown in other models of ALS in zebrafish (Ramesh et al. 2010). Additionally, due to the link between ALS and FTD in patients harbouring the repeat expansion in *C9orf72*, we observed for behavioural changes. Unfortunately, due to time constraints we were unable to study pathology in these zebrafish. In the future, it would be beneficial to conduct a thorough pathological investigation on these lines, including staining brain and spinal cord tissue for p62/SQSTM1, ubiquitin and phospho TDP-43, which are hallmarks of C9-ALS. However, as no pathological hallmarks of ALS were reported in *C9orf72* LOF mouse models, it is possible that we will not see any in the *C13H9orf72* LOF zebrafish either (Atanasio et al. 2016, Sudria-Lopez et al. 2016, Burberry et al. 2016, O'Rourke et al. 2016, Koppers et al. 2015).

### 6.3.1. Survival
We reported that loss of C13H9orf72 expression did not impact survival at any age in the zebrafish. These findings do not recapitulate the phenotype observe in human C9-ALS patients, whose mean disease duration has been reported to be 30.5 months (Cooper-Knock et al. 2012). These findings do agree with the *C13H9orf72* KD zebrafish which showed no difference in early viability (Ciura et al. 2013). Additionally, they agree with two *C9orf72* LOF mouse models, which did not show a decrease in survival (O'Rourke et al. 2016, Koppers et al. 2015). However, some studies have reported that *C9orf72* LOF mouse models have a reduced survival (Atanasio et al. 2016, Sudria-Lopez et al. 2016, Burberry et al. 2016). It is important to note that the reduction in survival observed in these mouse models may be linked to an immune defect and not neurodegeneration. The discrepancy reported in survival between these mouse models may suggest that environmental factors or differences in the genetic strain may influence survival in mice lacking C9orf72 expression.

### 6.3.2. Motor function

We demonstrated that the swim tunnel is a robust test to measure swimming ability in comparison to the spinning task. We suggest that the spinning task is not suitable for long-term phenotypic studies monitoring motor function, due to its high variability in comparison to the swim tunnel. Additionally, we highlighted the importance of controlling for both gender and size in experimental groups using the swim tunnel, which has important implications for future experimental design. Overall, our results showed that the *C13H9orf72* LOF adult zebrafish had a mild motor defect, but no corresponding defect in NMJs. These findings agree with one study which reports the *C9orf72* LOF mouse has mild motor impairments, but no corresponding neurodegeneration (Atanasio et al. 2016). The authors suggest that motor defects could be secondary to the already established lymphoid organ hyperplasia and glomerulonephropathy in these mice (Atanasio et al. 2016). However, we are yet to determine whether immune defects were the cause of the mild motor defect seen in the zebrafish (discussed below). However, these findings do not recapitulate what is observed in human C9-ALS/FTD patients, who experience neurodegeneration and severe motor defects as a result. Therefore, our data suggests LOF is not sufficient to cause C9-ALS. Additionally, this model does not support the *C.elegan* ALFA-1 deletion model, which showed age-dependent progressive motor defects with an increased sensitivity to stress induced paralysis (Therrien et al. 2013). As well as this, our model does not support the *C13H9orf72* KD zebrafish which showed locomotor deficits at the embryonic stage (Ciura et al. 2013), suggesting that this phenotype may be a result of off-target mediated effects. In the future we could microinject the same AMOs used in the KD study into both wild-type and stable *C13H9orf72* KO mutants. We would expect to see the same effect in wild-types as reported in the paper, but not in the stable KO zebrafish. However, if we did see the same effects in our mutants, it would suggest the AMOs used in the aforementioned study had off-target effects.

Overall, a major limitation of this study was that it was underpowered. Power analysis was originally performed using G*Power Version 3.0.3, based on $U_{crit}$ values obtained from a transgenic SOD-1 zebrafish model of ALS (Ramesh et al. 2010), indicating a sample of 11 zebrafish per group would provide 80% power to detect a 20% reduction in $U_{crit}$ (student's t-test, two-tailed, $\alpha = 0.05$, $\beta = 0.8$). This was then applied to the other characterisation tests. However, due to variability and the mild phenotype observed in the

*C13H9orf72* LOF zebrafish, this meant that the study was underpowered. As discussed, retrospective power calculations using G*Power Version 3.0.10, based on $U_{crit}$ values obtained in this study, revealed a sample of 25 zebrafish per group would provide 80% power to detect a 20% decrease in $U_{crit}$ (student's t-test, two-tailed, $\alpha = 0.05$, $\beta = 0.8$). A cohort of this size has been raised, for which we are currently measuring $U_{crit}$ in the swim tunnel test.

### 6.3.3. Behaviour

Finally, we characterised behaviour in the aforementioned lines. As FTD and ALS/FTD patients have been reported to display symptoms such as anxiety, we examined anxiety-like behaviour in adult zebrafish using two different tests: the novel tank diving test and the open field test (Mahoney et al. 2012). We did not report any difference in anxiety-like behaviour between *C13H9orf72* LOF mutants and their wild-type siblings. However, we cannot conclude from this that these fish do not have any FTD-like symptoms. There is robust evidence that these tests measure anxiety. For example, it has been reported that use of anxiolytic treatments significantly decrease the amount of time spent in the lower half of the tank during the novel tank diving test (Cachat et al. 2010, Parker et al. 2014, Bencan et al. 2009, Levin et al. 2007), which supports this protocols ability to measure anxiety. Additionally, the use of anxiolytic treatments such as diazepam and ethanol decreases thigmotaxic behaviour in the open field test, again supporting this tests ability to measure anxiety (Baiamonte et al. 2016). However, there is a lack of adult zebrafish models with stable mutations in dementia genes that report on behavioural phenotypes, such as anxiety. Therefore, it is possible this kind of phenotype doesn't manifest in such models without the use of anxiogenic drugs, for example.

In the future additional behavioural tests could be conducted. Patients carrying the repeat expansion in *C9orf72* often present with psychosis, as well as other aberrant social behaviours such as disinhibition and apathy (Mahoney et al. 2012, Cooper-Knock et al. 2014a). It is possible to study social interactions in adult zebrafish because they are a social species that have a tendency to form shoals, a type of group-forming behaviour which can be easily assessed in adult zebrafish (Miller and Gerlai 2007). It would also be interesting to examine their social approach behaviour in the future, to examine whether a focal zebrafish prefers to associate with conspecifics or be on its own (McRobert and Bradner 1998). This would be relatable to patients as a measure of disinhibition. As well as social interactions, memory and cognition can also be observed in adult zebrafish for

example by using a T-Maze, which is similar to a test used on rodents (Darland and Dowling 2001, Norton and Bally-Cuif 2010). This is relevant to patients because they are reported to have memory loss (Mahoney et al. 2012). It is essential that behaviour is monitored in animal models of *C9orf72*-related disease, due to the close link between ALS and FTD in patients carrying the repeat expansion in *C9orf72*. Studies of the *C9orf72* LOF mouse model do not report any attempt to observe behaviour and cognition in the mice, thus studies to evaluate this should be considered in the future. However, in order to do this effectively, behavioural tests need to be standardised to allow for consistency and cross-laboratory comparability. Lack of standardisation is a particular issue surrounding zebrafish behavioural tests. In the future, further scrutiny is needed to understand the effect that previous testing experience (test battery effect) and gender have on the outcome of behavioural tests, for example.

### 6.4. The function of C13H9orf72 *in vivo*
#### 6.4.1. Role in autophagy

Thus far, *C13H9orf72* LOF zebrafish and *C9orf72* LOF mouse models have not been reported to display ALS/FTD-like symptoms (O'Rourke et al. 2016, Sudria-Lopez et al. 2016, Koppers et al. 2015, Atanasio et al. 2016, Burberry et al. 2016). However, recent studies using *C9orf72* LOF mice have consistently implicated C9orf72 protein function in autophagy and immune regulation (Atanasio et al. 2016, Amick et al. 2016, O'Rourke et al. 2016, Yang et al. 2016, Ugolino et al. 2016). Regarding autophagy, the pathway is known to be important for neuronal health; for example, neuronal-specific knockout (KO) of essential autophagy genes - such as *ATG7, ATG5* and *FIP200* - results in the inhibition of autophagy in neurons and subsequently neurodegeneration in mouse models (Hara et al. 2006, Komatsu et al. 2006, Liang et al. 2010). Furthermore, defective autophagy has been implicated in the causation of several neurodegenerative disorders such as Alzheimer's disease and Parkinson's disease. There are also multiple reports that defective autophagy plays a role in the pathogenesis of ALS (Menzies et al. 2017). As mentioned, UBIs are a neuropathological hallmark of C9-linked ALS, as well as non-C9 linked ALS (Menzies et al. 2017). Additionally, several ALS-linked genes are known to encode proteins which function within the pathway, including: *p62/SQSTM1, UBQLN2, OPTN, TBK-1* and *VCP*. Regarding C9orf72, it has been reported in our lab and others that C9orf72 plays a role in the regulation of the autophagy pathway, therefore we examined this in our *C13H9orf72* LOF model (Farg et al. 2014, Yang et al. 2016, Sellier et al. 2016, Sullivan et al. 2016a, Webster et al. 2016a).

We reported that C13H9orf72 directly interacted with a component of the initiation complex, ATG13, in an *in vitro* binding assay, as has been shown in our lab with human C9orf72 previously (Webster et al. 2016a). Interestingly, we also report that loss of C13H9orf72 expression does not result in defective autophagy initiation, converse to previous reports *in vitro* (Webster et al. 2016a, Sellier et al. 2016, Sullivan et al. 2016a). We reasoned this may be because C13H9orf72 exerts its effect downstream from the initiation complex, which evidence has suggested from previous studies (Farg et al. 2014, Amick et al. 2016, O'Rourke et al. 2015). For example, there are an increasing number of studies reporting an increase, not a decrease, in LC3-II levels in response to reduced C9orf72 expression (Farg et al. 2014, O'Rourke et al. 2016). This increase in basal LC3-II levels could be a result of increased autophagic flux or defective clearance of autophagosomes via the lysosome. As a result, we investigated basal LC3-II levels in our zebrafish, but no statistically significant difference was observed between genotypes in two lines (SH451 and SH448). The disparity in results between our *C13H9orf72* LOF zebrafish and functional analysis completed in cell culture could be for several reasons. Firstly, we know that C13H9orf72 is not ubiquitously expressed in zebrafish, with expression of *C13H9orf72* mRNA reported in a subset of tissues, including regions of the CNS, such as the forebrain, midbrain, hindbrain and spinal cord (Ciura et al. 2013). Therefore, the effect of loss of C13H9orf72 expression on autophagy may be harder to observe via immunoblotting, as we are using the whole fish embryo in comparison to a homogenous population of cells, as used previously (Webster et al. 2016a). In the future, we could extract protein from relevant tissues taken from adult zebrafish, such as the brain, to examine LC3-II levels after treatment with the same drugs used in this study or to examine basal levels of LC3-II under normal conditions. Additionally, we could extend our *in vivo* study of autophagy into live embryos via injecting mCherry-LC3-EGFP into wild-type and *C13H9orf72* mutant zebrafish embryos (Pankiv et al. 2007). The fusion of acid-sensitive GFP and acid-insensitive mCherry to LC3 results in a pH-sensitive sensor to measure autophagy in live cells. This will allow us to probe delivery of autophagy substrates to the lysosome, as we will be able to distinguish autophagosomes (red and green fluorescence) from the acidic autolysosomes (red fluorescence only) in individual cells (Pankiv et al. 2007). Thus, utilising this technique would allow us to detect cell-specific defects, which is not possible using the western blot-based approach taken in this project. Secondly, there could be a compensatory mechanism *in vivo* which can activate autophagy in an mTOR-independent manner, protecting the zebrafish from a defect in the

autophagy pathway caused by loss of C13H9orf72 expression. Anecdotally, in support of this we have observed in our lab that *ATG5* LOF zebrafish could survive up to 30dpf, which is surprising as when *ATG5* is ablated in mice they are reported to die within 1 day of delivery (He et al. 2009) and suggests that alternative mechanisms may compensate for defects in the autophagy pathway. Finally, C9orf72 may have different functions in different systems. For example, there are multiple reports that *C9orf72* LOF mice have defects in autophagy (Atanasio et al. 2016, Amick et al. 2016, O'Rourke et al. 2016, Yang et al. 2016, Ugolino et al. 2016). Mouse C9orf72 (3110043021Rik) shares >90% nucleotide identity with human C9orf72, whereas zebrafish C9orf72 shares 76% nucleotide identity. Additionally, we have reported in this study that C13H9orf72 is missing an exon in comparison to higher vertebrates, such as mice and humans, which corresponds to coding exon 3. Thus, this difference in conservation may also explain why we do not see a defect in autophagy when C13H9orf72 expression is lost in the zebrafish. Although, we reported C13H9orf72 binds hATG13, supporting the idea that there is conservation of protein function between C13H9orf72 and hC9orf72, which does not support the latter theory.

### 6.4.2. Role in the immune system

Immune defects are also reported in *C9orf72* LOF mice (O'Rourke et al. 2016, Sudria-Lopez et al. 2016, Koppers et al. 2015, Atanasio et al. 2016, Burberry et al. 2016). As discussed in chapter 5, we decided to investigate whether the *C13H9orf72* LOF zebrafish we generated had defects in the immune system, in particular focussing on whether they showed signs of splenomegaly. We reported that *C13H9orf72* LOF zebrafish spleens were 35% larger than wild-type, but this was not significant due to a small sample size. However, we cannot confirm from these findings that loss of C13H9orf72 expression in these zebrafish has not affected the immune system, and further work will need to be done in the future to confirm this. For example, two groups found evidence of an increase in macrophage number in mutant animals suggesting that the inflammatory phenotypes observed may be due to dysfunction in this or other phagocytic cells (Atanasio et al. 2016, O'Rourke et al. 2016). Therefore, we could look at the levels of macrophages in haematopoietic tissues, such as the spleen, in the zebrafish. Multiple genes have been suggested as markers for macrophage lineage in zebrafish, such as *L-plastin* (Herbomel, Thisse and Thisse 1999). Use of L-plastin antibodies has been reported in zebrafish, thus could be used in the future (Mathias et al. 2009). Overall, it is important to note that

although the immune system in zebrafish and other teleosts is physiologically similar to higher vertebrates, like mice, there are some differences. For example, teleosts do not have lymph nodes and *C9orf72* LOF mice reportedly exhibit lymphadenopathy, enlarged lymph nodes, as well as splenomegaly (Uribe et al. 2011, O'Rourke et al. 2016, Atanasio et al. 2016, Sudria-Lopez et al. 2016). Additionally, it has been reported in the *C9orf72* LOF mouse model that *Trem2* expression is significantly upregulated in splenic tissue, but zebrafish do not harbour an orthologue for this gene (O'Rourke et al. 2016). Thus, despite the similarities, these differences may be why we do not see symptoms such as splenomegaly in the *C13H9orf72* LOF zebrafish.

### 6.5. A noncoding $(G_4C_2)_n$ hexanucleotide repeat expansion in C9orf72: one mutation, many mechanisms

Overall, the relative contribution of *C9orf72* haploinsufficiency, RNA toxicity and DPR toxicity in the pathogenesis of ALS/FTD is still unclear. Although there are contradictory results for all disease mechanisms, most *in vivo* models suggest that GOF mechanisms such as RNA toxicity and DPR proteins are neurotoxic, whereas LOF mechanisms are not. However, it is possible that a combination of multiple mechanisms results in the development of *C9orf72*-linked ALS/FTD in humans and not just one mechanism in isolation. Therefore, although *C9orf72* LOF may not be neurotoxic alone, it may modulate disease onset and/or progression in C9-ALS/FTD alongside proposed GOF mechanisms. For example, as C9orf72 is reported to function in autophagy, partial or complete loss of its function may disrupt the pathway and exacerbate RNA toxicity or dipeptide repeat (DPR) protein toxicity in disease. In the future, we need to develop models to further understand how these proposed disease mechanisms interact *in vivo,* as this may have more relevance to humans with C9-ALS/FTD.

We have the potential to use our *C9orf72* LOF zebrafish to generate models that harbour both LOF and GOF disease mechanisms to further investigate this in the future. Many cellular and animal models seem to suggest that the arginine rich DPR species (poly-GR and –PR) are highly toxic (Xu et al. 2013, Lee et al. 2013, Chew et al. 2015, Zhang et al. 2014, Ohki et al. 2017, Zhang et al. 2016, Wen et al. 2014, Mizielinska et al. 2014). Additionally, it is reported that poly-GA is the most abundant DPR species in patients carrying the repeat expansion (Mori et al. 2013c). Therefore, observing the interaction between these particular DPRs and *C9orf72* haploinsufficiency may be an interesting place to start. As we know that the *C13H9orf72* LOF mutants generated in this study are

able to breed and produce viable offspring, we could cross our mutants with transgenic zebrafish expressing these DPRs for further study. Interestingly, a recent study generated transgenic zebrafish expressing poly-GA (Ohki et al. 2017). However, as this zebrafish showed high levels of larval lethality, it would not be possible to cross this with our *C13H9orf72* LOF zebrafish (Ohki et al. 2017). In the future, it could be of interest to optimise microinjection the poly-GA, -GR and -PR constructs (available in our lab) into our *C13H9orf72* LOF zebrafish at larval stages. If C13H9orf72 does play an essential role in the autophagy pathway in zebrafish, a worsened phenotype may be observed in our mutants at this stage if the defective autophagy pathway is unable to clear the toxic, aggregated protein.

### 6.6. Oligogenic disease and a multi-hit model

Another point for consideration is the potential oligogenic nature of ALS. The *C13H9orf72* LOF zebrafish generated in this study could also be used to further investigate this in the future, especially as oligogenic inheritance of mutant *C9orf72* with other ALS-linked genes is the most commonly reported combination (Lattante et al. 2015a). For example, *OPTN* mutations have been reported in combination with *C9orf72* (Bury et al. 2016, Lattante et al. 2015a, Millecamps et al. 2011, Millecamps et al. 2012). However, mutations in *OPTN* are not the only ones that have been reported to be in combination with *C9orf72* and in total over 10 ALS-causing genetic variants have been described (Lattante et al. 2015a). As we know that the *C13H9orf72* LOF mutants generated in this study are able to breed and produce viable offspring, we have the potential to rapidly generate several novel oligogenic models in the future. This would enable us to identify whether both genes are needed to cause disease in a synergistic or additive way. Alternatively, it could reveal if one of the mutations, or whole gene itself, has been falsely related to ALS. Re-evaluation of ALS cases where a casual mutation was identified before the discovery of *C9orf72* may reveal further combinations which could also be studied. Additionally, it would be interesting to investigate the combinations which have been reported to be in pure FTD cases only (*C9orf72* with tau or p62/SQSTM1) and pure ALS cases only (*C9orf72* with TDP-43, FUS or SOD1), to see whether this recapitulates distinct phenotypes in zebrafish (Lattante et al. 2015a). This would provide insight into how *C9orf72* repeat expansions can be responsible for the ALS-FTD spectrum of disease. Overall, zebrafish are more efficient to use than mammalian models to define the degree of interaction among causative genes due to their

reduced cost, their ability to produce hundreds of eggs at weekly intervals and ease of genetic manipulation.

### 6.7. Conclusions

We have successfully generated and characterised a *C13H9orf72* LOF zebrafish. For a comparison between the *C9orf72* LOF models, including the model generated in this study, see table 6.1. Results from the characterisation completed so far do not support the hypothesis that *C9orf72* LOF is sufficient to cause C9-ALS/FTD alone, which complements published findings in *C9orf72* LOF mouse models (see table 6.1). However, our findings do not rule out that *C9orf72* LOF may modulate disease onset and/or progression in C9-ALS/FTD patients alongside proposed GOF mechanisms. Additionally, we examined C9orf72 protein function in these zebrafish and confirmed it interacts with a member of the autophagy initiation complex, but further work is needed to determine whether it plays a regulatory role in autophagy in zebrafish. Overall, we have generated a powerful tool to use in the future to test the potential interaction of LOF and GOF disease mechanisms, oligogenic nature of C9-ALS/FTD and the function of the C9orf72 protein. Understanding of these important areas is paramount in identifying novel targets for future therapies, which will benefit the largest proportion of ALS and FTD patients.

**Table 6.1 Summary of C9orf72 loss-of-function models.** Details of organism, orthologue name, method(s) used, phenotype(s) of null mutants and reference to the original study is given.

| Organism | Orthologue | Method(s) | Phenotype(s) | Original study |
|---|---|---|---|---|
| *C.elegan* | ALFA-1 | Knockout line *alfa-1(ok3062)* or RNA interference (RNAi) | Age-dependant motor phenotype<br>Neurodegeneration of GABAergic motor neurons<br>Hypersensitivity to osmotic stress | (Therrien et al. 2013) |
| *D.rerio* | C13H9orf72 | Knockdown using antisense morpholinos (AMOs) injected into fertilised embryos | Disrupted arborization and shortening of motor neuron axons<br>Impaired touch-evoked escape response (TEER) | (Ciura et al. 2013) |
| | | **CRISPR/Cas9- mediated frameshift mutation in exon 1, causing premature stop codon; TALEN-mediated frameshift mutation in exon 7, causing premature stop codon** | **No alteration in survival**<br>**Mild defect in motor function, but no corresponding defect in the NMJs**<br>**No change in anxiety-like behaviour**<br>**No evidence of dysfunctional autophagy pathway**<br>**No evidence of splenomegaly** | **Current study** |
| *M.musculus* | 3110043O21Rik | Intracerebroventricular (ICV) stereotactic injection of *C9orf72*-specific antisense oligonucleotides (ASO) | No evidence of C9-ALS/FTD associated pathology<br>No change in anxiety-like behaviour<br>No defect in motor function<br>Minimal genome-wide mRNA alterations | (Lagier-Tourenne et al. 2013) |
| | | Cre-lox mediated excision of exons 4-5 in neurons and glial cells only | No alteration in survival<br>No defect in motor function<br>No evidence of C9-ALS/FTD associated pathology (including motor neuron number, gliosis, TDP-43 mislocalisation or increased ubiquitination) | (Koppers et al. 2015) |
| | | Transgenic mice with exons 2-6 replaced with *LacZ* construct; CRISPR-Cas9 mediated disruption of exon 4 | Evidence of decreased survival<br>No evidence of neurodegeneration<br>Evidence of immune dysregulation | (Burberry et al. 2016) |
| | | Transgenic mice with exons 2-6 replaced with *LacZ* construct; Zinc Finger Nuclease (ZFN)-mediated deletion of exon 2 | No defect in motor function<br>No evidence of C9-ALS/FTD associated pathology<br>Evidence of immune dysregulation | (O'Rourke et al. 2016) |

| | | | |
|---|---|---|---|
| | Transgenic mice with exons 2-11 replaced with *LacZ* construct | Evidence of decreased survival<br>Mild defect in motor function<br>Evidence of immune dysregulation | (Atanasio et al. 2016) |
| | Cre-lox mediated excision of exons 4-5 in whole genome | Evidence of decreased survival<br>No defect in motor function<br>No evidence of C9-ALS/FTD associated pathology (including motor neuron number, gliosis, TDP-43 mislocalisation or increased ubiquitination)<br>Evidence of immune dysregulation | (Sudria-Lopez et al. 2016) |
| | CRISPR/Cas9-mediated frameshift mutation in exon 2, causing a premature stop codon, effecting transcripts 1 and 3 | Evidence of dysfunctional autophagy pathway<br>Evidence of immune dysregulation | (Sullivan et al. 2016b) |
| | Transgenic mice with exons 2-6 replaced with *LacZ* construct | Evidence of decreased survival<br>Mild defect in motor function, but no corresponding decrease in motor neuron number<br>No change in anxiety-like behaviour, but mild abnormalities in social interaction and recognition<br>No overt C9-ALS/FTD associated pathology<br>Evidence of immune dysregulation | (Jiang et al. 2016) |
| | Transgenic mice with exons 2-6 replaced with *LacZ* construct | Evidence of decreased survival<br>No evidence of neurodegeneration<br>Evidence of immune dysregulation<br>Evidence of dysfunctional autophagy pathway | (Ugolino et al. 2016) |

## References

Abe, K., M. Aoki, S. Tsuji, Y. Itoyama, G. Sobue, M. Togo, C. Hamada, M. Tanaka, M. Akimoto, K. Nakamura, F. Takahashi, K. Kondo, H. Yoshino & M. C. I. A. L. S. S. G. Edaravone (2017) Safety and efficacy of edaravone in well defined patients with amyotrophic lateral sclerosis: a randomised, double-blind, placebo-controlled trial. *Lancet Neurology,* 16**,** 505-512.

Ahmad, F., L. P. J. J. Noldus, R. A. J. Tegelenbosch & M. K. Richardson (2012) Zebrafish embryos and larvae in behavioural assays. *Behaviour,* 149**,** 1241-1281.

Al-Saif, A., F. Al-Mohanna & S. Bohlega (2011) A mutation in sigma-1 receptor causes juvenile amyotrophic lateral sclerosis. *Annals of Neurology,* 70**,** 913-919.

Al-Sarraj, S., A. King, C. Troakes, B. Smith, S. Maekawa, I. Bodi, B. Rogelj, A. Al-Chalabi, T. Hortobagyi & C. E. Shaw (2011) p62 positive, TDP-43 negative, neuronal cytoplasmic and intranuclear inclusions in the cerebellum and hippocampus define the pathology of C9orf72-linked FTLD and MND/ALS. *Acta Neuropathologica,* 122**,** 691-702.

Almeida, S., E. Gascon, H. Tran, H. J. Chou, T. F. Gendron, S. DeGroot, A. R. Tapper, C. Sellier, N. Charlet-Berguerand, A. Karydas, W. W. Seeley, A. L. Boxer, L. Petrucelli, B. L. Miller & F.-B. Gao (2013) Modeling key pathological features of frontotemporal dementia with C9ORF72 repeat expansion in iPSC-derived human neurons. *Acta Neuropathologica,* 126**,** 385-399.

Amick, J., A. Roczniak-Ferguson & S. M. Ferguson (2016) C9orf72 binds SMCR8, localizes to lysosomes, and regulates mTORC1 signaling. *Molecular Biology of the Cell,* 27**,** 3040-3051.

Ao, X., L. Zou & Y. Wu (2014) Regulation of autophagy by the Rab GTPase network. *Cell Death and Differentiation,* 21**,** 348-358.

Arai, T., T. Nonaka, M. Hasegawa, H. Akiyama, M. Yoshida, Y. Hashizume, K. Tsuchiya, T. Oda & K. Ikeda (2003) Neuronal and glial inclusions in frontotemporal dementia with or without motor neuron disease are immunopositive for p62. *Neuroscience Letters,* 342**,** 41-44.

Ariyomo, T. O. & P. J. Watt (2012) The effect of variation in boldness and aggressiveness on the reproductive success of zebrafish. *Animal Behaviour,* 83**,** 41-46.

Ariyomo, T. O. & P. J. Watt (2015) Effect of hunger level and time of day on boldness and aggression in the zebrafish Danio rerio. *Journal of Fish Biology,* 86**,** 1852-1859.

Ash, P. E. A., K. F. Bieniek, T. F. Gendron, T. Caulfield, W.-L. Lin, M. DeJesus-Hernandez, M. M. van Blitterswijk, K. Jansen-West, J. W. Paul, III, R. Rademakers, K. B. Boylan, D. W. Dickson & L. Petrucelli (2013) Unconventional Translation of C9ORF72 GGGGCC Expansion Generates Insoluble Polypeptides Specific to c9FTD/ALS. *Neuron,* 77**,** 639-646.

Atanasio, A., V. Decman, D. White, M. Ramos, B. Ikiz, H.-C. Lee, C.-J. Siao, S. Brydges, E. LaRosa, Y. Bai, W. Fury, P. Burfeind, R. Zamfirova, G. Warshaw, J. Orengo, A. Oyejide, M. Fralish, W. Auerbach, W. Poueymirou, J. Freudenberg, G. Gong, B. Zambrowicz, D. Valenzuela, G. Yancopoulos, A. Murphy, G. Thurston & K.-M. V. Lai (2016) C9orf72 ablation causes immune dysregulation characterized by leukocyte expansion, autoantibody production, and glomerulonephropathy in mice. *Scientific Reports,* 6.

Babin, P. J., C. Goizet & D. Raldua (2014) Zebrafish models of human motor neuron diseases: Advantages and limitations. *Progress in Neurobiology,* 118**,** 36-58.

Baborie, A., T. D. Griffiths, E. Jaros, R. Perry, I. G. McKeith, D. J. Burn, M. Masuda-Suzukake, M. Hasegawa, S. Rollinson, S. Pickering-Brown, A. C. Robinson, Y. S. Davidson & D. M. A. Mann (2015) Accumulation of dipeptide repeat proteins predates that of TDP-43 in frontotemporal lobar degeneration associated with

hexanucleotide repeat expansions in C9ORF72 gene. *Neuropathology and Applied Neurobiology,* 41**,** 601-612.

Baiamonte, M., M. O. Parker, G. P. Vinson & C. H. Brennan (2016) Sustained Effects of Developmental Exposure to Ethanol on Zebrafish Anxiety-Like Behaviour. *Plos One,* 11.

Baker, M., I. R. Mackenzie, S. M. Pickering-Brown, J. Gass, R. Rademakers, C. Lindholm, J. Snowden, J. Adamson, A. D. Sadovnick, S. Rollinson, A. Cannon, E. Dwosh, D. Neary, S. Melquist, A. Richardson, D. Dickson, Z. Berger, J. Eriksen, T. Robinson, C. Zehr, C. A. Dickey, R. Crook, E. McGowan, D. Mann, B. Boeve, H. Feldman & M. Hutton (2006) Mutations in progranulin cause tau-negative frontotemporal dementia linked to chromosome 17. *Nature,* 442**,** 916-919.

Bannwarth, S., S. Ait-El-Mkadem, A. Chaussenot, E. C. Genin, S. Lacas-Gervais, K. Fragaki, L. Berg-Alonso, Y. Kageyama, V. Serre, D. G. Moore, A. Verschueren, C. Rouzier, I. Le Ber, G. Auge, C. Cochaud, F. Lespinasse, K. N'Guyen, A. de Septenville, A. Brice, P. Yu-Wai-Man, H. Sesaki, J. Pouget & V. Paquis-Flucklinger (2014) A mitochondrial origin for frontotemporal dementia and amyotrophic lateral sclerosis through CHCHD10 involvement. *Brain,* 137**,** 2329-2345.

Beck, J., M. Poulter, D. Hensman, J. D. Rohrer, C. J. Mahoney, G. Adamson, T. Campbell, J. Uphill, A. Borg, P. Fratta, R. W. Orrell, A. Malaspina, J. Rowe, J. Brown, J. Hodges, K. Sidle, J. M. Polke, H. Houlden, J. M. Schott, N. C. Fox, M. N. Rossor, S. J. Tabrizi, A. M. Isaacs, J. Hardy, J. D. Warren, J. Collinge & S. Mead (2013) Large C9orf72 Hexanucleotide Repeat Expansions Are Seen in Multiple Neurodegenerative Syndromes and Are More Frequent Than Expected in the UK Population. *American Journal of Human Genetics,* 92**,** 345-353.

Behrends, C., M. E. Sowa, S. P. Gygi & J. W. Harper (2010) Network organization of the human autophagy system. *Nature,* 466**,** 68-U84.

Belzil, V. V., P. O. Bauer, M. Prudencio, T. F. Gendron, C. T. Stetler, I. K. Yan, L. Pregent, L. Daughrity, M. C. Baker, R. Rademakers, K. Boylan, T. C. Patel, D. W. Dickson & L. Petrucelli (2013) Reduced C9orf72 gene expression in c9FTD/ALS is caused by histone trimethylation, an epigenetic event detectable in blood. *Acta Neuropathologica,* 126**,** 895-905.

Benato, F., T. Skobo, G. Gioacchini, I. Moro, F. Ciccosanti, M. Piacentini, G. M. Fimia, O. Carnevali & L. Dalla Valle (2013) Ambra1 knockdown in zebrafish leads to incomplete development due to severe defects in organogenesis. *Autophagy,* 9**,** 476-495.

Bencan, Z., D. Sledge & E. D. Levin (2009) Buspirone, chlordiazepoxide and diazepam effects in a zebrafish model of anxiety. *Pharmacology Biochemistry and Behavior,* 94**,** 75-80.

Bensimon, G., L. Lacomblez, V. Meininger, P. Bouche, C. Delwaide, P. Couratier, O. Blin, F. Viader, H. Peyrostpaul, J. David, J. M. Maloteaux, J. Hugon, E. C. Laterre, A. Rascol, M. Clanet, J. M. Vallat, A. Dumas, G. Serratrice, B. Lechevallier, A. J. Peuch, T. Nguyen, C. Shu, P. Bastien, C. Papillon, S. Durrleman, E. Louvel, P. Guillet, L. Ledoux, E. Orvoenfrija & M. Dib (1994) A CONTROLLED TRIAL OF RILUZOLE IN AMYOTROPHIC-LATERAL-SCLEROSIS. *New England Journal of Medicine,* 330**,** 585-591.

Bento, C. F., M. Renna, G. Ghislat, C. Puri, A. Ashkenazi, M. Vicinanza, F. M. Menzies & D. C. Rubinsztein (2016) Mammalian Autophagy: How Does It Work? *Annual Review of Biochemistry, Vol 85,* 85**,** 685-713.

Benussi, L., G. Rossi, M. Glionna, E. Tonoli, E. Piccoli, S. Fostinelli, A. Paterlini, R. Flocco, D. Albani, R. Pantieri, C. Cereda, G. Forloni, F. Tagliavini, G. Binetti & R. Ghidoni (2014) C9ORF72 Hexanucleotide Repeat Number in Frontotemporal Lobar

Degeneration: A Genotype-Phenotype Correlation Study. *Journal of Alzheimers Disease,* 38**,** 799-808.

Bilsland, L. G., E. Sahai, G. Kelly, M. Golding, L. Greensmith & G. Schiavo (2010) Deficits in axonal transport precede ALS symptoms in vivo. *Proceedings of the National Academy of Sciences of the United States of America,* 107**,** 20523-20528.

Blazina, A. R., M. R. Vianna & D. R. Lara (2013) The Spinning Task: A New Protocol to Easily Assess Motor Coordination and Resistance in Zebrafish. *Zebrafish,* 10**,** 480-485.

Blokhuis, A. M., E. J. N. Groen, M. Koppers, L. H. van den Berg & R. J. Pasterkamp (2013) Protein aggregation in amyotrophic lateral sclerosis. *Acta Neuropathologica,* 125**,** 777-794.

Boettcher, M. & M. T. McManus (2015) Choosing the Right Tool for the Job: RNAi, TALEN, or CRISPR. *Molecular Cell,* 58**,** 575-585.

Boillee, S., K. Yamanaka, C. S. Lobsiger, N. G. Copeland, N. A. Jenkins, G. Kassiotis, G. Kollias & D. W. Cleveland (2006) Onset and progression in inherited ALS determined by motor neurons and microglia. *Science,* 312**,** 1389-1392.

Borroni, B., C. Bonvicini, A. Alberici, E. Buratti, C. Agosti, S. Archetti, A. Papetti, C. Stuani, M. Di Luca, M. Gennarelli & A. Padovani (2009) Mutation within TARDBP Leads to Frontotemporal Dementia without Motor Neuron Disease. *Human Mutation,* 30**,** E974-E983.

Brett, J. R. (1964) THE RESPIRATORY METABOLISM AND SWIMMING PERFORMANCE OF YOUNG SOCKEYE SALMON. *Journal of the Fisheries Research Board of Canada,* 21**,** 1183-1226.

Brook, J. D., M. E. McCurrach, H. G. Harley, A. J. Buckler, D. Church, H. Aburatani, K. Hunter, V. P. Stanton, J. P. Thirion & T. Hudson (1992) Molecular basis of myotonic dystrophy: expansion of a trinucleotide (CTG) repeat at the 3' end of a transcript encoding a protein kinase family member. *Cell,* 69**,** 385-385.

Bruijn, L. I., M. W. Becher, M. K. Lee, K. L. Anderson, N. A. Jenkins, N. G. Copeland, S. S. Sisodia, J. D. Rothstein, D. R. Borchelt, D. L. Price & D. W. Cleveland (1997) ALS-linked SOD1 mutant G85R mediates damage to astrocytes and promotes rapidly progressive disease with SOD1-containing inclusions. *Neuron,* 18**,** 327-338.

Buchman, V. L., J. Cooper-Knock, N. Connor-Robson, A. Higginbottom, J. Kirby, O. D. Razinskaya, N. Ninkina & P. J. Shaw (2013) Simultaneous and independent detection of C9ORF72 alleles with low and high number of GGGGCC repeats using an optimised protocol of Southern blot hybridisation. *Molecular Neurodegeneration,* 8.

Buhler, A., M. Kustermann, T. Bummer, W. Rottbauer, M. Sandri & S. Just (2016) Atrogin-1 Deficiency Leads to Myopathy and Heart Failure in Zebrafish. *International Journal of Molecular Sciences,* 17.

Bultmann, S., R. Morbitzer, C. S. Schmidt, K. Thanisch, F. Spada, J. Elsaesser, T. Lahaye & H. Leonhardt (2012) Targeted transcriptional activation of silent oct4 pluripotency gene by combining designer TALEs and inhibition of epigenetic modifiers. *Nucleic Acids Research,* 40**,** 5368-5377.

Burberry, A., N. Suzuki, J.-Y. Wang, R. Moccia, D. A. Mordes, M. H. Stewart, S. Suzuki-Uematsu, S. Ghosh, A. Singh, F. T. Merkle, K. Koszka, Q.-Z. Li, L. Zon, D. J. Rossi, J. J. Trowbridge, L. D. Notarangelo & K. Eggan (2016) Loss-of-function mutations in the C9ORF72 mouse ortholog cause fatal autoimmune disease. *Science Translational Medicine,* 8.

Burns, J. G. (2008) The Validity of Three Tests of Temperament in Guppies (Poecilia reticulata). *Journal of Comparative Psychology,* 122**,** 344-356.

Burrell, J. R., M. C. Kiernan, S. Vucic & J. R. Hodges (2011) Motor Neuron Dysfunction in Frontotemporal Dementia. *Neurology,* 76**,** A76-A77.

Bury, J. J., J. R. Highley, J. Cooper-Knock, E. F. Goodall, A. Higginbottom, C. J. McDermott, P. G. Ince, P. J. Shaw & J. Kirby (2016) Oligogenic inheritance of optineurin (OPTN) and C9ORF72 mutations in ALS highlights localisation of OPTN in the TDP-43-negative inclusions of C9ORF72-ALS. *Neuropathology,* 36**,** 125-134.

Byrne, S., M. Elamin, P. Bede, A. Shatunov, C. Walsh, B. Corr, M. Heverin, N. Jordan, K. Kenna, C. Lynch, R. L. McLaughlin, P. M. Iyer, C. O'Brien, J. Phukan, B. Wynne, A. L. Bokde, D. G. Bradley, N. Pender, A. Al-Chalabi & O. Hardiman (2012) Cognitive and clinical characteristics of patients with amyotrophic lateral sclerosis carrying a C9orf72 repeat expansion: a population-based cohort study. *Lancet Neurology,* 11**,** 232-240.

Cachat, J., A. Stewart, L. Grossman, S. Gaikwad, F. Kadri, K. M. Chung, N. Wu, K. Wong, S. Roy, C. Suciu, J. Goodspeed, M. Elegante, B. Bartels, S. Elkhayat, D. Tien, J. Tan, A. Denmark, T. Gilder, E. Kyzar, J. DiLeo, K. Frank, K. Chang, E. Utterback, P. Hart & A. V. Kalueff (2010) Measuring behavioral and endocrine responses to novelty stress in adult zebrafish. *Nature Protocols,* 5**,** 1786-1799.

Caligari, M., M. Godi, S. Guglielmetti, F. Franchignoni & A. Nardone (2013) Eye tracking communication devices in amyotrophic lateral sclerosis: Impact on disability and quality of life. *Amyotrophic Lateral Sclerosis and Frontotemporal Degeneration,* 14**,** 546-552.

Carvalho, M., M. S. Schwartz & M. Swash (1995) INVOLVEMENT OF THE EXTERNAL ANAL-SPHINCTER IN AMYOTROPHIC-LATERAL-SCLEROSIS. *Muscle & Nerve,* 18**,** 848-853.

Catani, M., M. Piccirilli, M. C. Geloso, A. Cherubini, G. Finali, G. Pelliccioli, U. Senin & P. Mecocci (2004) Rapidly progressive aphasic dementia with motor neuron disease: A distinctive clinical entity. *Dementia and Geriatric Cognitive Disorders,* 17**,** 21-28.

Ceballos-Diaz, C., A. M. Rosario, H.-J. Park, P. Chakrabarty, A. Sacino, P. E. Cruz, Z. Siemienski, N. Lara, C. Moran, N. Ravelo, T. E. Golde & N. R. McFarland (2015) Viral expression of ALS-linked ubiquilin-2 mutants causes inclusion pathology and behavioral deficits in mice. *Molecular Neurodegeneration,* 10.

Champagne, D. L., C. C. M. Hoefnagels, R. E. de Kloet & M. K. Richardson (2010) Translating rodent behavioral repertoire to zebrafish (Danio rerio): Relevance for stress research. *Behavioural Brain Research,* 214**,** 332-342.

Chang, N. N., C. H. Sun, L. Gao, D. Zhu, X. F. Xu, X. J. Zhu, J. W. Xiong & J. J. Xi (2013) Genome editing with RNA-guided Cas9 nuclease in Zebrafish embryos. *Cell Research,* 23**,** 465-472.

Chapman, A. L., E. J. Bennett, T. M. Ramesh, K. J. De Vos & A. J. Grierson (2013) Axonal Transport Defects in a Mitofusin 2 Loss of Function Model of Charcot-Marie-Tooth Disease in Zebrafish. *Plos One,* 8.

Chen, Y. Z., C. L. Bennett, H. M. Huynh, I. P. Blair, I. Puls, J. Irobi, I. Dierick, A. Abel, M. L. Kennerson, B. A. Rabin, G. A. Nicholson, M. Auer-Grumbach, K. Wagner, P. De Jonghe, J. W. Griffin, K. H. Fischbeck, V. Timmerman, D. R. Cornblath & P. F. Chance (2004) DNA/RNA helicase gene mutations in a form of juvenile amyotrophic lateral sclerosis (ALS4). *American Journal of Human Genetics,* 74**,** 1128-1135.

Chew, J., T. F. Gendron, M. Prudencio, H. Sasaguri, Y.-J. Zhang, M. Castanedes-Casey, C. Lee, K. Jansen-West, A. Kurti, M. E. Murray, K. F. Bieniek, P. O. Bauer, E. C. Whitelaw, L. Rousseau, J. N. Stankowski, C. Stetler, L. M. Daughrity, E. A. Perkerson, P. Desaro, A. Johnston, K. Overstreet, D. Edbauer, R. Rademakers, K. B. Boylan, D. W. Dickson, J. D. Fryer & L. Petrucelli (2015) C9ORF72 repeat expansions in mice cause TDP-43 pathology, neuronal loss, and behavioral deficits. *Science,* 348**,** 1151-1154.

Chio, A., G. Borghero, G. Restagno, G. Mora, C. Drepper, B. J. Traynor, M. Sendtner, M. Brunetti, I. Ossola, A. Calvo, M. Pugliatti, M. A. Sotgiu, M. R. Murru, M. G.

Marrosu, F. Marrosu, K. Marinou, J. Mandrioli, P. Sola, C. Caponnetto, G. Mancardi, P. Mandich, V. La Bella, R. Spataro, A. Conte, M. R. Monsurro, G. Tedeschi, F. Pisano, I. Bartolomei, F. Salvi, G. L. Pinter, I. Simone, G. Logroscino, A. Gambardella, A. Quattrone, C. Lunetta, P. Volanti, M. Zollino, S. Penco, S. Battistini, A. E. Renton, E. Majounie, Y. Abramzon, F. L. Conforti, F. Giannini, M. Corbo, M. Sabatelli & I. Consortium (2012) Clinical characteristics of patients with familial amyotrophic lateral sclerosis carrying the pathogenic GGGGCC hexanucleotide repeat expansion of C9ORF72. *Brain,* 135**,** 784-793.

Chio, A., G. Logroscino, O. Hardiman, R. Swingler, D. Mitchell, E. Beghi, B. G. Traynor & C. Eurals (2009) Prognostic factors in ALS: A critical review. *Amyotrophic Lateral Sclerosis,* 10**,** 310-323.

Chow, C. Y., J. E. Landers, S. K. Bergen, P. C. Sapp, A. E. Grant, J. M. Jones, L. Everett, G. M. Lenk, D. M. McKenna-Yasek, L. S. Weisman, D. Figlewicz, R. H. Brown & M. H. Meisler (2009) Deleterious Variants of FIG4. a Phosphoinositide Phosphatase, in Patients with ALS. *American Journal of Human Genetics,* 84**,** 85-88.

Christian, M., T. Cermak, E. L. Doyle, C. Schmidt, F. Zhang, A. Hummel, A. J. Bogdanove & D. F. Voytas (2010) Targeting DNA Double-Strand Breaks with TAL Effector Nucleases. *Genetics,* 186**,** 757-U476.

Cirulli, E. T., B. N. Lasseigne, S. Petrovski, P. C. Sapp, P. A. Dion, C. S. Leblond, J. Couthouis, Y. F. Lu, Q. L. Wang, B. J. Krueger, Z. Ren, J. Keebler, Y. J. Han, S. E. Levy, B. E. Boone, J. R. Wimbish, L. L. Waite, A. L. Jones, J. P. Carulli, A. G. Day-Williams, J. F. Staropoli, W. W. Xin, A. Chesi, A. R. Raphael, D. McKenna-Yasek, J. Cady, J. de Jong, K. P. Kenna, B. N. Smith, S. Topp, J. Miller, A. Gkazi, A. Al-Chalabi, L. H. van den Berg, J. Veldink, V. Silani, N. Ticozzi, C. E. Shaw, R. H. Baloh, S. Appel, E. Simpson, C. Lagier-Tourenne, S. M. Pulst, S. Gibson, J. Q. Trojanowski, L. Elman, L. McCluskey, M. Grossman, N. A. Shneider, W. K. Chung, J. M. Ravits, J. D. Glass, K. B. Sims, V. M. Van Deerlin, T. Maniatis, S. D. Hayes, A. Ordureau, S. Swarup, J. Landers, F. Baas, A. S. Allen, R. S. Bedlack, J. W. Harper, A. D. Gitler, G. A. Rouleau, R. Brown, M. B. Harms, G. M. Cooper, T. Harris, R. M. Myers, D. B. Goldstein & F. S. Consortium (2015) Exome sequencing in amyotrophic lateral sclerosis identifies risk genes and pathways. *Science,* 347**,** 1436-1441.

Ciura, S., S. Lattante, I. Le Ber, M. Latouche, H. Tostivint, A. Brice & E. Kabashi (2013) Loss of Function of C9orf72 Causes Motor Deficits in a Zebrafish Model of Amyotrophic Lateral Sclerosis. *Annals of Neurology,* 74**,** 180-187.

Ciura, S., C. Sellier, M. L. Campanari, N. Charlet-Berguerand & E. Kabashi (2016) The most prevalent genetic cause of ALS-FTD, C9orf72 synergizes the toxicity of ATXN2 intermediate polyglutamine repeats through the autophagy pathway. *Autophagy,* 12**,** 1406-1408.

Clement, A. M., M. D. Nguyen, E. A. Roberts, M. L. Garcia, S. Boillee, M. Rule, A. P. McMahon, W. Doucette, D. Siwek, R. J. Ferrante, R. H. Brown, J. P. Julien, L. S. B. Goldstein & D. W. Cleveland (2003) Wild-type nonneuronal cells extend survival of SOD1 mutant motor neurons in ALS mice. *Science,* 302**,** 113-117.

Comley, L. H., J. Nijssen, J. Frost-Nylen & E. Hedlund (2016) Cross-disease comparison of amyotrophic lateral sclerosis and spinal muscular atrophy reveals conservation of selective vulnerability but differential neuromuscular junction pathology. *Journal of Comparative Neurology,* 524**,** 1424-1442.

Cooper-Knock, J., J. J. Bury, P. R. Heath, M. Wyles, A. Higginbottom, C. Gelsthorpe, J. R. Highley, G. Hautbergue, M. Rattray, J. Kirby & P. J. Shaw (2015) C9ORF72 GGGGCC Expanded Repeats Produce Splicing Dysregulation which Correlates with Disease Severity in Amyotrophic Lateral Sclerosis. *Plos One,* 10.

Cooper-Knock, J., A. Frolov, J. R. Highley, G. Charlesworth, J. Kirby, A. Milano, J. Hartley, P. G. Ince, C. J. McDermott, T. Lashley, T. Revesz, P. J. Shaw, N. W. Wood & O.

Bandmann (2013) C9ORF72 expansions, parkinsonism, and Parkinson disease A clinicopathologic study. *Neurology,* 81**,** 808-811.

Cooper-Knock, J., C. Hewitt, J. R. Highley, A. Brockington, A. Milano, S. Man, J. Martindale, J. Hartley, T. Walsh, C. Gelsthorpe, L. Baxter, G. Forster, M. Fox, J. Bury, K. Mok, C. J. McDermott, B. J. Traynor, J. Kirby, S. B. Wharton, P. G. Ince, J. Hardy & P. J. Shaw (2012) Clinico-pathological features in amyotrophic lateral sclerosis with expansions in C9ORF72. *Brain,* 135**,** 751-764.

Cooper-Knock, J., P. J. Shaw & J. Kirby (2014a) The widening spectrum of C9ORF72-related disease; genotype/phenotype correlations and potential modifiers of clinical phenotype. *Acta Neuropathologica,* 127**,** 333-345.

Cooper-Knock, J., M. J. Walsh, A. Higginbottom, J. Robin Highley, M. J. Dickman, D. Edbauer, P. G. Ince, S. B. Wharton, S. A. Wilson, J. Kirby, G. M. Hautbergue & P. J. Shaw (2014b) Sequestration of multiple RNA recognition motif-containing proteins by C9orf72 repeat expansions. *Brain : a journal of neurology,* 137**,** 2040-51.

Corcia, P., W. Camu, J. M. Halimi, P. Vourc'h, C. Antar, S. Vedrine, B. Giraudeau, B. de Toffol, C. R. Andres & A. L. S. S. G. French (2006) SMN1 gene, but not SMN2, is a risk factor for sporadic ALS. *Neurology,* 67**,** 1147-1150.

Cruts, M., I. Gijselinck, J. van der Zee, S. Engelborghs, H. Wils, D. Pirici, R. Rademakers, R. Vandenberghe, B. Dermaut, J.-J. Martin, C. van Duijn, K. Peeters, R. Sciot, P. Santens, T. De Pooter, M. Mattheijssens, M. Van den Broeck, I. Cuijt, K. l. Vennekens, P. P. De Deyn, S. Kumar-Singh & C. Van Broeckhoven (2006) Null mutations in progranulin cause ubiquitin-positive frontotemporal dementia linked to chromosome 17q21. *Nature,* 442**,** 920-924.

Da Costa, M. M. J., C. E. Allen, A. Higginbottom, T. Ramesh, P. J. Shaw & C. J. McDermott (2014) A new zebrafish model produced by TILLING of SOD1-related amyotrophic lateral sclerosis replicates key features of the disease and represents a tool for in vivo therapeutic screening. *Disease Models & Mechanisms,* 7**,** 73-81.

Damiano, M., A. A. Starkov, S. Petri, K. Kipiani, M. Kiaei, M. Mattiazzi, M. F. Beal & G. Manfredi (2006) Neural mitochondrial Ca2+ capacity impairment precedes the onset of motor symptoms in G93A Cu/Zn-superoxide dismutase mutant mice. *Journal of Neurochemistry,* 96**,** 1349-1361.

Darland, T. & J. E. Dowling (2001) Behavioral screening for cocaine sensitivity in mutagenized zebrafish. *Proceedings of the National Academy of Sciences of the United States of America,* 98**,** 11691-11696.

De Vos, K. J., A. L. Chapman, M. E. Tennant, C. Manser, E. L. Tudor, K.-F. Lau, J. Brownlees, S. Ackerley, P. J. Shaw, D. M. McLoughlin, C. E. Shaw, P. N. Leigh, C. C. J. Miller & A. J. Grierson (2007) Familial amyotrophic lateral sclerosis-linked SOD1 mutants perturb fast axonal transport to reduce axonal mitochondria content. *Human Molecular Genetics,* 16**,** 2720-2728.

DeJesus-Hernandez, M., I. R. Mackenzie, B. F. Boeve, A. L. Boxer, M. Baker, N. J. Rutherford, A. M. Nicholson, N. A. Finch, H. Flynn, J. Adamson, N. Kouri, A. Wojtas, P. Sengdy, G. Y. R. Hsiung, A. Karydas, W. W. Seeley, K. A. Josephs, G. Coppola, D. H. Geschwind, Z. K. Wszolek, H. Feldman, D. S. Knopman, R. C. Petersen, B. L. Miller, D. W. Dickson, K. B. Boylan, N. R. Graff-Radford & R. Rademakers (2011) Expanded GGGGCC Hexanucleotide Repeat in Noncoding Region of C9ORF72 Causes Chromosome 9p-Linked FTD and ALS. *Neuron,* 72**,** 245-256.

Deng, H.-X., W. Chen, S.-T. Hong, K. M. Boycott, G. H. Gorrie, N. Siddique, Y. Yang, F. Fecto, Y. Shi, H. Zhai, H. Jiang, M. Hirano, E. Rampersaud, G. H. Jansen, S. Donkervoort, E. H. Bigio, B. R. Brooks, K. Ajroud, R. L. Sufit, J. L. Haines, E. Mugnaini, M. A. Pericak-Vance & T. Siddique (2011) Mutations in UBQLN2 cause

dominant X-linked juvenile and adult-onset ALS and ALS/dementia. *Nature,* 477**,** 211-U113.

Deretic, V., T. Saitoh & S. Akira (2013) Autophagy in infection, inflammation and immunity. *Nature Reviews Immunology,* 13**,** 722-737.

Doble, A. (1996) The pharmacology and mechanism of action of riluzole. *Neurology,* 47**,** S233-S241.

Domenici, P. (2003) Habitat, body design and the swimming performance of fish. *Vertebrate Biomechanics and Evolution***,** 137-160.

Donnelly, C. J., P.-W. Zhang, J. T. Pham, A. R. Heusler, N. A. Mistry, S. Vidensky, E. L. Daley, E. M. Poth, B. Hoover, D. M. Fines, N. Maragakis, P. J. Tienari, L. Petrucelli, B. J. Traynor, J. Wang, F. Rigo, C. F. Bennett, S. Blackshaw, R. Sattler & J. D. Rothstein (2013) RNA Toxicity from the ALS/FTD C9ORF72 Expansion Is Mitigated by Antisense Intervention. *Neuron,* 80**,** 415-428.

Drapeau, P., L. Saint-Amant, R. R. Buss, M. Chong, J. R. McDearmid & E. Brustein (2002) Development of the locomotor network in zebrafish. *Progress in Neurobiology,* 68**,** 85-111.

Dreosti, E., G. Lopes, A. R. Kampff & S. W. Wilson (2015) Development of social behavior in young zebrafish. *Frontiers in Neural Circuits,* 9.

Egan, R. J., C. L. Bergner, P. C. Hart, J. M. Cachat, P. R. Canavello, M. F. Elegante, S. I. Elkhayat, B. K. Bartels, A. K. Tien, D. H. Tien, S. Mohnot, E. Beeson, E. Glasgow, H. Amri, Z. Zukowska & A. V. Kalueff (2009) Understanding behavioral and physiological phenotypes of stress and anxiety in zebrafish. *Behavioural Brain Research,* 205**,** 38-44.

Eisen, J. S. & J. C. Smith (2008) Controlling morpholino experiments: don't stop making antisense. *Development,* 135**,** 1735-1743.

Elden, A. C., H. J. Kim, M. P. Hart, A. S. Chen-Plotkin, B. S. Johnson, X. D. Fang, M. Armakola, F. Geser, R. Greene, M. M. Lu, A. Padmanabhan, D. Clay-Falcone, L. McCluskey, L. Elman, D. Juhr, P. J. Gruber, U. Rub, G. Auburger, J. Q. Trojanowski, V. M. Y. Lee, V. M. Van Deerlin, N. M. Bonini & A. D. Gitler (2010) Ataxin-2 intermediate-length polyglutamine expansions are associated with increased risk for ALS. *Nature,* 466**,** 1069-U77.

Farg, M. A., V. Sundaramoorthy, J. M. Sultana, S. Yang, R. A. K. Atkinson, V. Levina, M. A. Halloran, P. A. Gleeson, I. P. Blair, K. Y. Soo, A. E. King & J. D. Atkin (2014) C9ORF72, implicated in amytrophic lateral sclerosis and frontotemporal dementia, regulates endosomal trafficking. *Human Molecular Genetics,* 23**,** 3579-3595.

Fecto, F., J. H. Yan, S. P. Vemula, E. D. Liu, Y. Yang, W. J. Chen, J. G. Zheng, Y. Shi, N. Siddique, H. Arrat, S. Donkervoort, S. Ajroud-Driss, R. L. Sufit, S. L. Heller, H. X. Deng & T. Siddique (2011) SQSTM1 Mutations in Familial and Sporadic Amyotrophic Lateral Sclerosis. *Archives of Neurology,* 68**,** 1440-1446.

Ferraiuolo, L., J. Kirby, A. J. Grierson, M. Sendtner & P. J. Shaw (2011) Molecular pathways of motor neuron injury in amyotrophic lateral sclerosis. *Nature Reviews Neurology,* 7**,** 616-630.

Fischer, L. R., D. G. Culver, P. Tennant, A. A. Davis, M. S. Wang, A. Castellano-Sanchez, J. Khan, M. A. Polak & J. D. Glass (2004) Amyotrophic lateral sclerosis is a distal axonopathy: evidence in mice and man. *Experimental Neurology,* 185**,** 232-240.

Fischer, L. R. & J. D. Glass (2007) Axonal degeneration in motor neuron disease. *Neurodegenerative Diseases,* 4**,** 431-442.

Fratta, P., M. Poulter, T. Lashley, J. D. Rohrer, J. M. Polke, J. Beck, N. Ryan, D. Hensman, S. Mizielinska, A. J. Waite, M.-C. Lai, T. F. Gendron, L. Petrucelli, E. M. C. Fisher, T. Revesz, J. D. Warren, J. Collinge, A. M. Isaacs & S. Mead (2013) Homozygosity for the C9orf72 GGGGCC repeat expansion in frontotemporal dementia. *Acta Neuropathologica,* 126**,** 401-409.

Freischmidt, A., T. Wieland, B. Richter, W. Ruf, V. Schaeffer, K. Muller, N. Marroquin, F. Nordin, A. Hubers, P. Weydt, S. Pinto, R. Press, S. Millecamps, N. Molko, E. Bernard, C. Desnuelle, M. H. Soriani, J. Dorst, E. Graf, U. Nordstrom, M. S. Feiler, S. Putz, T. M. Boeckers, T. Meyer, A. S. Winkler, J. Winkelman, M. de Carvalho, D. R. Thal, M. Otto, T. Brannstrom, A. E. Volk, P. Kursula, K. M. Danzer, P. Lichtner, I. Dikic, T. Meitinger, A. C. Ludolph, T. M. Strom, P. M. Andersen & J. H. Weishaupt (2015) Haploinsufficiency of TBK1 causes familial ALS and fronto-temporal dementia. *Nature Neuroscience,* 18**,** 631-+.

Frey, D., C. Schneider, L. Xu, J. Borg, W. Spooren & P. Caroni (2000) Early and selective loss of neuromuscular synapse subtypes with low sprouting competence in motoneuron diseases. *Journal of Neuroscience,* 20**,** 2534-2542.

Fu, Y. F., J. A. Foden, C. Khayter, M. L. Maeder, D. Reyon, J. K. Joung & J. D. Sander (2013) High-frequency off-target mutagenesis induced by CRISPR-Cas nucleases in human cells. *Nature Biotechnology,* 31**,** 822-+.

Ganley, I. G., D. H. Lam, J. Wang, X. Ding, S. Chen & X. Jiang (2009) ULK1 center dot ATG13 center dot FIP200 Complex Mediates mTOR Signaling and Is Essential for Autophagy. *Journal of Biological Chemistry,* 284**,** 12297-12305.

Gendron, T. F., K. F. Bieniek, Y.-J. Zhang, K. Jansen-West, P. E. A. Ash, T. Caulfield, L. Daughrity, J. H. Dunmore, M. Castanedes-Casey, J. Chew, D. M. Cosio, M. van Blitterswijk, W. C. Lee, R. Rademakers, K. B. Boylan, D. W. Dickson & L. Petrucelli (2013) Antisense transcripts of the expanded C9ORF72 hexanucleotide repeat form nuclear RNA foci and undergo repeat-associated non-ATG translation in c9FTD/ALS. *Acta Neuropathologica,* 126**,** 829-844.

Gendron, T. F. & L. Petrucelli (2011) Rodent Models of TDP-43 Proteinopathy: Investigating the Mechanisms of TDP-43-Mediated Neurodegeneration. *Journal of Molecular Neuroscience,* 45**,** 486-499.

Gijselinck, I., T. Van Langenhove, J. van der Zee, K. Sleegers, S. Philtjens, G. Kleinberger, J. Janssens, K. Bettens, C. Van Cauwenberghe, S. Pereson, S. Engelborghs, A. Sieben, P. De Jonghe, R. Vandenberghe, P. Santens, J. De Bleecker, G. Maes, V. Baumer, L. Dillen, G. Joris, I. Cuijt, E. Corsmit, E. Elinck, J. Van Dongen, S. Vermeulen, M. Van den Broeck, C. Vaerenberg, M. Mattheijssens, K. Peeters, W. Robberecht, P. Cras, J. J. Martin, P. P. De Deyn, M. Cruts & C. Van Broeckhoven (2012) A C9orf72 promoter repeat expansion in a Flanders-Belgian cohort with disorders of the frontotemporal lobar degeneration-amyotrophic lateral sclerosis spectrum: a gene identification study. *Lancet Neurology,* 11**,** 54-65.

Gijselinck, I., S. Van Mossevelde, J. van der Zee, A. Sieben, S. Engelborghs, J. De Bleecker, A. Ivanoiu, O. Deryck, D. Edbauer, M. Zhang, B. Heeman, V. Baumer, M. Van den Broeck, M. Mattheijssens, K. Peeters, E. Rogaeva, P. De Jonghe, P. Cras, J. J. Martin, P. P. de Deyn, M. Cruts, C. Van Broeckhoven & C. Belneu (2016) The C9orf72 repeat size correlates with onset age of disease, DNA methylation and transcriptional downregulation of the promoter. *Molecular Psychiatry,* 21**,** 1112-1124.

Gilbert, M. J. H., T. C. Zerulla & K. B. Tierney (2014) Zebrafish (Danio rerio) as a model for the study of aging and exercise: Physical ability and trainability decrease with age. *Experimental Gerontology,* 50**,** 106-113.

Gizzi, M., A. Dirocco, M. Sivak & B. Cohen (1992) OCULAR MOTOR FUNCTION IN MOTOR-NEURON DISEASE. *Neurology,* 42**,** 1037-1046.

Gleason, C. E., A. Ordureau, R. Gourlay, J. S. C. Arthur & P. Cohen (2011) Polyubiquitin Binding to Optineurin Is Required for Optimal Activation of TANK-binding Kinase 1 and Production of Interferon beta. *Journal of Biological Chemistry,* 286**,** 35663-35674.

Gordon, S. P., Y. Y. Chen, K. Yamashita, C. Bejar, A. Wilshire & V. Cheung (2015) Sex-specific genetic differences in endurance swimming of Trinidadian guppies. *Ecology and Evolution,* 5**,** 5318-5328.

Gorrie, G. H., F. Fecto, D. Radzicki, C. Weiss, Y. Shi, H. Dong, H. Zhai, R. Fu, E. Liu, S. Li, H. Arrat, E. H. Bigio, J. F. Disterhoft, M. Martina, E. Mugnaini, T. Siddique & H.-X. Deng (2014) Dendritic spinopathy in transgenic mice expressing ALS/dementia-linked mutant UBQLN2. *Proceedings of the National Academy of Sciences of the United States of America,* 111**,** 14524-14529.

Greenbaum, D., C. Colangelo, K. Williams & M. Gerstein (2003) Comparing protein abundance and mRNA expression levels on a genomic scale. *Genome Biology,* 4.

Greenway, M. J., P. M. Andersen, C. Russ, S. Ennis, S. Cashman, C. Donaghy, V. Patterson, R. Swingler, D. Kieran, J. Prehn, K. E. Morrison, A. Green, K. R. Acharya, R. H. Brown & O. Hardiman (2006) ANG mutations segregate with familial and 'sporadic' amyotrophic lateral sclerosis. *Nature Genetics,* 38**,** 411-413.

Guo, H., L. Lai, M. E. R. Butchbach, M. P. Stockinger, X. Shan, G. A. Bishop & C. Lin (2003) Increased expression of the glial glutamate transporter EAAT2 modulates excitotoxicity and delays the onset but not the outcome of ALS in mice. *Society for Neuroscience Abstract Viewer and Itinerary Planner,* 2003**,** Abstract No. 96.9-Abstract No. 96.9.

Gurney, M. E., H. F. Pu, A. Y. Chiu, M. C. Dalcanto, C. Y. Polchow, D. D. Alexander, J. Caliendo, A. Hentati, Y. W. Kwon, H. X. Deng, W. J. Chen, P. Zhai, R. L. Sufit & T. Siddique (1994) MOTOR-NEURON DEGENERATION IN MICE THAT EXPRESS A HUMAN CU,ZN SUPEROXIDE-DISMUTASE MUTATION. *Science,* 264**,** 1772-1775.

Haeusler, A. R., C. J. Donnelly, G. Periz, E. A. J. Simko, P. G. Shaw, M.-S. Kim, N. J. Maragakis, J. C. Troncoso, A. Pandey, R. Sattler, J. D. Rothstein & J. Wang (2014) C9orf72 nucleotide repeat structures initiate molecular cascades of disease. *Nature,* 507**,** 195-+.

Hand, C. K., J. Khoris, F. Salachas, F. Gros-Louis, A. A. S. Lopes, V. Mayeux-Portas, R. H. Brown, V. Meininger, W. Camu & G. A. Rouleau (2002) A novel locus for familial amyotrophic lateral sclerosis, on chromosome 18q. *American Journal of Human Genetics,* 70**,** 251-256.

Hara, T., K. Nakamura, M. Matsui, A. Yamamoto, Y. Nakahara, R. Suzuki-Migishima, M. Yokoyama, K. Mishima, I. Saito, H. Okano & N. Mizushima (2006) Suppression of basal autophagy in neural cells causes neurodegenerative disease in mice. *Nature,* 441**,** 885-889.

Hara, T., A. Takamura, C. Kishi, S.-i. Iemura, T. Natsume, J.-L. Guan & N. Mizushima (2008) FIP200, a ULK-interacting protein, is required for autophagosome formation in mammalian cells. *Journal of Cell Biology,* 181**,** 497-510.

Harms, M. B., J. Cady, C. Zaidman, P. Cooper, T. Bali, P. Allred, C. Cruchaga, M. Baughn, R. T. Libby, A. Pestronk, A. Goate, J. Ravits & R. H. Baloh (2013) Lack of C9ORF72 coding mutations supports a gain of function for repeat expansions in amyotrophic lateral sclerosis. *Neurobiology of Aging,* 34.

Harris, H. & D. C. Rubinsztein (2012) Control of autophagy as a therapy for neurodegenerative disease. *Nature Reviews Neurology,* 8**,** 108-117.

He, C., C. R. Bartholomew, W. Zhou & D. J. Klionsky (2009) Assaying autophagic activity in transgenic GFP-Lc3 and GFP-Gabarap zebrafish embryos. *Autophagy,* 5**,** 520-526.

He, C. & D. J. Klionsky (2010) Analyzing autophagy in zebrafish. *Autophagy,* 6**,** 642-644.

Herbomel, P., B. Thisse & C. Thisse (1999) Ontogeny and behaviour of early macrophages in the zebrafish embryo. *Development,* 126**,** 3735-3745.

Hewamadduma, C. A. A., A. J. Grierson, T. P. Ma, L. Pan, C. B. Moens, P. W. Ingham, T. Ramesh & P. J. Shaw (2013) Tardbpl splicing rescues motor neuron and axonal

development in a mutant tardbp zebrafish. *Human Molecular Genetics,* 22**,** 2376-2386.

Hicks, G. G., N. Singh, A. Nashabi, S. Mai, G. Bozek, L. Klewes, D. Arapovic, E. K. White, M. J. Koury, E. M. Oltz, L. Van Kaer & H. E. Ruley (2000) Fus deficiency in mice results in defective B-lymphocyte development and activation, high levels of chromosomal instability and perinatal death. *Nature Genetics,* 24**,** 175-179.

Hodges, J. R., R. Davies, J. Xuereb, J. Kril & G. Halliday (2003) Survival in frontotemporal dementia. *Neurology,* 61**,** 349-354.

Honda, S., S. Arakawa, Y. Nishida, H. Yamaguchi, E. Ishii & S. Shimizu (2014) Ulk1-mediated Atg5-independent macroautophagy mediates elimination of mitochondria from embryonic reticulocytes. *Nature Communications,* 5.

Howe, K., M. D. Clark, C. F. Torroja, J. Torrance, C. Berthelot, M. Muffato, J. E. Collins, S. Humphray, K. McLaren, L. Matthews, S. McLaren, I. Sealy, M. Caccamo, C. Churcher, C. Scott, J. C. Barrett, R. Koch, G.-J. Rauch, S. White, W. Chow, B. Kilian, L. T. Quintais, J. A. Guerra-Assuncao, Y. Zhou, Y. Gu, J. Yen, J.-H. Vogel, T. Eyre, S. Redmond, R. Banerjee, J. Chi, B. Fu, E. Langley, S. F. Maguire, G. K. Laird, D. Lloyd, E. Kenyon, S. Donaldson, H. Sehra, J. Almeida-King, J. Loveland, S. Trevanion, M. Jones, M. Quail, D. Willey, A. Hunt, J. Burton, S. Sims, K. McLay, B. Plumb, J. Davis, C. Clee, K. Oliver, R. Clark, C. Riddle, D. Eliott, G. Threadgold, G. Harden, D. Ware, B. Mortimer, G. Kerry, P. Heath, B. Phillimore, A. Tracey, N. Corby, M. Dunn, C. Johnson, J. Wood, S. Clark, S. Pelan, G. Griffiths, M. Smith, R. Glithero, P. Howden, N. Barker, C. Stevens, J. Harley, K. Holt, G. Panagiotidis, J. Lovell, H. Beasley, C. Henderson, D. Gordon, K. Auger, D. Wright, J. Collins, C. Raisen, L. Dyer, K. Leung, L. Robertson, K. Ambridge, D. Leongamornlert, S. McGuire, R. Gilderthorp, C. Griffiths, D. Manthravadi, S. Nichol, G. Barker, S. Whitehead, M. Kay, et al. (2013) The zebrafish reference genome sequence and its relationship to the human genome. *Nature,* 496**,** 498-503.

Howland, D. S., J. Liu, Y. J. She, B. Goad, N. J. Maragakis, B. Kim, J. Erickson, J. Kulik, L. DeVito, G. Psaltis, L. J. DeGennaro, D. W. Cleveland & J. D. Rothstein (2002) Focal loss of the glutamate transporter EAAT2 in a transgenic rat model of SOD1 mutant-mediated amyotrophic lateral sclerosis (ALS). *Proceedings of the National Academy of Sciences of the United States of America,* 99**,** 1604-1609.

Hruscha, A., P. Krawitz, A. Rechenberg, V. Heinrich, J. Hecht, C. Haass & B. Schmid (2013) Efficient CRISPR/Cas9 genome editing with low off-target effects in zebrafish. *Development,* 140**,** 4982-4987.

Hsiung, G.-Y. R., M. DeJesus-Hernandez, H. H. Feldman, P. Sengdy, P. Bouchard-Kerr, E. Dwosh, R. Butler, B. Leung, A. Fok, N. J. Rutherford, M. Baker, R. Rademakers & I. R. A. Mackenzie (2012) Clinical and pathological features of familial frontotemporal dementia caused by C9ORF72 mutation on chromosome 9p. *Brain,* 135**,** 709-722.

Huebers, A., N. Marroquin, B. Schmoll, S. Vielhaber, M. Just, B. Mayer, J. Hoegel, J. Dorst, T. Mertens, W. Just, A. Aulitzky, V. Wais, A. C. Ludolph, C. Kubisch, J. H. Weishaupt & A. E. Volk (2014) Polymerase chain reaction and Southern blot-based analysis of the C9orf72 hexanucleotide repeat in different motor neuron diseases. *Neurobiology of Aging,* 35.

Hutagalung, A. H. & P. J. Novick (2011) Role of Rab GTPases in Membrane Traffic and Cell Physiology. *Physiological Reviews,* 91**,** 119-149.

Hutton, M., C. L. Lendon, P. Rizzu, M. Baker, S. Froelich, H. Houlden, S. Pickering-Brown, S. Chakraverty, A. Isaacs, A. Grover, J. Hackett, J. Adamson, S. Lincoln, D. Dickson, P. Davies, R. C. Petersen, M. Stevens, E. de Graaff, E. Wauters, J. van Baren, M. Hillebrand, M. Joosse, J. M. Kwon, P. Nowotny, L. K. Che, J. Norton, J. C. Morris, L. A. Reed, J. Trojanowski, H. Basun, L. Lannfelt, M. Neystat, S. Fahn, F. Dark, T.

Tannenberg, P. R. Dodd, N. Hayward, J. B. J. Kwok, P. R. Schofield, A. Andreadis, J. Snowden, D. Craufurd, D. Neary, F. Owen, B. A. Oostra, J. Hardy, A. Goate, J. van Swieten, D. Mann, T. Lynch & P. Heutink (1998) Association of missense and 5 '-splice-site mutations in tau with the inherited dementia FTDP-17. *Nature,* 393**,** 702-705.

Hwang, W. Y., Y. F. Fu, D. Reyon, M. L. Maeder, S. Q. Tsai, J. D. Sander, R. T. Peterson, J. R. J. Yeh & J. K. Joung (2013) Efficient genome editing in zebrafish using a CRISPR-Cas system. *Nature Biotechnology,* 31**,** 227-229.

Imbert, G., F. Saudou, G. Yvert, D. Devys, Y. Trottier, J. M. Garnier, C. Weber, J. L. Mandel, G. Cancel, N. Abbas, A. Durr, O. Didierjean, G. Stevanin, Y. Agid & A. Brice (1996) Cloning of the gene for spinocerebellar ataxia 2 reveals a locus with high sensitivity to expanded CAG/glutamine repeats. *Nature Genetics,* 14**,** 285-291.

Ince, P. G., J. Lowe & P. J. Shaw (1998) Amyotrophic lateral sclerosis: current issues in classification, pathogenesis and molecular pathology. *Neuropathology and Applied Neurobiology,* 24**,** 104-117.

Jeong, J. Y., H. B. Kwon, J. C. Ahn, D. Kang, S. H. Kwon, J. A. Park & K. W. Kim (2008) Functional and developmental analysis of the blood-brain barrier in zebrafish. *Brain Research Bulletin,* 75**,** 619-628.

Jiang, J., Q. Zhu, T. F. Gendron, S. Saberi, M. McAlonis-Downes, A. Seelman, J. E. Stauffer, P. Jafar-nejad, K. Drenner, D. Schulte, S. Chun, S. Sun, S.-C. Ling, B. Myers, J. Engelhardt, M. Katz, M. Baughn, O. Platoshyn, M. Marsala, A. Watt, C. J. Heyser, M. C. Ard, L. De Muynck, L. M. Daughrity, D. A. Swing, L. Tessarollo, C. J. Jung, A. Delpoux, D. T. Utzschneider, S. M. Hedrick, P. J. de Jong, D. Edbauer, P. Van Damme, L. Petrucelli, C. E. Shaw, C. F. Bennett, S. Da Cruz, J. Ravits, F. Rigo, D. W. Cleveland & C. Lagier-Tourenne (2016) Gain of Toxicity from ALS/FTD-Linked Repeat Expansions in C9ORF72 Is Alleviated by Antisense Oligonucleotides Targeting GGGGCC-Containing RNAs. *Neuron,* 90**,** 535-550.

Johnson, J. O., J. Mandrioli, M. Benatar, Y. Abramzon, V. M. Van Deerlin, J. Q. Trojanowski, J. R. Gibbs, M. Brunetti, S. Gronka, J. Wuu, J. Ding, L. McCluskey, M. Martinez-Lage, D. Falcone, D. G. Hernandez, S. Arepalli, S. Chong, J. C. Schymick, J. Rothstein, F. Landi, Y.-D. Wang, A. Calvo, G. Mora, M. Sabatelli, M. R. Monsurro, S. Battistini, F. Salvi, R. Spataro, P. Sola, G. Borghero, G. Galassi, S. W. Scholz, J. P. Taylor, G. Restagno, A. Chio, B. J. Traynor & I. Consortium (2010) Exome Sequencing Reveals VCP Mutations as a Cause of Familial ALS. *Neuron,* 68**,** 857-864.

Johnson, J. O., E. P. Pioro, A. Boehringer, R. Chia, H. Feit, A. E. Renton, H. A. Pliner, Y. Abramzon, G. Marangi, B. J. Winborn, J. R. Gibbs, M. A. Nalls, S. Morgan, M. Shoai, J. Hardy, A. Pittman, R. W. Orrell, A. Malaspina, K. C. Sidle, P. Fratta, M. B. Harms, R. H. Baloh, A. Pestronk, C. C. Weihl, E. Rogaeva, L. Zinman, V. E. Drory, G. Borghero, G. Mora, A. Calvo, J. D. Rothstein, C. Drepper, M. Sendtner, A. B. Singleton, J. P. Taylor, M. R. Cookson, G. Restagno, M. Sabatelli, R. Bowser, A. Chio, B. J. Traynor & Italsgen (2014) Mutations in the Matrin 3 gene cause familial amyotrophic lateral sclerosis. *Nature Neuroscience,* 17**,** 664-+.

Johnston, C. A., B. R. Stanton, M. R. Turner, R. Gray, A. H.-M. Blunt, D. Butt, M.-A. Ampong, C. E. Shaw, P. N. Leigh & A. Al-Chalabi (2006) Amyotrophic lateral sclerosis in an urban setting - A population based study of inner city London. *Journal of Neurology,* 253**,** 1642-1643.

Joung, J. K. & J. D. Sander (2013) INNOVATION TALENs: a widely applicable technology for targeted genome editing. *Nature Reviews Molecular Cell Biology,* 14**,** 49-55.

Jung, C. H., C. B. Jun, S.-H. Ro, Y.-M. Kim, N. M. Otto, J. Cao, M. Kundu & D.-H. Kim (2009) ULK-Atg13-FIP200 Complexes Mediate mTOR Signaling to the Autophagy Machinery. *Molecular Biology of the Cell,* 20**,** 1992-2003.

Kabashi, E., N. Champagne, E. Brustein & P. Drapeau (2010a) In the swim of things: recent insights to neurogenetic disorders from zebrafish. *Trends in Genetics,* 26**,** 373-381.

Kabashi, E., L. Lin, M. L. Tradewell, P. A. Dion, V. Bercier, P. Bourgouin, D. Rochefort, S. B. Hadj, H. D. Durham, C. V. Velde, G. A. Rouleau & P. Drapeau (2010b) Gain and loss of function of ALS-related mutations of TARDBP (TDP-43) cause motor deficits in vivo. *Human Molecular Genetics,* 19**,** 671-683.

Kalueff, A. V., M. Gebhardt, A. M. Stewart, J. M. Cachat, M. Brimmer, J. S. Chawla, C. Craddock, E. J. Kyzar, A. Roth, S. Landsman, S. Gaikwad, K. Robinson, E. Baatrup, K. Tierney, A. Shamchuk, W. Norton, N. Miller, T. Nicolson, O. Braubach, C. P. Gilman, J. Pittman, D. B. Rosemberg, R. Gerlai, D. Echevarria, E. Lamb, S. C. F. Neuhauss, W. Weng, L. Bally-Cuif, H. Schneider & Znrc (2013) Towards a Comprehensive Catalog of Zebrafish Behavior 1.0 and Beyond. *Zebrafish,* 10**,** 70-86.

Kalueff, A. V., A. M. Stewart & R. Gerlai (2014) Zebrafish as an emerging model for studying complex brain disorders. *Trends in Pharmacological Sciences,* 35**,** 63-75.

Kang, S. H., Y. Li, M. Fukaya, I. Lorenzini, D. W. Cleveland, L. W. Ostrow, J. D. Rothstein & D. E. Bergles (2013) Degeneration and impaired regeneration of gray matter oligodendrocytes in amyotrophic lateral sclerosis. *Nature Neuroscience,* 16**,** 571-+.

Karam, C., S. N. Scelsa & D. J. L. MacGowan (2010) The clinical course of progressive bulbar palsy. *Amyotrophic Lateral Sclerosis,* 11**,** 364-368.

Kenna, K. P., R. L. McLaughlin, S. Byrne, M. Elamin, M. Heverin, E. M. Kenny, P. Cormican, D. W. Morris, C. G. Donaghy, D. G. Bradley & O. Hardiman (2013) Delineating the genetic heterogeneity of ALS using targeted high-throughput sequencing. *Journal of Medical Genetics,* 50**,** 776-783.

Kieran, D., M. Hafezparast, S. Bohnert, J. R. T. Dick, J. Martin, G. Schiavo, E. M. C. Fisher & L. Greensmith (2005) A mutation in dynein rescues axonal transport defects and extends the life span of ALS mice. *Journal of Cell Biology,* 169**,** 561-567.

Kiernan, M. C., S. Vucic, B. C. Cheah, M. R. Turner, A. Eisen, O. Hardiman, J. R. Burrell & M. C. Zoing (2011) Amyotrophic lateral sclerosis. *Lancet,* 377**,** 942-955.

Kim, H. J., N. C. Kim, Y. D. Wang, E. A. Scarborough, J. Moore, Z. Diaz, K. S. MacLea, B. Freibaum, S. Q. Li, A. Molliex, A. P. Kanagaraj, R. Carter, K. B. Boylan, A. M. Wojtas, R. Rademakers, J. L. Pinkus, S. A. Greenberg, J. Q. Trojanowski, B. J. Traynor, B. N. Smith, S. Topp, A. S. Gkazi, J. Miller, C. E. Shaw, M. Kottlors, J. Kirschner, A. Pestronk, Y. R. Li, A. F. Ford, A. D. Gitler, M. Benatar, O. D. King, V. E. Kimonis, E. D. Ross, C. C. Weihl, J. Shorter & J. P. Taylor (2013) Mutations in prion-like domains in hnRNPA2B1 and hnRNPA1 cause multisystem proteinopathy and ALS. *Nature,* 495**,** 467-+.

Kimmel, C. B., W. W. Ballard, S. R. Kimmel, B. Ullmann & T. F. Schilling (1995) STAGES OF EMBRYONIC-DEVELOPMENT OF THE ZEBRAFISH. *Developmental Dynamics,* 203**,** 253-310.

Klionsky, D. J., F. C. Abdalla, H. Abeliovich, R. T. Abraham, A. Acevedo-Arozena, K. Adeli, L. Agholme, M. Agnello, P. Agostinis, J. A. Aguirre-Ghiso, H. J. Ahn, O. Ait-Mohamed, S. Ait-Si-Ali, T. Akematsu, S. Akira, H. M. Al-Younes, M. A. Al-Zeer, M. L. Albert, R. L. Albin, J. Alegre-Abarrategui, M. F. Aleo, M. Alirezaei, A. Almasan, M. Almonte-Becerril, A. Amano, R. Amaravadi, S. Amarnath, A. O. Amer, N. Andrieu-Abadie, V. Anantharam, D. K. Ann, S. Anoopkumar-Dukie, H. Aoki, N. Apostolova, G. Arancia, J. P. Aris, K. Asanuma, N. Y. O. Asare, H. Ashida, V. Askanas, D. S. Askew, P. Auberger, M. Baba, S. K. Backues, E. H. Baehrecke, B. A. Bahr, X.-Y. Bai, Y. Bailly, R. Baiocchi, G. Baldini, W. Balduini, A. Ballabio, B. A. Bamber, E. T. W. Bampton, G. Banhegyi, C. R. Bartholomew, D. C. Bassham, R. C. Bast, Jr., H. Batoko, B.-H. Bay, I. Beau, D. M. Bechet, T. J. Begley, C. Behl, C. Behrends, S. Bekri, B. Bellaire, L. J. Bendall, L. Benetti, L. Berliocchi, H. Bernardi, F. Bernassola, S. Besteiro, I. Bhatia-Kissova, X. Bi, M. Biard-Piechaczyk, J. S. Blum,

L. H. Boise, P. Bonaldo, D. L. Boone, B. C. Bornhauser, K. R. Bortoluci, I. Bossis, F. Bost, J.-P. Bourquin, P. Boya, M. Boyer-Guittaut, P. V. Bozhkov, N. R. Brady, C. Brancolini, A. Brech, J. E. Brenman, A. Brennand, E. H. Bresnick, P. Brest, D. Bridges, M. L. Bristol, P. S. Brookes, E. J. Brown, J. H. Brumell, et al. (2012) Guidelines for the use and interpretation of assays for monitoring autophagy. *Autophagy,* 8**,** 445-544.

Klionsky, D. J., K. Abdelmohsen, A. Abe, M. J. Abedin, H. Abeliovich, A. A. Arozena, H. Adachi, C. M. Adams, P. D. Adams, K. Adeli, P. J. Adhihetty, S. G. Adler, G. Agam, R. Agarwal, M. K. Aghi, M. Agnello, P. Agostinis, P. V. Aguilar, J. Aguirre-Ghiso, E. M. Airoldi, S. Ait-Si-Ali, T. Akematsu, E. T. Akporiaye, M. Al-Rubeai, G. M. Albaiceta, C. Albanese, D. Albani, M. L. Albert, J. Aldudo, H. Alguel, M. Alirezaei, I. Alloza, A. Almasan, M. Almonte-Beceril, E. S. Alnemri, C. Alonso, N. Altan-Bonnet, D. C. Altieri, S. Alvarez, L. Alvarez-Erviti, S. Alves, G. Amadoro, A. Amano, C. Amantini, S. Ambrosio, I. Amelio, A. O. Amer, M. Amessou, A. Amon, Z. An, F. A. Anania, S. U. Andersen, U. P. Andley, C. K. Andreadi, N. Andrieu-Abadie, A. Anel, D. K. Ann, S. Anoopkumar-Dukie, M. Antonioli, H. Aoki, N. Apostolova, S. Aquila, K. Aquilano, K. Araki, E. Arama, A. Aranda, J. Araya, A. Arcaro, E. Arias, H. Arimoto, A. R. Ariosa, J. L. Armstrong, T. Arnould, I. Arsov, K. Asanuma, V. Askanas, E. Asselin, R. Atarashi, S. S. Atherton, J. D. Atkin, L. D. Attardi, P. Auberger, G. Auburger, L. Aurelian, R. Autelli, L. Avagliano, M. L. Avantaggiati, L. Avrahami, S. Awale, N. Azad, T. Bachetti, J. M. Backer, D.-H. Bae, J.-S. Bae, O.-N. Bae, S. H. Bae, E. H. Baehrecke, S.-H. Baek, S. Baghdiguian, A. Bagniewska-Zadworna, et al. (2016) Guidelines for the use and interpretation of assays for monitoring autophagy (3rd edition). *Autophagy,* 12**,** 1-222.

Kloepper, T. H., N. Kienle, D. Fasshauer & S. Munro (2012) Untangling the evolution of Rab G proteins: implications of a comprehensive genomic analysis. *Bmc Biology,* 10.

Kok, F. O., M. Shin, C.-W. Ni, A. Gupta, A. S. Grosse, A. van Impel, B. C. Kirchmaier, J. Peterson-Maduro, G. Kourkoulis, I. Male, D. F. DeSantis, S. Sheppard-Tindell, L. Ebarasi, C. Betsholtz, S. Schulte-Merker, S. A. Wolfe & N. D. Lawson (2015) Reverse Genetic Screening Reveals Poor Correlation between Morpholino-Induced and Mutant Phenotypes in Zebrafish. *Developmental Cell,* 32**,** 97-108.

Komatsu, M., S. Waguri, T. Chiba, S. Murata, J. Iwata, I. Tanida, T. Ueno, M. Koike, Y. Uchiyama, E. Kominami & K. Tanaka (2006) Loss of autophagy in the central nervous system causes neurodegeneration in mice. *Nature,* 441**,** 880-884.

Koppers, M., A. M. Blokhuis, H.-J. Westeneng, M. L. Terpstra, C. A. C. Zundel, R. V. de Sa, R. D. Schellevis, A. J. Waite, D. J. Blake, J. H. Veldink, L. H. van den Berg & R. J. Pasterkamp (2015) C9orf72 ablation in mice does not cause motor neuron degeneration or motor deficits. *Annals of Neurology,* 78**,** 426-438.

Kurosaki, T. & L. E. Maquat (2016) Nonsense-mediated mRNA decay in humans at a glance. *Journal of Cell Science,* 129**,** 461-467.

Kwiatkowski, T. J., Jr., D. A. Bosco, A. L. LeClerc, E. Tamrazian, C. R. Vanderburg, C. Russ, A. Davis, J. Gilchrist, E. J. Kasarskis, T. Munsat, P. Valdmanis, G. A. Rouleau, B. A. Hosler, P. Cortelli, P. J. de Jong, Y. Yoshinaga, J. L. Haines, M. A. Pericak-Vance, J. Yan, N. Ticozzi, T. Siddique, D. McKenna-Yasek, P. C. Sapp, H. R. Horvitz, J. E. Landers & R. H. Brown, Jr. (2009) Mutations in the FUS/TLS Gene on Chromosome 16 Cause Familial Amyotrophic Lateral Sclerosis. *Science,* 323**,** 1205-1208.

La Spada, A. R. & J. P. Taylor (2010) Repeat expansion disease: progress and puzzles in disease pathogenesis. *Nature Reviews Genetics,* 11**,** 247-258.

Laaksovirta, H., T. Peuralinna, J. C. Schymick, S. W. Scholz, S. L. Lai, L. Myllykangas, R. Sulkava, L. Jansson, D. G. Hernandez, J. R. Gibbs, M. A. Nalls, D. Heckerman, P. J.

Tienari & B. J. Traynor (2010) Chromosome 9p21 in amyotrophic lateral sclerosis in Finland: a genome-wide association study. *Lancet Neurology,* 9**,** 978-985.

Lacomblez, L., G. Bensimon, P. N. Leigh, P. Guillet & V. Meininger (1996) Dose-ranging study of riluzole in amyotrophic lateral sclerosis. *Lancet,* 347**,** 1425-1431.

Lagier-Tourenne, C., M. Baughn, F. Rigo, S. Sun, P. Liu, H.-R. Li, J. Jiang, A. T. Watt, S. Chun, M. Katz, J. Qiu, Y. Sun, S.-C. Ling, Q. Zhu, M. Polymenidou, K. Drenner, J. W. Artates, M. McAlonis-Downes, S. Markmiller, K. R. Hutt, D. P. Pizzo, J. Cady, M. B. Harms, R. H. Baloh, S. R. Vandenberg, G. W. Yeo, X.-D. Fu, C. F. Bennett, D. W. Cleveland & J. Ravits (2013) Targeted degradation of sense and antisense C9orf72 RNA foci as therapy for ALS and frontotemporal degeneration. *Proceedings of the National Academy of Sciences of the United States of America,* 110**,** E4530-E4539.

Laird, F. M., M. H. Farah, S. Ackerley, A. Hoke, N. Maragakis, J. D. Rothstein, J. Griffin, D. L. Price, L. J. Martin & P. C. Wong (2008) Motor neuron disease occurring in a mutant dynactin mouse model is characterized by defects in vesicular trafficking. *Journal of Neuroscience,* 28**,** 1997-2005.

Langerhans, R. B. (2009) Trade-off between steady and unsteady swimming underlies predator-driven divergence in Gambusia affinis. *Journal of Evolutionary Biology,* 22**,** 1057-1075.

Larson, M. H., L. A. Gilbert, X. Wang, W. A. Lim, J. S. Weissman & L. S. Qi (2013) CRISPR interference (CRISPRi) for sequence-specific control of gene expression. *Nature Protocols,* 8**,** 2180-2196.

Lattante, S., S. Ciura, G. A. Rouleau & E. Kabashi (2015a) Defining the genetic connection linking amyotrophic lateral sclerosis (ALS) with frontotemporal dementia (FTD). *Trends in Genetics,* 31**,** 263-273.

Lattante, S., H. de Calbiac, I. Le Ber, A. Brice, S. Ciura & E. Kabashi (2015b) Sqstm1 knock-down causes a locomotor phenotype ameliorated by rapamycin in a zebrafish model of ALS/FTLD. *Human Molecular Genetics,* 24**,** 1682-1690.

Lee, Y.-B., H.-J. Chen, João N. Peres, J. Gomez-Deza, J. Attig, M. talekar, C. Troakes, Agnes L. Nishimura, Emma L. Scotter, C. Vance, Y. Adachi, V. Sardone, Jack W. Miller, Bradley N. Smith, J.-M. Gallo, J. Ule, F. Hirth, B. Rogelj, C. Houart & Christopher E. Shaw (2013) Hexanucleotide Repeats in ALS/FTD Form Length-Dependent RNA Foci, Sequester RNA Binding Proteins, and Are Neurotoxic. *Cell Reports,* 5**,** 1178-1186.

Leigh, P. N., B. H. Anderton, A. Dodson, J. M. Gallo, M. Swash & D. M. Power (1988) UBIQUITIN DEPOSITS IN ANTERIOR HORN CELLS IN MOTOR NEURON DISEASE. *Neuroscience Letters,* 93**,** 197-203.

Leigh, P. N., A. Dodson, M. Swash, J. P. Brion & B. H. Anderton (1989) CYTOSKELETAL ABNORMALITIES IN MOTOR NEURON DISEASE - AN IMMUNOCYTOCHEMICAL STUDY. *Brain,* 112**,** 521-535.

Levin, E. D., Z. Bencan & D. T. Cerutti (2007) Anxiolytic effects of nicotine in zebrafish. *Physiology & Behavior,* 90**,** 54-58.

Levine, T. P., R. D. Daniels, A. T. Gatta, L. H. Wong & M. J. Hayes (2013) The product of C9orf72, a gene strongly implicated in neurodegeneration, is structurally related to DENN Rab-GEFs. *Bioinformatics,* 29**,** 499-503.

Levivier, E., B. Goud, M. Souchet, T. P. G. Calmels, J. P. Mornon & I. Callebaut (2001) uDENN, DENN, and dDENN: Indissociable domains in Rab and MAP kinases signaling pathways. *Biochemical and Biophysical Research Communications,* 287**,** 688-695.

Li, Q., A. Lau, T. J. Morris, L. Guo, C. B. Fordyce & E. F. Stanley (2004) A syntaxin 1, G alpha(o), and N-type calcium channel complex at a presynaptic nerve terminal:

Analysis by quantitative immunocolocalization. *Journal of Neuroscience,* 24**,** 4070-4081.

Li, X. & W. D. Heyer (2008) Homologous recombination in DNA repair and DNA damage tolerance. *Cell Research,* 18**,** 99-113.

Li, Y., Y. Guo, X. Wang, X. Yu, W. Duan, K. Hong, J. Wang, H. Han & C. Li (2015) TREHALOSE DECREASES MUTANT SOD1 EXPRESSION AND ALLEVIATES MOTOR DEFICIENCY IN EARLY BUT NOT END-STAGE AMYOTROPHIC LATERAL SCLEROSIS IN A SOD1-G93A MOUSE MODEL. *Neuroscience,* 298**,** 12-25.

Liang, C.-C., C. Wang, X. Peng, B. Gan & J.-L. Guan (2010) Neural-specific Deletion of FIP200 Leads to Cerebellar Degeneration Caused by Increased Neuronal Death and Axon Degeneration. *Journal of Biological Chemistry,* 285**,** 3499-3509.

Lieber, M. R. (2010) The Mechanism of Double-Strand DNA Break Repair by the Nonhomologous DNA End-Joining Pathway. *Annual Review of Biochemistry, Vol 79,* 79**,** 181-211.

Lieschke, G. J. & P. D. Currie (2007) Animal models of human disease: zebrafish swim into view. *Nature Reviews Genetics,* 8**,** 353-367.

Lillo, P., B. Garcin, M. Hornberger, T. H. Bak & J. R. Hodges (2010) Neurobehavioral Features in Frontotemporal Dementia With Amyotrophic Lateral Sclerosis. *Archives of Neurology,* 67**,** 826-830.

Lindlof, A. (2003) Gene identification through large-scale EST sequence processing. *Applied bioinformatics,* 2**,** 123-9.

Link, V., A. Shevchenko & C. P. Heisenberg (2006) Proteomics of early zebrafish embryos. *Bmc Developmental Biology,* 6.

Liu, E. Y., J. Russ, K. Wu, D. Neal, E. Suh, A. G. McNally, D. J. Irwin, V. M. Van Deerlin & E. B. Lee (2014) C9orf72 hypermethylation protects against repeat expansion-associated pathology in ALS/FTD. *Acta Neuropathologica,* 128**,** 525-541.

Liu, F., Q. Liu, C. X. Lu, B. Cui, X. N. Guo, R. R. Wang, M. S. Liu, X. G. Li, L.-Y. Cui & X. Zhang (2016) Identification of a novel loss-of-function C9orf72 splice site mutation in a patient with amyotrophic lateral sclerosis. *Neurobiology of Aging,* 47.

Logroscino, G., B. J. Traynor, O. Hardiman, A. Chio, D. Mitchell, R. J. Swingler, A. Millul, E. Benn, E. Beghi & Eurals (2010) Incidence of amyotrophic lateral sclerosis in Europe. *Journal of Neurology Neurosurgery and Psychiatry,* 81**,** 385-390.

Lomen-Hoerth, C., S. Langmore, M. Cotts & R. K. Olney (2002) The overlap of Amyotrophic Lateral Sclerosis and Frontotemporal Lobar Dementia. *Neurology,* 58**,** A412-A412.

Lomen-Hoerth, C., J. Murphy, S. Langmore, J. H. Kramer, R. K. Olney & B. Miller (2003) Are amyotrophic lateral sclerosis patients cognitively normal? *Neurology,* 60**,** 1094-1097.

Long, L., H. Guo, D. Yao, K. Xiong, Y. Li, P. Liu, Z. Zhu & D. Liu (2015) Regulation of transcriptionally active genes via the catalytically inactive Cas9 in C-elegans and D-rerio. *Cell Research,* 25**,** 638-641.

Lopez-Patino, M. A., L. Yu, H. Cabral & I. V. Zhdanova (2008) Anxiogenic effects of cocaine withdrawal in zebrafish. *Physiology & Behavior,* 93**,** 160-171.

Lowe, J., G. Lennox, D. Jefferson, K. Morrell, D. McQuire, T. Gray, M. Landon, F. J. Doherty & R. J. Mayer (1988) A FILAMENTOUS INCLUSION BODY WITHIN ANTERIOR HORN NEURONS IN MOTOR NEURON DISEASE DEFINED BY IMMUNOCYTOCHEMICAL LOCALIZATION OF UBIQUITIN. *Neuroscience Letters,* 94**,** 203-210.

Luty, A. A., J. B. J. Kwok, C. Dobson-Stone, C. T. Loy, K. G. Coupland, H. Karlstrom, T. Sobow, J. Tchorzewska, A. Maruszak, M. Barcikowska, P. K. Panegyres, C. Zekanowski, W. S. Brooks, K. L. Williams, I. P. Blair, K. A. Mather, P. S. Sachdev, G. M. Halliday & P. R. Schofield (2010) Sigma Nonopioid Intracellular Receptor 1

Mutations Cause Frontotemporal Lobar Degeneration-Motor Neuron Disease. *Annals of Neurology,* 68**,** 639-649.

Mackenzie, I. R. A., E. H. Bigio, P. G. Ince, F. Geser, M. Neumann, N. J. Cairns, L. K. Kwong, M. S. Forman, J. Ravits, H. Stewart, A. Eisen, L. McClusky, H. A. Kretzschmar, C. M. Monoranu, J. R. Highley, J. Kirby, T. Siddique, P. J. Shaw, V. M. Y. Lee & J. Q. Trojanowski (2007) Pathological TDP-43 distinguishes sporadic amyotrophic lateral sclerosis from amyotrophic lateral sclerosis with SOD1 mutations. *Annals of Neurology,* 61**,** 427-434.

Mackenzie, I. R. A., P. Frick, F. A. Graesser, T. F. Gendron, L. Petrucelli, N. R. Cashman, D. Edbauer, E. Kremmer, J. Prudlo, D. Troost & M. Neumann (2015) Quantitative analysis and clinico-pathological correlations of different dipeptide repeat protein pathologies in C9ORF72 mutation carriers. *Acta Neuropathologica,* 130**,** 845-861.

Mackenzie, I. R. A., P. Frick & M. Neumann (2014) The neuropathology associated with repeat expansions in the C9ORF72 gene. *Acta Neuropathologica,* 127**,** 347-357.

Mahadevan, M., C. Tsilfidis, L. Sabourin, G. Shutler, C. Amemiya, G. Jansen, C. Neville, M. Narang, J. Barcelo, K. Ohoy, S. Leblond, J. Earlemacdonald, P. J. Dejong, B. Wieringa & R. G. Korneluk (1992) MYOTONIC-DYSTROPHY MUTATION - AN UNSTABLE CTG REPEAT IN THE 3' UNTRANSLATED REGION OF THE GENE. *Science,* 255**,** 1253-1255.

Mahoney, C. J., J. Beck, J. D. Rohrer, T. Lashley, K. Mok, T. Shakespeare, T. Yeatman, E. K. Warrington, J. M. Schott, N. C. Fox, M. N. Rossor, J. Hardy, J. Collinge, T. Revesz, S. Mead & J. D. Warren (2012) Frontotemporal dementia with the C9ORF72 hexanucleotide repeat expansion: clinical, neuroanatomical and neuropathological features. *Brain,* 135**,** 736-750.

Makky, K., J. Tekiela & A. N. Mayer (2007) Target of rapamycin (TOR) signaling controls epithelial morphogenesis in the vertebrate intestine. *Developmental Biology,* 303**,** 501-513.

Marit, J. S. & L. P. Weber (2011) Acute exposure to 2,4-dinitrophenol alters zebrafish swimming performance and whole body triglyceride levels. *Comparative Biochemistry and Physiology C-Toxicology & Pharmacology,* 154**,** 14-18.

Maruyama, H., H. Morino, H. Ito, Y. Izumi, H. Kato, Y. Watanabe, Y. Kinoshita, M. Kamada, H. Nodera, H. Suzuki, O. Komure, S. Matsuura, K. Kobatake, N. Morimoto, K. Abe, N. Suzuki, M. Aoki, A. Kawata, T. Hirai, T. Kato, K. Ogasawara, A. Hirano, T. Takumi, H. Kusaka, K. Hagiwara, R. Kaji & H. Kawakami (2010) Mutations of optineurin in amyotrophic lateral sclerosis. *Nature,* 465**,** 223-U109.

Mathai, B. J., A. H. Meijer & A. Simonsen (2017) Studying Autophagy in Zebrafish. *Cells,* 6.

Mathias, J. R., M. E. Dodd, K. B. Walters, S. K. Yoo, E. A. Ranheim & A. Huttenlocher (2009) Characterization of zebrafish larval inflammatory macrophages. *Developmental and Comparative Immunology,* 33**,** 1212-1217.

Mattiazzi, M., M. D'Aurelio, C. D. Gajewski, K. Martushova, M. Kiaei, M. F. Beal & G. Manfredi (2002) Mutated human SOD1 causes dysfunction of oxidative phosphorylation in mitochondria of transgenic mice. *Journal of Biological Chemistry,* 277**,** 29626-29633.

Matus, S., V. Valenzuela, D. B. Medinas & C. Hetz (2013) ER Dysfunction and Protein Folding Stress in ALS. *International journal of cell biology,* 2013**,** 674751-674751.

McGown, A., J. R. McDearmid, N. Panagiotaki, H. Tong, S. Al Mashhadi, N. Redhead, A. N. Lyon, C. E. Beattie, P. J. Shaw & T. M. Ramesh (2013) Early interneuron dysfunction in ALS: Insights from a mutant sod1 zebrafish model. *Annals of Neurology,* 73**,** 246-258.

McGown, A., D. P. J. Shaw & T. Ramesh (2016) ZNStress: a high-throughput drug screening protocol for identification of compounds modulating neuronal stress in the transgenic

mutant sod1G93R zebrafish model of amyotrophic lateral sclerosis. *Molecular Neurodegeneration,* 11.

McRobert, S. P. & J. Bradner (1998) The influence of body coloration on shoaling preferences in fish. *Animal Behaviour,* 56**,** 611-615.

Mendez, M. F., J. S. Shapira, R. J. Woods, E. A. Licht & R. E. Saul (2008) Psychotic symptoms in frontotemporal dementia: Prevalence and review. *Dementia and Geriatric Cognitive Disorders,* 25**,** 206-211.

Meng, L. H. & X. F. S. Zheng (2015) Toward rapamycin analog (rapalog)-based precision cancer therapy. *Acta Pharmacologica Sinica,* 36**,** 1163-1169.

Menzies, F. M., M. R. Cookson, R. W. Taylor, D. M. Turnbull, Z. M. A. Chrzanowska-Lightowlers, L. C. Dong, D. A. Figlewicz & P. J. Shaw (2002) Mitochondrial dysfunction in a cell culture model of familial amyotrophic lateral sclerosis. *Brain,* 125**,** 1522-1533.

Menzies, F. M., A. Fleming, A. Caricasole, C. F. Bento, S. P. Andrews, A. Ashkenazi, J. Fullgrabe, A. Jackson, M. J. Sanchez, C. Karabiyik, F. Licitra, A. L. Ramirez, M. Pavel, C. Puri, M. Renna, T. Ricketts, L. Schlotawa, M. Vicinanza, H. Won, Y. Zhu, J. Skidmore & D. C. Rubinsztein (2017) Autophagy and Neurodegeneration: Pathogenic Mechanisms and Therapeutic Opportunities. *Neuron,* 93**,** 1015-1034.

Millecamps, S., S. Boillee, E. Chabrol, W. Camu, C. Cazeneuve, F. Salachas, P. F. Pradat, V. Danel-Brunaud, N. Vandenberghe, P. Corcia, N. Le Forestier, L. Lacomblez, G. Bruneteau, D. Seilhean, A. Brice, J. Feingold, V. Meininger & E. LeGuern (2011) Screening of OPTN in French familial amyotrophic lateral sclerosis. *Neurobiology of Aging,* 32.

Millecamps, S., S. Boillee, I. Le Ber, D. Seilhean, E. Teyssou, M. Giraudeau, C. Moigneu, N. Vandenberghe, V. Danel-Brunaud, P. Corcia, P.-F. Pradat, N. Le Forestier, L. Lacomblez, G. Bruneteau, W. Camu, A. Brice, C. Cazeneuve, E. LeGuern, V. Meininger & F. Salachas (2012) Phenotype difference between ALS patients with expanded repeats in C9ORF72 and patients with mutations in other ALS-related genes. *Journal of Medical Genetics,* 49**,** 258-263.

Miller, J. C., S. Tan, G. Qiao, K. A. Barlow, J. Wang, D. F. Xia, X. Meng, D. E. Paschon, E. Leung, S. J. Hinkley, G. P. Dulay, K. L. Hua, I. Ankoudinova, G. J. Cost, F. D. Urnov, H. S. Zhang, M. C. Holmes, L. Zhang, P. D. Gregory & E. J. Rebar (2011) A TALE nuclease architecture for efficient genome editing. *Nature Biotechnology,* 29**,** 143-U149.

Miller, N. & R. Gerlai (2007) Quantification of shoaling behaviour in zebrafish (Danio rerio). *Behavioural Brain Research,* 184**,** 157-166.

Mitchell, J. C., P. McGoldrick, C. Vance, T. Hortobagyi, J. Sreedharan, B. Rogelj, E. L. Tudor, B. N. Smith, C. Klasen, C. C. J. Miller, J. D. Cooper, L. Greensmith & C. E. Shaw (2013) Overexpression of human wild-type FUS causes progressive motor neuron degeneration in an age- and dose-dependent fashion. *Acta Neuropathologica,* 125**,** 273-288.

Mizielinska, S., S. Groenke, T. Niccoli, C. E. Ridler, E. L. Clayton, A. Devoy, T. Moens, F. E. Norona, I. O. C. Woollacott, J. Pietrzyk, K. Cleverley, A. J. Nicoll, S. Pickering-Brown, J. Dols, M. Cabecinha, O. Hendrich, P. Fratta, E. M. C. Fisher, L. Partridge & A. M. Isaacs (2014) C9orf72 repeat expansions cause neurodegeneration in Drosophila through arginine-rich proteins. *Science,* 345**,** 1192-1194.

Mizielinska, S., T. Lashley, F. E. Norona, E. L. Clayton, C. E. Ridler, P. Fratta & A. M. Isaacs (2013) C9orf72 frontotemporal lobar degeneration is characterised by frequent neuronal sense and antisense RNA foci. *Acta Neuropathologica,* 126**,** 845-857.

Mizuno, Y., M. Amari, M. Takatama, H. Aizawa, B. Mihara & K. Okamoto (2006a) Immunoreactivities of p62, an ubiqutin-binding protein, in the spinal anterior horn

cells of patients with amyotrophic lateral sclerosis. *Journal of the Neurological Sciences,* 249**,** 13-18.

Mizuno, Y., M. Amari, M. Takatama, H. Aizawa, B. Mihara & K. Okamoto (2006b) Transferrin localizes in Bunina bodies in amyotrophic lateral sclerosis. *Acta Neuropathologica,* 112**,** 597-603.

Monson, C. A. & K. C. Sadler (2010) Inbreeding Depression and Outbreeding Depression Are Evident in Wild-Type Zebrafish Lines. *Zebrafish,* 7**,** 189-197.

Mori, K., T. Arzberger, F. A. Graesser, I. Gijselinck, S. May, K. Rentzsch, S.-M. Weng, M. H. Schludi, J. van der Zee, M. Cruts, C. Van Broeckhoven, E. Kremmer, H. A. Kretzschmar, C. Haass & D. Edbauer (2013a) Bidirectional transcripts of the expanded C9orf72 hexanucleotide repeat are translated into aggregating dipeptide repeat proteins. *Acta Neuropathologica,* 126**,** 881-893.

Mori, K., S. Lammich, I. R. A. Mackenzie, I. Forne, S. Zilow, H. Kretzschmar, D. Edbauer, J. Janssens, G. Kleinberger, M. Cruts, J. Herms, M. Neumann, C. Van Broeckhoven, T. Arzberger & C. Haass (2013b) hnRNP A3 binds to GGGGCC repeats and is a constituent of p62-positive/TDP43-negative inclusions in the hippocampus of patients with C9orf72 mutations. *Acta Neuropathologica,* 125**,** 413-423.

Mori, K., S.-M. Weng, T. Arzberger, S. May, K. Rentzsch, E. Kremmer, B. Schmid, H. A. Kretzschmar, M. Cruts, C. Van Broeckhoven, C. Haass & D. Edbauer (2013c) The C9orf72 GGGGCC Repeat Is Translated into Aggregating Dipeptide-Repeat Proteins in FTLD/ALS. *Science,* 339**,** 1335-1338.

Morita, M., A. Al-Chalabi, P. M. Andersen, B. Hosler, P. Sapp, E. Englund, J. E. Mitchell, J. J. Habgood, J. de Belleroche, J. Xi & R. H. Brown (2006) A locus on chromosome 9p confers susceptibility to ALS and frontotemporal dementia. *Neurology,* 66**,** 839-844.

Mostowy, S., L. Boucontet, M. J. M. Moya, A. Sirianni, P. Boudinot, M. Hollinshead, P. Cossart, P. Herbomel, J. P. Levraud & E. Colucci-Guyon (2013) The Zebrafish as a New Model for the In Vivo Study of Shigella flexneri Interaction with Phagocytes and Bacterial Autophagy. *Plos Pathogens,* 9.

Mukaka, M. M. (2012) Statistics Corner: A guide to appropriate use of Correlation coefficient in medical research. *Malawi Medical Journal,* 24**,** 69-71.

Mussolino, C., R. Morbitzer, F. Luetge, N. Dannemann, T. Lahaye & T. Cathomen (2011) A novel TALE nuclease scaffold enables high genome editing activity in combination with low toxicity. *Nucleic Acids Research,* 39**,** 9283-9293.

Nagabhushana, A. & R. K. Mishra (2016) Finding clues to the riddle of sex determination in zebrafish. *Journal of Biosciences,* 41**,** 145-155.

Nagai, M., D. B. Re, T. Nagata, A. Chalazonitis, T. M. Jessell, H. Wichterle & S. Przedborski (2007) Astrocytes expressing ALS-linked mutated SOD1 release factors selectively toxic to motor neurons. *Nature Neuroscience,* 10**,** 615-622.

Nasevicius, A. & S. C. Ekker (2000) Effective targeted gene 'knockdown' in zebrafish. *Nature Genetics,* 26**,** 216-220.

Nasiadka, A. & M. D. Clark (2012) Zebrafish Breeding in the Laboratory Environment. *Ilar Journal,* 53**,** 161-168.

Neumann, M., D. M. Sampathu, L. K. Kwong, A. C. Truax, M. C. Micsenyi, T. T. Chou, J. Bruce, T. Schuck, M. Grossman, C. M. Clark, L. F. McCluskey, B. L. Miller, E. Masliah, I. R. Mackenzie, H. Feldman, W. Feiden, H. A. Kretzschmar, J. Q. Trojanowski & V. M. Y. Lee (2006) Ubiquitinated TDP-43 in frontotemporal lobar degeneration and amyotrophic lateral sclerosis. *Science,* 314**,** 130-133.

Nijssen, J., L. H. Comley & E. Hedlund (2017) Motor neuron vulnerability and resistance in amyotrophic lateral sclerosis. *Acta Neuropathologica,* 133**,** 863-885.

Nishihira, Y., C.-F. Tan, O. Onodera, Y. Toyoshima, M. Yamada, T. Morita, M. Nishizawa, A. Kakita & H. Takahashi (2008) Sporadic amyotrophic lateral sclerosis: two

pathological patterns shown by analysis of distribution of TDP-43-immunoreactive neuronal and glial cytoplasmic inclusions. *Acta Neuropathologica,* 116**,** 169-182.

Nishimura, A. L., M. Mitne-Neto, H. C. A. Silva, A. Richieri-Costa, S. Middleton, D. Cascio, F. Kok, J. R. M. Oliveira, T. Gillingwater, J. Webb, P. Skehel & M. Zatz (2004) A mutation in the vesicle-trafficking protein VAPB causes late-onset spinal muscular atrophy and amyotrophic lateral sclerosis. *American Journal of Human Genetics,* 75**,** 822-831.

Norton, W. & L. Bally-Cuif (2010) Adult zebrafish as a model organism for behavioural genetics. *Bmc Neuroscience,* 11.

O'Rourke, J. G., L. Bogdanik, A. K. M. G. Muhammad, T. F. Gendron, K. J. Kim, A. Austin, J. Cady, E. Y. Liu, J. Zarrow, S. Grant, R. Ho, S. Bell, S. Carmona, M. Simpkinson, D. Lall, K. Wu, L. Daughrity, D. W. Dickson, M. B. Harms, L. Petrucelli, E. B. Lee, C. M. Lutz & R. H. Baloh (2015) C9orf72 BAC Transgenic Mice Display Typical Pathologic Features of ALS/FTD. *Neuron,* 88**,** 892-901.

O'Rourke, J. G., L. Bogdanik, A. Yanez, D. Lall, A. J. Wolf, A. K. M. G. Muhammad, R. Ho, S. Carmona, J. P. Vit, J. Zarrow, K. J. Kim, S. Bell, M. B. Harms, T. M. Miller, C. A. Dangler, D. M. Underhill, H. S. Goodridge, C. M. Lutz & R. H. Baloh (2016) C9orf72 is required for proper macrophage and microglial function in mice. *Science,* 351**,** 1324-1329.

Ohki, Y., A. Wenninger-Weinzierl, A. Hruscha, K. Asakawa, K. Kawakami, C. Haass, D. Edbauer & B. Schmid (2017) Glycine-alanine dipeptide repeat protein contributes to toxicity in a zebrafish model of C9orf72 associated neurodegeneration. *Molecular Neurodegeneration,* 12.

Okamoto, K., S. Hirai, M. Amari, M. Watanabe & A. Sakurai (1993) BUNINA BODIES IN AMYOTROPHIC-LATERAL-SCLEROSIS IMMUNOSTAINED WITH RABBIT ANTI-CYSTATIN-C SERUM. *Neuroscience Letters,* 162**,** 125-128.

Orban, L., R. Sreenivasan & P.-E. Olsson (2009) Long and winding roads: Testis differentiation in zebrafish. *Molecular and Cellular Endocrinology,* 312**,** 35-41.

Orlacchio, A., C. Babalini, A. Borreca, C. Patrono, R. Massa, S. Basaran, R. P. Munhoz, E. A. Rogaeva, P. H. St George-Hyslop, G. Bernardi & T. Kawarai (2010) SPATACSIN mutations cause autosomal recessive juvenile amyotrophic lateral sclerosis. *Brain,* 133**,** 591-598.

Ostberg, P. & N. Bogdanovic (2011) Semantic dementia with lower motor neuron disease showing FTLD-TDP type 3 pathology (sensu Mackenzie). *Neuropathology,* 31**,** 271-279.

Pankiv, S., T. H. Clausen, T. Lamark, A. Brech, J.-A. Bruun, H. Outzen, A. Overvatn, G. Bjorkoy & T. Johansen (2007) p62/SQSTM1 binds directly to Atg8/LC3 to facilitate degradation of ubiquitinated protein aggregates by autophagy. *Journal of Biological Chemistry,* 282**,** 24131-24145.

Panula, P., V. Sallinen, M. Sundvik, J. Kolehmainen, V. Torkko, A. Tiittula, M. Moshnyakov & P. Podlasz (2006) Modulatory Neurotransmitter Systems and Behavior: Towards Zebrafish Models of Neurodegenerative Diseases. *Zebrafish,* 3**,** 235-247.

Parker, M. O., L. V. Annan, A. H. Kanellopoulos, A. J. Brock, F. J. Combe, M. Baiamonte, M.-T. Teh & C. H. Brennan (2014) The utility of zebrafish to study the mechanisms by which ethanol affects social behavior and anxiety during early brain development. *Progress in Neuro-Psychopharmacology & Biological Psychiatry,* 55**,** 94-100.

Parker, M. O., M. E. Millington, F. J. Combe & C. H. Brennan (2012) Housing Conditions Differentially Affect Physiological and Behavioural Stress Responses of Zebrafish, as well as the Response to Anxiolytics. *Plos One,* 7.

Parkinson, N., P. G. Ince, M. O. Smith, R. Highley, G. Skibinski, P. M. Andersen, K. E. Morrison, H. S. Pall, O. Hardiman, J. Collinge, P. J. Shaw, E. M. C. Fisher, M. R. C.

P. A. Study & F. R. Consortium (2006) ALS phenotypes with mutations in CHMP2B (charged multivesicular body protein 2B). *Neurology,* 67**,** 1074-1077.

Pattanayak, V., J. P. Guilinger & D. R. Liu (2014) Determining the Specificities of TALENs, Cas9, and Other Genome-Editing Enzymes. *Use of Crispr/Cas9, Zfns, and Talens in Generating Site-Specific Genome Alterations,* 546**,** 47-78.

Peters, O. M., G. T. Cabrera, H. Tran, T. F. Gendron, J. E. McKeon, J. Metterville, A. Weiss, N. Wightman, J. Salameh, J. Kim, H. Sun, K. B. Boylan, D. Dickson, Z. Kennedy, Z. Lin, Y.-J. Zhang, L. Daughrity, C. Jung, F.-B. Gao, P. C. Sapp, H. R. Horvitz, D. A. Bosco, S. P. Brown, P. de Jong, L. Petrucelli, C. Mueller & R. H. Brown, Jr. (2015a) Human C9ORF72 Hexanucleotide Expansion Reproduces RNA Foci and Dipeptide Repeat Proteins but Not Neurodegeneration in BAC Transgenic Mice. *Neuron,* 88**,** 902-909.

Peters, O. M., M. Ghasemi & R. H. Brown (2015b) Emerging mechanisms of molecular pathology in ALS. *Journal of Clinical Investigation,* 125**,** 1767-1779.

Philips, T. & W. Robberecht (2011) Neuroinflammation in amyotrophic lateral sclerosis: role of glial activation in motor neuron disease. *Lancet Neurology,* 10**,** 253-263.

Philips, T. & J. D. Rothstein (2015) Rodent Models of Amyotrophic Lateral Sclerosis. *Current protocols in pharmacology,* 69**,** 5.67.1-21.

Phillips, J. B. & M. Westerfield (2014) Zebrafish models in translational research: tipping the scales toward advancements in human health. *Disease Models & Mechanisms,* 7**,** 739-743.

Piao, Y. S., K. Wakabayashi, A. Kakita, M. Yamada, S. Hayashi, T. Morita, F. Ikuta, K. Oyanagi & H. Takahashi (2003) Neuropathology with clinical correlations of sporadic amyotrophic lateral sclerosis: 102 autopsy cases examined between 1962 and 2000. *Brain Pathology,* 13**,** 10-22.

Picher-Martel, V., P. N. Valdmanis, P. V. Gould, J. P. Julien & N. Dupre (2016) From animal models to human disease: a genetic approach for personalized medicine in ALS. *Acta Neuropathologica Communications,* 4.

Plaut, I. (2000) Effects of fin size on swimming performance, swimming behaviour and routine activity of zebrafish Danio rerio. *Journal of Experimental Biology,* 203**,** 813-820.

Plaut, I. (2002) Does pregnancy affect swimming performance of female Mosquitofish, Gambusia affinis? *Functional Ecology,* 16**,** 290-295.

Puls, I., C. Jonnakuty, B. H. LaMonte, E. L. F. Holzbaur, M. Tokito, E. Mann, M. K. Floeter, K. Bidus, D. Drayna, S. J. Oh, R. H. Brown, C. L. Ludlow & K. H. Fischbeck (2003) Mutant dynactin in motor neuron disease. *Nature Genetics,* 33**,** 455-456.

Ramesh, T., A. N. Lyon, R. H. Pineda, C. Wang, P. M. L. Janssen, B. D. Canan, A. H. M. Burghes & C. E. Beattie (2010) A genetic model of amyotrophic lateral sclerosis in zebrafish displays phenotypic hallmarks of motoneuron disease. *Disease Models & Mechanisms,* 3**,** 652-662.

Ran, F. A., P. D. Hsu, C. Y. Lin, J. S. Gootenberg, S. Konermann, A. E. Trevino, D. A. Scott, A. Inoue, S. Matoba, Y. Zhang & F. Zhang (2013) Double Nicking by RNA-Guided CRISPR Cas9 for Enhanced Genome Editing Specificity. *Cell,* 154**,** 1380-1389.

Reddy, K., B. Zamiri, S. Y. R. Stanley, R. B. Macgregor, Jr. & C. E. Pearson (2013) The Disease-associated r(GGGGCC)(n) Repeat from the C9orf72 Gene Forms Tract Length-dependent Uni- and Multimolecular RNA G-quadruplex Structures. *Journal of Biological Chemistry,* 288**,** 9860-9866.

Reimer, M. M., I. Soerensen, V. Kuscha, R. E. Frank, C. Liu, C. G. Becker & T. Becker (2008) Motor neuron regeneration in adult zebrafish. *Journal of Neuroscience,* 28**,** 8510-8516.

Renna, M., C. F. Bento, A. Fleming, F. M. Menzies, F. H. Siddiqi, B. Ravikumar, C. Puri, M. Garcia-Arencibia, O. Sadiq, S. Corrochano, S. Carter, S. D. M. Brown, A. Acevedo-

Arozena & D. C. Rubinsztein (2013) IGF-1 receptor antagonism inhibits autophagy. *Human Molecular Genetics,* 22**,** 4528-4544.

Renton, A. E., A. Chio & B. J. Traynor (2014) State of play in amyotrophic lateral sclerosis genetics. *Nature Neuroscience,* 17**,** 17-23.

Renton, A. E., E. Majounie, A. Waite, J. Simon-Sanchez, S. Rollinson, J. R. Gibbs, J. C. Schymick, H. Laaksovirta, J. C. van Swieten, L. Myllykangas, H. Kalimo, A. Paetau, Y. Abramzon, A. M. Remes, A. Kaganovich, S. W. Scholz, J. Duckworth, J. H. Ding, D. W. Harmer, D. G. Hernandez, J. O. Johnson, K. Mok, M. Ryten, D. Trabzuni, R. J. Guerreiro, R. W. Orrell, J. Neal, A. Murray, J. Pearson, I. E. Jansen, D. Sondervan, H. Seelaar, D. Blake, K. Young, N. Halliwell, J. B. Callister, G. Toulson, A. Richardson, A. Gerhard, J. Snowden, D. Mann, D. Neary, M. A. Nalls, T. Peuralinna, L. Jansson, V. M. Isoviita, A. L. Kaivorinne, M. Holtta-Vuori, E. Ikonen, R. Sulkava, M. Benatar, J. Wuu, A. Chio, G. Restagno, G. Borghero, M. Sabatelli, D. Heckerman, E. Rogaeva, L. Zinman, J. D. Rothstein, M. Sendtner, C. Drepper, E. E. Eichler, C. Alkan, Z. Abdullaev, S. D. Pack, A. Dutra, E. Pak, J. Hardy, A. Singleton, N. M. Williams, P. Heutink, S. Pickering-Brown, H. R. Morris, P. J. Tienari, B. J. Traynor & I. Consortium (2011) A Hexanucleotide Repeat Expansion in C9ORF72 Is the Cause of Chromosome 9p21-Linked ALS-FTD. *Neuron,* 72**,** 257-268.

Ringholz, G. M., S. H. Appel, M. Bradshaw, N. A. Cooke, D. M. Mosnik & P. E. Schulz (2005) Prevalence and patterns of cognitive impairment in sporadic ALS. *Neurology,* 65**,** 586-590.

Rosen, D. R., T. Siddique, D. Patterson, D. A. Figlewicz, P. Sapp, A. Hentati, D. Donaldson, J. Goto, J. P. Oregan, H. X. Deng, Z. Rahmani, A. Krizus, D. McKennayasek, A. Cayabyab, S. M. Gaston, R. Berger, R. E. Tanzi, J. J. Halperin, B. Herzfeldt, R. Vandenbergh, W. Y. Hung, T. Bird, G. Deng, D. W. Mulder, C. Smyth, N. G. Laing, E. Soriano, M. A. Pericakvance, J. Haines, G. A. Rouleau, J. S. Gusella, H. R. Horvitz & R. H. Brown (1993) MUTATIONS IN CU/ZN SUPEROXIDE-DISMUTASE GENE ARE ASSOCIATED WITH FAMILIAL AMYOTROPHIC-LATERAL-SCLEROSIS. *Nature,* 362**,** 59-62.

Rothstein, J. D., M. DykesHoberg, C. A. Pardo, L. A. Bristol, L. Jin, R. W. Kuncl, Y. Kanai, M. A. Hediger, Y. F. Wang, J. P. Schielke & D. F. Welty (1996) Knockout of glutamate transporters reveals a major role for astroglial transport in excitotoxicity and clearance of glutamate. *Neuron,* 16**,** 675-686.

Rothstein, J. D., G. C. Tsai, R. W. Kuncl, L. Clawson, D. R. Cornblath, D. B. Drachman, A. Pestronk, B. L. Stauch & J. T. Coyle (1990) ABNORMAL EXCITATORY AMINO-ACID-METABOLISM IN AMYOTROPHIC-LATERAL-SCLEROSIS. *Annals of Neurology,* 28**,** 18-25.

Rowland, L. P. & N. A. Shneider (2001) Medical progress: Amyotrophic lateral sclerosis. *New England Journal of Medicine,* 344**,** 1688-1700.

Sakowski, S. A., J. S. Lunn, A. S. Busta, S. S. Oh, G. Zamora-Berridi, M. Palmer, A. A. Rosenberg, S. G. Philip, J. J. Dowling & E. L. Feldman (2012) Neuromuscular effects of G93A-SOD1 expression in zebrafish. *Molecular Neurodegeneration,* 7.

Sapp, P. C., B. A. Hosler, D. McKenna-Yasek, W. Chin, A. Gann, H. Genise, J. Gorenstein, M. Huang, W. Sailer, M. Scheffler, M. Valesky, J. L. Haines, M. Pericak-Vance, T. Siddique, H. R. Horvitz & R. H. Brown (2003) Identification of two novel loci for dominantly inherited familial amyotrophic lateral sclerosis. *American Journal of Human Genetics,* 73**,** 397-403.

Sareen, D., J. G. O'Rourke, P. Meera, A. K. M. G. Muhammad, S. Grant, M. Simpkinson, S. Bell, S. Carmona, L. Ornelas, A. Sahabian, T. Gendron, L. Petrucelli, M. Baughn, J. Ravits, M. B. Harms, F. Rigo, C. F. Bennett, T. S. Otis, C. N. Svendsen & R. H. Baloh (2013) Targeting RNA foci in iPSC-derived motor neurons from ALS patients with a C9ORF72 repeat expansion. *Science translational medicine,* 5**,** 208ra149-208ra149.

Sasaki, S. & M. Iwata (2006) Neuronal inclusions in sporadic motor neuron disease are negative for alpha-synuclein. *Neuromuscular Disorders,* 16**,** S66-S66.

Sasaki, S. & M. Iwata (2007) Mitochondrial alterations in the spinal cord of patients with sporadic amyotrophic lateral sclerosis. *Journal of Neuropathology and Experimental Neurology,* 66**,** 10-16.

Schaefer, A. M., J. R. Sanes & J. W. Lichtman (2005) A compensatory subpopulation of motor neurons in a mouse model of amyotrophic lateral sclerosis. *Journal of Comparative Neurology,* 490**,** 209-219.

Schmid, B. & C. Haass (2013) Genomic editing open new avenues for zebrafish as a model for neurodegeneration. *Journal of Neurochemistry,* 127**,** 461-470.

Schmid, B., A. Hruscha, S. Hogl, J. Banzhaf-Strathmann, K. Strecker, J. van der Zee, M. Teucke, S. Eimer, J. Hegermann, M. Kittelmann, E. Kremmer, M. Cruts, B. Solchenberger, L. Hasenkamp, F. van Bebber, C. Van Broeckhoven, D. Edbauer, S. F. Lichtenthaler & C. Haass (2013) Loss of ALS-associated TDP-43 in zebrafish causes muscle degeneration, vascular dysfunction, and reduced motor neuron axon outgrowth. *Proceedings of the National Academy of Sciences of the United States of America,* 110**,** 4986-4991.

Schnorr, S. J., P. J. Steenbergen, M. K. Richardson & D. L. Champagne (2012) Measuring thigmotaxis in larval zebrafish. *Behavioural Brain Research,* 228**,** 367-374.

Seibenhener, M. L., J. R. Babu, T. Geetha, H. C. Wong, N. R. Krishna & M. W. Wooten (2004) Sequestosome 1/p62 is a polyubiquitin chain binding protein involved in ubiquitin proteasome degradation. *Molecular and Cellular Biology,* 24**,** 8055-8068.

Sellier, C., M.-L. Campanari, C. J. Corbier, A. Gaucherot, I. Kolb-Cheynel, M. Oulad-Abdelghani, F. Ruffenach, A. Page, S. Ciura, E. Kabashi & N. Charlet-Berguerand (2016) Loss of C9ORF72 impairs autophagy and synergizes with polyQ Ataxin-2 to induce motor neuron dysfunction and cell death. *Embo Journal,* 35**,** 1276-1297.

Sephton, C. F., A. A. Tang, A. Kulkarni, J. West, M. Brooks, J. J. Stubblefield, Y. Liu, M. Q. Zhang, C. B. Green, K. M. Huber, E. J. Huang, J. Herz & G. Yu (2014) Activity-dependent FUS dysregulation disrupts synaptic homeostasis. *Proceedings of the National Academy of Sciences of the United States of America,* 111**,** E4769-E4778.

Serra, E. L., C. C. Medalha & R. Mattioli (1999) Natural preference of zebrafish (Danio rerio) for a dark environment. *Brazilian Journal of Medical and Biological Research,* 32**,** 1551-1553.

Sha, S. J., L. T. Takada, K. P. Rankin, J. S. Yokoyama, N. J. Rutherford, J. C. Fong, B. Khan, A. Karydas, M. C. Baker, M. DeJesus-Hernandez, M. Pribadi, G. Coppola, D. H. Geschwind, R. Rademakers, S. E. Lee, W. Seeley, B. L. Miller & A. L. Boxer (2012) Frontotemporal dementia due to C9ORF72 mutations Clinical and imaging features. *Neurology,* 79**,** 1002-1011.

Shatunov, A., K. Mok, S. Newhouse, M. E. Weale, B. Smith, C. Vance, L. Johnson, J. H. Veldink, M. A. van Es, L. H. van den Berg, W. Robberecht, P. Van Damme, O. Hardiman, A. E. Farmer, C. M. Lewis, A. W. Butler, O. Abel, P. M. Andersen, I. Fogh, V. Silani, A. Chio, B. J. Traynor, J. Melki, V. Meininger, J. E. Landers, P. McGuffin, J. D. Glass, H. Pall, P. N. Leigh, J. Hardy, R. H. Brown, Jr., J. F. Powell, R. W. Orrell, K. E. Morrison, P. J. Shaw, C. E. Shaw & A. Al-Chalabi (2010) Chromosome 9p21 in sporadic amyotrophic lateral sclerosis in the UK and seven other countries: a genome-wide association study. *Lancet Neurology,* 9**,** 986-994.

Shaw, P. J., P. G. Ince, G. Falkous & D. Mantle (1995) OXIDATIVE DAMAGE TO PROTEIN IN SPORADIC MOTOR-NEURON DISEASE SPINAL-CORD. *Annals of Neurology,* 38**,** 691-695.

Simpson, E. P., Y. K. Henry, J. S. Henkel, R. G. Smith & S. H. Appel (2004) Increased lipid peroxidation in sera of ALS patients - A potential biomarker of disease burden. *Neurology,* 62**,** 1758-1765.

Singleman, C. & N. G. Holtzman (2014) Growth and Maturation in the Zebrafish, Danio Rerio: A Staging Tool for Teaching and Research. *Zebrafish,* 11**,** 396-406.

Smith, B. N., N. Ticozzi, C. Fallini, A. S. Gkazi, S. Topp, K. P. Kenna, E. L. Scotter, J. Kost, P. Keagle, J. W. Miller, D. Calini, C. Vance, E. W. Danielson, C. Troakes, C. Tiloca, S. Al-Sarraj, E. A. Lewis, A. King, C. Colombrita, V. Pensato, B. Castellotti, J. De Belleroche, F. Baas, A. ten Asbroek, P. C. Sapp, D. McKenna-Yasek, R. L. McLaughlin, M. Polak, S. Asress, J. Esteban-Perez, J. L. Munoz-Blanco, M. Simpson, W. van Rheenen, F. P. Diekstra, G. Lauria, S. Duga, S. Corti, C. Cereda, L. Corrado, G. Soraru, K. E. Morrison, K. L. Williams, G. A. Nicholson, I. P. Blair, P. A. Dion, C. S. Leblond, G. A. Rouleau, O. Hardiman, J. H. Veldink, L. H. van den Berg, A. Al-Chalabi, H. Pall, P. J. Shaw, M. R. Turner, K. Talbot, F. Taroni, A. Garcia-Redondo, Z. Y. Wu, J. D. Glass, C. Gellera, A. Ratti, R. H. Brown, V. Silani, C. E. Shaw, J. E. Landers & S. Consortium (2014) Exome-wide Rare Variant Analysis Identifies TUBA4A Mutations Associated with Familial ALS. *Neuron,* 84**,** 324-331.

Smith, B. N., S. D. Topp, C. Fallini, H. Shibata, H.-J. Chen, C. Troakes, A. King, N. Ticozzi, K. P. Kenna, A. Soragia-Gkazi, J. W. Miller, A. Sato, D. M. Dias, M. Jeon, C. Vance, C. H. Wong, M. de Majo, W. Kattuah, J. C. Mitchell, E. L. Scotter, N. W. Parkin, P. C. Sapp, M. Nolan, P. J. Nestor, M. Simpson, M. Weale, M. Lek, F. Baas, J. M. V. de Jong, A. L. M. A. ten Asbroek, A. Garcia Redondo, J. Esteban-Perez, C. Tiloca, F. Verde, S. Duga, N. Leigh, H. Pall, K. E. Morrison, A. Al-Chalabi, P. J. Shaw, J. Kirby, M. R. Turner, K. Talbot, O. Hardiman, J. D. Glass, J. de Belleroche, M. Maki, S. E. Moss, C. Miller, C. Gellera, A. Ratti, S. Al-Sarraj, R. H. Brown, Jr., V. Silani, J. E. Landers & C. E. Shaw (2017) Mutations in the vesicular trafficking protein annexin A11 are associated with amyotrophic lateral sclerosis. *Science Translational Medicine,* 9.

Snowden, J. S., S. Rollinson, J. C. Thompson, J. M. Harris, C. L. Stopford, A. M. T. Richardson, M. Jones, A. Gerhard, Y. S. Davidson, A. Robinson, L. Gibbons, Q. Hu, D. DuPlessis, D. Neary, D. M. A. Mann & S. M. Pickering-Brown (2012) Distinct clinical and pathological characteristics of frontotemporal dementia associated with C9ORF72 mutations. *Brain,* 135**,** 693-708.

Sobue, G., Y. Hashizume, T. Yasuda, E. Mukai, T. Kumagai, T. Mitsuma & J. Q. Trojanowski (1990) PHOSPHORYLATED HIGH-MOLECULAR-WEIGHT NEUROFILAMENT PROTEIN IN LOWER MOTOR NEURONS IN AMYOTROPHIC LATERAL SCLEROSIS AND OTHER NEURODEGENERATIVE DISEASES INVOLVING VENTRAL HORN CELLS. *Acta Neuropathologica,* 79**,** 402-408.

Sreedharan, J., I. P. Blair, V. B. Tripathi, X. Hu, C. Vance, B. Rogelj, S. Ackerley, J. C. Durnall, K. L. Williams, E. Buratti, F. Baralle, J. de Belleroche, J. D. Mitchell, P. N. Leigh, A. Al-Chalabi, C. C. Miller, G. Nicholson & C. E. Shaw (2008) TDP-43 mutations in familial and sporadic amyotrophic lateral sclerosis. *Science,* 319**,** 1668-1672.

Sternberg, S. H., S. Redding, M. Jinek, E. C. Greene & J. A. Doudna (2014) DNA Interrogation by the CRISPR RNA-Guided Endonuclease Cas9. *Biophysical Journal,* 106**,** 695A-695A.

Stewart, A. M., O. Braubach, J. Spitsbergen, R. Gerlai & A. V. Kalueffl (2014) Zebrafish models for translational neuroscience research: from tank to bedside. *Trends in Neurosciences,* 37**,** 264-278.

Stewart, H., N. J. Rutherford, H. Briemberg, C. Krieger, N. Cashman, M. Fabros, M. Baker, A. Fok, M. DeJesus-Hernandez, A. Eisen, R. Rademakers & I. R. A. Mackenzie (2012) Clinical and pathological features of amyotrophic lateral sclerosis caused by

mutation in the C9ORF72 gene on chromosome 9p. *Acta Neuropathologica,* 123**,** 409-417.

Sudria-Lopez, E., M. Koppers, M. de Wit, C. van der Meer, H.-J. Westeneng, C. A. C. Zundel, S. A. Youssef, L. Harkema, A. de Bruin, J. H. Veldink, L. H. van den Berg & R. J. Pasterkamp (2016) Full ablation of C9orf72 in mice causes immune system-related pathology and neoplastic events but no motor neuron defects. *Acta Neuropathologica,* 132**,** 145-147.

Sullivan, P. M., X. Zhou, A. M. Robins, D. H. Paushter, D. Kim, M. B. Smolka & F. Hu (2016a) The ALS/FTLD associated protein C9orf72 associates with SMCR8 and WDR41 to regulate the autophagy-lysosome pathway. *Acta Neuropathologica Communications,* 4.

Sullivan, P. M., X. L. Zhou, A. M. Robins, D. H. Paushter, D. Kim, M. B. Smolka & F. H. Hu (2016b) The ALS/FTLD associated protein C9orf72 associates with SMCR8 and WDR41 to regulate the autophagy-lysosome pathway. *Acta Neuropathologica Communications,* 4.

Summerton, J. & D. Weller (1997) Morpholino antisense oligomers: Design, preparation, and properties. *Antisense & Nucleic Acid Drug Development,* 7**,** 187-195.

Swinnen, B. & W. Robberecht (2014) The phenotypic variability of amyotrophic lateral sclerosis. *Nature Reviews Neurology,* 10**,** 661-670.

Sztal, T. E., A. A. Ruparelia, C. Williams & R. J. Bryson-Richardson (2016) Using Touch-evoked Response and Locomotion Assays to Assess Muscle Performance and Function in Zebrafish. *Journal of visualized experiments : JoVE.*

Takahashi, H. (1977) JUVENILE HERMAPHRODITISM IN THE ZEBRAFISH BRACHYDANIO-RERIO. *Bulletin of the Faculty of Fisheries Hokkaido University,* 28**,** 57-65.

Takahashi, Y., Y. Fukuda, J. Yoshimura, A. Toyoda, K. Kurppa, H. Moritoyo, V. V. Belzil, P. A. Dion, K. Higasa, K. Doi, H. Ishiura, J. Mitsui, H. Date, B. Ahsan, T. Matsukawa, Y. Ichikawa, T. Moritoyo, M. Ikoma, T. Hashimoto, F. Kimura, S. Murayama, O. Onodera, M. Nishizawa, M. Yoshida, N. Atsuta, G. Sobue, J. A. Fifita, K. L. Williams, I. P. Blair, G. A. Nicholson, P. Gonzalez-Perez, R. H. Brown, M. Nomoto, K. Elenius, G. A. Rouleau, A. Fujiyama, S. Morishita, J. Goto, S. Tsuji & JaCals (2013) ERBB4 Mutations that Disrupt the Neuregulin-ErbB4 Pathway Cause Amyotrophic Lateral Sclerosis Type 19. *American Journal of Human Genetics,* 93**,** 900-905.

Talbot, K. (2009) Motor neuron disease: the bare essentials. *Practical neurology,* 9**,** 303-9.

Therrien, M., G. A. Rouleau, P. A. Dion & J. A. Parker (2013) Deletion of C9ORF72 Results in Motor Neuron Degeneration and Stress Sensitivity in C-elegans. *Plos One,* 8.

Tong, S.-K., H.-J. Hsu & B.-c. Chung (2010) Zebrafish monosex population reveals female dominance in sex determination and earliest events of gonad differentiation. *Developmental Biology,* 344**,** 849-856.

Turner, M. R., O. Hardiman, M. Benatar, B. R. Brooks, A. Chio, M. de Carvalho, P. G. Ince, C. Lin, R. G. Miller, H. Mitsumoto, G. Nicholson, J. Ravits, P. J. Shaw, M. Swash, K. Talbot, B. J. Traynor, L. H. Van den Berg, J. H. Veldink, S. Vucic & M. C. Kiernan (2013) Controversies and priorities in amyotrophic lateral sclerosis. *Lancet Neurology,* 12**,** 310-322.

Ugolino, J., Y. J. Ji, K. Conchina, J. Chu, R. S. Nirujogi, A. Pandey, N. R. Brady, A. Hamacher-Brady & J. Wang (2016) Loss of C9orf72 Enhances Autophagic Activity via Deregulated mTOR and TFEB Signaling. *Plos Genetics,* 12.

Underwood, B. R., S. Imarisio, A. Fleming, C. Rose, G. Krishna, P. Heard, M. Quick, V. I. Korolchuk, M. Renna, S. Sarkar, M. Garcia-Arencibia, C. J. O'Kane, M. P. Murphy & D. C. Rubinsztein (2010) Antioxidants can inhibit basal autophagy and enhance

neurodegeneration in models of polyglutamine disease. *Human Molecular Genetics,* 19**,** 3413-3429.

Uribe, C., H. Folch, R. Enriquez & G. Moran (2011) Innate and adaptive immunity in teleost fish: a review. *Veterinarni Medicina,* 56**,** 486-503.

van Blitterswijk, M., M. Dejesus-Hernandez, E. Niemantsverdriet, M. E. Murray, M. G. Heckman, N. N. Diehl, P. H. Brown, M. C. Baker, N. A. Finch, P. O. Bauer, G. Serrano, T. G. Beach, K. A. Josephs, D. S. Knopman, R. C. Petersen, B. F. Boeve, N. R. Graff-Radford, K. B. Boylan, L. Petrucelli, D. W. Dickson & R. Rademakers (2013) Association between repeat sizes and clinical and pathological characteristics in carriers of C90RF72 repeat expansions (Xpansize-72): a cross-sectional cohort study. *Lancet Neurology,* 12**,** 978-988.

van Blitterswijk, M., M. DeJesus-Hernandez & R. Rademakers (2012a) How do C9ORF72 repeat expansions cause amyotrophic lateral sclerosis and frontotemporal dementia: can we learn from other noncoding repeat expansion disorders? *Current Opinion in Neurology,* 25**,** 689-700.

van Blitterswijk, M., M. A. van Es, E. A. M. Hennekam, D. Dooijes, W. van Rheenen, J. Medic, P. R. Bourque, H. J. Schelhaas, A. J. van der Kooi, M. de Visser, P. I. W. de Bakker, J. H. Veldink & L. H. van den Berg (2012b) Evidence for an oligogenic basis of amyotrophic lateral sclerosis. *Human Molecular Genetics,* 21**,** 3776-3784.

Van Deerlin, V. M., J. B. Leverenz, L. M. Bekris, T. D. Bird, W. Yuan, L. B. Elman, D. Clay, E. M. Wood, A. S. Chen-Plotkin, M. Martinez-Lage, E. Steinbart, L. McCluskey, M. Grossman, M. Neumann, I. L. Wu, W.-S. Yang, R. Kalb, D. R. Galasko, T. J. Montine, J. Q. Trojanowski, V. M. Y. Lee, G. D. Schellenberg & C.-E. Yu (2008) TARDBP mutations in amyotrophic lateral sclerosis with TDP-43 neuropathology: a genetic and histopathological analysis. *Lancet Neurology,* 7**,** 409-416.

Van Deerlin, V. M., P. M. A. Sleiman, M. Martinez-Lage, A. Chen-Plotkin, L.-S. Wang, N. R. Graff-Radford, D. W. Dickson, R. Rademakers, B. F. Boeve, M. Grossman, S. E. Arnold, D. M. A. Mann, S. M. Pickering-Brown, H. Seelaar, P. Heutink, J. C. van Swieten, J. R. Murrell, B. Ghetti, S. Spina, J. Grafman, J. Hodges, M. G. Spillantini, S. Gilman, A. P. Lieberman, J. A. Kaye, R. L. Woltjer, E. H. Bigio, M. Mesulam, S. al-Sarraj, C. Troakes, R. N. Rosenberg, C. L. White, III, I. Ferrer, A. Llado, M. Neumann, H. A. Kretzschmar, C. M. Hulette, K. A. Welsh-Bohmer, B. L. Miller, A. Alzualde, A. Lopez de Munain, A. C. McKee, M. Gearing, A. I. Levey, J. J. Lah, J. Hardy, J. D. Rohrer, T. Lashley, I. R. A. Mackenzie, H. H. Feldman, R. L. Hamilton, S. T. Dekosky, J. van der Zee, S. Kumar-Singh, C. Van Broeckhoven, R. Mayeux, J. P. G. Vonsattel, J. C. Troncoso, J. J. Kril, J. B. J. Kwok, G. M. Halliday, T. D. Bird, P. G. Ince, P. J. Shaw, N. J. Cairns, J. C. Morris, C. A. McLean, C. DeCarli, W. G. Ellis, S. H. Freeman, M. P. Frosch, J. H. Growdon, D. P. Perl, M. Sano, D. A. Bennett, J. A. Schneider, T. G. Beach, E. M. Reiman, B. K. Woodruff, J. Cummings, H. V. Vinters, C. A. Miller, H. C. Chui, I. Alafuzoff, P. Hartikainen, D. Seilhean, D. Galasko, E. Masliah, C. W. Cotman, M. T. Tunon, M. C. C. Martinez, D. G. Munoz, S. L. Carroll, D. Marson, P. F. Riederer, N. Bogdanovic, G. D. Schellenberg, H. Hakonarson, J. Q. Trojanowski & V. M. Y. Lee (2010) Common variants at 7p21 are associated with frontotemporal lobar degeneration with TDP43 inclusions. *Nature Genetics,* 42**,** 234-U34.

van Es, M. A., J. H. Veldink, C. G. J. Saris, H. M. Blauw, P. W. J. van Vught, A. Birve, R. Lemmens, H. J. Schelhaas, E. J. N. Groen, M. H. B. Huisman, A. J. van der Kooi, M. de Visser, C. Dahlberg, K. Estrada, F. Rivadeneira, A. Hofman, M. J. Zwarts, P. T. C. van Doormaal, D. Rujescu, E. Strengman, I. Giegling, P. Muglia, B. Tomik, A. Slowik, A. G. Uitterlinden, C. Hendrich, S. Waibel, T. Meyer, A. C. Ludolph, J. D. Glass, S. Purcell, S. Cichon, M. M. Noethen, H. E. Wichmann, S. Schreiber, S. H. H. M. Vermeulen, L. A. Kiemeney, J. H. J. Wokke, S. Cronin, R. L. McLaughlin, O.

Hardiman, K. Fumoto, R. J. Pasterkamp, V. Meininger, J. Melki, P. N. Leigh, C. E. Shaw, J. E. Landers, A. Al-Chalabi, R. H. Brown, Jr., W. Robberecht, P. M. Andersen, R. A. Ophoff & L. H. van den Berg (2009) Genome-wide association study identifies 19p13.3 (UNC13A) and 9p21.2 as susceptibility loci for sporadic amyotrophic lateral sclerosis. *Nature Genetics,* 41**,** 1083-U53.

Van Hoecke, A., L. Schoonaert, R. Lemmens, M. Timmers, K. A. Staats, A. S. Laird, E. Peeters, T. Philips, A. Goris, B. Dubois, P. M. Andersen, A. Al-Chalabi, V. Thijs, A. M. Turnley, P. W. van Vught, J. H. Veldink, O. Hardiman, L. Van Den Bosch, P. Gonzalez-Perez, P. Van Damme, R. H. Brown, Jr., L. H. van den Berg & W. Robberecht (2012) EPHA4 is a disease modifier of amyotrophic lateral sclerosis in animal models and in humans. *Nature Medicine,* 18**,** 1418-+.

Van Langenhove, T., J. van der Zee & C. Van Broeckhoven (2012) The molecular basis of the frontotemporal lobar degeneration-amyotrophic lateral sclerosis spectrum. *Annals of Medicine,* 44**,** 817-828.

Vance, C., A. Al-Chalabi, D. Ruddy, B. N. Smith, X. Hu, J. Sreedharan, T. Siddique, H. J. Schelhaas, B. Kusters, D. Troost, F. Baas, V. de Jong & C. E. Shaw (2006) Familial amyotrophic lateral sclerosis with frontotemporal dementia is linked to a locus on chromosome 9p13.2-21.3. *Brain,* 129**,** 868-876.

Vance, C., B. Rogelj, T. Hortobagyi, K. J. De Vos, A. L. Nishimura, J. Sreedharan, X. Hu, B. Smith, D. Ruddy, P. Wright, J. Ganesalingam, K. L. Williams, V. Tripathi, S. Al-Saraj, A. Al-Chalabi, P. N. Leigh, I. P. Blair, G. Nicholson, J. de Belleroche, J.-M. Gallo, C. C. Miller & C. E. Shaw (2009) Mutations in FUS, an RNA Processing Protein, Cause Familial Amyotrophic Lateral Sclerosis Type 6. *Science,* 323**,** 1208-1211.

Vossel, K. A. & B. L. Miller (2008) New approaches to the treatment of frontotemporal lobar degeneration. *Current Opinion in Neurology,* 21**,** 708-716.

Waite, A. J., D. Baeumer, S. East, J. Neal, H. R. Morris, O. Ansorge & D. J. Blake (2014) Reduced C9orf72 protein levels in frontal cortex of amyotrophic lateral sclerosis and frontotemporal degeneration brain with the C9ORF72 hexanucleotide repeat expansion. *Neurobiology of Aging,* 35.

Wang, H. Y., H. Yang, C. S. Shivalila, M. M. Dawlaty, A. W. Cheng, F. Zhang & R. Jaenisch (2013) One-Step Generation of Mice Carrying Mutations in Multiple Genes by CRISPR/Cas-Mediated Genome Engineering. *Cell,* 153**,** 910-918.

Wang, T., J. J. Wei, D. M. Sabatini & E. S. Lander (2014) Genetic Screens in Human Cells Using the CRISPR-Cas9 System. *Science,* 343**,** 80-84.

Wang, Y., W. Liu, J. Yang, F. Wang, Y. Sima, Z.-m. Zhong, H. Wang, L.-F. Hu & C.-F. Liu (2017) Parkinson's disease-like motor and non-motor symptoms in rotenone-treated zebrafish. *Neurotoxicology,* 58**,** 103-109.

Watts, S. A., M. Powell & L. R. D'Abramo (2012) Fundamental Approaches to the Study of Zebrafish Nutrition. *Ilar Journal,* 53**,** 144-160.

Webb, P. W. (1994) Exercise performance of fish. *Advances in Veterinary Science and Comparative Medicine; Comparative vertebrate exercise physiology: Phyletic adaptations,* 38B**,** 1-49.

Webster, C. P., E. F. Smith, C. S. Bauer, A. Moller, G. M. Hautbergue, L. Ferraiuolo, M. A. Myszczynska, A. Higginbottom, M. J. Walsh, A. J. Whitworth, B. K. Kaspar, K. Meyer, P. J. Shaw, A. J. Grierson & K. J. De Vos (2016a) The C9orf72 protein interacts with Rab1a and the ULK1 complex to regulate initiation of autophagy. *Embo Journal,* 35**,** 1656-1676.

Webster, C. P., E. F. Smith, A. J. Grierson & K. J. De Vos (2016b) C9orf72 plays a central role in Rab GTPase-dependent regulation of autophagy. *Small GTPases***,** 1-10.

Wen, X., W. Tan, T. Westergard, K. Krishnamurthy, S. S. Markandaiah, Y. Shi, S. Lin, N. A. Shneider, J. Monaghan, U. B. Pandey, P. Pasinelli, J. K. Ichida & D. Trotti (2014)

Antisense Proline-Arginine RAN Dipeptides Linked to C9ORF72-ALS/FTD Form Toxic Nuclear Aggregates that Initiate In Vitro and In Vivo Neuronal Death. *Neuron,* 84**,** 1213-1225.

Wen, X., T. Westergard, P. Pasinelli & D. Trotti (2017) Pathogenic determinants and mechanisms of ALS/FTD linked to hexanucleotide repeat expansions in the C9orf72 gene. *Neuroscience Letters,* 636**,** 16-26.

Westerfield, M., J. V. McMurray & J. S. Eisen (1986) IDENTIFIED MOTONEURONS AND THEIR INNERVATION OF AXIAL MUSCLES IN THE ZEBRAFISH. *Journal of Neuroscience,* 6**,** 2267-2277.

Wiedemann, F. R., G. Manfredi, C. Mawrin, F. Beal & E. A. Schon (2002) Mitochondrial DNA and respiratory chain function in spinal cords of ALS patients. *Journal of Neurochemistry,* 80**,** 616-625.

Wilke, C., J. K. Pomper, S. Biskup, C. Puskas, D. Berg & M. Synofzik (2016) Atypical parkinsonism in C9orf72 expansions: a case report and systematic review of 45 cases from the literature. *Journal of Neurology,* 263**,** 558-574.

Williams, K. L., J. A. Fifita, S. Vucic, J. C. Durnall, M. C. Kiernan, I. P. Blair & G. A. Nicholson (2013) Pathophysiological insights into ALS with C9ORF72 expansions. *Journal of Neurology Neurosurgery and Psychiatry,* 84**,** 931-935.

Williamson, T. L. & D. W. Cleveland (1999) Slowing of axonal transport is a very early event in the toxicity of ALS-linked SOD1 mutants to motor neurons. *Nature Neuroscience,* 2**,** 50-56.

Wilson, C. (2012) Aspects of Larval Rearing. *Ilar Journal,* 53**,** 169-178.

Wittkopp, N., E. Huntzinger, C. Weiler, J. Sauliere, S. Schmidt, M. Sonawane & E. Izaurralde (2009) Nonsense-Mediated mRNA Decay Effectors Are Essential for Zebrafish Embryonic Development and Survival. *Molecular and Cellular Biology,* 29**,** 3517-3528.

Wolman, M. & M. Granato (2012) Behavioral genetics in larval zebrafish: Learning from the young. *Developmental Neurobiology,* 72**,** 366-372.

Wu, C. H., C. Fallini, N. Ticozzi, P. J. Keagle, P. C. Sapp, K. Piotrowska, P. Lowe, M. Koppers, D. McKenna-Yasek, D. M. Baron, J. E. Kost, P. Gonzalez-Perez, A. D. Fox, J. Adams, F. Taroni, C. Tiloca, A. L. Leclerc, S. C. Chafe, D. Mangroo, M. J. Moore, J. A. Zitzewitz, Z. S. Xu, L. H. van den Berg, J. D. Glass, G. Siciliano, E. T. Cirulli, D. B. Goldstein, F. Salachas, V. Meininger, W. Rossoll, A. Ratti, C. Gellera, D. A. Bosco, G. J. Bassell, V. Silani, V. E. Drory, R. H. Brown & J. E. Landers (2012) Mutations in the profilin 1 gene cause familial amyotrophic lateral sclerosis. *Nature,* 488**,** 499-+.

Wullimann, M. F. & T. Mueller (2004) Teleostean and mammalian forebrains contrasted: Evidence from genes to behavior. *Journal of Comparative Neurology,* 475**,** 143-162.

Xi, Z., L. Zinman, D. Moreno, J. Schymick, Y. Liang, C. Sato, Y. Zheng, M. Ghani, S. Dib, J. Keith, J. Robertson & E. Rogaeva (2013) Hypermethylation of the CpG Island Near the G(4)C(2) Repeat in ALS with a C9orf72 Expansion. *American Journal of Human Genetics,* 92**,** 981-989.

Xiao, S., L. MacNair, P. McGoldrick, P. M. McKeever, J. R. McLean, M. Zhang, J. Keith, L. Zinman, E. Rogaeva & J. Robertson (2015) Isoform-Specific Antibodies Reveal Distinct Subcellular Localizations of C9orf72 in Amyotrophic Lateral Sclerosis. *Annals of Neurology,* 78**,** 568-583.

Xu, Z., M. Poidevin, X. Li, Y. Li, L. Shu, D. L. Nelson, H. Li, C. M. Hales, M. Gearing, T. S. Wingo & P. Jin (2013) Expanded GGGGCC repeat RNA associated with amyotrophic lateral sclerosis and frontotemporal dementia causes neurodegeneration. *Proceedings of the National Academy of Sciences of the United States of America,* 110**,** 7778-7783.

Yamanaka, K., S. J. Chun, S. Boillee, N. Fujimori-Tonou, H. Yamashita, D. H. Gutmann, R. Takahashi, H. Misawa & D. W. Cleveland (2008) Astrocytes as determinants of disease progression in inherited amyotrophic lateral sclerosis. *Nature Neuroscience,* 11**,** 251-253.

Yang, M., C. Liang, K. Swaminathan, S. Herrlinger, F. Lai, R. Shiekhattar & J.-F. Chen (2016) A C9ORF72/SMCR8-containing complex regulates ULK1 and plays a dual role in autophagy. *Science Advances,* 2.

Yang, Y., A. Hentati, H. X. Deng, O. Dabbagh, T. Sasaki, M. Hirano, W. Y. Hung, K. Ouahchi, J. H. Yan, A. C. Azim, N. Cole, G. Gascon, A. Yagmour, M. Ben-Hamida, M. Pericak-Vance, F. Hentati & T. Siddique (2001) The gene encoding alsin, a protein with three guanine-nucleotide exchange factor domains, is mutated in a form of recessive amyotrophic lateral sclerosis. *Nature Genetics,* 29**,** 160-165.

Zerial, M. & H. McBride (2001) Rab proteins as membrane organizers. *Nature Reviews Molecular Cell Biology,* 2**,** 107-117.

Zhang, D., L. M. Iyer, F. He & L. Aravind (2012) Discovery of Novel DENN Proteins: Implications for the Evolution of Eukaryotic Intracellular Membrane Structures and Human Disease. *Frontiers in genetics,* 3**,** 283-283.

Zhang, H., C.-F. Tan, F. Mori, K. Tanji, A. Kakita, H. Takahashi & K. Wakabayashi (2008) TDP-43-immunoreactive neuronal and glial inclusions in the neostriatum in amyotrophic lateral sclerosis with and without dementia. *Acta Neuropathologica,* 115**,** 115-122.

Zhang, K., C. J. Donnelly, A. R. Haeusler, J. C. Grima, J. B. Machamer, P. Steinwald, E. L. Daley, S. J. Miller, K. M. Cunningham, S. Vidensky, S. Gupta, M. A. Thomas, I. Hong, S.-L. Chiu, R. L. Huganir, L. W. Ostrow, M. J. Matunis, J. Wang, R. Sattler, T. E. Lloyd & J. D. Rothstein (2015) The C9orf72 repeat expansion disrupts nucleocytoplasmic transport. *Nature,* 525**,** 56-+.

Zhang, Y.-J., T. F. Gendron, J. C. Grima, H. Sasaguri, K. Jansen-West, Y.-F. Xu, R. B. Katzman, J. Gass, M. E. Murray, M. Shinohara, W.-L. Lin, A. Garrett, J. N. Stankowski, L. Daughrity, J. Tong, E. A. Perkerson, M. Yue, J. Chew, M. Castanedes-Casey, A. Kurti, Z. S. Wang, A. M. Liesinger, J. D. Baker, J. Jiang, C. Lagier-Tourenne, D. Edbauer, D. W. Cleveland, R. Rademakers, K. B. Boylan, G. Bu, C. D. Link, C. A. Dickey, J. D. Rothstein, D. W. Dickson, J. D. Fryer & L. Petrucelli (2016) C9ORF72 poly(GA) aggregates sequester and impair HR23 and nucleocytoplasmic transport proteins. *Nature Neuroscience,* 19**,** 668-+.

Zhang, Y.-J., K. Jansen-West, Y.-F. Xu, T. F. Gendron, K. F. Bieniek, W.-L. Lin, H. Sasaguri, T. Caulfield, J. Hubbard, L. Daughrity, J. Chew, V. V. Belzil, M. Prudencio, J. N. Stankowski, M. Castanedes-Casey, E. Whitelaw, P. E. A. Ash, M. DeTure, R. Rademakers, K. B. Boylan, D. W. Dickson & L. Petrucelli (2014) Aggregation-prone c9FTD/ALS poly(GA) RAN-translated proteins cause neurotoxicity by inducing ER stress. *Acta Neuropathologica,* 128**,** 505-524.

Zhang, Y. X., D. T. Nguyen, E. M. Olzomer, G. P. Poon, N. J. Cole, A. Puvanendran, B. R. Phillips & D. Hesselson (2017) Rescue of Pink1 Deficiency by Stress-Dependent Activation of Autophagy. *Cell Chemical Biology,* 24**,** 471-+.

Zhu, P., C. J. Sieben, X. L. Xu, P. C. Harris & X. Y. Lin (2017) Autophagy activators suppress cystogenesis in an autosomal dominant polycystic kidney disease model. *Human Molecular Genetics,* 26**,** 158-172.

Ziv, L., A. Muto, P. J. Schoonheim, S. H. Meijsing, D. Strasser, H. A. Ingraham, M. J. M. Schaaf, K. R. Yamamoto & H. Baier (2013) An affective disorder in zebrafish with mutation of the glucocorticoid receptor. *Molecular Psychiatry,* 18**,** 681-691.

Zu, T., B. Gibbens, N. S. Doty, M. Gomes-Pereira, A. Huguet, M. D. Stone, J. Margolis, M. Peterson, T. W. Markowski, M. A. C. Ingram, Z. Nan, C. Forster, W. C. Low, B. Schoser, N. V. Somia, H. B. Clark, S. Schmechel, P. B. Bitterman, G. Gourdon, M.

S. Swanson, M. Moseley & L. P. W. Ranum (2011) Non-ATG-initiated translation directed by microsatellite expansions. *Proceedings of the National Academy of Sciences of the United States of America,* 108**,** 260-265.

Zu, T., Y. Liu, M. Baez-Coronel, T. Reid, O. Pletnikova, J. Lewis, T. M. Miller, M. B. Harms, A. E. Falchook, S. H. Subramony, L. W. Ostrow, J. D. Rothstein, J. C. Troncoso & L. P. W. Ranum (2013) RAN proteins and RNA foci from antisense transcripts in C9ORF72 ALS and frontotemporal dementia. *Proceedings of the National Academy of Sciences of the United States of America,* 110**,** E4968-E4977.